

UNIVERSITÀ
DEGLI STUDI
DI PADOVA

TESI DI DOTTORATO

Sede Amministrativa: Università degli Studi di Padova
Facoltà di Scienze MM. FF. NN.
Dipartimento di Scienze Chimiche

SCUOLA DI DOTTORATO DI RICERCA IN: SCIENZE MOLECOLARI
INDIRIZZO: SCIENZE CHIMICHE
CICLO XXIII°

ADVANCED EPR SPECTROSCOPY PROVIDES NEW INSIGHTS INTO TRIPLET-TRIPLET ENERGY TRANSFER IN PHOTOSYNTHESIS

Direttore della Scuola: Ch.mo Prof. Maurizio Casarin
Coordinatore d'indirizzo: Ch.mo Prof. Maurizio Casarin
Supervisore: Ch.ma Prof. ssa Donatella Carbonera

Dottorando: Enrico Salvadori

A Bruna e Giovanni

Contents

		Abstract	5
		Sommario	9
		Thesis Outline	13
Chapter I		**The Light-Harvesting Complexes**	15
	1.1	Photosynthetic Pigments	19
		1.1.1 Chlorophylls	19
		1.1.2 Carotenoids	21
	1.2	Light-Harvesting Complexes and triplet triplet energy transfer	24
		1.2.1 LHC-II from *Spinacia oleracea*	25
		1.2.1.1 TTET	25
		1.2.2 LHC from *Amphidinium carterae*	27
		1.2.2.1. TTET	28
		1.2.3 PCPs from *Amphidinium carterae* and *Heterocapsa pygmaea*	28
		1.2.3.1- TTET	30
		1.2.4 Chlorosomes from *Chlorobaculum tepidum*	31
		1.2.4.1 TTET	32
	1.3	References	33
Charter II		**The triplet State**	39
	2.1	Triplet state description	41
		2.1.1 Zero Field Splitting Interaction	42
		2.1.2 Electron Zeeman Interaction	46
		2.1.3 Hyperfine Interaction	47
	2.2	Spin Polarization	49
	2.3	Triplet-Triplet Energy Transfer	51
	2.4	References	53
Chapter III		**The Triplet State EPR Spectroscopy**	55
	3.1	Time-Resolved EPR	57
	3.2	Pulsed EPR	59
	3.3	Pulsed ENDOR	67
	3.4	References	71
Chapter IV		**LHC-II from *Spinacia Oleracea***	73
	4.1	Pulsed ENDOR and Density Functional Theory on the Lutein Triplet State in LHC-II of *Spinacia oleracea*. Comparison with the Peridinin Triplet State in PCP of *Amphidinum carterae*.	75

Chapter V **LHC from *Amphidinium carterae*** 103

5.1 Triplet-triplet energy transfer in the major intrinsic light-harvesting complex of *Amphidinium carterae* as revealed by ODMR and EPR spectroscopies 105
5.1.1 Supplemantary Materials 115

Charter VI **PCPs protein from *Amphidinium Carterae* and *Heterocapsa Pygmaea*** 121

6.1 Spectroscopic properties of the peridinins involved in chlorophyll triplet quenching in high-salt peridinin-chlorophyll a-protein from *Amphidinium carterae* as revealed by optically detected magnetic resonance, pulse EPR and pulse ENDOR spectroscopies. 123
6.2 Triplet-triplet energy transfer in Peridinin-Chlorophyll *a*-protein reconstituted with Chl *a* and Chl *d* as revealed by optically detected magnetic resonance and pulse EPR: Comparison with the native PCP complex from *Amphidinium carterae* 133
6.3 Pulsed EPR and ENDOR on the Peridinin Triplet State Involved in the Photoprotective Mechanism in Peridinin-Chlorophyll *a*-Protein 141
6.4 Conservation of Spin-polarization during Triplet-Triplet Energy transfer in Reconstituted Peridinin-Chlorophyll *a*-Proteins from *Amphidinium carterae* 157
6.4.1 Supporting Information 179

Chapter VII **Chlorosomes from *Chlorobium tepidum*** 183

7.1 A time-resolved EPR investigation of the triplet-triplet energy transfer in the chlorosomes of *Chlorobaculum tepidum* reveals the molecular organization of the pigments in the baseplate 185

Acknowledgements 203

Abstract

Carotenoids are essential in photosynthesis. These molecules play several roles in the photosynthetic apparatus: they share with chlorophylls the light-harvesting function, stabilize the pigment-protein complexes and are responsible for the protection of the whole apparatus against the hazardous singlet oxygen. The structural function has been investigated in many different organisms by several biochemical methods: the main finding is that carotenoids are essential for the protein stability. Without carotenoids light-harvesting complexes would not fold and their selective removal from intact proteins often causes unfolding. The light-harvesting function of the carotenoids has been object of extensive investigations. The photo-physics of their singlet states is very complex: it is characterized by the presence of forbidden states, fast dynamics of the excited states and low fluorescence yield. The singlet energy transfer pathways between carotenoids and chlorophylls, which are important for the light-harvesting function, have been also well characterized. Less has been done on the study of the photoprotective role that makes carotenoids essential for the photosynthetic organisms. Carotenoids are involved in photoprotection in many ways and at different stages of the photosynthetic process, in relation to the intensity and duration of the stress conditions. When the sunlight intensity suddenly increases the first photoprotection mechanism activated is the photo-physical triplet-triplet energy transfer from chlorophylls molecules to carotenoids molecules. This interaction scavenges the formation of highly oxidant oxygen species which could be produced by the chlorophyll triplet states, whose production increases under light excess. Carotenoid triplet states are thus very important from a physiological point of view.

In contrast to photosynthetic reaction centres, which have very similar structural architecture, light-harvesting complexes show more variability due to different habitat adaptation of the photosynthetic organisms. This heterogeneity stimulated a comparative investigation on light harvesting complexes in order to point out the common and the different key features adopted by the different organisms for reaching an efficient triplet-triplet energy transfer.

This thesis represents one of the few detailed studies entirely focused on the role of carotenoids molecules in the triplet-triplet energy transfer mechanism in naturally occurring light-harvesting complexes. By means of EPR spectroscopy, the magnetic

properties of the carotenoid triplet states have been exploited to characterize the energy transfer pathways in four different light-harvesting complexes: the LHC-II from higher plants, the LHC and the PCPs from dinoflagellates and the chlorosomes from green sulphur bacteria. These antenna proteins have been selected as representative for the light-harvesting strategy variability adopted by different photosynthetic species.

The main results obtained, which have a physiological relevance, can be summarized as follows:

- Among all the pigments present in each protein considered, only specific carotenoids are devoted to the dissipation of chlorophyll triplet energy. It is worth noting that the examined proteins belong to different organisms which are not close in the evolutionary scale. Thus, the presence of a specific triplet energy sink seems to be an important point in the photoprotection mechanism played by triplet-triplet energy transfer.
- EPR spectroscopy does not show any evidence for the existence of triplet excitons involving carotenoids and chlorophylls. Moreover multiple triplet-triplet energy transfers among carotenoids can also be ruled out. Therefore a localized carotenoid triplet state seems to be a common feature for all the pigment-protein complexes.
- The triplet electron density distribution over the conjugate chain of the carotenoids is not heavily influenced by the chemical substitution. It has the same pattern and the same extent even though triplet states belonging to carotenoids with very different molecular structure are considered. This characteristic makes the relative geometry of the chlorophyll/carotenoid couples involved in the triplet-triplet energy transfer not very dependent on the center-to-center distance of the two pigments. Instead the minimum distance between the π-conjugated systems results to be most the important structural requirement.
- Triplet-triplet energy transfer in antenna complexes seems to be properly described by a superexchange mechanism involving a molecular bridge interposed between the chlorophyll/carotenoid couple. This bridge is represented by the fifth ligand of the Mg atom bound to the chlorophyll. The mechanism is supported by ENDOR measurements and DFT calculations: the

highest electron density calculated for the carotenoid triplet state is located on the carbon atom closest to the Mg fifth ligand. Thus the bridge likely increases the triplet-triplet energy transfer rate leading to a very efficient quenching.

Together with the 'functional' results, this thesis demonstrates also how triplet state EPR techniques, applied to the study of the molecules involved in triplet-triplet energy transfer, can be used to derive structural information if the crystallographic structure of the light-harvesting protein is not known. As a matter of fact, EPR spectra can be conveniently used to extract some experimental constraints useful in the modelling of protein structure, since their shapes strictly depend on the relative geometry of the couples involved in the triplet-triplet energy transfer. In photosynthesis this is particularly relevant since many proteins involved in the process are large, embedded in the membrane and bound many cofactors. All these characteristics are severe limitations in using x-ray diffraction or NMR

Sommario

I caroteni sono assi portanti del processo fotosintetico. A queste molecole sono affidati molteplici ruoli: condividono con le clorofille la funzione di raccolta dell'energia luminosa, stabilizzano i complessi proteina-pigmento e sono responsabili della protezione dell'intero apparato fotosintetico contro l'azione ossidante dell'ossigeno di singoletto. La funzione strutturale è stata studiata mediante diverse tecniche biochimiche in molteplici organismi: è stato dimostrato che i carotenoidi sono essenziali per la stabilità strutturale dei complessi proteici. Senza carotenoidi i complessi antenna non sono in grado di assemblarsi e la loro rimozione selettiva da proteine intatte ne causa la denaturazione. La funzione di raccolta della luce è stata estensivamente studiata tramite spettroscopie ottiche. La foto-fisica degli stati di singoletto nei caroteni è molto complessa e caratterizzata dalla presenza di transizioni proibite, dalla dinamica veloce tra stati eccitati e dalla bassa resa di fluorescenza. Anche i cammini di trasferimento di energia di singoletto tra caroteni e clorofille, importanti per la funzione di raccolta della luce, sono stati ampiamente caratterizzati. Molto meno è stato fatto riguardo al ruolo fotoprotettivo che rende i carotenoidi essenziali per gli organismi fotosintetici. I carotenoidi sono implicati nella fotoprotezione in moti modi e in diversi gradi in relazione alla durata e all'intensità delle condizioni di stress. Quando l'intensità della luce solare aumenta improvvisamente il primo meccanismo di fotoprotezione attivato è il trasferimento di energia tripletto-tripletto dalle molecole di clorofilla verso le molecole di carotenoide: questo trasferimento di energia previene la formazione di specie all'ossigeno altamente ossidanti che potrebbero essere prodotte dalla clorofilla in stato di tripletto. Lo stato di tripletto di carotenoide è quindi fisiologicamente importante.

A differenza dei centri di reazione fotosintetici, che condividono tutti un'architettura strutturale molto simile, i complessi antenna esibiscono una più spiccata variabilità dovuta ai differenti adattamenti ambientali. Questa eterogeneità ha stimolato un'indagine comparativa al fine di evidenziare le caratteristiche fondamentali comuni o particolari adottate dai diversi organismi per rendere il trasferimento di energia di tripletto efficiente.

Questa tesi rappresenta uno dei pochi studi dettagliati completamente focalizzati sul ruolo delle molecole carotenoidi nel meccanismo di trasferimento di energia tripletto-ripletto in complessi antenna naturali. Attraverso la spettroscopia EPR, si sono sfruttate le proprietà magnetiche degli stati di tripletto dei caroteni per caratterizzare i cammini di trasferimento di energia in quattro diversi complessi antenna: la proteina LHC-II caratteristica delle piante superiori, le proteine LHC e PCP caratteristiche dei dinoflagellati ed i clorosomi caratteristici dei batteri verdi sulfurei. Queste proteine sono state selezionate come campione rappresentativo della variabilità nelle strategie di fotoprotezione adottate dai diversi organismi fotosintetici.

I risultati ottenuti con rilevanza fisiologica possono essere schematizzati come segue:

- Tra tutti i pigmenti presenti in ogni proteina considerata, solo specifici carotenoidi sono deputati alla dissipazione dell'energia di tripletto delle clorofille. Vale la pena notare che le proteine considerate appartengono ad organismi distanti nella scala evolutiva. Sembra perciò che la presenza di specifiche 'trappole di energia' sia centrale nella fotoprotezione giocata dai trasferimenti di energia tripletto-tripletto

- I dati EPR non mostrano alcuna evidenza circa la formazione di eccitoni di tripletto che coinvolgano caroteni e clorofille. Inoltre, permettono di escludere la presenza trasferimenti multipli di energia di tripletto tra carotenoidi. Perciò, la presenza di uno stato di tripletto di carotenoide localizzato sembra essere una caratteristica comune a tutti i complessi antenna considerati.

- La distribuzione della densità elettronica dello stato di tripletto lungo la catena coniugata della molecola di carotenoide non risulta essere particolarmente influenzata dalla presenza di sostituenti chimici: presenta la stesso andamento e la stessa estensione anche tra carotenoidi con strutture chimiche molto differenti. Questa evidenza rende la geometria relativa della coppia clorofilla/carotenoide coinvolta nel trasferimento di energia non particolarmente dipendente dalla distanza tra i centri dei sistemi coniugati delle due molecole. Mentre sembra che la minima distanza tra i sistemi coniugati sia il requisito strutturale fondamentale.

- Il trasferimento di energia tripletto-tripletto nei complessi antenna sembra essere correttamente descritto dal meccanismo di super-scambio che coinvolge un ponte molecolare intercalato tra la coppia clorofilla/carotenoide. Questo ponte è

rappresentato dal quinto legando dell'atomo di Mg legato al centro della molecola di clorofilla. Gli esperimenti ENDOR ed i calcoli DFT condotti supportano questa conclusione: la densità elettronica più alta riscontrata appartiene all'atomo di carbonio più vicino al quinto legando dell'atomo di Mg. Verosimilmente il ponte molecolare aumenta la velocità di trasferimento di energia garantendo un processo molto efficiente.

Parallelamente a questi conclusioni 'funzionali', questa tesi dimostra anche come le tecniche EPR, applicate allo studio di molecole coinvolte nei trasferimenti di energia tripletto-tripletto, possano essere utilizzate per ricavare informazioni strutturali quando la struttura cristallografica non sia nota. Infatti, poiché la loro forma spettrale dipende direttamente dalla geometria della coppia coinvolta nel trasferimento di energia di tripletto, gli spettri EPR possono essere opportunamente impiegati per estrarre vincoli sperimentali da impiegare nella modellizzazione di strutture proteiche.
In ambito fotosintetico questo risultato è particolarmente rilevante dal momento che molte proteine coinvolte nel processo sono grandi, di membrana e legano molti cofattori. Tutte queste caratteristiche costituiscono importanti limitazioni nell'utilizzo della diffrazione ai raggi x o delle tecniche NMR.

Thesis Outline

The thesis is structured with an introductory part with a general presentation of the biological problem, the physics of the triplet state and an overview about the EPR techniques adopted. The second part is completely devoted to the experimental results and it is divided into four chapters concerning the different light-harvesting complexes. All the experimental chapters are in scientific-article layout: this is to offer the possibility of a selective consultation. If the experimental work has been already published it is presented without any modification.

Together with the EPR results, some ODMR data are also present: they are not strictly part of this Ph.D. work but they have been reported because intimately connected with the investigation.

The experimental work has been done mostly in the EPR laboratory of the 'Dipartimento di Scienze Chimiche, Università degli Studi di Padova', even though some experiments on the LHC-II and on the chlorosomes have been carried out in the EPR laboratory of the University College of London. The biological samples of dinoflagellate algae have been provided by Prof. Roger Hiller (Macquarie University, Australia) and Prof. Hugo Scheer (Ludwig-Maximilian University, Munich). The chlorosome samples have been provided by Prof. Alberto Vianelli (Università dell'Insubria, Varese) while the atomic coordinates of the baseplate structural model has been provided by Prof. Juha Linnato (University of Jyväskylä, Finland) as personal communication. Theoretical DFT calculations are a collaboration with Prof. Vincenzo Barone (Scuola Normale Superiore di Pisa, Italy) and Dr. Alfonso Pedone (Università di Modena e Reggio Emilia, Italy).

Chapter I

The Light-Harvesting Complexes

Photosynthesis is the physical-chemical process by which plants, algae and some bacteria convert carbon dioxide into high-energy organic compounds, using the solar energy. Photosynthesis provides the energy and the reduced carbon required for the survival of virtually all life on our planet, as well as the molecular oxygen for the survival of oxygen consuming organisms [Ort and Yocum].

Although photosynthesis can be performed in different ways in different species, some features are common. The process always begins when energy from light is absorbed and delivered to specialized chlorophylls-proteins complexes, called photosynthetic reaction centers (RCs). In plants, these RCs are held inside the thylakoid membranes of organelles, called chloroplasts, while in bacteria they are embedded in the plasma membrane. Some of the light energy gathered by chlorophylls is stored in the form of adenosine triphosphate (ATP). The rest of the energy is used to remove electrons from a reductant such as water. These electrons are then used in the reactions that reduce carbon dioxide into carbohydrates.

As already stated, the photosynthetic organisms need to collect the sunlight energy which is necessary to drive the charge-separation reactions that are at the heart of the photosynthetic process; the so called light-harvesting complexes (or antenna complexes) are devoted to fulfil this preliminary task. A light-harvesting complex is a pigments-protein complex used by photosynthetic organisms to harvest more of the incoming light than would be captured by the photosynthetic reaction centere itsef. Light-harvesting complexes are found in wide variety among the different photosynthetic species, in relation to different habitats and different position in the evolutionary scale. Light-harvesting complexes are located around the reaction centre and bind pigments, carotenoids and chlorophylls, to funnel the absorbed energy to the special pair in the RCs. Reaction centre chlorophyll–protein complexes would be able to directly absorb light and perform the charge separation events, However their absorption cross section (the probability of absorbing a photon under a given light intensity) is rather small. Thus, the pigments, associated with the antenna complexes cooperatively absorb and funnel light energy to the reaction centers.

Besides light-harvesting, a further crucial function of the carotenoids molecules in the apparatus is to avoid the damaging photochemical reactions, in particular those

including oxygen products, which can be induced, under high light conditions (stress conditions), via an increased production of chlorophyll triplet states. It has been demonstrated, by many authors, that plants lacking carotenoids quickly die by exposure to light and oxygen [Codgell et al. 1987, Young et al. 1993].

The possible fates of the chlorophyll excited singlet states are depicted in figure 1.1.

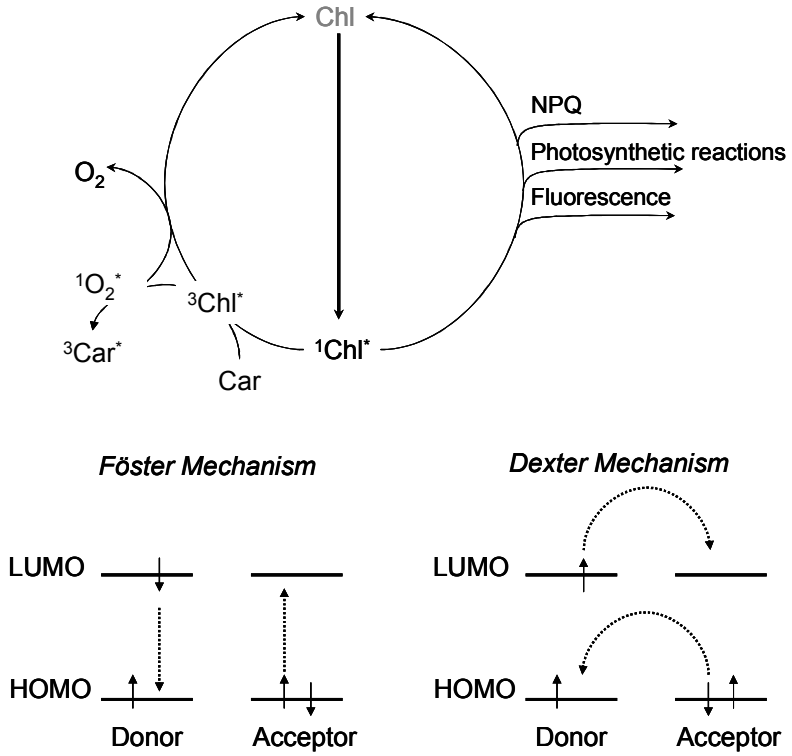


Figure 1.1: Top – Possible fate of excited Chl. When Chl absorbs light it is excited from its ground state to its singlet excited state, $^1Chl^*$. From there, it has several ways to relax back to the ground state. It can relax by fluorescence, its excitation can be used to fuel photosynthetic reactions, or it can be de-excited by dissipating heat (NPQ, non-photochemical quenching). Last, $^1Chl^*$ can undergo intersystem crossing and produce $^3Chl^*$ which in turn can generate the very reactive singlet oxygen $^1O_2{}^*$. Carotenoids are able to deactivate both $^3Chl^*$ and $^1O_2{}^*$ by virtue of their low lying triplet state which relaxes by non-radiative process. Bottom – Schematic representations for the Föster and Dexter energy transfer mechanisms.

The energy transfer processes are fundamental for the photosynthetic process. In this context, two different mechanisms are worth to be mentioned: the Förster mechanism and the exchange mechanism, also known as Dexter mechanism, see figure 1.1. The former is based on the electronic dipole-dipole interaction between the transition

dipoles of a donor and an acceptor: it is efficient for long distances and it depends on the superposition of the donor emission spectrum and the acceptor absorption spectrum. In this mechanism, the excited electron of the donor relaxes back to the ground state and simultaneously an electron of the acceptor is lead to an excited state. Oppositely, the exchange mechanism results in the transfer of two electrons, one electron passing from the donor LUMO to the acceptor LUMO, the second electron tunnelling simultaneously from the acceptor ground state to the donor one. The Förster mechanism is suitable to describe the singlet-singlet energy transfer among (bacterio)chlorophylls [Struve 1995, Sundström et al. 1995]. On the other hand, when carotenoids are involved, since their fluorescence yield is very low, the energy transfer from them to the (bacterio)chlorophylls is better described by the Dexter mechanism. More importantly, the Dexter mechanism is active in the energy transfer between triplet states.

Figure 1.2 schematically reports the energy transfer pathways involving chlorophylls and carotenoids active in photosynthetic proteins.

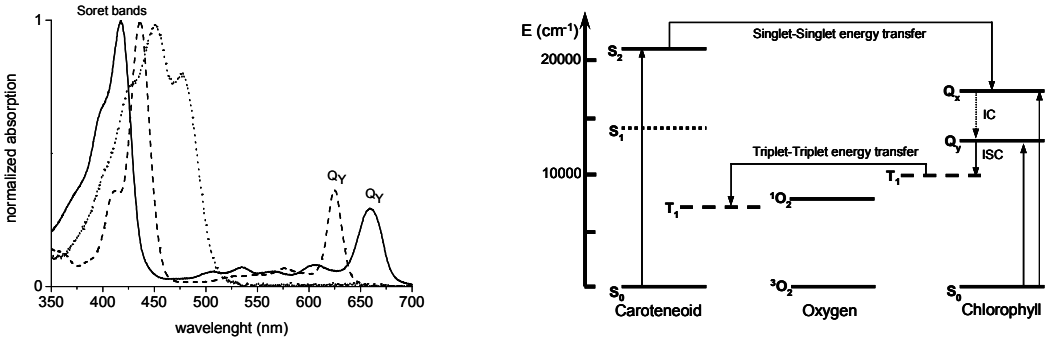


Figure 1.2: Left - Absorption spectra of Chl a in methanol (straight line), Chl b in diethyl-ether (dashed line) and β-carotene in diethyl-ether (dotted line), all the spectra are normalized to the absorption maximum. Right – Schematic energy diagram showing the electronic transitions of chlorophyll, carotenoid and oxygen.

1.1 Photosynthetic pigments

1.1.1 Chlorophylls

Chlorophyll is the vital cofactor in photosynthesis, which allows plants to obtain energy from light. Bacteria use slightly different molecules called bacterio-

chlorophylls. (Bacterio)Chlorophylls derive from the (bacterio)chlorin structure, which is structurally similar, and are produced through the same metabolic pathway as other porphyrin pigments. In addition, they are characterized by a fifth isocyclic ring. Some molecular structures of chlorophylls are reported in figure 1.3. In the center of the chlorin ring a magnesium ion is coordinated by the four nitrogen atoms. The chlorin ring can have several different side chains, usually including a long phytol chain that often serves as an anchor to the protein structure. Usually, in bacteriochlorophyll, the ring B is saturated.

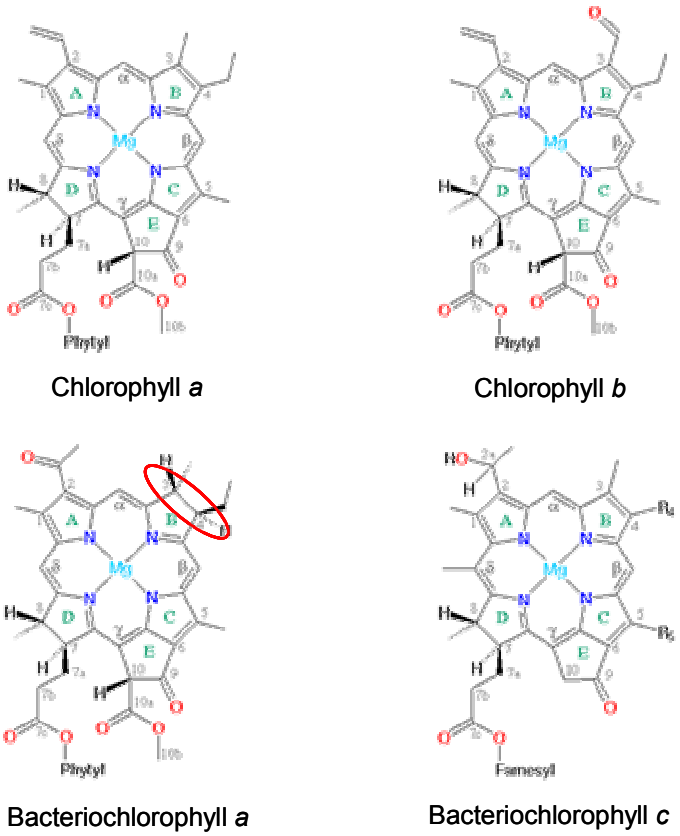


Figure 1.3: Molecular structures of the most common (bacterio)chlorophylls discussed in this thesis. In bacteriochlorophyll *a*, the saturated ring B is highlighted. Rings A, B, C, D and E are also called I, II, III, IV and V.

There are a few different forms that naturally occur: the most widely distributed form in higher plants and algae is chlorophyll *a*, whereas in bacteria is bacteriochlorophyll *a*. The different chemical substitutions at the porphyrin ring are able to modulate the interactions with the environment varying the strength of hydrophobic interaction or the presence of hydrogen-bonds.

The (bacterio)chlorophyll absorption spectrum usually presents two groups of transitions: the weakly allowed Q-bands in the visible-near IR region ad the strongly allowed B-bands, or Soret, in the blue part of the spectrum (see figure 2). Indeed the relative transition strength of the absorption bands depends on the chemical substitutions and on the environmental polarity. In the Chl *a* spectrum in methanol, a strong Soret band at 430 nm and a relative strong Q_Y transition at 662 nm are present. The weak band at 578 nm is the Q_X transition. The substitution of the methyl into formyl group in ring B going from Chl *a* to Chl *b* is reflected in the red-shift of the Chl *b* Soret band, in the blue-shift of the Q_Y band and in the lower extinction coefficient. All these changes are due to a small substitution that increases the electronic distribution symmetry making Chl *b* more porphyrin-like. The BChl *a* absorption spectrum shows the absorption maximum at 770 nm (Q_Y band), with the Q_X transition at 594 nm and the Soret at 364 nm. The red shift of the Q_Y band, compared to Chl *a*, is due to the presence of the acetyl at the C2 and to the saturation of the ring B. Conversely, the BChl *c* spectrum resembles more that of Chl *a* rather than the of BChl *a*. In fact its molecular structure is more similar to that of Chls molecules. In general, the molar extinction coefficient of the Q_Y transition is directly related to the electronic distribution: the more asymmetric the π-electron distribution becomes, the more intense the Q_Y transition will be. The *in vivo* environment conditions (such as hydrogen bonding, charged aminoacids proximity, excitonic interactions, etc..) could also have strong effects on frequency, intensity and line-width of the Q_Y transition.

1.1.2 Carotenoids

Carotenoids are long linear organic molecules. The basic structure is a symmetrical tetraterpene skeleton formed by tail-to-tail linkage of two C_{20} units [Young et al. 1993]. These molecules absorb light most efficiently in the 400 – 600 nm range and are able to extend the absorption of the antenna complexes in the green region, [Young et al. 1993, Polìvka et al. 2010]. In nature, many kinds of carotenoids occur differing in the extent of their π-electron system, in the nature of their cyclic end-groups, methyl side-groups, presence of triple bonds, allene, carbonyl and other

moieties. Carotenoids can be split into two classes, xanthopylls (which contain oxygen) and carotenes (which contain no oxygen so they are purely hydrocarbons). Their colour, ranging from pale yellow to deep red through bright orange, is related to their electronic structure. Xanthophylls are often yellow, hence their class name. Some carotenoid structures, relevant in photosynthesis, are reported in figure 1.4. The spectroscopic properties of carotenoids are mostly determined by the conjugated π-electrons of the polyene chain. Each double bond reduces the energy gap required for electrons to move to higher energy states, allowing the molecule to absorb visible light of progressively lower energy.

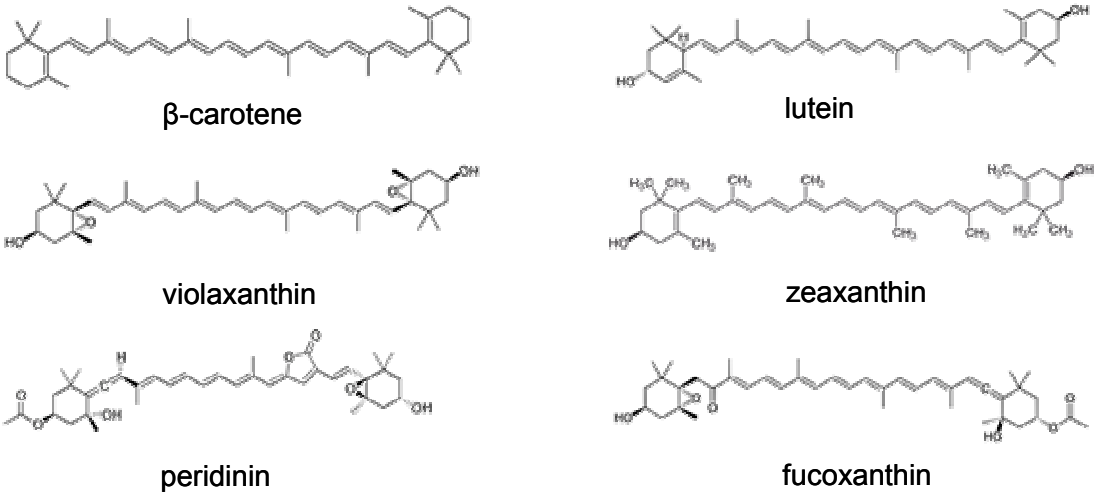


Figure 1.4: Molecular structure of the carotenoid molecules considered in the experimental chapters. The β-carotene structure is also reported for comparison.

Typically, the absorption spectrum of a carotenoid in solution exhibits a characteristic three-peaks structure, in which each peak corresponds to the transition from the ground state to a different vibronic sub-level of S_2, see figure 1.2. The $S_0 \rightarrow S_2$ ($^1A_g \rightarrow {}^1B_u$) transition is strongly allowed and is associated with a large change in dipole moment. Linear polyenes have also an additional state located at lower energy (^2A_g). The transition to this state is optically forbidden for symmetry reasons, however it may become weakly allowed due to symmetry breaking, (for a recent comparative review see [Polìvka et al. 2010]). The energy of S_2 state shows a 1/N dependence on the conjugation length. Carotenoids fulfil several roles in the photosynthetic apparatus: they participate in structural assembly and stabilization of protein complexes in the thylakoid membrane; they absorb the light in the energy region where Chls do not absorb and transfer the energy to them; above all,

carotenoids protect the whole system from photo-oxidation. As a matter of the fact, the carotenoids are able to quench the chlorophyll triplet states and deactivate the harmful singlet oxygen. The reactions involved in the entire process can be summarized as follow:

- singlet oxygen generation and photo-oxidative processes

$Chl + h\nu \rightarrow {}^1Chl^*$

${}^1Chl^* \rightarrow {}^3Chl^*$

${}^3Chl^* + {}^3O_2 \rightarrow {}^1Chl + {}^1O_2{}^*$

${}^1O_2{}^* + \text{organic compounds} \rightarrow \text{oxidation products}$

- Photo-physical photoprotection

${}^3Chl^* + {}^1Car \rightarrow {}^1Chl + {}^3Car^*$

${}^1O_2{}^* + {}^1Car \rightarrow {}^3O_2 + {}^3Car^*$

${}^3Car^* \rightarrow {}^1Car + \text{heat}$

Note that, the photo-physical reactions between singlet oxygen and carotenoid species are simply energy transfer processes and they do not lead to oxidation products and hence to carotenoid degradation [Codgell et al. 1987]. The photo-physical photoprotection played by carotenoids is the fastest response among the mechanisms found in nature, and it is particularly suitable for sudden variations of light intensity during the day-time. If the stress conditions extend for longer periods, other photoprotection strategies are activated, known under the name of "*Non-photochemical quenching"*. Those mechanisms are more efficient but need longer time to build up and longer period to recover when the stress conditions come over [Müller et al. 2001].

1.2 Light-harvesting complexes and triplet-triplet energy transfer

Energy transfer mechanisms critically depend on the distance and on the relative position between the partners. To reach a high efficiency in energy delivery from antenna pigments to the special pair, all the cofactors must be held at optimal distance and orientation. The protein scaffold in the light-harvesting complexes holds the pigments in defined positions and provides the possibility of fine-tuning their absorption properties by specific pigment-protein interactions. All Cars and Chls are non-covalently attached to the proteins. The binding is realized via either a weak ligand-metal interaction of the central Mg to nucleophilic aminoacid side chains, or other non-covalent interactions such as π-π interactions, hydrogen-bonding,

This thesis is focused on the triplet-triplet energy transfer (TTET) mechanism taking place among chlorophylls and carotenoids in the light-harvesting proteins. This mechanism will be described in some details in chapter II..

Triplet-triplet energy transfer is the fastest response to light stress conditions. It is known that when the number of collected photons exceeds the RCs turnover, the absorbed excitation becomes localized on specific chlorophyll molecules increasing their probability of populating triplet states. Chlorophyll triplet is not harmful by its own but it has the right energy to populate singlet oxygen, a very reactive species which is able to damage the whole apparatus.Carotenoids are able to scavenge the singlet oxygen formation by virtue of their triplet state (see Carotenoids section).

Light-harvesting complexes are strongly influenced by the habitat in a much more deep way compared to RCs. For this reason it is interesting to apply a comparative approach in studying the energy transfer process and the photoprotective strategy in naturally occurring antenna complexes. Four different proteins from three different organisms belonging to higher plants, algae and bacteria have been chosen. These proteins are different in terms of origin, location in the photosynthetic apparatus and pigment content and stoichiometry. However they are all able to perform efficiently the photoprotection mechanism by means of the triplet Chl quenching, denoting a possible common molecular strategy in the optimization of the process. In particular, we are interested in identifying the specific pigments involved in the triplet-triplet energy transfer mechanism and in pointing out common structural and physical-chemical features in the photoprotection process.

1.2.1 LHC-II from Spinacia oleracea

LHC-II is the peripheral antenna complex associated with the photosystem II. It is the most abundant membrane protein in the chloroplast of higher plants. LHC-II plays a crucial role in absorbing light, controlling the structure of the membrane and in the regulation and adaptation to high-light conditions.

The crystal structure of LHC-II from spinach (*Spinacia oleracea*) has been resolved at 2.72 Å resolution [Liu et al. 2004] and that of pea at 2.5 Å resolution [Standfuss et al. 2005] revealing a trimeric assembly of the protein. Each LHC-II monomer has three trans-membrane helices which bind 14 chlorophylls molecules (8 Chl *a* and 6 Chl *b*) and 4 carotenoids molecules (two luteins, one neoxanthin and one carotenoid belonging to the xanthophylls cycle [Müller et al. 2001]). The chlorophylls are vertically distributed in two layers within the membrane, one close to the stromal surface, the other to the luminal, as reported in figure 1.5. The luteins are bound in the centre of the protein in sites L1 and L2 (nomenclature as [Liu et al. 2004]). The binding site N1 is specific for neoxanthin and is located near the helix C. The last site, V1, may bind violaxanthin, antheraxanthin or zeaxanthin depending on the light conditions and it is located in the periphery of the monomeric subunits. In LHC-II the solar energy is absorbed independently by each pigment but it is transferred selectively to Chl *a* molecules [Holt et al. 2003, Mozzo et al. 2008, Muh et al. 2010].

1.2.1.1 TTET

In LHC-II the main photoprotective mechanism responsible for excess energy dissipation is represented by the *non-photochemical quenching* process based on the de-epoxidation of violaxanthin to antheraxanthin and zeaxanthin by the enzyme violaxanthin de-epoxidase, which is activated by low luminal pH [Demming-Adams et al. 1996], and probably involves the V1 site [Ruban et al. 1999]. It has been demonstrated that carotenoids in V1 site are not involved in light-harvesting and singlet energy transfer [Caffarri et al. 2001].

In a recent paper [Di Valentin et al. 2009] the triplet state EPR spectrum of photoexcited LHC-II has been analyzed to get insight into the triplet-triplet energy transfer mechanism of this protein. TTET in LHC-II is efficient but not complete,

leaving about 5% of the chlorophylls triplet unquenched [Mozzo et al. 2008]. In fact, the EPR spectrum shows two distinct contributions: the major assigned to a carotenoid populated via triplet-triplet energy transfer and the minor assigned to unquenched chlorophylls. It has been demonstrated that the molecules involved in triplet-triplet energy transfer to prevent the singlet oxygen formation are the couples Chl603/Lut621 and Chl612/Lut620, even though some contribution from Chl602/610 cannot be excluded [Caffarri et al. 2001, Di Valentin et al. 2009].

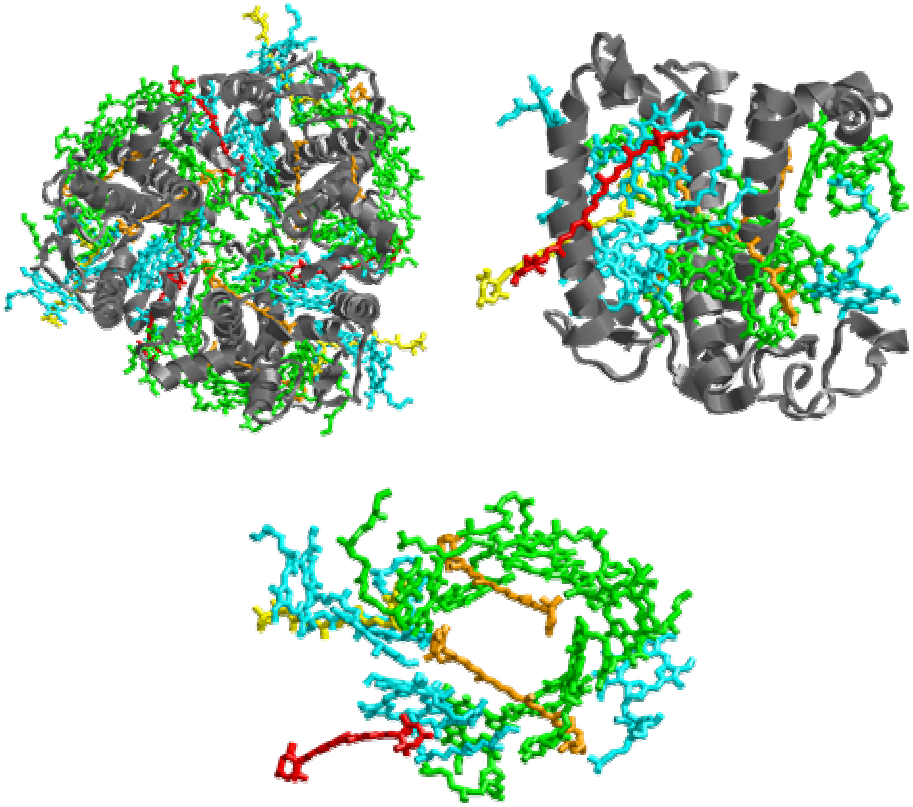


Figure 1.5: Top left – view of the trimeric organization of LHC-II in crystal along the C_3 axis. Top right – LHC-II monomer. Bottom – pigment organization within the monomer, the pseudo-C_2 symmetry is clearly visible [Liu et al. 2004]. In all figures, lutein is depicted in orange, violaxanthin in red, neoxanthin in yellow, chlorophyll *a* in green and chlorophyll *b* in cyan.

It has been suggested that the His and Asn residues, coordinated to the central Mg atom of Chl603 and Chl612 respectively, pull the porphyrin rings toward the luteins, favouring the overlap of the conjugated systems. A similar molecular arrangement has been found in PCP from *A. carterae* [Di Valentin et al. 2008a] (see infra). The unquenched chlorophyll triplet state present in LHC-II complex after illumination is putatively located in Chl604, Chl611, Chl613 and Chl614 sites since they do not contribute to the formation of the observed carotenoid triplet state [Di Valentin et al.

2009]. It has been demonstrated, by optical spectroscopy [Mozzo et al. 2008], that these unquenched chlorophylls are present even at room temperature in isolated LHC-II preparations.,

1.2.2 LHC from Amphidinium carterae

LHC (Light-Harvesting Complex) is the major intrinsic antenna system of the photosynthetic apparatus of dinoflagellates. Purified from thylakoids membranes, the LHC is a 19 kDa protein with an estimated pigment composition of 7 Chl *a*, 4 Chl c_2, 12 peridinins and 2 diadinoxanthins [Hiller 1993]. Note that in this complex, unlike LHC-II from higher plants and algae but as PCP from the same organism (see infra), the carotenoid content exceeds that of Chl *a*. This unusual pigment ratio strengthens the idea that carotenoids are the main light-harvesting pigments for water-living species. Marine eukaryotic algae employ carotenoids such as peridinin, fucoxanthin and siphonaxanthin, characterized by the presence of a carbonyl group conjugated with the π-system. In these algae carotenoids paly the major light-harvesting function [Bautista et al. 1999]. After direct light absorption, both peridinin and Chl c_2 transfer their singlet excitation efficiently to Chl *a* [Hiller 1993, Polívka 2006]. Although the overall identity between the sequences of LHC and LHC-II from higher plants is low, a model, based on alignment of the sequences with the three dimensional structure of LHC-II, has been proposed [Hiller 1995a]. By sequence alignment five conserved Chl *a* ligands have been identified in LHC with respect LHC-II [Hiller 1995a], which correspond to the ligands of Cla610-612-613-602-603 in the LHC-II structure, according to the nomenclature reported in [Liu et al. 2004]. Also the two central carotenoid (Car) binding sites (L1 and L2) are most probably preserved in LHC. On the other hand, the two extra carotenoid binding sites found in LHC-II located at the periphery of the monomeric subunits are not conserved in LHC. Moreover, in LHC the total number of Chl molecules is reduced (11 instead of 14), thus the additional Car molecules may be inserted in sites which are occupied by Chls in LHC-II or may form clusters as in PCP. The interactions between PCP and LHC light-harvesting proteins are still unknown.

1.2.2.1 TTET

The literature about TTET in LHC is poor. The singlet-singlet energy transfer efficiency varies within the 400-600 nm spectral region. It is about 90% in the peridinin spectral region but is drops in the diadinixanthin spectral region, indicating that this carotenoid is less involved in the energy transfer. By time resolved absorption spectroscopy Polìvka et al. [Polìvka et al. 2006] suggested that diadinoxanthin could form triplet states, but not via TTET. Moreover, it has been demonstrated that diadinoxanthin is involved in photo-protection of algae apparatus in a similar way as violaxanthin in LHC-II

1.2.3 PCPs from Amphidinium carterae and Heterocapsa pygmaea

PCP (Peridinin – Chlorophyll *a* – Protein) is the water-soluble external light-harvesting complex characteristic of dinoflagellate algae. This complex is optimized for photon capture especially in the blue-green spectral region because water is like a filter for light in the red. The x-ray structure of PCP from *A. carterae* has been solved in the past at 2 Å resolution [Hoffman et al. 1996] and it has been recently redefined at 1.5 Å [Shulte et al. 2009]. The basic structural and functional unit is a trimer. Each monomer binds only peridinin and Chl *a* in a stoichiometric ratio of 4:1; the cofactors are arranged as two pseudo-identical domains of four peridinins and one Chl *a* molecule. All the pigments are located in the hydrophobic cavity isolated by the protein. The peptide primary sequence of the N- and C- terminal regions are largely homologus (56%), probably due to a gene duplication and fusion, and form structurally most identical domains each consisting of eight alpha-helices. The holo-protein including the lipid molecules associated has a molecular weight of 38.1 kDa. Distances between peridinins in the same domain range from 4 to 11 Å, and the conjugated system of all the peridinins are in van der Waals contact (3.3 - 3.8 Å) with the tetrapyrrole rings of the Chl *a* molecules. The distance between the Mg atoms of the two Chl *a* molecules in the same monomer is 17.4 Å. The PCP structure is shown in figure 1.6. Along with the PCP form already discussed, named Main-Form *Amphidinium* PCP (MF-APCP), a minor component has also been discovered which is eluted from an anion exchange column at high-salt concentration [Sharples,

1996]. This minor variant, denoted High-Salt *Amphidinium* PCP (HS-APCP), presents 31% identity in amino acid sequence with MF-APCP. It contains only six peridinins and two Chl *a* molecules and has a molecular weight of 34 kDa. The crystallographic structure of HS-APCP has also been determined [Shulte et al. 2009a]. It shows a large similarity with the MF-APCP structure in terms of pigments arrangement, except for the absence of two symmetry related peridinins called PID612/PID622 (nomenclature according to [Hoffman et al. 1996]). Moreover, the porphyrin rings are more distant, 18.4 Å Mg-Mg distance, and the phytol tails occupy the regions where the missing carotenoids were located. More recently, reconstitution of functional PCP from heterologously-expressed apoprotein mixed with pigments extracted from native PCP or from other organisms, has been obtained. Constructs of full-length, as well as N-terminal domain PCP (N-PCP), have been reproduced and reconstituted *in vitro* with native or altered pigment compositions.

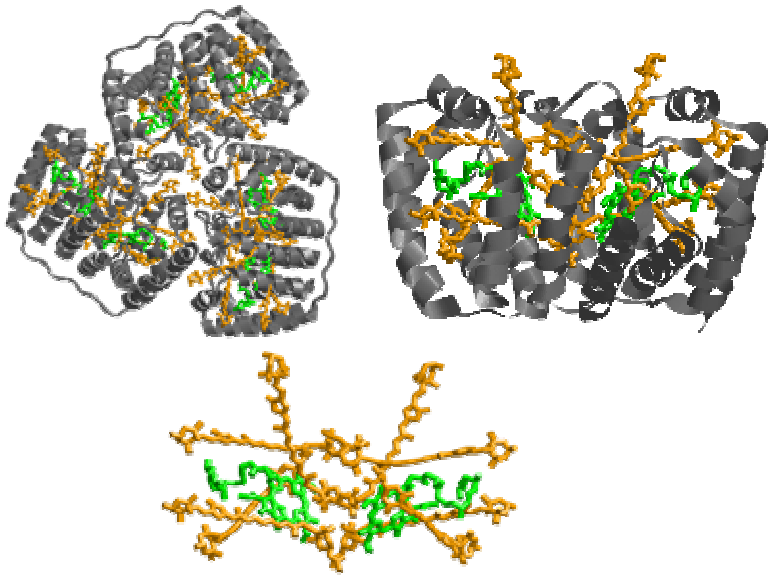


Figure 1.6: Top left – view of the trimeric organization of PCP in crystal along the C_3 axis. Top right – Structure of the monomer. Bottom – pigment organization within the monomer; the pseudo-C_2 symmetry is clearly visible [Hofmann et al. 1996]. In all figures, peridinin is depicted in orange, chlorophyll *a* in green.

The N-PCP is a 16 kDa protein corresponding to the 'half-mer' of the monomeric MF-APCP. When N-PCP is reconstituted, it forms a 32 kDa homo-dimer. It was also possible to obtain dimers with different pigments composition in each monomer

[Brotosudarmo et al. 2006, Brotosudarmo et al. 2008]. All the optical spectroscopy techniques employed so far (absorption, fluorescence, excitation fluorescence and circular dichroism [Miller et al. 2005, Wörmke et al. 2007, Mackowski et al. 2008]) have demonstrated that the reconstituted samples are characterized by behaviours very similar to those of the native proteins. The crystal structures of all these reconstituted forms have been solved at atomic resolution (< 2 Å) [Shulte et al. 2010]. Another dinoflagellate alga, *Heterocapsa pygmaea*, exhibits a 15 kDa PCP form (HPCP) which binds 4 peridinins and 1 Chl *a* molecules. This form derives most likely from the gene ancestor from which MF-APCP evolved. The structure of HPCP is not known but it has been demonstrated that it forms an homo-dimer structure in solution. HPCP shows no evident differences in its spectroscopic behaviour with respect MF-APCP.

1.2.3.1 TTET

The peridinin molecules in PCP are able to play the TTET with 100% efficiency in terms of energy transfer [Bautista et al. 1999, Di Valentin et al. 2008a]. Time-resolved EPR measurements on MF-APCP, allowed us to assign the triplet energy sink to the PID614 / PID624 molecules [Di Valentin et al. 2008a]. This in turn means that the triplet-triplet energy transfer involves the couples Chl601/PID614 and Chl602/PID624. These two pairs are characterized by the shortest distance between the centre of the π-systems and by the presence of a water molecule, the fifth ligand of the Mg atom of the Chl *a*, bridging the two partners. This water molecule has been suggested to play a role on extending the overlap between the peridinin and chlorophyll wavefunctions, see figure 1.7. The EPR results confuted the hypothesis of a triplet exciton which was debated for long time, in favour of a triplet localization on one specific peridinin molecule in each subcluster. To support this hypothesis the photo-excited peridinin triplet state in MF-APCP has been studied combining pulsed ENDOR (Electron Nuclear Double Resonance) spectroscopy (see chapter III) and DFT computations [Di Valentin et al 2008b]. The triplet spin density as derived by this approach, is delocalized over the whole π-conjugated system with an alternate pattern lost in the central region of the polyene chain, as reported in figure 1.7. The same conclusions have been reported independently by Niklas et al. on reconstituted

N-PCP [Niklas et al. 2007]. The ENDOR spectra are not temperature dependent supporting the hypothesis of a triplet localization. Moreover, high spin density has been found specifically at the carbon atom position which for PID614/PID624 is in close contact with the water molecule, above mentioned.

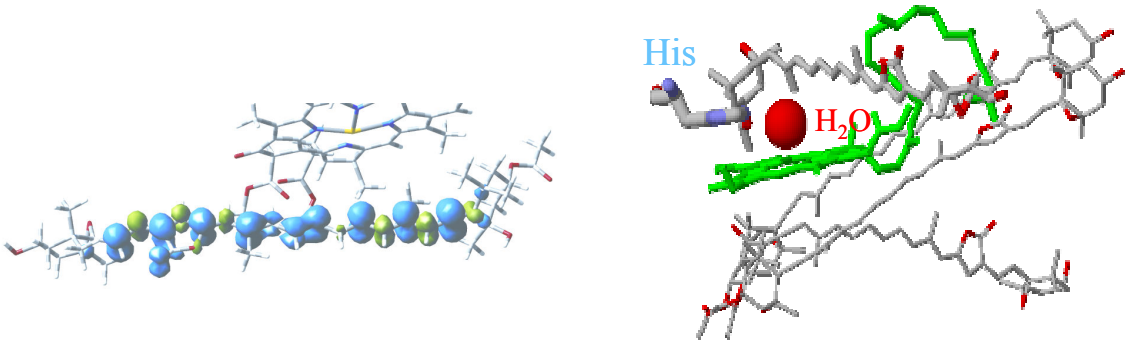


Figure 1.7: Left – Spin density distribution on the peridinin triplet state (Pid614) as derived by DFT calculations at level B3LYP/EPR-II, the chlorophyll is shown for sake of clarity [Di Valentin et al. 2008b]. Right – Structure of the Chl601/Pid614 as derived by 1PPR pdb file. The position of the water molecule is highlighted.

1.2.4 Chlorosomes from Chlorobaculum tepidum

Chlorosomes are the peripheral membrane antenna complexes of green photosynthetic bacteria [Olson 1998, Olson et al. 2004]. Organisms that use chlorosomes as light-harvesting systems are able to grow at extraordinary low light intensities, under which no other phototrophic organism can live [Blankenship et al. 2003]. The chlorosome is unusual in that it contains a relative small amount of proteins compared to the very high pigment content. Moreover, the organization of the pigments inside the antenna is largely dominated by pigment-pigment interaction instead of pigment-protein interaction as found for the other antenna complexes [Pedersen et al. 2010, Oostergetel et al. 2010]. In relation to the species, a single chlorosome can contain about 200,000 to 250,000 BChl *c* (or BChl *d*/*e*) molecules, 2,500 BChl *a* molecules (i.e. BChl *c* : BChl *a* = 100 : 1), 20,000 carotenoids molecules, 18,000 quinone-type molecules, 5,000 protein molecules of 10 different types and about 20,000 lipid molecules. Chlorosomes are found in two rather different groups of photosynthetic green bacteria: the green sulphur bacteria

(*Chlorobiaceae*) and the green filamentous bacteria (*Chloroflexaceae*) [Blankenship et al. 2003]. One of the most studied and characterized system belong to the green sulfur bacterium *Chlorobaculum tepidum*. The chlorosome core is composed of highly aggregated BChls structures. There are several models for the organization of the BChl *c* molecules inside the chlorosome which have been proposed: originally it has been proposed that BChl molecules assemble into road like elements [Staehelin et al. 1978, 1980]; alternatively a lamellar model was put forwards for the pigment arrangement in *Cba. tepidum* [Psencik et al. 2004]. Recently, further support for the lamellar model was obtained by electron microscopy on whole cells [Hohmann-Marriot et al. 2005].

A small amount of BChl *a* is also present in the chlorosome structure and it is located in the so called "baseplate" region, which is the contact region between the chlorosome and the membrane. It has been demonstrated by many experiments (cross-linking, selective detergent extraction, studies on carotenosomes [Bryant et al. 2002, Frigaard et al. 2005, Li et al. 2006]) that BChl *a* is selectively bound to CsmA protein [Sakuragi et al. 1999], the most abundant chlorosome envelope protein. In the *Cba. tepidum* apparatus, another protein is located between the baseplate and the membrane: the FMO (Fenna-Matthews-Olson) protein which was the first chlorophyll binding protein to have its structure solved at atomic resolution. FMO is a water-soluble protein associated with the membrane in trimeric form, each monomer consists of a hollow protein β-barrel surrounding seven BChl *a* molecules. Although the x-ray structure of FMO is known and that of CsmA has been recently determined [Pedersen et al. 2008], the structure of the whole chlorosome is still missing, figure 1.8 represents a putative model for the photosynthetic apparatus of *Cba. tepidum*.

TTET

It is worth noting that *Chlorobiaceae* are strict anaerobes so in principle they should not avoid the formation of singlet oxygen. Anyway, it has been found that also in these organisms, carotenoids are present. These carotenoids have structural [Ikonen et al. 2007] and light-harvesting functions but it has been demonstrated that their triplet state can be populated starting from BChl *a* triplet states [Carbonera et al.

2001]. Likely they preserve the organism in case of oxygen contamination in the habitat due to water mixing., Carotenoid-free chlorosomes photodegrade about 3 times faster than wild-type chlorosomes, supporting a photo-protective function for carotenoids. On the other hand, it has been demonstrated that BChl *c* aggregates form long-lived, triplet states that do not interact with carotenoids or with oxygen. These states can be attributed to triplet excitons that form due to the interaction between the closely packed BChls. It has been suggested that the energy of these triplet excitons could fall below that of singlet oxygen and carotenoid triplet state. Thus, the formation of triplet excitons in chlorosomes could represent an alternative photoprotection mechanism taking place in the core of the chlorosomes[Kim et al. 2007].

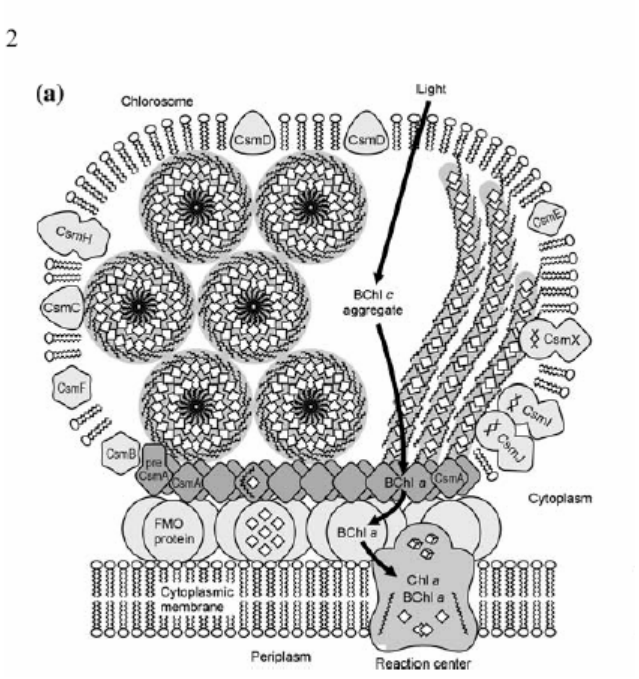


Figure 1.8: Putative model for the photosynthetic apparatus of *Cba. Tepidum* (figure taken from [Frigaard et al. 2005]). The singlet energy transfer pathways are also shown.

1.3 References

[Bautista 1999] J.A. Bautista, R.G. Hiller, F.P. Sharples, D. Gosztola, M.Wasielewski, H.A.Frank, *J. Phys. Chem. A*, **1999**, 103

[Blankenship et al. 2003] Blankenship R. E., Matsuura K., Antenna complex from green photosynthetic bacteria. In: Green B.R., Parson W. W. (eds), Light harvesting antennas in photosynthesis. Kluwer, Dordrecht, The Netherlands, 2003

[Brotosudarmo et al. 2006] Brotosudarmo T. H. P., Hofmann E., Hiller R. G., Wörmke S., Mackowski S., Zumbusch A., Bräuchle C., Sheer H., *FEBS Letters*, **2006**, 580: 5257-5262

[Brotosudarmo et al. 2008] Brotosudarmo T. H. P., Mackowski S., Hofmann E., Hiller R. G., Bräuchle C., Sheer H., *Photosynthesis Research*, **2008**, 95, 247-252

[Bryant et al. 2002] Bryant D. A., Vassilieva E. V., Frigaard N. U., et al., *Biochemistry*, **2002**, 41, 14403-14411

[Caffarri et al. 2001] Caffarri S., Croce R., Breton J., Bassi R., *J. Biolog. Chem*., **2001**, 276(38), 35924-35933

[Carbonera et al. 2001] Carbonera D., Bordignon E., Giacometti G., Agostini G., Vianelli A.,Vannini C., *J. Phys. Chem. B*, **2001**, 105, 246-255

[Codgell et al. 1987] Codgell R. J., Frank H. A., *Biochim. Biophys. Acta*, **1987**, 859, 63-79

[Di Valentin et al. 2008a] M. Di Valentin, S. Ceola, E. Salvadori, G. Agostini, D. Carbonera, *Biochim. Biophys. Acta*, **2008**, 1777, 186–195.

[Di Valentin et al. 2008b] M. Di Valentin, S. Ceola, G. Agostini, G. M. Giacometti, A. Angerhofer, O. Crescenzi, V. Barone, D. Carbonera, *Biochim. Biophys. Acta*, **2008**, 1777, 295-307

[Di Valentin et al. 2009] Di Valentin M., F. Biasibetti, S. Ceola, D. Carbonera, *J. Phys.Chem. B*, **2009**, 113, 13071-13078

[Demming-Adams et al. 1996] Demming-Adams B., Adams W. W., *Trends Plant. Sci.*, **1996**, 1, 21-26

[Frigaard et al. 2005] Frigaard N.-U., Li H., Martinsson P., Das S. K., Franck H. A., Aartsma T. J., Bryant D. A., *Photosynth. Res*., **2005**, 86 : 101-111

[Gerola and Olson 1986] Gerola P. D., Olson J. M., *Biochim. Biophys. Acta*, **1986**, 848: 69-76

[Grossman 1990] Grossman A. R., Manodori, A., Snyder D., *Mol. Gen. Genet.*, **1990**, 224, 91-100

[Hiller, 1993] Hiller R. G., Wrench P. M., Gooley A. P., Shoebridge G., Breton J., *Photochem. Photobiol. 57*, **1993**, 125-131.

[Hiller, 1995] Hiller R. G., Wrench P. M., Sharples F. P., *FEBS Lett.*, **1995**, 363, 175-178.

[Hoffman et al. 1996] Hofmann E., Wrench P. M., Sharples F.P., Hiller R.H., Welte W., Diederichs K., *Science*, **1996**,272, 1788–1791.

[Hohmann-Marriott et al. 2005] Hohmann-Marriott M. F., Balnkenship R. E., Roberson R. W., *Photosynth. Res.*, **2005**, 86, 145-154

[Holt et al. 2003] Holt N. E., Kennis J. T. M., Dall'Osto L., Bassi R., Fleming G. R., *Chem. Phys. Let.*, **2003**, 379(3-4), 305-313

[Kim et al. 2007] Kim H., Li H., Maresca J., Bryant D. A., Savikhin S., *Biophys. J.*, **2007**, 93, 192-201

[Ikonen et al. 2007] Ikonen T. P., Li H., Psencik J., Laurinmaki P. A., Butcher S. J., Frigaard N.-U., Serimaa R. E., Bryant D. A., Tuma R., *Byophys. J.*, **2007**, 93(2), 620-628

[Li et al. 2006] Li H., Frigaard N.-U., Bryant D. A., *Biochemistry*, **2006,** 45, 9095-9103

[Liu et al. 2004] Liu Z., Yan H., Wang K., Kuang T., Zhang J., Gui L., An X.; Chang W., *Nature,* **2004**, *428*, 287-292.

[Mackowski et al. 2008] Mackowski S., Wörmke S., Brotosudarmo T. H. P., Sheer H., Bräuchle C., *Photosynth. Res.*, **2008**, 95, 253-260

[Miller et al. 2005] Miller D. J., Catmull J., Puskeiler R., Tweedale H., Sharples F. P., Hiller R. G., *Photosynth. Res.*, **2005**, 86, 229-240

[Mozzo et al. 2008] Mozzo M., Dall'Osto L., Hienerwadel R., Bassi R., Croce R., *J. Biol. Chem*., **2008**, 283(10), 6184-6192

[Muh et al. 2010] Muh F., Madjet M. E. A., Renger T., *J. Phys. Chem. B*, **2010**, 114(42), 13517-13535

[Müller et al. 2001] Müller P., Li X. P., Niyogi K. K., *Plant. Physiology*, **2001**, 125, 1558-1566.

[Niklas et al. 2007] Niklas J., Schulte T., Prakash M., van Gastel M., Hofmann E., Lubitz W., *J. Am. Chem. Soc*., **2007**, 129, 1542-15443

[Olson 1998] Olson J. M., *Photochem. Photobiol*., **1998**, 67, 61-75

[Olson et al. 2004] Olson J. M., Blanckenship R. E., *Photosynth. Res.*, **2004**, 80(1-3), 378-386

[Oostergetel et al. 2010] Oostergetel G. T., van Amerongen H., Boekema E. J., *Photosynth. Res*., **2010**, 104: 245-255

[Ort and Yocum] Advances in Photosynthesis col. 4. Oxygenic Photosynthesis: the light reactions. Edited by Ort D. R. & Yocum C. K., Kluwer Academic Press

[Pedersen et al. 2008] Pedersen M. Ø., Underhaug J., Dittmer J., Miller M., Nielsen N. C., *FEBS Letters*, **2008**, 582, 2869-2874

[Polívka 2006] Polívka T.,. van Stokkum I. H. M., Zigmantas D., van Grondelle R., Sundström V., Hiller R. G. *Biochemistry*, **2006**, *45* (28), 8516-8526

[Polìvka et al. 2010] Polìvka T., Frank H., *Accounts of chemical research*, **2010**, 43(8), 1125-1134

And references therein.

[Ruban et al. 1999] Ruban A. V., Lee P. J., Wentworth M., Young A. J., Horton P., *J. Biol. Chem.*, **1999**, 274, 10458-10465

[Psencik et al. 2004] Psencik J., Ilkonen T. P., Laurinmaki P., Merckel M. C., Butcher S. J., Serimaa R. E., Tuma R., *Biophys. J.*, **2004**, 87, 1165-1172

[Sakuragi et al. 1999] Sakuragi Y., Frigaard N. U., Shimada K., Matsuura K., *Biochemistry*, **2007**, 46: 7062-7068

[Sharples, 1996] Sharples, F. P., Wrench, P. M., Ou, K. L., and Hiller, R. G., *Biochim. Biophys. Acta*, **1996**, *1276*, 117-123.

[Shulte et al. 2009] Shulte T., Niedzwiedzki D. M., Birge R. R., Hiller R. G., Polìvka T., Hofmann E., Frank H. A., , *Proc. Natl. Acad. Sci. USA*, **2009**, 106, 20764-20769

[Shulte et al. 2010**]** Shulte T., Hiller R. G., Hofmann E., *FEBS Letters*, **2010**, 584, 973-978

[Shulte et al. 2009a] Schulte T., Sharples F. P., Hiller R. G., Hofmann E., *Biochemistry*, **2009**, 48(21), 4466-4475

[Staehelin et al. 1978] Staehelin L. A., Golecki J. R., Fuller R. C., Drews G., *Arch. Microbiol*., **1978**, 119, 269-277

[Staehelin et al. 1980] Staehelin L. A., Golecki J. R., Drews G., *Biochim. Biophys. Acta*, **1980**, 589, 30-45

[Standfuss et al. 2005] Standfuss J.; Terwisscha van Scheltinga A. C.; Lamborghini M., Kuehlbrandt W., *EMBO J.,* **2005**, *24*, 919-928.

[Struve 1995] Struve W.S., Anoxygenic Photosynthetic Bacteria, Kluwer Academic Publishers: Dordrecht, cap. 15, p.297, **1995**

[Sundström et al. 1995] Sundström V., van Grondelle R., Anoxygenic Photosynthetic Bacteria, Kluwer Academic Publishers: Dordrecht, cap. 17, p.349, **1995**

[Wörmke et al. 2007] Wörmke S., Mackowski S., Brotosudarmo T. H. P., Jung C., Zumbusch A., Ehrl M., Sheer H., Hofmann E., Hiller R. G., Bräuchle C., *Biochim. et Biophys. Acta*, **2007**, 1767, 956-964

[Young et al. 1993] Young A., Britton G., Carotenoids in Photosynthesis, Chapman & Hall, 1993

Chapter II
The Triplet State

Triplet state is an electronic state characterized by two unpaired parallel electrons in the outer shell and by total spin angular momentum S = 1. Usually the organic molecules ground state is a singlet state, i.e. the highest occupied electronic orbital is shared by two paired electrons. If one of these electrons is excited to one of the unoccupied orbitals, by absorption of a proper energy quantum (typically by photoexcitation), the molecule is still in a singlet state since energy absorption cannot vary the spin multiplicity. However there is a probability that the molecule undergoes an *intersystem crossing* (ISC) from an excited singlet state to a meta-stable excited triplet state changing its spin multiplicity. ISC mechanism is due mainly to the spin-orbit coupling.. The population of the triplet sub-levels is a very selective process and leads to spin polarization..

2.1 Triplet state description

The total spin Hamiltonian for a molecule in the triplet state, in the presence of an applied magnetic field, as in an EPR experiment, is:

$$\hat{H} = g\beta_e\hbar^{-1}B_0\hat{S} + \hat{S}D\hat{S} + \sum_{k=1}^{m}\hat{S}A_k\hat{I}_K - \sum_{k=1}^{m}g_{n,k}\beta_n\hbar^{-1}B_0\hat{I}_k + \sum_{I>1/2}\hat{I}_kP_k\hat{I}_k + \sum_{i\neq k}I_id^{(i,k)}I_k \qquad (2.1)$$

Where the first term represents the electron Zeeman interaction between the electron spin and the applied magnetic field; the second is the dipolar interaction between the two unpaired electrons, also known as zero field splitting; the third is the hyperfine couplings between the electron spin and the *m* nuclear spins (I_k); the fourth is the nuclear Zeeman interactions; the fifth is the nuclear quadrupole interaction (only for nuclear spins with quantum number I > ½); the sixth is the spin-spin interactions between pairs of nuclear spins [Schweiger et al. 2001].

The exact description of all the terms is not necessary for the comprehensions of the triplet state EPR experiments presented in this thesis, thus in the following only the relevant contributions will be analyzed.

2.1.1 Zero Field Splitting Interaction

For the triplet state of organic molecules, this term is not the dominant in the presence of an applied magnetic field. However it will be considered firstly because it is the most characteristic for a triplet state.

Generally the total electronic wavefunction Ψ of a molecule can be expressed as a product of a spatial function Φ, which depends on the electronic spatial coordinates, and a spin function Ξ, which depends on the spin coordinates:

$$\Psi = \Phi * \Xi \tag{2.2}$$

As stated by the Pauli's principle the wavefunction must be antisymmetric with respect to the electronic exchange operation.

To describe the triplet state in its general features it is adequate to consider the spin Hamiltonian for two interacting electrons. In the coupled representation, two interacting electrons lead to four different spin configurations that can be divided into two states in relation to their behaviour with respect the electronic exchange operation: one singlet and one triplet.

The symmetric state with respect to electronic exchange:

$$\frac{1}{\sqrt{2}}[\alpha(1)\beta(2)-\alpha(2)\beta(1)] \tag{2.3}$$

has total spin quantum number S = 0 and thus unitary spin multiplicity (2S+1), for this reason it is called singlet state.

The anti-symmetric states respect to the exchange:

$$\alpha(1)\alpha(2) \tag{2.4}$$

$$\frac{1}{\sqrt{2}}[\alpha(1)\beta(2)+\alpha(2)\beta(1)] \tag{2.5}$$

$$\beta(1)\beta(2) \tag{2.6}$$

have total spin quantum number S = 1 and thus spin multiplicity equal to 3, for this reason they are collectively called triplet. The wavefunctions above mentioned are eigenfunctions of operators $\hat{S}^2$ (S = 1) and $\hat{S}_z$ (M_S = 1, 0, -1); usually they are labelled considering the $\hat{S}_z$ eigenvalues:

$$|+1\rangle = |\alpha\alpha\rangle \tag{2.7}$$

$$|0\rangle = \frac{1}{\sqrt{2}}\left(|\alpha\beta\rangle + |\beta\alpha\rangle\right) \tag{2.8}$$

$$|-1\rangle = |\beta\beta\rangle \tag{2.9}$$

Because of the coulumbic interaction between the two unpaired electrons, the triplet and the singlet states are not iso-energetic: the energy difference is equal to twice the exchange integral value:

$$\Delta E = 2\langle\phi_a(1)\phi_b(2)|\frac{e^2}{4\pi\varepsilon_0 r}|\phi_a(2)\phi_b(1)\rangle \tag{2.10}$$

Where Φ_a and Φ_b are the spatial part of the normalized monoelectronic wavefunctions, calculated for two not interacting electrons, ε_0 is the vacuum permittivity and r is the inter-electronic distance.

While the exchange interaction differentiates the triplet and the singlet states, the magnetic dipole-magnetic dipole interaction further splits the triplet state energy levels. Due to this contribution the triplet sublevels are no longer iso-energetic even in the absence of an applied magnetic field. This effect is called *zero field splitting* (ZFS). The dipole-dipole interaction between two unpaired electrons is analogous to the classical counterpart for magnetic dipoles. The corresponding spin Hamiltonian being expressed as:

$$\hat{H}_{SS} = \frac{\mu_0}{4\pi} g_1 g_2 \beta_e^2 \left[\frac{\hat{S}_1\hat{S}_2}{r_{12}^3} - \frac{3\left(\hat{S}_1\cdot\bar{r}\right)\left(\hat{S}_2\cdot\bar{r}\right)}{r_{12}^5}\right] \tag{2.11}$$

Where g_1 and g_2 are the electronic g factors considered isotropic, μ_0 is the vacuum magnetic permeability and β_e is the electronic Bohr magneton. In the following it will be assumed that $g_1 = g_2 = g$.

Since the electrons are considered to be interacting, it is worth writing the expression as a function of the total spin angular momentum S defined as the sum of individual spin momenta:

$$\hat{S} = \sum_i \hat{S}_i \tag{2.12}$$

In matrix notation, the dipolar Hamiltonian takes the form:

$$\hat{H}_{SS} = \hat{S}\ D\ \hat{S} \tag{2.13}$$

Where D is the dipolar interaction tensor, also known as *zero field splitting* tensor, and the general element can be expressed as:

$$D_{ij} = \frac{g^2 \beta^2 \mu_0}{8\pi} \left\langle \frac{3ij - r^2 \delta_{ij}}{r^5} \right\rangle \tag{2.14}$$

With $i,j = x, y, z$. The angular brackets accounts for the delocalized nature of the electrons, and they indicate the average distribution over the spatial part of the electronic wavefunction, while x, y, z are the three components of the distance vector r_{12} in the reference frame.

The tensor D is diagonal in the principal axis frame and the three sublevels are not degenerate with energies corresponding to $X = -D_{XX}$, $Y = -D_{YY}$ e $Z = -D_{ZZ}$.

In the principal axis system the dipolar Hamiltonian could be written as:

$$\hat{H}_{SS} = D_{XX} \hat{S}_X^2 + D_{YY} \hat{S}_Y^2 + D_{ZZ} \hat{S}_Z^2 \tag{2.15}$$

As it is clear from the definition of the general element ij, D has rank 2 and it is traceless: thus in the principal reference frame the spin sub-levels energies can be described by only two linearly-independent parameters. These parameters, named *zero field splitting* parameters, are usually indicated by D and E and have the form:

$$D = -\frac{3}{2} Z = 3 \frac{g^2 \beta^2 \mu_0}{16\pi} \left\langle \frac{r^2 - 3z^2}{r^5} \right\rangle \tag{2.16}$$

$$E = -\frac{1}{2}(Y - X) = 3 \frac{g^2 \beta^2 \mu_0}{16\pi} \left\langle \frac{x^2 - y^2}{r^5} \right\rangle \tag{2.17}$$

Hence, the triplet sub-levels energies can be expressed as function of the ZFS parameters:

$$X = \frac{1}{3}(D - E) \tag{2.18}$$

$$Y = \frac{1}{3}(D + E) \tag{2.19}$$

$$Z = -\frac{2}{3} D \tag{2.20}$$

The dipolar Hamiltonian can be re-written using D and E as:

$$\hat{H}_{SS} = D\hat{S}_Z^2 + E\left(S_Y^2 - S_X^2\right) \tag{2.21}$$

Note that the ZFS parameters are not univocally defined, since their values depend on which axis is labelled as Z. By convention, the ZFS X, Y, Z axes are according to the condition |D| > 3|E|.

The absolute value of the D and E parameters is strongly dependent on the average distance between the two interacting electrons and on the geometry of the electronic distribution of the triplet state. If the symmetry is high (spherical or cubic), the three principal axes are equivalent: D and E are both equal to zero and the triplet sublevels are degenerate. If the symmetry is cylindrical, only E is equal to zero and the degeneration is partially removed.

For a molecule such as chlorophyll, planar in the *xy* plane, $r^2\text{-}3z^2 > 0$, thus *D* is positive. On the other hand, for a molecule with a long molecular axis, as a carotenoid, D is negative. Figure 2.1 shows the order of the energy levels and the orientation of the ZFS axes on the chlorophyll and carotenoid molecular structures.

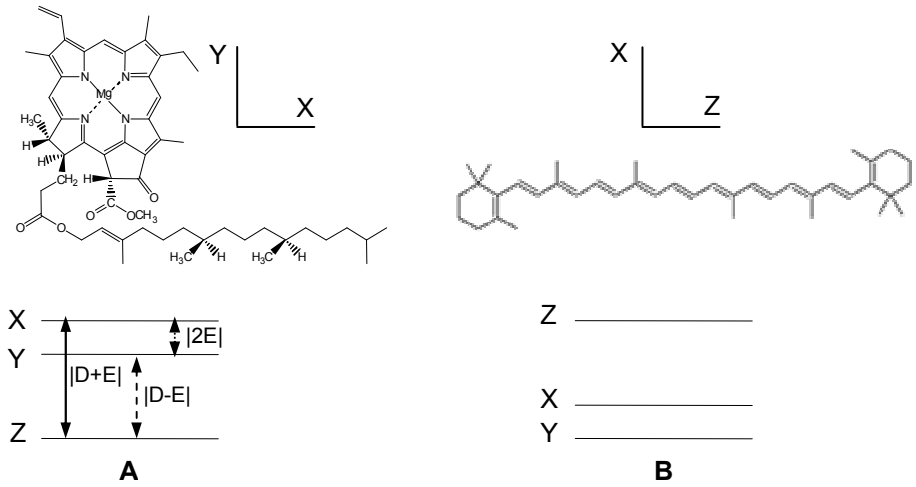


Figure 2.1: A) Chlorophyll *a* ZFS axes orientation (the Z axis is perpendicular to the molecular plane), the triplet energy level diagram at zero field [Vrieze et al. 1995]. B) β-carotene ZFS axes orientation (the Y axes is perpendicular to the conjugated chain), the triplet energy level diagram at zero field is also shown [Frick et al. 1990, Kok et al. 1996]. For the chlorophyll triplet state, the three possible magnetic transitions in zero field, 2|E|, |D|-|E| and |D+E|, are also depicted.

The eigenfunctions of the dipolar Hamiltonian can be expressed also on the basis of triplet state functions:

$$|X\rangle = \frac{1}{\sqrt{2}}\left(|-1\rangle - |+1\rangle\right) = \frac{1}{\sqrt{2}}\left(\beta\beta - \alpha\alpha\right) \tag{2.22}$$

$$|Y\rangle = \frac{i}{\sqrt{2}}\left(|-1\rangle + |+1\rangle\right) = \frac{i}{\sqrt{2}}\left(\beta\beta + \alpha\alpha\right) \tag{2.23}$$

$$|Z\rangle = |0\rangle = \frac{1}{\sqrt{2}}\left(\alpha\beta + \beta\alpha\right) \tag{2.24}$$

2.1.2 Electron Zeeman Interaction

Considering an EPR experiment, besides the magnetic dipolar interaction between the electronic spins, the interaction between the spin angular momentum S and the applied magnetic field B_0 must be considered. The spin Hamiltonian is thus the sum of the Zeeman and the dipolar contributions:

$$\hat{H} = \hat{H}_Z + \hat{H}_{SS} \tag{2.25}$$

$$= g\beta B_0 \hat{S} + \hat{S} D \hat{S} \tag{2.26}$$

where the g factor is assumed to be isotropic. The functions (2.7), (2.8) end (2.9) can be used to calculate the eigenfunctions and the eigenvalues of the spin Hamiltonian (2.26). The matrix representation of (2.26) for an arbitrary orientation of the external magnetic field $\overline{B}_0$, with components B_x, B_y and B_z, is:

$$H = \begin{vmatrix} g\beta B_z - \frac{1}{2}(X+Y) - Z & \frac{1}{\sqrt{2}} g\beta (B_x - iB_y) & -\frac{1}{2}(X-Y) \\ \frac{1}{\sqrt{2}} g\beta (B_x + iB_y) & -(X+Y) & \frac{1}{\sqrt{2}} g\beta (B_x - iB_y) \\ -\frac{1}{2}(X-Y) & \frac{1}{\sqrt{2}} g\beta (B_x + iB_y) & -g\beta B_z - \frac{1}{2}(X+Y) - Z \end{vmatrix} \tag{2.27}$$

The exact diagonalization of the Hamiltonian is simplified if the special cases with B_0 parallel to one of the ZFS axes are considered. For instance, if B_0 is parallel to the Z axis, the eigenfunctions are:

$$|T_+\rangle = \cos\vartheta |+1\rangle - \sin\vartheta |-1\rangle \tag{2.28}$$

$$|T_-\rangle = \sin\vartheta |+1\rangle + \cos\vartheta |-1\rangle \tag{2.29}$$

$$|T_0\rangle = |0\rangle \tag{2.30}$$

with eigenvalues

$$E_+ = g\beta B + \frac{1}{2}(X+Y) + \frac{1}{2}(X-Y) tg\vartheta \tag{2.31}$$

$$E_{-} = -g\beta B + \frac{1}{2}(X+Y) - \frac{1}{2}(X-Y)tg\vartheta \tag{2.32}$$

$$E_0 = Z \tag{2.33}$$

where $\vartheta = arctg\left(\frac{X-Y}{2g\beta B}\right)$. (2.34)

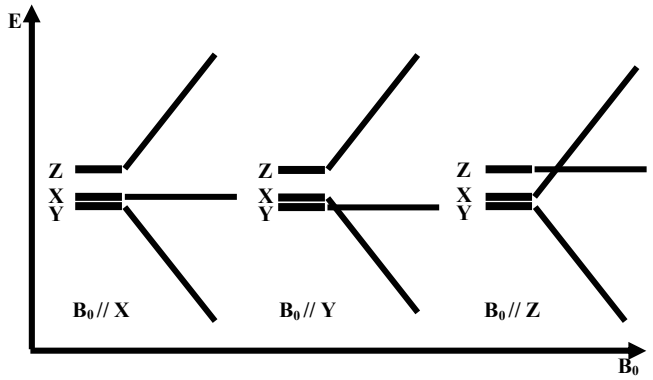


Figure 2.2: Triplet state sub-level energy as a function of the applied magnetic field. B_0 is alternatively parallel to the *X*, *Y* or *Z* ZFS axes. The energy scheme depicts the case D<0, E<0.

Clearly, if the condition $g\beta B >> D, E$ is verified, the eigenfunctions are those of the Zeeman Hamiltonian and the eigenvalues are corrected to the first order for the dipolar contribution. The energy of the Z sub-level is independent on the value of the applied magnetic field [Weil et al. 2007].
Analogous results are obtained when the applied magnetic field is parallel to the X or the Y axis (figure 2)

2.1.3 Hyperfine interaction

The last term of the spin Hamiltonian that we have to consider is the hyperfine interaction between the electron spin and the nuclear spins present in the molecule. Usually the hyperfine contributions are unresolved in a triplet state EPR spectrum of organic molecules and needs special techniques, such as ENDOR, to be measured. The hyperfine interaction is particularly meaningful since it gives information about the electronic structure of the excited triplet state.

Some nuclei have nuclear spin angular momentum *I* and thus an associated magnetic moment:

$$\mu_n = g_n \beta_n \hat{I} \tag{2.35}$$

where g_n is the Landè factor characteristic for each nucleus and β_n is the nuclear magneton. This nuclear magnetic moment interacts with the electronic magnetic moment. The proton (I=1/2) is the most important nucleus with magnetic properties.

The hyperfine interaction between the electronic spin and a nuclear spin is a magnetic dipole-magnetic dipole interaction. It has the form:

$$\hat{H}_{SI} = \frac{g_n \beta_n g_e \beta_e \hat{S} \cdot \hat{I}}{r^3} - 3\frac{g_n \beta_n g_e \beta_e \left(\hat{I} \cdot \bar{r}\right)\left(\hat{S} \cdot \bar{r}\right)}{r^5} \tag{2.36}$$

where *r* is the vector connecting the electron and the nuclear spins. The dipolar interaction acts through the space between the nucleus and the electrons. As unpaired electrons are localized in their orbitals, the dipolar interaction depends on the integral over the spatial distribution. If (2.36) is averaged over the electronic spatial distribution an expression which depends only on the spin variables is derived:

$$\hat{H}_{SI} = \hat{S}\, T\, \hat{I} \tag{2.37}$$

Where *T* is a second rank tensor with generic element equal to:

$$T_{ij} = g_n \beta_n g_e \beta_e \left(\left\langle \frac{1}{r^3} \right\rangle \delta_{ij} - 3\left\langle \frac{ij}{r^5} \right\rangle \right) \tag{2.38}$$

with *i, j = x, y, z*

Note that, the energy of magnetic interaction between spins varies as r^{-3} in all elements, and that the average depends on which orbital the unpaired electron occupies.

From the definition of T_{ij} it follows that $\sum_i T_{ii} = 0$, i.e. *T* is a traceless tensor. For this reason the EPR spectrum of a paramagnetic species in solution at high temperature (i.e. fast re-orientational motion) will not present dipolar hyperfine contributions. *T* has its own principal reference frame, in which it is diagonal. In general, the principal axes systems of *T* and *D* tensors are not parallel [Weil et al. 2007].

Besides the dipolar hyperfine contribution, Fermi theorized another contribution called isotropic hyperfine interaction:

$$\hat{H}_{iso} = \left(-\frac{2\mu_0}{3} \right) \psi(0)^2 g_n \beta_n g_e \beta_e \hat{S} \cdot \hat{I} \tag{2.39}$$

where $\psi(r)$ is the electronic wavefunction and hence $\psi(0)^2$ is the probability of finding the electrons at the nucleus. The (2.39) accounts for the hyperfine couplings detectable in solution at high temperature. Usually, the isotropic hyperfine coupling constant is indicated by a_{iso} and has the form:

$$a_{iso} = \left(-\frac{2\mu_0}{3} \right) \psi(0)^2 g_n \beta_n g_e \beta_e \tag{2.40}$$

And the corresponding term in the spin Hamiltonian is:

$$\hat{H}_{iso} = a_{iso} \hat{S} \hat{I} \tag{2.41}$$

Since a_{iso} is proportional to $\psi(0)^2$, the isotropic coupling is present only if the electron has some probability to be located at the nucleus.

If the unpaired electrons belong to orbitals with a node at the nucleus, the observed spin density (i.e. the measured hyperfine constant) is induced by configuration interactions [Carrington et al. 1979, Brustolon et al. 2009].

Anisotropic and isotropic hyperfine contributions can be collected in one hyperfine Hamiltonian:

$$\hat{H} = \hat{H}_{iso} + \hat{H}_{SI} \tag{2.42}$$

$$= a_{iso} \hat{S} \cdot \hat{I} + \hat{S} \cdot T \cdot \hat{I} \tag{2.43}$$

$$= \hat{S} \cdot A \cdot \hat{I} \tag{2.44}$$

A is obtained by adding a_{iso} to each diagonal term of T.

In the presence of *m* nuclei, the (2.44) becomes:

$$\hat{H} = \sum_{k=1}^{m} \hat{S} \cdot A \cdot \hat{I}_k \tag{2.45}$$

2.2 Spin Polarization

The triplet state of carotenoids and chlorophyll molecules in photosynthetic antenna systems are populated by different mechanisms.

Whereas carotenoid triplet states are populated by triplet-triplet energy transfer, chlorophyll triplet states are populated by *intersystem crossing* (ISC) from the

excited singlet states. Photo-excitation is the most common method to produce chlorophyll triplet states.

The ISC matrix elements that describe the interaction between the excited singlet state and the triplet state are different for each triplet sub-level.

$$\langle S_1 | \hat{H}_{SO} | T_X \rangle \neq \langle S_1 | \hat{H}_{SO} | T_Y \rangle \neq \langle S_1 | \hat{H}_{SO} | T_Z \rangle \quad (2.46)$$

Where $\hat{H}_{SO}$ is the spin-orbit coupling Hamiltonian, S_1 is the excited singlet state wavefunction and $T_{X,Y,Z}$ are the three wavefunctions for the sub-levels of the triplet state without any applied magnetic field.

Without the external magnetic field, the population rates of the three sub-levels depend linearly on the square of the matrix elements above mentioned, thus they will be different for each sub-level:

$$p_i \propto \left| \langle S_1 | \hat{H}_{SO} | T_i \rangle \right|^2 \quad (2.47)$$

For this reason each triplet sub-level will be populated in a selective way. By definition, a system possessing not-degenerate sub-levels which at thermal equilibrium does not respect the population distribution expected by Boltzmann statistic is said to be polarized.

In the same way, even the decaying rates of the triplet sub-levels to the singlet ground state, at zero field, will present an analogue dependence:

$$w_i \propto \left| \langle T_i | \hat{H}_{SO} | S_0 \rangle \right|^2 \quad (2.48)$$

where S_0 is the wavefunction for the singlet ground state.

In the presence of a static external magnetic field, the population (P_i) and decay rates, (W_i) of the triplet sub-levels can be expressed as function of the same rates in zero field (p_i, w_i):

$$P_i = \sum_u |c_{iu}|^2 p_i \quad (2.49)$$

$$W_i = \sum_v |c_{iv}|^2 w_i \quad (2.50)$$

where c_{iu} and c_{iv} are the coefficients of the high field functions expressed as combination of the zero-field functions.

In the high field limit ($g\beta B_0 >> D, E$) and with $B_0 // i$, the populating and decay rates of the T_0, $T_{\pm 1}$ sub-levels are easily correlated to those at zero-field as following:

$$P_0 = P_i \qquad P_{\pm 1} = \tfrac{1}{2} (P_j + P_k) \quad (2.51)$$

$W_0 = W_i \quad W_{\pm 1} = \frac{1}{2}(K_j + K_w)$ (2.52)

With $i, j, k = X, Y, Z$ representing the principal axes directions of the ZFS tensor.

In an EPR spectrum the intensity of the EPR lines is proportional to the population difference between the sublevels involved in each transition. For polarized triplet states and in relation, for instance, to equations (2.51)-(2.52), the transition between the level $m_S = 0$ and the level $m_S = +1$ will be directly proportional to:

$$I_{0\to+1} \propto P_i - \left[\frac{1}{2}\left(P_j + P_k\right)\right] \tag{2.53}$$

Thus, if P_i is greater than $\frac{1}{2}(P_j + P_k)$ the line will be in absorption, vice versa it will be in emission. Note that if the transition $m_S(0) \rightarrow m_S(+1)$ is in absorption, the corresponding $m_S(-1) \rightarrow m_S(0)$ must be in emission.

2.3 Triplet-Triplet Energy Transfer

For carotenoids molecules, the ISC contribution is negligible and TTET is the mechanism by which the triplet state can be populated. The TTET process implies the concurrent exchange of two electrons between the interacting molecules [Dexter 1953, El-Sayed et al. 1969]. In zero magnetic field, the probability of energy transfer from one of the ZFS levels of the donor to one of the ZFS levels of the acceptor is proportional to the square of the electronic exchange integral:

$$P_T^{i'} \propto \left| \sum_{k,l}{}' \left\langle \sum_{i'} S_{0(A)}\varphi_A \tau_{i'}\varphi_D^* \left| \frac{1}{r_{kl}} \right| S_{0(A)}\varphi_A \tau_i \varphi_D^* \right\rangle \right|^2 \tag{2.54}$$

$$= \left|\left\langle S_{0(D)} \middle| S_{0(A)} \right\rangle\right|^2 \left| \sum_{i'} \left\langle \tau_{i'} \middle| \tau_i \right\rangle \right|^2 \left| \sum_{k,l}{}' \left\langle \varphi_D \varphi_A^* \left| \frac{1}{r_{kl}} \right| \varphi_A \varphi_D^* \right\rangle \right|^2 \tag{2.55}$$

$$= C \left| \sum_i \left\langle \tau_{i'} \tau_i \cos\theta_{i'i} \right\rangle \right|^2 \tag{2.56}$$

Where the total state functions of the donor are $\tau_{i'}\varphi_D^*$ and $S_{0(D)}\varphi_D$ for the excited triplet and the ground singlet states respectively, and the corresponding functions for the acceptor are $\tau_i\varphi_A^*$ and $S_{0(A)}\varphi_A$ (S_0 and τ are the spin functions and the $\varphi's$ are the

spatial functions); C is constant for a constant donor-acceptor configuration and r_{kl} is the distance between the electrons k and l.

Equation (2.56) states that the probability of the transfer between the spin direction *i'* in the molecular frame of the donor to the three spin directions (ZFS axes) i in the molecular frame of the acceptor is proportional to the squares of the projection of the spin direction *i'* of the donor into the spin directions of the acceptor.

The exchange operator has no effect on the spin functions: for this reason the donor spin direction is conserved in the acceptor during the triple-triplet energy transfer [El-Sayed et al. 1969, El-Sayed 1971, Imamura et al. 19 84, Akiyama et al. 1994, Di Valentin et al. 2008-2009].

The exchange integral represents the coulombic interaction between the charge densities $\varphi_A\varphi_D^*$ and $\varphi_D\varphi_A^*$, where the asterisk marks the excited molecule. It depends on the superposition of the electron density of donor and acceptor; it is very sensitive to the relative position and distance between the donor and the acceptor. As a result, an efficient TTET requires a close contact between the two partners.

EPR spectroscopy allows studying the spin polarization. The donor spin polarization, created by ISC, is inherited by the acceptor triplet during triplet-triplet energy transfer. The population probabilities of the acceptor triplet sublevels are proportional to population probabilities of the donor triplet and the projections of the ZFS axes systems. Accordingly the eq.2.56 can be rewritten as:

$$P_k^A = \sum_h \cos^2 \theta_{hk} P_h^D \tag{2.57}$$

With an applied magnetic field, the spin eigenfunctions can be expressed as a function of those in zero-field

$$\left|T_j\right\rangle = \sum_i c_{ji} \left|T_i\right\rangle \tag{2.58}$$

The same holds for the population probabilities

$$P_j = \sum \left|c_{ji}\right|^2 P_i' \tag{2.59}$$

with j = -1, 0, +1 and i = X, Y, Z.

The population probability of each triplet sublevels of the acceptor becomes:

$$P_j^A = \sum_h \sum_k \left|c_{ik}\right|^2 \cos^2 \theta_{hk} \; P_h^D \tag{2.60}$$

The term ($cos^2\theta_{hk}$) contains the structural information. The initial polarization preserves the memory of the donor-acceptor relative orientation.

Note that the exact description of the triplet-state time evolution needs to consider also the spin-lattice relaxation terms between the triplet state sub-levels that are not considered here. In Chapter III, the kinetic equations for a photo-excited triplet state are reported in relation to the experiment used for their detection.

2.4 References

[Akiyama et al. 1994] Akiyama K. Tero-Kubota S., Ikoma T., IIkegami Y., *J. Am. Chem. Soc.*, **1994**, 116 5324-5327

[Carrington et al. 1979] Carrington A., McLachlan A. D., Introduction to Magnetic Resonance, Science Paperbacks, 1979

[Dexter 1953] Dexter D. L., *J. Chem. Phys*., **1953**, 21, 836-850

[Di Valentin et al. 2008] M. Di Valentin, S. Ceola, E. Salvadori, G. Agostini, D. Carbonera, *Biochim. Biophys. Acta*, **2008**, 1777, 186–195

[Di Valentin et al. 2009] Di Valentin M., F. Biasibetti, S. Ceola, D. Carbonera, *J. Phys.Chem. B*., **2009**, 113, 13071-13078

[El-Sayed et al. 1969] El-Sayed M. A., Tinti D. S., Yee E. M., *J. Chem. Phys.*, **1969**, 51, 5721-5723

[El-Sayed 1971] El-Sayed M. A., *J. Chem. Phys.*, **1971**, 54 680-692

[Frick et al. 1990**]** Frick J., von Schutz U., Wolf H. C., Kothe G., *Mol. Cryst. Liq. Cryst.*, **1990**,183, 269-272

[Imamura et al. 1984] Imamura T., Onitsuka O., Murai H., Obi K., J. *Phys. Chem.*, **1984**, 88, 4028-4031

[Kok et al. 1996] Kok E., Groenen E. J. J., *J. Am. Chem. Soc.*, **1996**, 118, 770-7794

[Schweiger et al. 2001] Schweiger A., Jeschke G., Principles of pulse electron paramagnetic resonance, Oxford press, 2001

[Vrieze et al. 1995] Vrieze J., Hoff A. J., *Chem. Phys. Letters*, **1995**, 237, 493-501

[Weil et al. 2007] Weil J. A., Bolton J. R., Electron Paramagnetic Resonance - Elementary Theory and Practical Applications, Second Edition. Wiley-Ineterscience, 2007

Chapter III

The Triplet State EPR Spectroscopy

Electron Paramagnetic Resonance (EPR) is a spectroscopic technique for determining the structure, the dynamics and the spatial distribution of paramagnetic species [Berliner et al. 2000, Seyedsayamdost et al. 2007]. Species with at least one unpaired electron are often involved in biochemical reactions. Metalloproteins contain paramagnetic metal ions for catalytic purposes [Bertini et al. 2001, Tocheva et al. 2007, Lyubenova et al. 2010] whereas organic free radicals are usually generated by one-electron transfer processes, as intermediates. In photosynthesis many radicals are involved in the electron transfer chain [Lubitz 2002, Lubitz et al. 2002a]. Furthermore in the photosynthetic apparatus, the presence of paramagnetic triplet states is correlated to the photoprotection from singlet oxygen [Lubitz 2002, Lubitz et al. 2002a]. EPR and related spectroscopies, such as ENDOR (Electron Nuclear DOuble Resonance), can provide unique information on the electronic structure since the magnetic observables are intimately correlated to the electronic wavefunction of the unpaired electron(s) and to the spatial arrangement of the surrounding nuclei. Focusing the attention on triplet states, the zero-field splitting parameters can provide information on the type of paramagnetic species while the hyperfine couplings (hfcs) give an insight on the spin density distribution and hence on the electronic structure (see Chapter II). In this thesis continuous-wave (cw) and pulsed methods are employed in a complementary manner: the former allows to study the spin-polarization of the triplet state, the latter permits to get utmost resolution by separating the different interactions entangled in the cw-spectrum and gives signals that contain only the desired information (in this context hyperfine couplings).

In chapter II, the essential concepts about the triplet state spin Hamiltonian have been presented. In this section some fundamental principles of the EPR experiments are given. Moreover, the relevant magnetic observables considered in the experimental part of this thesis are illustrated.

3.1 Time-resolved EPR

The steady state continuous wave (cw) experiment consists in measuring a signal proportional to the absorption of a monochromatic microwave (mw) radiation by the

sample while the external magnetic field is swept slowly (in relation to the spin relaxation time) through the resonance for each possible transition [Poole 1983, Brustolon et al. 2009]. The selection rule for observing an EPR transition is $\Delta m_S = \pm 1$.

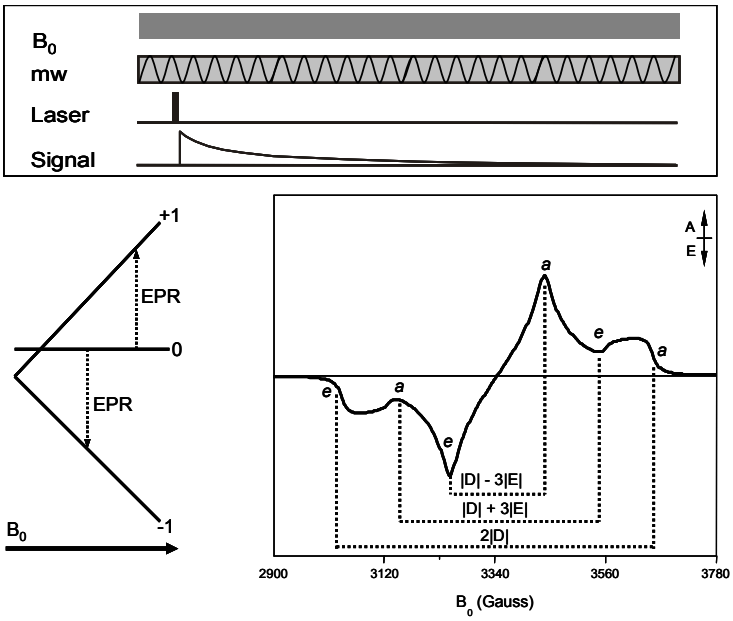


Figure 3.1: Top – Schematic representation of the TR-EPR experiment: at a fixed magnetic field B_0, and under monochromatic mw irradiation, a laser pulse generates the paramagnetic species whose time-evolution is detected. Bottom left – Triplet state energy levels scheme where only the electron Zeeman interaction have been taken into account, the two EPR transitions with opposite polarization are shown. Bottom right – Spin-polarized EPR spectrum of a powder triplet state with $D > 0$, $E < 0$ and $P_y > P_x > P_z$. The polarization at the canonical orientations (*a* = enhanced absorption, *e* = enhanced emission) and the relations to calculate the ZFS parameters are reported.

For meta-stable species as photo-induced triplet states a variant called time-resolved EPR (TR-EPR) is more suitable. In a photo-excited TR-EPR experiment (see figure 3.1), the time evolution of the EPR signal is monitored at a fixed magnetic field after a laser pulse. By collecting together the time traces, detected at different magnetic fields, over the resonance region, it is possible to obtain a bidimensional spectrum that correlates the EPR signal intensity to both the time and the magnetic field. TR-EPR has a great advantage with respect to the conventional cw-spectra: it permits to record the initial spin-polarization that occurs at short delay time from the laser pulse. The initial polarization gives insight into the mechanism of triplet formation (see Chapter II).

EPR spectra of triplet states are characterized by two EPR transitions according to the energy level scheme shown in 3.1. In single crystal where all the molecules have

the same orientation with respect to the applied field, these two transitions lead to a two-line spectrum. In addition if the triplet state sub-levels populations are polarized, as for a photoinduced triplet state, these two lines have opposite polarization: one is in absorption and one in emission (see chapter II). In the case of a powder sample, as a protein frozen solution is, all the possible orientations with respect to the magnetic field are present, and the spectral shape is the envelope of all the two-line spectra, representing a weighted distribution of all possible resonance fields. Ultimately the spectrum is determined by the absolute values of the ZFS parameters: these values determine the magnetic fields at which the turning points of the powder pattern occur, as shown in 3.1 [Brustolon et al. 2009]. These points represent the special cases when the applied magnetic field is parallel to one of the ZFS axis; usually they are labelled as $X^{\pm}$, $Y^{\pm}$ and $Z^{\pm}$ in relation to the particular ZFS axis and to the transition ($m_S(0) \rightarrow m_S(1)$ or $m_S(-1) \rightarrow m_S(0)$). It is worth noting that the g and hyperfine anisotropies are often too small to be resolved in the EPR spectrum of a triplet state of organic molecules.

3.2 Pulsed-EPR

The standard pulsed experiment consists in measuring the signal emitted by the spin system following a series of one or more microwave pulses. In this case the signal is due to the dynamics of the spin-system state prepared by the pulses.

In the following a simple description of pulse experiment based on the vector model is presented [Weil et al. 2007, Brustolon et al. 2009]. This formalism is very intuitive and is equivalent to the quantum mechanical density matrix formalism describing a single unpaired electron (S = ½) where only two energy levels have to be considered. It is appropriate also for S = 1 systems if the two transitions, $m_S(0) \rightarrow m_S(1)$ and $m_S(-1) \rightarrow m_S(0)$, can be treated individually as a two-levels system. Nevertheless, the exact description requires the full quantum treatment and the interested reader is addressed to [Schweiger et al. 2001].

A ‘spin packet’ is defined as a collection of spins with the same resonance frequency. Usually, different resonance frequencies are due to different molecular environments and they can be exactly determined on the basis of the spin Hamiltonian parameters introduced in chapter II. If in the sample there are many different spin packets they

are supposed to be not-interacting and the total magnetization is the sum of the individual spin packet magnetization. The magnetization vector is a classical quantity since it is a sum over a large number of spins.

$$\overline{M} = \sum \overline{\mu}_i$$

Where $\overline{\mu}_i$ is the magnetic moment of each spin. (3.1)

At thermal equilibrium and in the presence of a static magnetic field, for instance along the laboratory Z axis, the magnetization aligns to it. The magnetization time-evolution depends on its interaction with any external magnetic fields, static or time-dependent:

$$d\overline{M}/dt = \overline{M} \times g\mu_B \overline{B} \tag{3.2}$$

If only the static magnetic field B_0 is present the motion consists in the precession of $\overline{M}$ around the Z axis at Larmor frequency ω_L ($\omega_L = g\mu_B B_0 / \hbar$).

If a time-dependent magnetic field is also present, for instance along the X direction $\overline{B}_{1X}(t) = B_1 \cos(\omega t)$ the equation of motion must consider both fields:

$$dM/dt = g\mu_B(\overline{M} \times \overline{B}_0) + g\mu_B(\overline{M} \times \overline{B}_1(t)) - \frac{\left(iM_x + jM_y\right)}{T_2} - \frac{k\left(M_z - M_0\right)}{T_1} \tag{3.3}$$

where *i, j, k* are unit vectors along the X, Y, Z axes, M_x, M_y, M_z are the magnetization components, M_0 is the magnetization at the equilibrium, finally T_1 and T_2 are two phenomenological time constants. T_1 is the spin-lattice relaxation time and accounts for the recovering of the equilibrium value of the magnetization *z* component. T_1 characterizes the energy transfer processes from the spin system to the lattice and vice versa. T_2 is the transverse relaxation time and accounts for the vanishing of *x* and *y* components. T_2 is related to the energy transfer processes within the spin system, which do not involve the lattice.

An easy method to simplify the description is to use a rotating reference frame of axis, with *x*, *y* rotating around Z at angular frequency ω; *z* = Z and $\overline{B}_1$ oscillates along *x*. In the rotating frame $\overline{B}_1$ is seen constant by $\overline{M}$ and the motion becomes a precession of $\overline{M}$ around the $\overline{B}_1$ direction at frequency $\omega_1 = g\mu_B B_1 / \hbar$. The time evolution of the M components (M_x', M_y' and M_z) in this frame are:

$$dM'_x/dt = M'_y(\omega - \omega_0) - \frac{M'_x}{T_2} \tag{3.4a}$$

$$dM'_y/dt = M_z\omega_1 - M'_x(\omega - \omega_0) - \frac{M'_y}{T_2} \tag{3.4b}$$

$$dM_z/dt = -M'_y\omega_1 - \frac{(M_z - M_0)}{T_1} \tag{3.4c}$$

Where ω is the frequency of the microwaves. From the equations (3.4a)-(3.4b) and considering $\omega = \omega_0$ (resonance condition) follows:

$$dM'_x/dt = -\frac{M'_x}{T_2} \tag{3.5a}$$

$$dM'_y/dt = M_z\omega_1 - \frac{M'_y}{T_2} \tag{3.5b}$$

$$dM_z/dt = -M'_y\omega_1 - \frac{(M_z - M_0)}{T_1} \tag{3.5c}$$

which describe the precession of M around B_1 (i.e. x axis). If we neglect the relaxation, for a magnetization aligned along Z at time t = 0 with value M_0, the solution of (3.5a)-(3.5c) gives:

$$M'_x = 0 \tag{3.6a}$$

$$M'_y = M_0 \sin\omega_1 t \tag{3.6b}$$

$$M_z = M_0 \cos\omega_1 t \tag{3.6c}$$

If the time-dependent magnetic field B_1 is applied for a certain time *t*, the magnetization is turned away from *z* toward *y* by the angle:

$$\theta = g\mu_B B_1 t \tag{3.7}$$

The flip-angle depends on B_1, the magnetic field strength, and *t*, the duration of the perturbation.

A microwave pulse of length t_p is formed by turning the radiation on at time $t = 0$ and turning it off at time t_p. In general, a microwave pulse can be used to rotate de magnetization of any desired angle. It is generally assumed that the microwave pulses are short and intense so that T_1 and T_2 relaxation can be neglected and that $B_1 >> B_0$ during the pulses.

If $\theta = \pi/2$ the magnetization becomes aligned along the *y* axis, if $\theta = \pi$ the magnetization becomes aligned to *-z* axis. A pulse with $\theta = \pi$ inverts the magnetization and consequently the populations of the spin states. Usually the pulses are labelled in relation to their flip angles, thus a pulse with $\theta = \pi/2$ is called $\pi/2$-

pulse while a pulse with $\theta = \pi$ is called π-pulse. The effect of a $\pi/2$-pulse is depicted in figure 3.2.

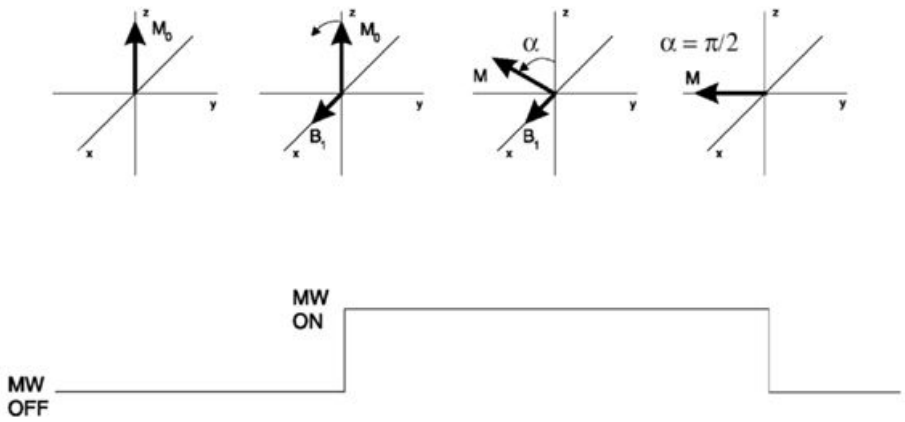


Figure 3.2: Precession of the magnetization vector under the influence of a $\pi/2$-pulse (image from Bruker BioSpin).

The behaviour of the three components of the magnetization is quite simple in the absence of any applied microwave field: M_z simply relaxes with a time constant T_1 towards its initial value (for a radical, this value is determined by the temperature and the splitting between the two energy levels of the spin: M_z is directly proportional to the population difference between these two levels) whereas M'_x and M'_y precess around B_0 at the EPR frequency of that particular spin packet. At the same time, they decay toward zero with a time constant T_2. Resonant microwave pulses convert M_z into M'_x and M'_y or vice versa.

The pulsed EPR signal is proportional to the transverse magnetization i.e. M'_x and M'_y components and it is maximum when the magnetization at $t = 0$ (equilibrium magnetization for a stable species or initial magnetization for a meta-stable species) is aligned to x (or y) axis by a pulse. Thus, a $\pi/2$-pulse gives the maximum signal intensity.

As in NMR spectroscopy, the simplest experiment consists in a single pulse able to rotate the magnetization of $\pi/2$. This will cause the appearance of a FID (Free Induction Decay) signal.

After the $\pi/2$-pulse, along the x rotating axis, the M'_y component starts precessing around z at its own precession frequency while decaying with a time constant T_2.

During this precession the M'_x and M'_y components induce a microwave signal in the EPR spectrometer: this signal is the FID.

The FID has some important properties:

- it occurs at precisely the resonance frequency of the spin packet
- it decays with the T_2 of that spin packet
- if the pulse deviates from the ideal π/2-pulse the frequency and they lifetime of the FID are not affected

Thus, the frequency and T_2 of a spin packet can be measured by the FID.

If the sample is composed by many spin packets, the FID is the sum of the FIDs of all the individual spin packets.

In principle, the EPR spectrum can be extract from the FID by Fourier transformation procedure [Schweiger et al. 2001].

Such an experiment is not common in EPR since the relaxation times are roughly 10^6 times faster than those concerning the nuclei (i.e. the FID relaxes within the instrument dead-time) and the pulse band-width is not larger enough to cover the whole spectrum (i.e. the π/2-pulse cannot rotate all the spin packets). For these reasons most of the pulsed EPR experiments are based on the spin-echo sequences.

The Hahn echo sequence, or primary-echo sequence, is: π/2 – τ – π – τ – echo (figure 3.3a).

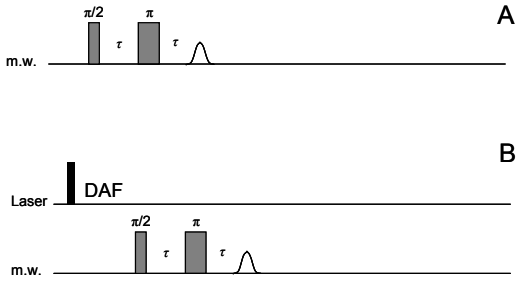


Figure 3.3: Pulse sequence for: A) primary echo scheme; B) photoexcited primary echo sequence.

In this description it is assumed that both the π/2 and π pulses are aligned along the *x* axis of the rotating frame. The first π/2-pulse converts the initial magnetization M into M'_y that in turn starts precessing and decaying in the rotating frame immediately after the first pulse.

After the delay time τ the magnetization in the *xy* plane has became:

$$M'_y(\tau) = Me^{\frac{-\tau}{T_2}} \cos(\omega_a \tau) \tag{3.8a}$$

$$M'_x(\tau) = Me^{\frac{-\tau}{T_2}} \sin(-\omega_a \tau) \tag{3.8b}$$

Where ω_a is the precession frequency of the spin packet. The equations (3.8a) and (3.8b) combine the effect of the precession and of the relaxation.

They can be combined to describe the precessig magnetization:

$$M(\tau) = M'_x(\tau) + iM'_y(\tau) = Me^{-i\omega_a - \frac{\tau}{T_2} - \frac{i\pi}{2}} \tag{3.9}$$

which shows both the phase and the amplitude of the precessing magnetization and of the FID induced in the spectrometer. The terms in the exponential are function of the precession of the magnetization, the T_2 decay and the overall phase shift of - π/2 between M(0) and the microwave magnetic field.

At time τ the π-pulse is applied with B_1 along the *x* axis of the rotating frame. This pulse will convert M'_y into $-M'_y$ and M_z into $-M_z$ (which will be ignored since does not contribute to the signal). Mathematically, the π-pulse converts M(τ) into its complex conjugate, thus at a time t after the second pulse the magnetization is:

$$M(\tau + t) = M^*(\tau)e^{-i\omega_a t - \frac{t}{T_2}} = Me^{-i\omega_a(t-\tau) - \frac{(t+\tau)}{T_2} + \frac{i\pi}{2}} \tag{3.10}$$

This strongly resembles the previous equation (3.9). The magnetization of the spin packet after the π-pulse is precessing with the same frequency and decaying with T_2 although with a different phase.

The echo phenomenon takes place when there are present many spin packets i.e. broad distributions of precession frequencies. The signal following the first pulse eq. (3.9) from each spin packet is proportional to $e^{-i\omega_a - \frac{\tau}{T_2} - \frac{i\pi}{2}}$ so that for a broad distribution of ω_a, the signals from the individual spin packets interfere with each other and the sum of the FID goes to zero before the magnetization has decayed from T_2 relaxation, as above mentioned. The second pulse reverses the M'_y magnetization for every spin packet. Because of the phase conjugation [Schweiger et al. 2001], the destructive interference that attenuated the FID from the collection of spin packets now is reverse because the $\omega_a(t-\tau)$ terms get smaller for all the spin packets. At the instant t = τ, the magnetization from each spin packet is:

$$M(2\tau) = Me^{-\frac{(2\tau)}{T_2} + \frac{i\pi}{2}} \tag{3.11}$$

and the signal from each spin packet is independent from ω_a. All the signals are in phase and add together: from little (or no) signal after the second pulse a signal appears at time 2τ. At 2τ the magnetization is the same as after the first pulse except for same T_2 decay. After $t = 2\tau$ the signal starts to decrease toward zero. All these events are schematically depicted in figure 3.4.

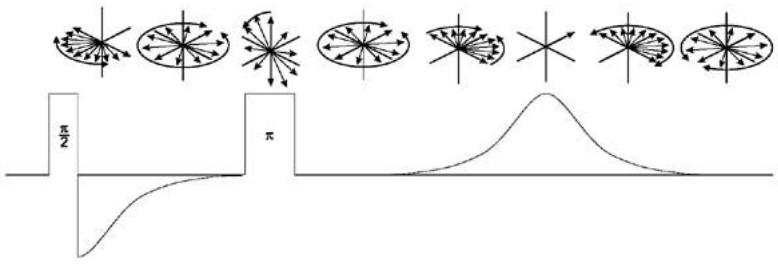


Figure 3.4: Magnetization behaviour during an echo experiment (Figure from Bruker BioSpin).

The Hahn echo can be used for different purposes, for instance: if the echo amplitude is recorded as a function of τ information about relaxation time T_2, Heisenberg exchange and ESEEM (Electron Spin Echo Envelope Modulation, i.e. an alternative spectroscopy technique to measure hyperfine couplings) effect can be obtained [Lin 1984, Dikanov et al. 1992, Schweiger et al. 2001]; if it is introduced in a pulse sequence it allows the generation of a signal for the detection period (see Davies-ENDOR). Moreover, the primary echo sequence is used to detect the EPR spectrum by recording the echo amplitude as the magnetic field is swept at a constant delay τ; in this thesis, such experiment is called field-swept ESE (Electron Spin Echo) detected EPR. Not always such a spectrum resembles the cw-spectrum, because the generation and the detection of the echo influence the shape of the resulting spectrum. The main influence is due to the relaxation times and to the hyperfine interactions. Sometimes these effects help on disentangle the contributions to the different spectra coming from different species.

In the case of photo-generated species, as triplet states, the EPR spectrum can be measured by a laser pulse followed by the Hahn sequence (see figure 3.3B). Also the kinetics of the triplet population, decay and relaxation rates, can be easily examined by the Hahn sequence [Lin 1984]. The general scheme for a laser-induced species is flash – DAF– $\pi/2 - \tau - \pi - \tau$ – echo, where DAF means Delay After Flash (see figure 3.3B). If the DAF length is varied, for a fixed value of τ, the time evolution of the

photo-induced magnetization can be recorded by considering the echo evolution. Basically, each primary echo sequence at different DAF probes the status of the triplet born after each laser flash [Lin 1984].

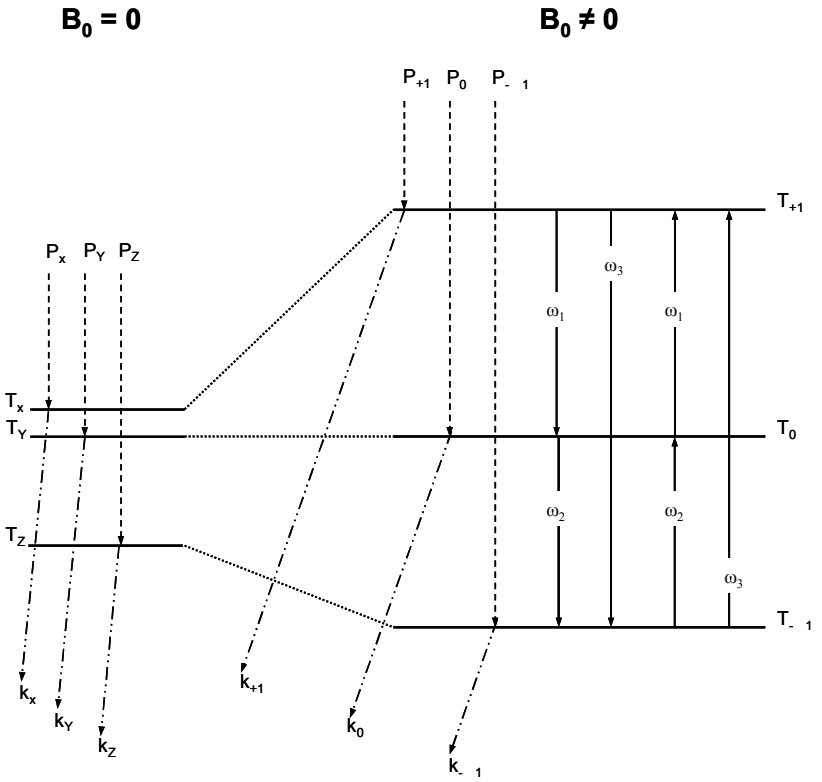


Figure 3.5: Kinetics of the triplet state.

Since during the detection and the evolution there are no microwaves present, the data analysis is simplified. Actually, the microwave stimulated absorption/emission contributions can be ignored. This is a great advantage of the pulsed techniques with respect to the TR-EPR which, in principle, also allows revealing the time evolution of the signal [McGann et al. 1985]. The kinetics of triplet excitation in the absence of a microwave field, (schematically reported in figure 3.5), are governed by the following differential equations:

$$dN_1/dt = -(\omega_1 + \omega_3 + k_1 + P_1)N_1 + (\omega_1 - P_1)N_0 + (\omega_3 - P_1)N_{-1} + P_1 N_T \quad (3.12a)$$

$$dN_0/dt = (\omega_1 - P_0)N_1 - (\omega_1 + \omega_2 + k_0 + P_0)N_0 + (\omega_2 - P_0)N_{-1} + P_0 N_T \quad (3.12b)$$

$$dN_{-1}/dt = (\omega_3 - P_{-1})N_1 + (\omega_2 - P_{-1})N_0 - (\omega_3 + \omega_2 + k_{-1} + P_{-1})N_{-1} + P_{-1} N_T \quad (3.12c)$$

$$N_T = N_S + N_1 + N_0 + N_{-1} \tag{3.12d}$$

where N_T is the total population of the species, N_S is the population of the singlet ground state, N_i is the population of the i sublevel, ω_i is the spin-lattice relaxation rate, P_i the population rate and k_i the decay rate [Lin 1984], see also chapter II. For carotenoid triplet states it is often possible to neglect the spin-lattice relaxation rates, since the major contribution is due to the sublevels decay.

3.3 Pulsed-ENDOR

ENDOR is a magnetic double resonance spectroscopy suitable for obtaining detailed molecular and structural information about paramagnetic species. ENDOR allows detecting, via the electron spin properties, the NMR frequencies of the nuclei coupled to electron spin [Kemple]. As stated by the acronym, two different electromagnetic fields are necessary: one in the microwave (mw) region to excite the electron spin transitions and one in the radio frequency (rf) region to excite the nuclear spin transitions. The energy level scheme in figure 3.6 is referred to a triplet state coupled to a proton (I = ½) with positive hfc ($A_{ZZ} > 0$) and with the magnetic field parallel to the Z axis of the hfc tensor (see Chapter II). The ENDOR selection rule is $\nu_{ENDOR} = |\nu_H - m_S A_{ZZ}|$, hence for each EPR transition, $m_S(0) \rightarrow m_S(1)$ and $m_S(-1) \rightarrow m_S(0)$, there are two resonance frequencies:

$$\nu_{ENDOR}(0) = \nu_H \tag{3.13a}$$

$$\nu_{ENDOR}(\pm 1) = \nu_H \mp A_{ZZ} \tag{3.13b}$$

where ν_H is the proton free Larmor frequency at that particular B_0. Clearly the transition at ν_H stems for the proton Zeeman transition in the $m_S = 0$ manifold and it is common to all protons. Therefore the triplet state ENDOR spectra are asymmetric, unlike the radical spectra. The hfcs can be read as a deviation from the ν_H transition. More important, if the sign of D is known the signs of the hfcs can be directly derived.

In the standard cw-ENDOR experiment, a particular EPR transition is saturated by a strong mw field. Simultaneously, a rf field induces nuclear transitions, which are detected by observing the desaturation of the EPR transition as a function of the rf.

Cw-ENDOR suffers of a strong dependence from the temperature since electronic and nuclear relaxation times must be controlled. Therefore its application is restricted to a narrow temperature range [Brustolon et al. 2009].

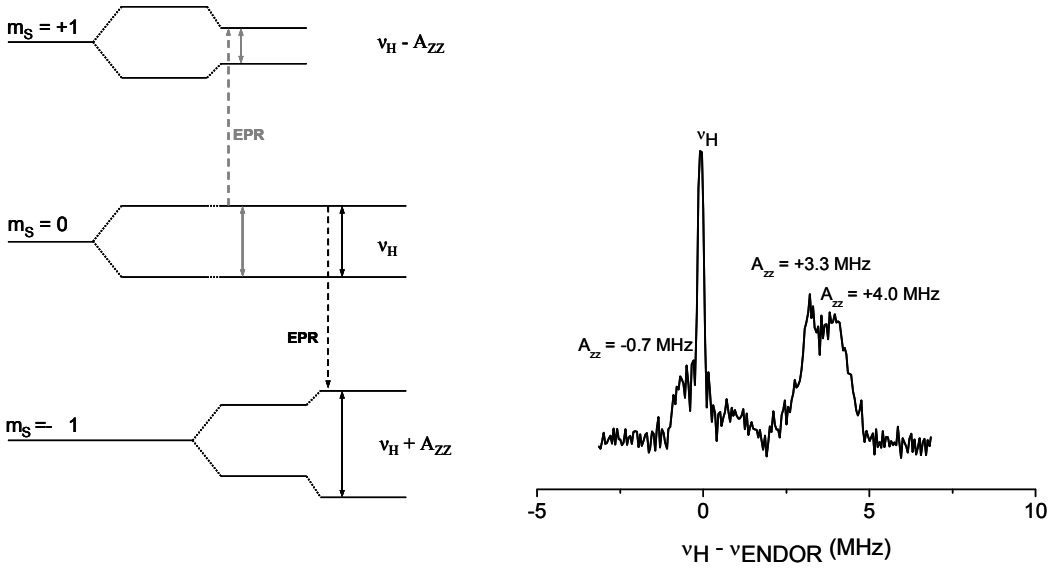


Figure 3.6: Left - Energy levels scheme for a triplet state (S = 1), coupled with an I = ½ with a positive hfc ($A_{ZZ} > 0$). The electronic Zeeman, the nuclear Zeeman and the fist order hyperfine contribution are shown. The EPR transitions are depicted with dashed arrows, while the ENDOR transitions are in continuous. Right – Triplet state ENDOR spectrum of a photoexcited porphyrin, the major ENDOR lines are labelled with the corresponding hfcs.

In 1965 Mims [Mims 1965] demonstrated that analogous ENDOR experiments can be carried out with pulsed mw and rf excitations. In this kind of pulse experiments, the intensity of the electron spin echo is recorded as a function of the radio frequency. Pulse-ENDOR can be often performed in conditions in which cw-ENDOR would be undetectable.

Like all the pulsed experiments, the ENDOR sequences can be divided into three different periods, the preparation, the mixing and the detection. In the preparation period, the mw pulse(s) create(s) the nuclear polarization. During the mixing period, the nuclear polarization is modified by a selective rf pulse. Finally, during the detection period, the nuclear polarization is transferred to electron coherence and indirectly observed via an electron spin echo (see infra ENDOR Davies as an example). The pulse sequences of the two ENDOR experiments used in this thesis are depicted in figure 3.7, where also the laser pulse is indicated since the

experiments have been performed in the characterization of photo-excited triplet states.

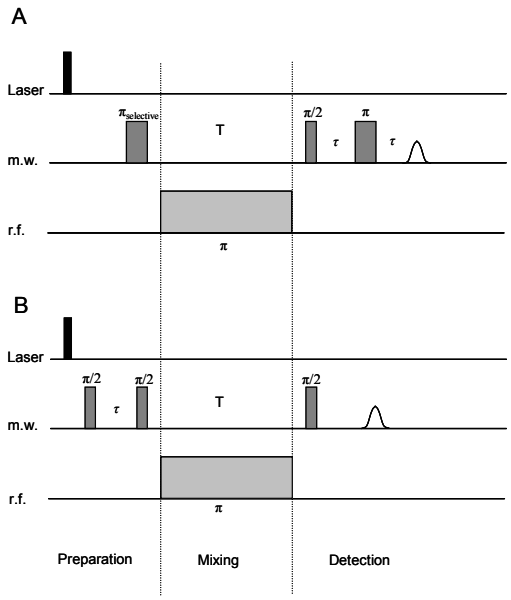


Figure 3.7: A) Photo-excited Davies-ENDOR pulse sequence; B) Photo-excited Mims-ENDOR pulse sequence. In both cases, the mw and rf pulses are triggered by the laser pulse.

The pulsed ENDOR Davies, introduced in 1974, is based on an inversion recovery sequence, $\pi_{selective} - T - \pi/2 - \tau - \pi - \tau -$ echo, where the first mw π pulse is selective and inverts the polarization (i.e. the populations) of a particular EPR transition [Davies 1974, Schweiger et al. 2001]. During the mixing period (T), a selective rf pulse (with flip angle θ_{rf}) is applied on-resonance with one of the nuclear frequencies: the polarization of this transition is changed accordingly to θ_{rf}. In turn, this change also alters the polarization of the observed transition and it is measured via a primary electron spin echo sub-sequence (detection period).

The echo can disappear completely if the rf field matches exactly one of the two allowed NMR transitions frequencies and if the pulse flip angle corresponds to an rf π-pulse for the nuclear spin. The effect of the pulse sequence in the case of S = 1 coupled to I = ½ is reported in figure 3.8, only the EPR transition $m_S(0) \rightarrow m_S(+1)$ is considered. The initial selective mw π pulse has a critical role in determining the spectral resolution: an unselective π-pulse (i.e. a short pulse) will cause the suppression of small hfcs [Schweiger et al. 2001].

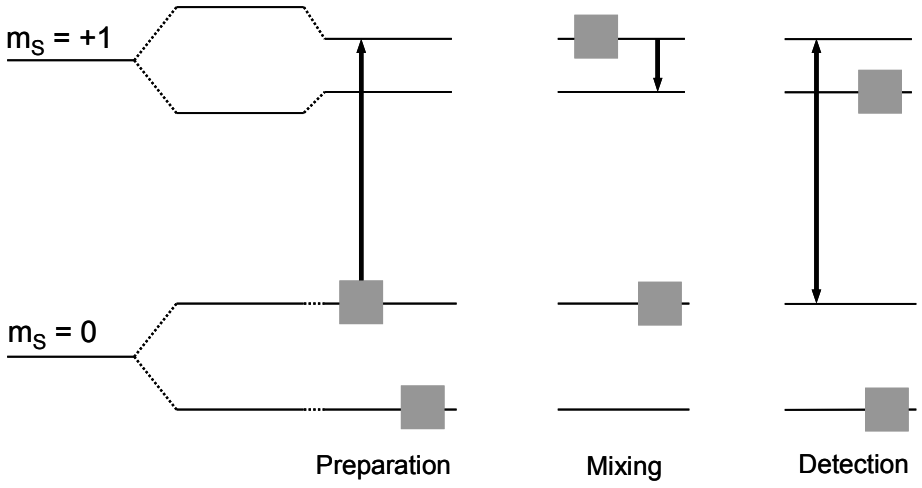


Figure 3.8: Polarization time evolution for a system S = 1, I = ½ (electron Zeeman and hyperfine interactions) during a Davies-ENDOR pulse sequence. Only the EPR transition $m_S(0) \rightarrow m_S(+1)$ is considered.

If small coupling constants have to be determined it is convenient to use the Mims ENDOR pulse sequence [Mims 1965, Schweiger et al. 2001]. The pulse sequence is based on the stimulated echo sequence with three non-selective π/2 pulses (see figure 3.9a): π/2 – τ – π/2 – T – π/2 – τ – echo. This sequence creates a stimulated echo at time τ after the third π/2-pulse. The first π/2-pulse transfers the initial magnetization (figure 3.9b) to M'_y magnetization (figure 3.9c). During the evolution time τ, M'_y starts precessing and relaxing (figure 3.9d). The second pulse rotates the magnetization vectors into the *xz* plane, storing some magnetization along *z* (figure 3.9e). All the information carried by the magnetization which is not stored along *z* will be lost during the detection. During time T, the magnetization in *xy* plane decays (figure 3.9f). At time T+τ the third π/2-pulse transfers the z-magnetization pattern into *xy* magnetization (figure 3.9g), which forms an echo at time T+2τ.

This kind of pulse sequence is sensitive to T_1 and its major application is in ESEEM spectroscopy where it provides higher spectral resolution (compere to the Hahn sequence) due to different selection rules [Lin 1984, Dikanov et al. 1992, Schweiger et al. 2001]. It is also used in Mims-ENDOR.

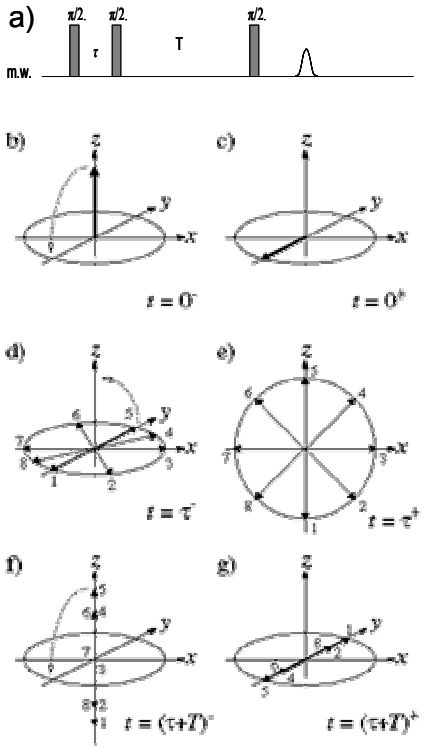


Figure 3.9: a) Stimulated echo pulse sequence; b-f) formation of the stimulated echo.

In Mims ENDOR, the preparation sequence, $\pi/2 - \tau - \pi/2$, creates a sinusoidal polarization pattern across the EPR spectrum [Schweiger et al. 2001] which is changed by the selective rf pulse and is recorded in function of the rf frequency via the stimulated electron spin echo. The choice of τ can have substantial effects since in Mims-ENDOR measurements there are blind spots that depend on the hyperfine constant value and the time τ. Usually, blind spots are overcome by adding several spectra recorded with different τ values. Considering an isotropic hyperfine constant a_{iso}, the corresponding ENDOR line intensity is zero for $\tau = 2n\pi/a_{iso}$ and maximum for $\tau = (2n + 1)\pi/a_{iso}$

3.4 References

[Berliner et al. 2000] Berliner L. J., Eaton S. S., Eaton G. R., Biological Magnetic Resonance, volume 19 – Distance measurements in Biological system by EPR, Kluwer Academic Press

[Bertini et al. 2001] Bertini I., Sigel A., Helmut S., Hendbook on Metalloproteins, Marcel Dekker, Inc., 2001

[Brustolon et al. 2009] Brustolon M., Giamello E., Electron Paramagnetic Resonance, a practitioner's toolkit, Wiley, 2009

[Carrington et al. 1967] Carrington A., McLachlan A. D., Introduction to magnetic resonance, Science Paperbacks, 1967

[Davies 1974] Davies E. R., *Phys Lett.*, **1974**, A47, 1

[Dikanov et al. 1992] Dikanov S. A., Tsvetkov Y. D., Electron spin echo envelope modulation (ESEEM) spectroscopy, CRC Press, 1992

[Kemple] Kemple M. D., ENDOR of triplet state systems in solids, in Multiple electron resonance spectroscopy, ed. Dorio M. M. and Freed J.

[Lin 1984] Lin T. S., *Chemical Reviews*, **1984**, 84(1), 1-15

[Lyubenova et al. 2010] Lyubenova S., Maly T., Zwicker K., Brandt U., Ludwig B., Prisner T., *Accounts of chemical research*, **2010**, 43(2). 181-189

[Lubitz 2002] Lubitz W., *Phys. Chem. Chem. Phys.*, **2002**, 4(22), 5539-5545

[Lubitz et al. 2002a] Lubitz W., Lendzian F., Bittl R., *Accounts of chemical research*, **2002**, 35(5). 313-320

[McGann et al. 1985] McGann W. J., Franck H.A., *Chem.. Phys. Lett.*, **1985**, 121, 253

[Mims 1965] Mims W. B., *Proc. Roy. Soc. London*, **1965**, 283, 452-457

[Poole 1983] Poole C. P. Jr., Electron spin resonance – a comprehensive treatise on experimental techniques, Wiley-interscience publication, 1983

[Seyedsayamdost et al. 2007] Seyedsayamdost M. R., Chan C. T. Y., Mugnaini V., Stubbe J., Bennati M., *J. Am. Chem. Soc.*, **2007**, 129(51), 15748-+

[Schweiger et al. 2001] Schweiger A., Jeschke G., Principles of pulse electron paramagnetic resonance, Oxford University Press, 2001

[Tocheva et al. 2007] Tocheva E. I., Rosell F. I., Mauk A. G., Murphy M. E. P., *Biochemistry*, **2007**, 46(43), 12366-12374

[Weil et al. 2007] Weil J. A., Bolton J. R., Electron paramagentic resonance – elementary theory and practical applications II edition, Wiley, 2007

Chapter IV

LHC-II from *Spinacia oleracea*

Pulsed ENDOR and Density Functional Theory on the Lutein Triplet State in LHC-II of *Spinacia Oleracea*. Comparison with the Peridinin Triplet State in PCP of *Amphidinum Carterae*.

Enrico Salvadori[1], Marilena Di Valentin[1], Christopher M. W. Kay[2], Alfonso Pedone[3,4], Vincenzo Barone[3] and Donatella Carbonera[1]

[1]Dipartimento di Scienze Chimiche, Università di Padova, via Marzolo 1, 35131 Padova, Italy

[2]Institute of Structural and Molecular Biology, Darwin Building, University College London, Gower Street, London WC1E 6BT, UK

[3]Scuola Normale Superiore, Piazza dei Cavalieri 7, I-56126 Pisa, Italy

[4]Dipartimento di Chimica, Università di Modena e Reggio Emilia, via G. Campi 183, 41100, Modena, Italy

Abstract

Carotenoid molecules are essential for the life of photosynthetic organisms. They protect the whole apparatus from the photo-oxidative damage induced by light-stress conditions. One of the photo-protective mechanisms implies triplet-triplet energy transfer from the chlorophyll molecules. The process is strongly dependent on the electronic distribution of the triplet states involved. In this contribution we used pulsed-ENDOR experiments on LHC-II from *Spinacia oleracea* as experimental constraints to validate DFT calculations on the electronic distribution of the lutein triplet state. In turn, DFT predictions allow us to discuss the electronic requirements for an efficient triplet-triplet energy transfer. The experimental results on LHC-II are compare with those on the carotenoid peridinin in PCP from *Amphidinium carterae* to point out common features of the photo-protective mechanism in the two different light-harvesting systems.

1. Introduction

Antenna proteins are specialized pigment-protein complexes for light-harvesting functions in the photosynthetic apparatus. Their role is to maximize the number of collected photon and to deliver them to the reaction centres (RC). Since *in vivo* the photosynthetic process works in fluctuating light intensity the light-harvesting machinery has to be highly flexible. When the light intensity is low all the collected energy is used for the charge separation reactions in the RCs, when the light intensity increases, and not all the absorbed energy can be used for the photosynthesis, several mechanism to get rid of the excess of energy are activated. In higher plants and algae, the most important photo-protection mechanism is connected to the xanthophyll cofactors bound to the major membrane antenna complexes, namely LHC-II and LHC. It is activated by the pH gradient in the lumen and it implicates the action of several enzymes. In this process, high light intensity induces the reversible de-epoxidation of violaxanthin to antheraxanthin up to zeaxanthin which has a fundamental role in photo-protection, even though the precise function is under debate [Müller et al. 2001]. On the other hand, the fastest response to light-excess conditions is played within the antenna complexes by the carotenoid (Car) molecules that are present in photosynthetic proteins: this mechanism implies the quenching of chlorophyll (Chl) triplet states. As a matter of fact, when the rate of excitation delivery exceed the turnover rate of the RCs the excitation became localized on one Chl molecule increasing the probability of inter system crossing and thus of triplet formation. Chl triplet (^{T}Chl) state is know to be a good sensitizer for singlet oxygen formation which in turn is a powerful oxidant agent able to damage the whole photosynthetic apparatus. By virtue of their low lying triplet state carotenoids (^{T}Car) are able to quench the Chl triplet states and also the singlet oxygen if it is present. For this reason carotenoids are of vital importance for oxygenic organisms [Polìvka et al. 2010].

Light-harvesting complexes are proteins common to all the photosynthetic systems but they are preset in many different forms in relation to pigment composition and stoichiometry and to their location in the apparatus. LHC-II (Light-Harvesting-Complex II) form higher plants and PCP (Peridinin-Chloropyll *a*-Protein) from dinoflagellate algae exemplify well this variability: these two proteins whose x-ray

structures have been resolved at high resolution, have been widely investigated and used as model systems to study the energy transfer pathways between cofactors in natural occurring antennae. LHC-II and PCP represent opposite strategies of light-harvesting in terms of pigments composition: while LHC-II is a membrane protein and the most abundant cofactors are chlorophylls molecules, PCP is water-soluble and the chlorophyll /carotenoid ratio is in favour of carotenoids.

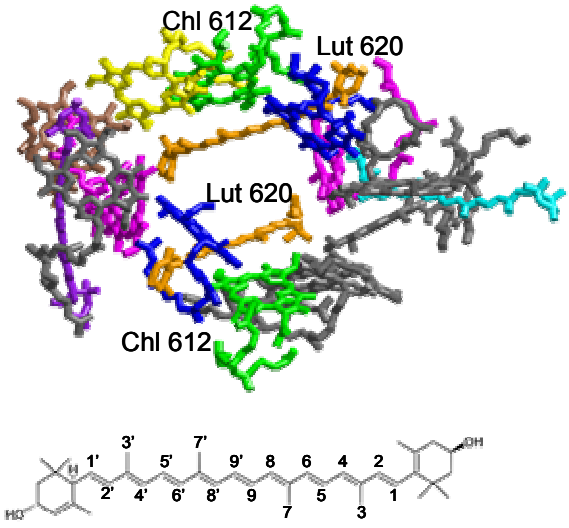


Figure 1: Structure of the pigments associated with the monomeric unit of LHC-II complex. Structure derived from coordinates deposited in the Brookhaven Data Bank (1RWT). Orange, luteins; purple, violaxanthin; cyan, neoxanthin; green, Chl *a* 603 (lower) and Chl *a* 612 (upper); blue, Chl *a* 602 (left) and Chl *a* 610 (right); magenta, Chl *a* 604 (left) and Chl *a* 613 (right); yellow, Chl *a* 611; brown, Chl *a* 614. The molecular structure of carotenoid lutein (upper), and of carotenoid peridinin are also shown. The numbering of lutein protons is the same as figure 1.

LHC-II is the main antenna protein associated with the photosystem II of higher plants and it is the most abundant membrane protein in the chloroplast. The x-ray structure of LHC-II has been resolved for both spinach (2.72 Å) [Liu et al. 2004] and pea (2.5 Å) [Standfuss et al. 2005]: it has been demonstrated the two structures are the same within the experimental error. LHC-II is a Chl a/b binding protein, it is structured as three trans membrane helices and it is observed in trimeric form. Each monomer binds 14 Chl molecules (8 Chl a and 6 Chl b) and 4 carotenoids (2 lutein, 1 neoxanthine and 1 carotenoid belonging to xanthophylls cycle). Among the carotenoids present in LHC-II, lutein (Lut) is the only one identify as Chl triplet quencher by means of optical and EPR spectroscopies [Mozzo et al. 2008, Di Valentin et al 2009]. Lutein is a polyene with a C_{40} carbon skeleton and 10 conjugated double bonds with no particular substituents along the π-system [Young

et al. 1993]. The geometries of the pigment cluster in LHC-II and the molecular structure of lutein are also shown in figure 1. Hereafter we will refer to the pigments numbering of the x-ray structure in Liu et al. [Liu et al. 2004].

On the other hand, PCP is the outer and water-soluble antenna complex characteristic of dinoflagellate algae; it contains only Chl *a* and peridinin (Per) in the ratio of 1:4. The structure of PCP from *Amphidinium carterae* (*A. carterae*) has been resolved by x-ray diffraction at 1.5 Å resolution [Shulte et al. 2009]. Other forms of PCP coming from the same organism and from related ones are also found in nature: High Salt PCP (HSPCP) from *A. carterae* is a minor variant which contains six Per and two Chl a molecules [Sharples et al. 1996, Shulte et al. 2009a] and PCP from *Heterocapsa pygmaea* which is half-size respect to PCP of *A. carterae* though conserving the same pigment composition. In addition, PCP can be reconstituted with a different pigment composition compared to the native one [Shulte et al. 2009, 2010]. These antennae employ predominantly Per as light-harvesting pigment, an unusual and highly substituted carotenoid with a C_{37} carbon skeleton, an allene moiety and a lactone ring conjugated with the π-electron system and with acetate and epoxidic groups in the two terminal β-rings. The number of conjugated double bonds is 9 including the allene moiety: the presence of the substituents breaks the C_{2h} symmetry of an idealized conjugated chain [Young et al. 1993].

Although peridinin and lutein share the conjugated skeleton as basic motif their optical properties are very different, mostly due to the minor extend of the double bond system and the high substitution with oxygen containing moieties for the peridinin. These chemical differences result in observable fluorescence from the S_1 state - usually not detectable for carotenoids – and in the appearance of a low singlet exited state with internal charge transfer (ICT) character. This ICT state is stabilized in polar environments and it modulates the lifetime of the S_1 state with which it is electronically coupled. The ICT state enhances the energy transfer efficiency to the Chl Q_y because in contrast to S_1 it has appreciable dipole moment [Zigmantas et al. 2002, Vaswani et al. 2003]. Most importantly the conjugated carbonyl group decreases the S_2-S_1 energy gap because the S_2 state energy is significantly lower in carbonyl carotenoids with respect to non-carbonyl analogues but the S_1 energy is largely unaffected. For these reasons carbonyl carotenoids are able to efficiently capture the green light which is fundamental for underwater life [Polìvka et al. 2010].

Lutein does not need any of these features since it is used by earth-living organisms and it is located in unpolar environment as the chloroplast membrane is. The oxydryl groups located at the terminal rings are involved in hydrogen-bonds with the protein scaffold. But they are not related to the photo-physical properties of the molecule.

As already pointed out, the photo-protection mechanism we are interested is a triplet-triplet energy transfer (TTET) process. The interaction was first theorized by Dexter [Dexter 1953]. TTET can be formalized as a simultaneous double electron transfer and it can be characterized by a non adiabatic rate constant which depends on the exchange integral between the two electrons and in turn on the electronic distribution over the molecular architectures. An efficient transfer demands two main conditions: (i) the interacting molecules have to be in van der Waals contact and (ii) the wave-functions of the donor and the acceptor must have a good spatial overlap. The paramagnetic character of triplet states makes EPR spectroscopy the method of choice to investigate TTET in photosynthetic antenna complexes: Time-Resolved electron spin resonance (TR-EPR) and pulsed EPR techniques coupled with photo-excitation are the most appropriate tools to investigate the triplet state electronic structure. Among the advance pulsed EPR techniques, in particular, electron-nuclear double resonance (ENDOR) is the most powerful method to map the spin density distribution of photo-induced triplet states: the determination of the atoms at which large electron spin density is located is fundamental to recognize the requisites for efficient TTET.

In our previous studies on this issue, it was demonstrated that in both PCP and LHC-II there is a specific Chl-Car pair involved in the TTET: in both complexes this couple is characterized by the shortest distance between the centres of the conjugated systems and by the presence of a bridging molecule between the Chl and the Car moieties which is the fifth ligand for Mg in Chl macrocycle (a water molecule in PCP, an aminoacidic residue in LHC-II) [Di Valentin et al. 2008a, 2009]. We derived the spin density distribution on peridinin triplet state in several PCP proteins (MF-APCP [Di Valentin et al. 2008b] and HS-APCP [Di Valentin et al. 2008c] from *A. carterae* and HPCP from *H. pygmaea* [Di Valentin et al. 2010]) by coupling pulsed ENDOR experiments on the photoexcited pigments in the proteins with theoretical calculation [Di Valentin et al. 2008b]. We found that the triplet spin density is delocalized over the whole π-conjugated system with an alternate spin pattern with

positive spin densities alternating with gradually smaller negative spin densities. This alternate pattern is lost in the central region of the polyene chain where all positive densities are found. The same approach, with similar results, was also applied by Nicklas et al. on the peridinin triplet state in reconstituted PCP sample at Q-band [Niklas et al. 2007].

In this contribution we have extended the work on the photo-excited triplet state of carotenoids in antenna complexes to the lutein molecule in LHC-II by means of Davies ENDOR measurements and density functional theory (DFT) calculation. For the first time, we present a picture of the electronic properties of the triplet state of the lutein. These results are used to discuss the electronic properties requirement for an efficient TTET. We also compare the lutein and peridinin triplet state properties in order to recognize common features in the TTET photo-protection mechanism.

2. Materials and Methods

Sample preparation: The LHC-II complex were isolated from spinach by using *n*-octil-*β*-D- glucopyranoside after which the LHC-II trimers were purified by using *n*-dodecyl-*β*-D-maltoside and were ultacentrifuged. For measurements, the samples were diluted in 10 mM Tricine, pH 7.8, 0.3 M sucrose, and 0.03% w/v *β*-dodecylmaltoside, to a final protein concentration of 3 mg/mL.

Oxygen was removed from the sample by flushing argon in the EPR sample tube befor freezing. Glycerol, previously degassed by several cycles of freezing and pumping, was added (60% v/v) to obtain a transparent matrix.

Pulsed EPR and ENDOR measurements: Pulsed EPR and ENDOR measurements were performed on a Bruker Elexsys pulsed EPR spectrometer equipped with a Bruker ENDOR accessory (E560D-P) and a radiofrequency (RF) amplifier (AR751-150W). Laser excitation at 532 nm (10mJ per pulse and repetition rate of 10Hz) was provided by the second harmonic of a Nd:YAG laser (Quantel Brilliant) in the optically transparent dielectric ring ENDOR resonator (EN4118X-MD4). The resonator was placed in a helium cryostat (Oxford CF935) for the cryogenic temperature experiments. After pulsed laser excitation, the EPR signals were directly detected and had a non derivative shape (A = enhanced absorption, E = enhanced emission).

Field-swept electron spin echo (ESE) spectra were recorded using a 2-pulse (flash-DAF-π/2-τ-π-τ-echo) ESE sequence for a delay between the laser flash and the first microwave pulse of 50 ns. The π/2 pulse was of 16 ns and he delay τ was set at 200 ns.

Devies-ENDOR experiments were performed using the microwave pulse sequence (flash-DAF-π-T- π /2-τ-π-τ-echo) with a selective inversion π pulse of 160 ns, T of 7 μs and a RF pulse of 6 μs. The detection sequence was the same to the field-swept ESE experiments but with τ of 500 or 700 ns. The DAF was normally of 50 ns or 9 μs for th X transition.

Quantum Chemical computation: Density functional theory calculations on the triplet states of the isolated Lut620 and Lut621 molecules and of the complexes with Chlorophyll *a* have been carried out by using the G03 package [Frisch et al. 2004]. The structures of Lut620 and Lut621 have been taken from x-ray diffraction experiments (pdb entry: 1RWT) and re-oriented so that the axes of dipolar couplings lie along the experimentally determined zero-field splitting (ZFS) axes. Hydrogens and methyl groups for both the singlet and triplet state of the two luteins have been optimized at the B3LYP/6-31G(d) level while freezing all the other atoms in the positions found in the x-ray study [Becke et al. 1993, Lee et al. 1988]. A free rotation of methyl groups has been assumed, so that the corresponding hfcs are averages over the three protons for four representative values of the C-C-C-H dihedral angles (0°, 30°, 60° and 90°). The isotropic hpcs and the hfc tensor components have been computed by using the purposely tailored EPR-II basis set [Barone 1994a, 1994b] for carbon, hydrogen, oxygen and nitrogen atoms and the 6-31G(d) basis set for the magnesium ion of the chlorophyll. Several experimental evidences have demonstrated that the EPR parameters of a molecule exhibit a more or less marked dependence on the nature of the embedded medium. Bulk solvent contributions can be accounted for by at least two theoretical methods, that is, explicit and implicit models [Pedone et al. 2010, Barone et al. 2010]. In this work environmental effects have been included by employing the Polarisable Continuum Method (PCM) [Tomasi et al. 2005] with a dielectric constant of 3.0 which is in the range of that found for proteins.

3. Results

3.1 Pulsed EPR

The 2-pulse ESE spectrum of photo-excited LHC-II from *S. oleracea* recorded immediately after the laser flash (DAF = 50 ns) at 20 K is shown in figure 2 panel A. The spectrum is the same as the previously reported in [Di Valentin et al. 2009], it shows the typical spin polarization pattern *eeaeaa* and ZFS parameter (|D| = 414 G, |E| = 40.7 G [Di Valentin et al. 2009]) compatible with the lutein triplet state. A minor contribution of unquenched Chl triplet state (^{T}Chl) is visible as small shoulders (marked with asterisks in the spectrum).

In the same panel the corresponding spectral simulations (dashed lines) decompose the powder spectrum in the $m_S = 0$ to $m_S = +1$ transition (X^+, Y^+, Z^+) and the $m_S = -1$ to $m_S = 0$ transition (X^-, Y^-, Z^-); the parameters are summarized in the figure caption. By convention, the order of the ZFS energy levels is $Z^2 > Y^2 > X^2$. The corresponding axes of the lutein triplet state have been assigned analogously to those determined for β-carotene in single-crystal: the long molecular axis is the Z axis, the X axis is parallel to the C-H bonds in the conjugated chain while the Y axis is perpendicular to the ZX plane [Frick et al. 1990, Ros et al. 1991], the axes direction with respect to the lutein molecular structure are also shown in figure 2 panel B.

Analysis of the spectral shape reveals that the lutein triplet has been populated by TTET from Chl603/612 as demonstrated in [Di Valentin et al. 2009].

3.2 Pulsed ENDOR

Considering the canonical transitions marked in the ESE-detected spectrum reported in figure 2 panel A, the total set of the A_{ii} hyperfine coupling (hfc) tensor components of protons coupled to lutein triplet state can by measured by photo-excited triplet ENDOR experiments, in the reference frame of ZFS tensor. The large ZFS interaction enables single-crystal-like ENDOR spectra to be recorded, using different field positions of the EPR spectrum to excite selectively only molecules with particular orientations. In figure 2 panel C, the ENDOR spectra of the photo-excited triplet state in LHC-II from *S. oleracea* at 20 K for the Y^+ and Y^- transitions are shown for comparison.

The frequency scale in this figure is plotted as deviations from the Larmor frequency (ν_H) and the hfcs values correspond to the frequency shift between the corresponding ENDOR line and ν_H. The ENDOR transitions are labelled as positive or negative in relation to their appearance in the spectrum with respect to ν_H. The original polarization of the ENDOR signals has not been maintained to allow a better comparison.

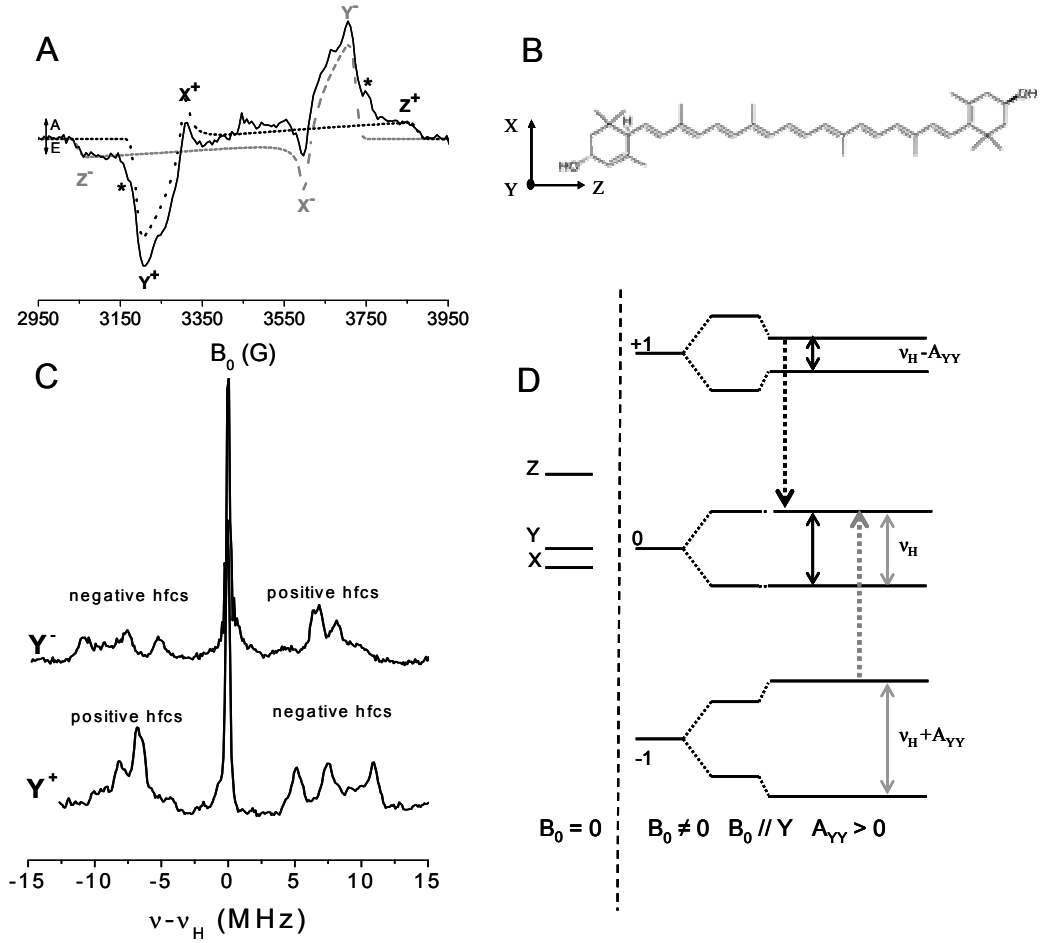


Figure 2:. (A) Field-swept ESE spectrum of LHC-II from *S. oleracea* at 20 K as it was in [Di Valentin et al. 2009]. Powder simulation (dashed lines) for the m_S = -1 to the m_S = 0 transitions (index +) ant the m_S = 0 to m_S = -1 transitions (index -) are also reported. The parameters used for the simulation are those already discussed in [Di Valentin et al. 2009] : |D| = 414 G, |E| = 40.7 G, Px : Py : Pz = 0.40 : 0.20 : 0.40, $g_{ii} = g_e$. (B) Molecular structure of Lutein, the orientations of ZFS axes are shown; (C) Photoexcited triplet state ENDOR spectra relative to Y^+ and Y^- transitions recorded at DAF = 50 ns and at 20 K. The frequency scale gives the deviation from the ν_H and the hfcs correspond to the shift between the corresponding ENDOR line and the ν_H. The expected spectral symmetry relative to the ν_H transition is clearly visible. (D) Spin energy levels for a triplet state showing positive hyperfine interaction with a nucleus with spin I = ½ for the applied magnetic field parallel to Y ZFS axis. The EPR transitions are marked with dashed arrows (gray $m_{-1} \rightarrow m_0$, black $m_0 \rightarrow m_{+1}$), while the NMR transitions are represented with continuous line. For comparison the energy level without external magnetic field is also shown.

The triplet spin energy levels for applied magnetic field parallel to the Y axis, including first-order hyperfine interaction with one proton with $A_{YY} > 0$, for $D < 0$ as expected for a molecule with a long axis as lutein, are shown in figure 2 panel D. The EPR transitions are depicted as dashed arrows, while the ENDOR transitions are in continuous. Considering the selection rule $\nu_{ENDOR} = |\nu_H - m_S A_{YY}|$, for each EPR transition, there are two ENDOR resonance frequencies at:

$\nu_{ENDOR}(0) = \nu_H$

$\nu_{ENDOR}(1) = \nu_H + A_{YY}$ if $A_{YY} > 0$ or $\nu_{ENDOR}(1) = \nu_H - A_{YY}$ if $A_{YY} < 0$

corresponding to the Y^+ EPR transition or

$\nu_{ENDOR}(0) = \nu_H$

$\nu_{ENDOR}(-1) = \nu_H + A_{YY}$ if $A_{YY} > 0$ or $\nu_{ENDOR}(-1) = \nu_H - A_{YY}$ if $A_{YY} < 0$

corresponding to the Y^- EPR transition.

Analogue conditions hold for X and Z transitions.

Several conclusions can be carried out from the inspection of the energy level diagram: (i) the ENDOR transitions corresponding to the $\Delta mS = \pm 1$ EPR transitions in the low-field spectrum are reflected on the opposite side in the high-field spectrum in relation to ν_H; (ii) the resulting ENDOR spectra are asymmetric because of the orientation selection; (iii) the line at resonance frequency ν_H is common for all protons and thus attains a high intensity and (iv) once the sign of D is known, as for lutein, the sign of the hfcs can be directly read from the spectrum.

The sign and the absolute value of the hfcs are very important quantities since they allow to identify the type of protons and they are directly related to the spin density distribution. From theoretical consideration, rotating methyl groups are expected to show up positive hfcs with axial symmetry and an anisotropy less than 10% of the respective isotropic hfcs. Furthermore the largest values is expected along the $C\text{-}CH_3$ bond direction, which should correspond to the ZFS X axis canonical orientation. On the other hand, the majority of the α-protons hfcs are expected to be negative and characterized by broad features because of their anisotropy; positive α-protons hfcs should have small absolute values.

The ENDOR spectra corresponding to both Y transitions show two set of well-resolved and structured signals, one of them is located in the positive couplings region and the other in the negative region. The expected symmetry between the two spectra about the ν_H line is clearly visible. The most intense signals present in the

positive region and corresponding to A_{YY} = 8.1 MHz and A_{YY} = 6.6 MHz can be attributed to rotating methyl groups directly bound to the conjugated chain [Di Valentin et al 2008b]. Those signals also present minor splitting (figure 2 panel C) that reveal some protein-induced molecular distortion of the lutein moiety that make the two pairs of methyl groups not exactly symmetric. In addition at A_{YY} = 9.6 MHz, corresponding to an hfc higher than the strong methyl groups lines, there is a weaker signal: on the basis of the literature hfcs for ^{T}Chl [Di Valentin et al. 1996, Lendzian et al. 2003] and since α-protons hfcs when positive are smaller than the ones of methyl groups, we attribute this transitions to one of the methyl groups of the unquenched ^{T}Chl visible in the ESE spectrum. In principle this signal could also be attributed to one of the four methyl groups present in lutein structure but it would represent a severe structural distortion for the almost symmetric structure of the lutein molecule. Another broad signal is present with A_{YY} = 4.2 MHz which is attributed again to ^{T}Chl only on the basis of DFT calculations as it would be discuss in the next section. Finally, some signals near the free proton line are also detected but it is worth noting that Davies-ENDOR spectroscopy is not very sensitive to small hfcs. The ENDOR transitions present in negative hfcs region (A_{YY} = -5.1 MHz, A_{YY} = -7.6 MHz, A_{YY} = -9.9 MHz and A_{YY} = -10.9 MHz) are quite broad and can be attributed to α-protons.

Figure 3 reports the experimental Davies-ENDOR spectra for all the three canonical orientations (X^+, Y^+ and Z^+) of the photo-excited triplet state of lutein in LHC-II at 20 K. All the spectra show, besides the strong line at ν_H, both positive and negative hyperfine couplings. The ENDOR spectrum corresponding to the Y^+ transition is the same as figure 2 and is report here for direct comparison with the other transitions.

The ENDOR spectrum corresponding to Z^+ transition shows two set of signals in the low RF (radiofrequency) region (around hfcs = 4 MHz or hfcs = 8 MHz), an unresolved structure near the free proton line and one broad and unstructured signal in the high RF region (A_{ZZ} = -6.2 ± 1.4 MHz). The strongest and more positive hfcs are attributed to the A_{ZZ} component of methyl groups (A_{ZZ} = 7.5 MHz and A_{ZZ} = 9.4 MHz): even though these signals are not split, they are not perfectly symmetric, as in the caso of the Y transitions. The other signals, present in both regions, can be attributed to α-protons because they are less intense and broader.

The ENDOR spectrum corresponding to the X^+ transition is more noisy due to the low initial polarization of the EPR signal at this orientation. The spectrum is quite crowded and it exhibits also signals with opposite polarization. This is due to the fact that this transition is the most affected by chlorophyll contributions: at the magnetic field corresponding to X^+ the ^{T}Lut spectrum is polarized in absorption, while the ^{T}Chl spectrum is polarized in emission [Di Valentin et al. 2009]. This explains why the free proton line has opposite sign with respect to the strongest hfcs transitions of the lutein triplet. The signals with the same polarization of the free proton line are attributed to the ^{T}Chl and are marked with asterisks in figure 3.

The lutein triplet signals are the following: A_{XX} = 9.5 MHz and A_{XX} = 8.1 MHz assigned to methyl groups couplings, A_{XX} = 3.2 MHz, A_{XX} = 1.8 MHz, A_{XX} = -2.2 MHz and A_{XX} = -6.6 MHz attributed to α-protons.

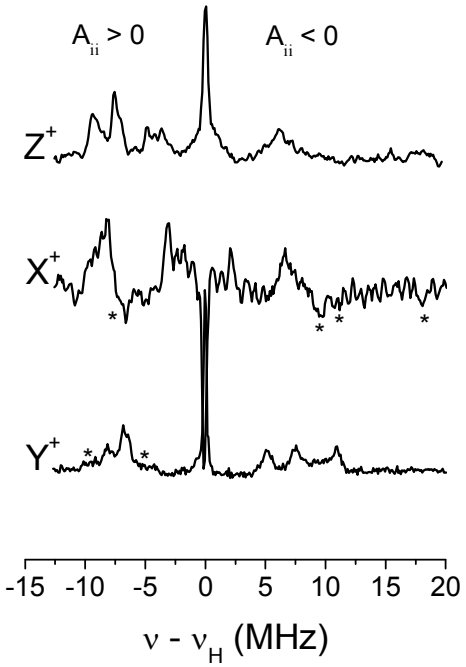


Figure 3: Photoexcited triplet state ENDOR spectra of LHC-II sample from *S.oleracea* with DAF = 50 ns and at 20 K. The figure reports the ENDOR spectra relative to the three transitions belonging to plus manifold (see figure 2). The frequency scale gives the deviation from the ν_H and the hfcs correspond to the shift between the corresponding ENDOR line and the ν_H. According to the energy level scheme present in figure 2, the ENDOR lines have been labeled as positive or negative. The lines relative to the unquenched chlorophyll triplet contributions are marked with an asterisks in all spectra.

To summarize, in the low RF side of all spectra a couple of intense lines corresponding to positive hfcs is visible which have been assigned to rotating methyl protons: A_{XX} = 8.1 MHz / A_{YY} = 6.6 MHz / A_{ZZ} = 7.5 MHz and A_{XX} = 9.5 MHz / A_{YY} = 8.1 MHz / A_{ZZ} = 9.4 MHz. From the experimental hfcs values, the isotropic contribution can be directly calculated: a_{sio} = 7.4 MHz and a_{sio} = 9.0 MHz. As expected the more anisotropic component is A_{XX} (C-CH_3 bond direction) and the anisotropy is not larger than 10% of the relative a_{sio}. Other signals related to both positive and negative hfcs are also present in all the spectra, indicating a negative and positive pattern of the spin density along the π-system. All these hfcs can be attributed to the α-protons directly bound to the polyene chain. The other methyl groups and the other protons present on the terminal rings are expected to not contribute to the ENDOR spectra since they are unconjugated.

Table 1 summarize the hfcs values as derived from the experiments at X, Y and Z canonical orientation in the ZFS frame. It is useful to remind that the ZFS and hfc tensor axes for α-protons and for the two sets of rotating methyl protons can be consider collinear within ± 10° so the measured hfcs are the diagonal components of the hyperfine tensors.

Table 1: Comparison between the experimental and the computed hfcs for the carotenoid lutein triple state in LHC-II. The atom positions are define according to figure 1.

Position	**Experimental values (MHz)**				**Computed values (MHz)**			
	A_{XX}	A_{YY}	A_{ZZ}	a_{iso}	A_{XX}	A_{YY}	A_{ZZ}	a_{iso}
1	-5.4*	-7.6	-6.2#	-6.4	-4.0	-6.3	-8.3	-6.2
1’					-4.0	-6.1	-8.2	-6.1
2	3.2	0.9	3.6	2.6	2.2	1.5	3.5	2.4
2’					2.3	1.6	3.6	2.5
4	3.2	0.9	4.8	3.0	2.3	1.7	4.4	2.8
4’					2.3	1.6	4.5	2.8
5	-6.6	-10.9	---	---	-4.5	-10.0	-13.1	-9.2
5’					-4.6	-10.2	-13.4	-9.4
6	1.8	0†	1.3£	1.0	1.7	0.2	3.2	1.7
6’					1.6	0.0	2.8	1.5
8	0†	-5.1	-1.3£	-1.3	0.2	-3.9	-2.6	-2.1
8’					0.1	-4.4	-3.3	-2.6
9	-2.2	-9.9	---	---	-2.8	-8.8	-10.3	-7.3
9’					-2.5	-8.3	-9.9	-6.9
Me-3	8.1	6.6§	7.5	7.4	7.2	6.1	6.8	6.7
Me-3’					7.4	6.2	7.1	6.9
Me-7	9.5	8.1	9.4	9.0	10.1	7.9	8.7	8.9
Me-7’					9.7	7.7	8.7	8.7

*present only in ENDOR spectrum at DAF = 9 μs
† Unresolved near the ν_H transition
§ a minor splitting is present in the spectra
…… # broad signal -6.2 ± 1.4 MHz
£ broad ν_H ± 1.3 MHz

As it is clearly visible by simple inspection of figure 3 and of table 1, we found experimentally less signals than those we expected on the basis of the lutein molecular structure (figure 1): this could mean that some ENDOR signals are missing or that the spin density on lutein triplet state has some symmetry properties. Of course, this is not obvious since the conjugated system extend over just one of the terminal rings but not on the other braking the overall symmetry. By inspecting the x-ray structure we hypothesize that the last conjugated double bond present in one of the terminal rings is not conjugated and does not contribute to the π-system: this lowers the number of conjugated double bonds from 10 to 9 but increases the symmetry of the delocalized system.

In the low and high RF regions of X^+ ENDOR spectrum signals with inverted polarization are also present: these signals can be attributed to the unquenched ^{T}Chl present in the isolated LHC-II preparation [Di Valentin et al. 2009]. To get insight into this issue, we performed ENDOR experiments also at DAF longer than 50 ns. In fact, while the carotenoid X transition is expected to invert its spin-polarization at longer DAF, the chlorophyll triplet at the same field will preserve the same polarization. It is known that in photosynthetic systems, all carotenoid triplet states present a polarization pattern *eaeaea* at long DAF [Carbonera et al. 1996, 1997] and thus change their initial polarization; on the other hand chlorophyll triplet states do not change their polarization at long DAF [Plato et al. 1991]. To an inversion in the initial polarization of the ESE spectrum corresponds an inverted polarization also of the hfcs signals.

In figure 4 the ENDOR spectrum corresponding to X^+ at DAF = 50 ns is compared with the same spectrum recorded at DAF = 9 μs. It is clearly visible that while some transitions invert their sign at longer DAF (lutein hfcs), some others do not (chlorophyll hfcs). The chlorophyll hfcs are marked by dotted lines. Moreover, at longer DAF at least one new signal becomes detectable (A_{XX} = -5.4 MHz) and it is highlighted in figure 4 by an arrow. We make the hypothesis that both the lutein and chlorophyll triplet states contribute to this signal since this line is not detectable at short DAF when their polarization is opposite but it became visible at longer DAF when the polarizations sum up.

No signals ascribable to unquenched ^{T}Chl have been found in correspondence to the Z transition field, as expected considering the TR-EPR spectral reconstruction of

LHC-II triplet, reported in [Di Valentin et al. 2009]. As a matter of fact, the chlorophyll triplet-state spectrum does not overlap with the Z transitions of the lutein triplet-state spectrum. The hfcs signals found in photoexcited ENDOR spectra of LHC-II experimentally assignable to chlorophyll triplet can be summarized as follows: A_{YY} = + 9.6 MHz, A_{XX} = +6.6 MHz, -5.4 MHz (only at DAF = 9 μs), -8.4 MHz, -9.4 MHz, -10.6 MHz and -17.8 MHz. Since the orientation of the unquenched molecule(s) with respect to the ZFS axes of the lutein triplet state is(are) not known we can not assign these hfcs to a particular ZFS transition of the chlorophyll triplet state.

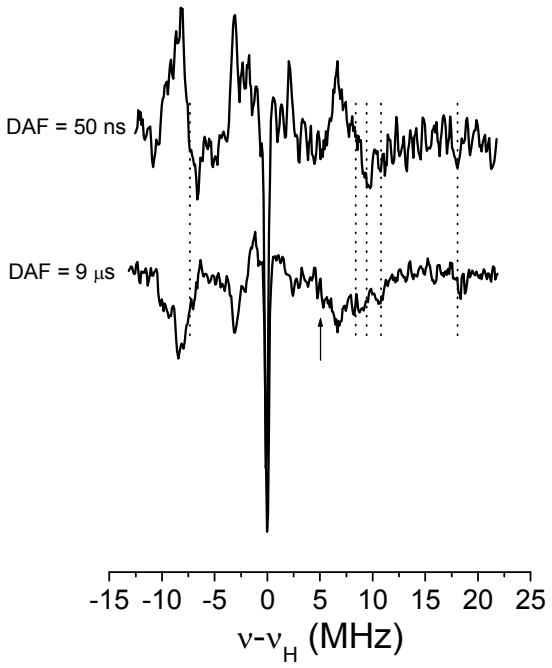


Figure 4: Pulsed Davies-ENDOR spectra of LHC-II sample from *S.oleracea* at 20 K for the X^+ transitions at different delay with respect to the laser pulse: DAF = 50 ns for the upper spectrum and DAF = 9 μs for the lower spectrum, all other experimental conditions are the same. The vertical lines show the time evolution of chlorophyll ENDOR transitions. The frequency scale gives the deviation from the ν_H and the hfcs correspond to the shift between the corresponding ENDOR line and the ν_H.

These experimental finding are in line with previous ENDOR experiments on chlorophyll [Di Valentin et al. 1996, Lendzian et al. 2003] and bacteriochlorophyll [Marchanka et al. 2009] triplet states where the number of observed hfcs is much smaller than those observed for the cation and anion radicals [Sinnecker et al. 2002,

Lendzian et al. 2003] and expected from theoretical calculations. The ENDOR spectra of chlorophyll *a* triplet state in organic solvent [Lendzian et al. 2003] or in polymeric matrix [Di Valentin et al. 1996] typically show one line corresponding to positive hfc around 8-9 MHz assigned to the methyl group connected to ring 3 and few negative hfcs between –6 MHz and –11 MHz attributed to methine protons.

3.3 Quantum mechanical computations

In order to assign all the hfcs experimentally found and to draw a clearer picture about the electronic properties of the triplet state of the lutein carotenoid in LHC-II we performed DFT calculations using theory levels that have been validated in a number of studies [Improta et al. 2004, Di Valentin et al. 2008b]. The calculations were performed on the whole Lut-Chl complex, considering the Chl603/Lut621 and Chl613/Lut620 couples involved in TTET as previously demonstrated [Di Valentin et al. 2009]. These lead to the identification of two low-lying triplet states (as for Per-Chl couple in PCP [Di Valentin et al. 2008b]) localized respectively on the chlorophyll and lutein moiety. The spin density of the triplet localized on lutein in the complex is indistinguishable from that obtained for the isolated lutein in the same geometry (as it is for the chlorophyll triplet state, not shown): the Mulliken spin densities computed in this latter case are shown in figure 5. DFT calculations confirm the hypothesis made on the basis of the x-ray structure inspection and of the ENDOR data: the terminal double bond does not show a significant spin density as it is not involved in the π-system.

The Mulliken spin densities have been computed also for the triplet state of the peridinin molecule embedded in a dielectric medium (ε = 3.0) and reported in Figure 6 for a proper comparison with the one calculated for lutein.

Looking at figure 5 and 6, a rough prediction on the relative values of hfcs can be done: in a first approximation, the isotropic hfc constants of hydrogen atoms lying in the nodal plane of π open-shell systems are proportional to the spin density of the carbon atoms to which they are attached, because of the spin polarization mechanism. For methyl groups lying out the nodal plane there is a direct contribution from singly occupied orbitals leading to quite large and positive hfcs.

A tentative assignment of the measured couplings to molecular position in lutein structure is achieved comparing with DFT calculation of the hfc tensors, see table 1.

The assignment is made considering the symmetry of the conjugated chain as derived by DFT computation: thus excluding any involvement of the last double bond present on the terminal ring. The computed couplings are the mean value of the hfcs relative to the two luteins presents in each LHC-II monomer.

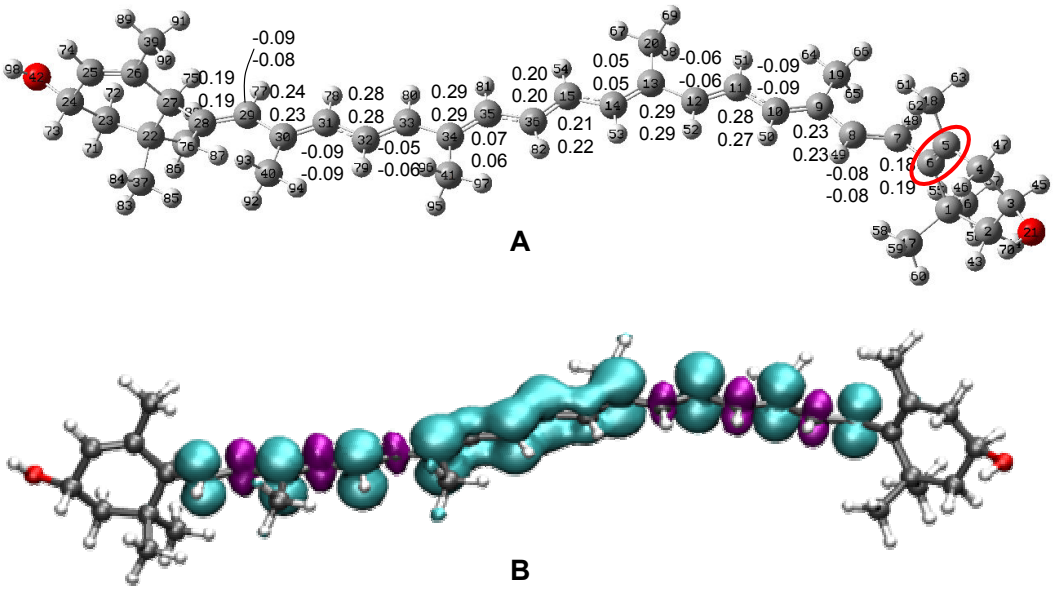


Figure 5: (A) Computed spin densities (B3LYP/EPR-II) for the excited triplet state localized on Lut620/Lut621. The unconjugate double bond present on the terminal ring is highlighted. (B) Mulliken spin densities computed at the B3LYP/EPR-II level for the triplet of Lut620 are reported on the lutein molucular skeleton. All the atoms are at the experimental X-ray geometry, except for methyl groups and hydrogens atoms (see Materials and Methods and Results sections for details). Only densities larger than 0.02 (in absolute value) are reported.

The computed values for methyl groups are in remarkable agreement with the experiment. We can therefore unequivocally assign the large positive hfcs measured in the ZFS axes directions to two sets of equivalent methyl protons: the largest a_{iso} = 9.0 MHz can be attributed to methyl 7 and a_{iso} = 7.4 MHz to methyl group 3 (for the molecular positions see Fig. 1B).

The triplet state studied above is obtained by an HOMO→LUMO excitation with one unpaired electron is present in each the HOMO and LUMO orbitals. In same cases, when the HOMO-1 is nearby in energy, the triplet state might in part, comprise an HOMO-1→LUMO excitation.

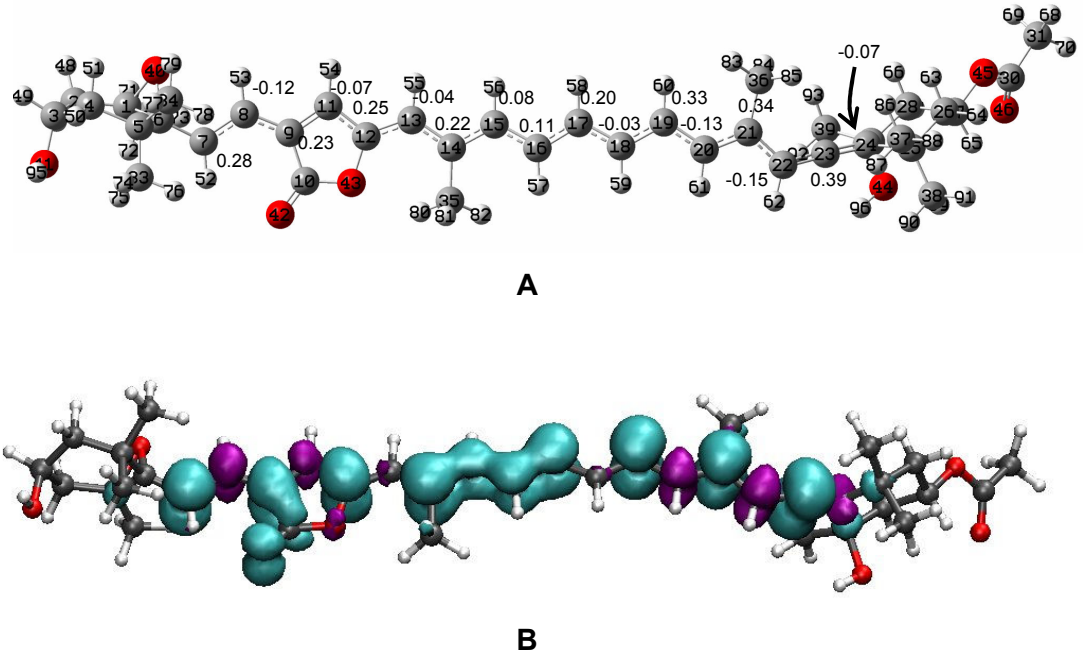


Figure 6: (a) Computed spin densities (B3LYP/EPR-II) for the excited triplet state localized on the Per614 (b) Mulliken spin densities computed at the B3LYP/EPR-II level for the triplet of peridinin are reported on the carotenoid molucular skeleton. All atoms are at the experimental X-ray geometry, except for methyl groups, allene moiety and hydrogen atoms (see ref. [Di Valentin et al. 2008b] for details). Only densities larger than 0.02 (in absolute value) are reported

Although the difference between the HOMO-1 and the HOMO orbitals is about 0.03 a.u. and the mixing of these orbitals is unlikely the triplet wave function with respect to participation of the HOMO, HOMO-1 and LUMO has been theoretically investigated by redistributing the unpaired electrons over the set of frontier orbitals (HOMO-1,HOMO and LUMO).

In table 2 the isotropic coupling constants considering a pure HOMO→LUMO excitation, a pure HOMO-1→LUMO transition and a 50% HOMO→LUMO and 50% HOMO-1→LUMO transition are reported for the Lut620 molecule.

In the latter case, the isotropic hyperfine coupling constants have been computed by using the equation:

$$a_{iso}(H) = \cos^2\varphi \cdot a_{H,L}(H) + \sin^2\varphi \cdot a_{H-1,L}(H)$$

Where φ determines the amount of mixing (φ=0° corresponds exclusively to a HOMO→LUMO excitation and φ=90° corresponds exclusively to a HOMO-1→LUMO excitation) and $a_{H,L}(H)$ and $a_{H-1,L}(H)$ are the isotropic coupling constants for pure HOMO→LUMO and HOMO-1→LUMO excitations.

The good agreement between the hyperfine coupling constants measured experimental and those computed by considering a pure HOMO→LUMO excitation confirms that the triplet state of the Lutein molecule is not mixed with the HOMO-1→LUMO excitation.

Table 2. Calculated Isotropic Hyperfine Couplings (of Lut620 for a pure HOMO→LUMO excitation, a pure HOMO-1→LUMO excitation and 50% HOMO→LUMO and 50% HOMO-1→LUMO excitation. The atom positions are define according to figure 1.

Position[a]	a_{iso} **(MHz)**			
	H→L	**H-1→L**	**50% H→L 50% H-1→L**	**Exp.**
1	-6.0	-7.3	-6.6	-6.4
1’	-6.1	-7.3	-6.7	
2	2.6	1.9	2.2	2.6
2’	2.5	1.7	2.1	
4	2.8	-2.0	0.4	3.0
4’	2.6	-1.7	0.4	
5	-9.2	-4.5	-6.8	---
5’	-9.1	-4.6	-6.9	
6	1.4	-5.9	-2.2	1.0
6’	1.1	-5.4	-2.1	
8	-2.3	-4.5	-3.4	-1.3
8’	-2.7	-4.6	-3.6	
9	-7.3	-3.1	-5.2	---
9’	-7.0	-3.0	-5.0	
Me-3	6.6	6.8	6.7	7.4
Me-3’	6.9	6.7	6.8	
Me-7	8.5	1.3	4.9	9.0
Me-7’	8.2	1.3	4.8	

The HOMO, HOMO-1 and LUMO are depicted in figure 7 for both the lutein and peridinin molecules. The orbitals are similar and they are distributed evenly over the carotenoid skeleton of the two molecules. However, looking at the LUMO orbital it seems that the electron density decays slightly faster for lutein at the extremities of the chain while the lactonic ring in the peridinin molecule contrasts the reduction of the electron density.

The population analysis of the frontier orbitals reveals that the p atomic orbitals of carbon 8 and 9 (See Fig. 1 for the numbering) provide the highest contribution (expanding coefficient of 0.10) to the LUMO of lutein while carbon 12 contributes more (coefficient of 0.11) to the LUMO of peridinin. The other p atomic orbitals having expanding coefficients less than 0.09.

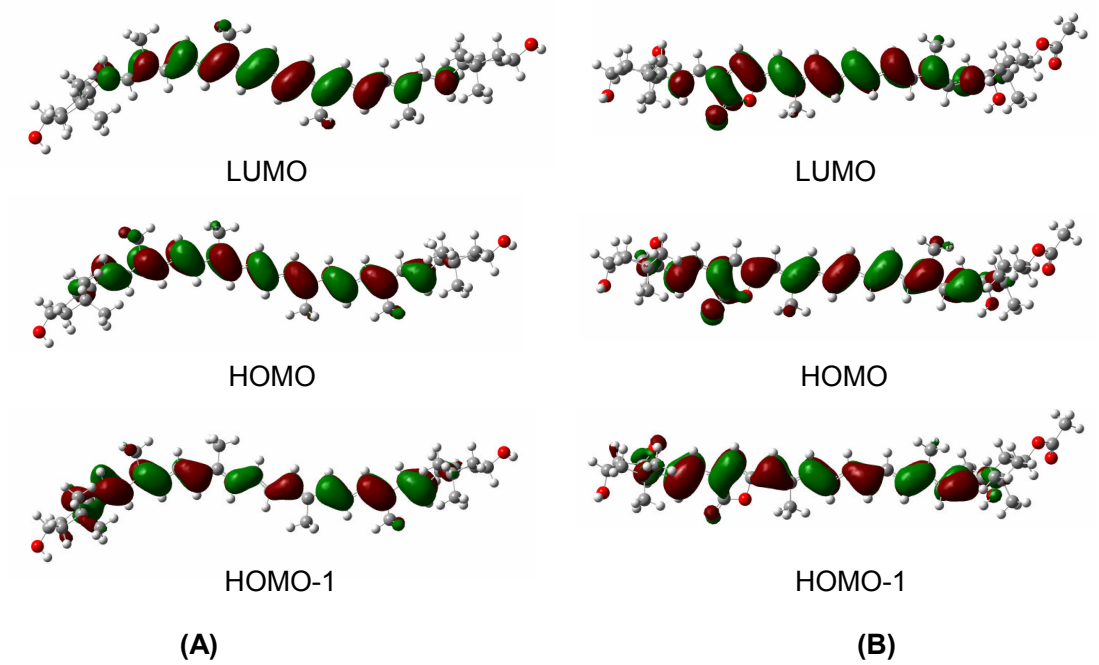


Figure 7: Kohn-Sham HOMO-1, HOMO and LUMO orbitals for (a) lutein and (b) peridinin molecules, respectively.

4. Discussion

Triplet-triplet energy transfer is the fastest photo-protection mechanisms evolved by photosynthetic organisms to prevent photo-oxidative damages. This process is active when chlorophyll triplet and or singlet oxygen are formed under light stress conditions. Carotenoid molecules play the important role of quenching via TTET the ^{T}Chl avoiding in this way singlet oxygen formation. To fulfil this task carotenoids must be in van der Waals contact with the chlorophyll moiety since a large spatial overlap between the carotenoid and chlorophyll wave-functions is needed. Detailed knowledge of the interaction between the two partners is particularly meaningful for the comprehension of pigments interaction *in vivo* and, in the future, for the development or the implementation of organic-based photovoltaic cells. In fact the introduction of well-designed carotenoid molecules in the photovoltaic devices could contribute to a higher photo-conversion and to a longer duration.

In this work we extend the approach adopted to investigate the electronic structure of the triplet state of the peridinin in PCP [Di Valentin 2008a, 2008b, 2008c, 2010] to lutein in LHC-II from *S. oleracea*. We already demonstrated that in LHC-II a

specific Lut-Chl pair (Lut620/Chl612 and Lut621/Chl603) is appointed to quench chlorophyll triplet state [Di Valentin et al. 2009]. In this contribution, we complete our study on the TTET in LHC-II mapping the spin density and the electronic distributions of the lutein photo-excited triplet state by ENDOR spectroscopy and DFT calculations. The detailed knowledge of the spin density distribution and, above all, of the electron density distribution in the triplet state of the pigments involved in the photoprotection mechanism is fundamental to point out the key features that account for an efficient TTET.

ENDOR measurements at all canonical orientations, where the static magnetic field is parallel to the ZFS tensor axes, has allowed us to obtain a suitable description of the hfcs of α and β protons bound to the conjugate chain. For each transition, several positive and negative hfcs have been detected indicating a non uniform spin density pattern along the conjugated system. The higher and positive hfcs are attributed to two different couple of rotating methyl groups, while the more anisotropic positive and negative signals are attributed to α-protons. Some ENDOR transitions detectable in Y and X transitions spectra have been assigned to the unquenched chlorophyll triplet observable in TR-EPR and ESE-detected spectra of LHC-II sample [Di Valentin et al. 2009].

DFT predictions (at level B3LYP/EPR-II) are in good agreement with the experimental hfcs values. However, even taking into account the molecular symmetry of lutein, some of the large and negative hyperfine components, predicted by DFT computation and belonging to α-protons, are missing in the ENDOR spectra. By comparison between experiments and calculations a tentative assignment of all the measured couplings has been made (see table 1).

In our previous works on PCPs from dinoflagellates we demonstrated that the triplet state is localized on one specific peridinin molecule which is responsible for triplet energy dissipation [Di Valentin 2008a, 2010]. Also we provided a detailed picture of spin density distribution on the peridinin photo-exicted triplet state in those proteins by means of ENDOR spectroscopy and DFT calculations [Di Valentin et al. 2008b]. Since all the experimental hfcs have been assigned to protons belonging to the peridinin molecule we conclude that on ENDOR experiments time scale the triplet is completely localized on one peridinin molecule. Moreover, no indication for any Per-Chl delocalization is came out from DFT calculations. While Niklas et al. [Niklas et

al. 2007] confirm these findings considering independently ENDOR experiments on reconstituted PCP, van Gronedelle's group propose a delocalized triplet model between peridinin and the adjacent Chl molecule to interpret step-scan Fourier transform infrared spectroscopy on PCP from *A. carterae* [Alexandre et al. 2007] and on *H. pygmaea* [Bonetti et al. 2009]. On the other hand, coupling the same infrared spectroscopic approach and DFT computations Mezzetti et al. [Mezzetti et al. 2008] support our results. Starting from the knowledge that a specific Lut-Chl pair (Lut620/Chl612 and Lut621/Chl603) is involved in TTET [Di Valentin et al. 2009], in this contribution we have investigated the electronic nature of the lutein triplet state: both DFT calculations and ENDOR spectroscopy on the LHC-II complex strongly support the localization of the excited triplet state. Although some of the hfcs lines visible in the ENDOR spectra (figure 3) are attributed to the unquenched ^{T}Chl detectable in the TR-EPR spectrum [Di Valentin et al. 2009], this experimental fact does not imply that the triplet state is delocalized between the chlorophyll and the lutein moieties. In fact, the experimental TR-EPR and ESE spectra can be satisfactory simulated taking into account two different contributions one relative to lutein and the other relative to Chl: the simulation parameter are in agreement with those reported for isolated Chl and Car species [Plato et al. 1991]. Any delocalization between the two molecules should produce a variation in the ZFS parameters. Above all, the hfcs assigned to ^{T}Chl in the ENDOR spectra, are compatible with the triplet-state hfcs of the chlorophyll monomer in organic solvent [Lendzian et al. 2003] or in polymeric matrix [Di Valentin et al. 1996] as reported by other authors. This means that no delocalization between the chlorophyll and the lutein moieties occurs, in fact a triplet state shared between two different molecules should exhibit hfcs different from the monomeric counterparts [Lendzian et al. 1998]. With similar argumentations, it has been demonstrated that ^{3}P680 is localized on just one of the chlorophyll molecules that make up the special pair [Lendzian et al. 2003]. All these experimental findings are supported by DFT calculations which have been performed on the chlorophyll-lutein complex .

DFT calculations show that the spin density of the triplet localized on lutein in the complex is indistinguishable from that obtained for the isolated lutein in the same geometry and also for the isolated chlorophyll triplet state. The unpaired spins are quite delocalized over the whole conjugated system of the lutein molecule: the

pattern is alternate with positive spin density followed by gradually smaller negative spin densities. This alternate pattern is lost in the central region of the conjugated chain where all positive spin densities are predicted. Similar behaviour has been calculated for carotenoid radical cations employing B3LYP hybrid DFT methods [Himo 2001, Guo et al. 2002]. More intriguing the same pattern has been found for the carotenoid peridinin in PCP antenna complex [Di Valentin et al. 2008b]: the peridinin triplet state spin density is distributed over all the π-system with an alternate pattern which is lost in the central region where the densities are all positive and have the highest values. No particular differences between the two carotenoid triplet spin density distributions can be highlighted.

The overall agreement between the computed and the experimental hyperfine couplings allow us to draw some conclusions about the triplet state electronic distribution in the frontier orbitals. First of all, the hfc experimental constrain has allowed us to prove that for both the lutein and peridinin triplet state is well-described by an HOMO→LUMO excitation with one unpaired electron is present in each the HOMO and LUMO orbitals. can be used to define which molecular orbitals are involved in the triplet state. Any contribution from the HOMO-1→LUMO, that have been found to contribute significantly to bacteriochlorophylls triplet state [Marchanka et al. 2009], can be neglected.

The redistributing of the unpaired electrons over the set of frontier orbitals has a central meaning in defining the requirements for efficient TTET. Formally the TTET can be describe as a simultaneous two-electrons transfer, i.e. the matrix element determining the rate in triplet transfer is a four-orbitals two-electrons exchange integral [Closs et al. 1988, 1989]:

$$V_{TTET} = \left\langle \psi^{D}_{LUMO}(1)\psi^{A}_{HOMO}(2) \left| e^2/r_{12} \right| \psi^{A}_{LUMO}(1)\psi^{D}_{HOMO}(2) \right\rangle .$$

Therefore, to calculate properly the exchange integral the electronic wave-functions involved must be properly described. The best and less ambiguous way is to constrain the theoretical calculation with experimental data. ENDOR spectroscopy provides extremely specific constrains for the carotenoid triplet state wave-functions, as proved in this investigation and previously [Di Valentin et al. 2008b]. Note that, our data give access only to the carotenoid triplet state electronic distribution: the TTET is too fast compare to the instrumental time-resolution and we cannot get any

information about the donor chlorophyll triplet state. The information on the chlorophyll triplet state has to be constrained in a different way.

As depicted in figure 7, the HOMO and LUMO electron densities are distributed all over the conjugated chain for both the lutein and peridinin moieties. The oxygen-containing substituents present in peridinin do not alter such a pattern. On the other hand, while in peridinin the electron density is almost equally distributed along all the conjugated chain, for the lutein the electron density becomes smaller at the edges near the terminal rings.

In our previous papers on TTET in PCP [Di Valentin et al. 2008a] and LHC-II [Di Valentin et al. 2009] we found that the Chl/Car couples involved in the photoprotection mechanisms are those characterized by the shortest centre – to – centre distance between π-systems and by and by the presence of a molecular bridge (a water molecule in PCP or an aminoacid residue His coordinating Chl603 and Asn coordinating Chl612 in LHC-II) inserted between the donor and the acceptor. As already pointed out in these studies, all the possible Chl/Car couples show van der Waals contacts, although in different molecular regions. In the present investigation, DFT calculations prove that the electron density is almost equally distributed all over the conjugated system, although the central region of the conjugated chain is indeed an high electron density region. The most relevant outcome of the DFT calculations is that the carbon atoms with the highest contribution to the LUMO molecular orbital (C8 for the lutein and C12 for the peridinin, for the nomenclature see figure 1 and [Di Valentin et al. 2008b]) are indeed those in closest contact with the molecular bridge. This result strengthens the hypothesis that TTET in both LHCII and PCP antenna complexes can be properly described as a super-exchange mechanism and that the molecular bridge is an important molecular feature in the selection of the most efficient energy transfer pathways [Di Valentin et al. 2008a, 2009].

As a conclusive remark, the use of advanced EPR techniques has allowed to properly described the triplet state of the carotenoid pigments involved in the photo-protection mechanism. The triplet state is localized on carotenoids which fulfil specific structural requirements. These carotenoids are characterized by the closest center-to-center distance with the nearby chlorophyll and are interfaced to the chlorophyll through a molecular bridge. The comparison between the lutein and peridinin clearly shows how singlet states behaviours are much more influenced by the chemical

structure than triplet state properties. The triplet-state spin density and the electronic density distributions do not show any significant dependence on the chemical nature of the carotenoid.

5. References

[Alexandre et al. 2007] Alexandre M. T. A., Luhrs D. C., van Stokkum I. H. M., Hiller R., Groot M. L., Kennis J. T. M., Van Grondelle R., *Biophys. J.*, **2007**, 93, 2118-2128

[Barone 1994a] Barone V., , *J. Chem. Phys*., **1994**,101, 10666–10676.

[Barone 1994b] Barone V., *J. Chem. Phys*., **1994**, 101, 6834–6838.

[Barone et al. 2010] Barone V., Cimino P., Pedone A., *Magnetic Resonance in Chemistry*, **2010**, 48, S11-S22

[Becke et al. 1993] A. D. Becke, *J. Chem. Phys.*, **1993**, 98, 5648-52.

[Bonetti et al. 2009] Bonetti C., Alexandre M. T. A., Hiller R .G., Kennis J. T. M., van Grondelle R., *Chemical Physics*, **2009**, 375(1-3), 63-69

[Carbonera et al. 1996] Carbonera D., Di Valentin M., Corvaja C., Giacometti G., Agostini G., Liddell P. A., Moore A. L., Moore T. A., Gust D., *Photochem. Photobiol.*, **1996**, 105, 329-335

[Carbonera et al. 1997] Carbonera D., Di Valentin M., Agostini G., Giacometti G., Liddell P. A., Gust D., Moore A. L., Moore T. A., *Appl. Magn. Res*., **1997**, 13, 487-504

[Closs et al. 1988] Closs G. L., Piotrowiak P., MacInnis J. M., Fleming G. R., *J. Am. Chem. Soc.*, **1988**, 110, 2652-2653

[Closs et al. 1989] Closs G. L., Johnson M. D., Miller J. R., Piotrowiak P., *J. Am. Chem. Soc.*, **1989**, 111, 3751-3753

[Dexter 1953] Dexter D. L*., J. Chem. Phys*., **1953**, 21, 836-850

[Di Valentin et al. 1996] Di Valentin M., Kay C. W. M., Giacometti G., Möebius K., *Chem. Phys. Letters*, **1996,** 248, 434-441

[Di Valentin et al. 2008a] M. Di Valentin, S. Ceola, E. Salvadori, G. Agostini, D. Carbonera, *Biochim. Biophys. Acta*, **2008**, 1777, 186–195.

[Di Valentin et al. 2008b] M. Di Valentin, S. Ceola, G. Agostini, G. M. Giacometti, A. Angerhofer, O. Crescenzi, V. Barone, D. Carbonera, *Biochim. Biophys. Acta*, **2008**, 1777, 295-307

[Di Valentin et al. 2008c] Di Valentin M., Ceola S., Salvadori E., Agostini G., Giacometti G. M., Carbonera D., *Biochim. Biophys. Acta*, **2008**, 1777, 1355-1363

[Di Valentin et al. 2009] Di Valentin M., F. Biasibetti, S. Ceola, D. Carbonera, *J. Phys.Chem*. *B*, **2009**, 113, 13071-13078

[Di Valentin et al. 2010] Di Valentin M., Salvadori E., Ceola S., Carbonera D., *Appl. Magn. Reson*., **2010** 37:191-205

[Frick et al. 1990] Frick J., von Schütz J. U., Wolfe H. C., Kothe G., *Mol. Liq. Crys.*, **1990**, 183, 269-272

[Frisch et al. 2004] Gaussian 03, Revision C.02, M. J. Frisch, G. W. Trucks, H. B. Schlegel, G. E. Scuseria, M. A. Robb, J. R. Cheeseman, J. A. Montgomery, Jr., T. Vreven, K. N. Kudin, J. C. Burant, J. M. Millam, S. S. Iyengar, J. Tomasi, V. Barone, B. Mennucci, M. Cossi, G. Scalmani, N. Rega, G. A. Petersson, H. Nakatsuji, M. Hada, M. Ehara, K. Toyota, R. Fukuda, J. Hasegawa, M. Ishida, T. Nakajima, Y. Honda, O. Kitao, H. Nakai, M. Klene, X. Li, J. E. Knox, H. P. Hratchian, J. B. Cross, V. Bakken, C. Adamo, J. Jaramillo, R. Gomperts, R. E. Stratmann, O. Yazyev, A. J. Austin, R. Cammi, C. Pomelli, J. W. Ochterski, P. Y. Ayala, K. Morokuma, G. A. Voth, P. Salvador, J. J. Dannenberg, V. G. Zakrzewski, S. Dapprich, A. D. Daniels, M. C. Strain, O. Farkas, D. K. Malick, A. D. Rabuck, K. Raghavachari, J. B. Foresman, J. V. Ortiz, Q. Cui, A. G. Baboul, S. Clifford, J. Cioslowski, B. B. Stefanov, G. Liu, A. Liashenko, P. Piskorz, I. Komaromi, R. L. Martin, D. J. Fox, T. Keith, M. A. Al-Laham, C. Y. Peng, A. Nanayakkara, M. Challacombe, P. M. W. Gill, B. Johnson, W. Chen, M. W. Wong, C. Gonzalez, and J. A. Pople, Gaussian, Inc., Wallingford CT, **2004**.

[Guo et al. 2002] Guo J. D., Luo Y., Himo F., *Chem. Phys. Letters*, **2002**, 366, 73-81

[Himo 2001] Himo F., *J. Phys. Chem*., **2001**, 105, 7933-7937

[Improta et al. 2004] R. Improta, V. Barone, *Chemical Reviews*, **2004**, 104, 1231-1253

[Lee et al. 1988] C. Lee, W. Yang, and R. G. Parr, *Phys. Rev. B*, **1988**, 37, 785-89.

[Lendzian et al. 1998] Lendzian F., Bittl R., Lubitz W., *Photosynth. Res*, **1998**, 55, 189-197

[Lendzian et al. 2003] Lendzian F., Bittl R., Telfer A., Lubitz W., *Biochim. Biophys. Acta*, **2003**,1605, 35-46

[Liu et al. 2004] Liu Z., Yan H., Wang K., Kuang T., Zhang J., Gui L., An X., Chang W., *Nature,* **2004**, *428*, 287-292.

[Marchanka et al. 2009] Marchanka A., Lubitz W., van Gastel M., *Phys. Chem. B*, **2009**, 113, 6917-6927

[Mezzetti et al. 2008] Mezzetti A., Spezia R., *Spectroscopy-an international journal*, **2008**, 22(4), 235-250

[Mozzo et al. 2008] Mozzo, M.; Dall'Osto, L.; Hienerwadel, R.; Bassi, R. Croce, R. *J. Biol. Chem.* **2008**, *283*, 6184-6192.

[Müller et al. 2001] Müller P., Li X. P., Niyogi K. K., *Plant. Physiology*, **2001**, 125, 1558-1566.

[Niklas et al. 2007] Niklas J., Schulte T., Prakash M., van Gastel M., Hofmann E., Lubitz W., *J. Am. Chem. Soc.*, **2007**, 129, 1542-15443

[Pedone et al. 2010] Pedone A., Biczysko M., Barone V., *Chem. Phys. Chem*., **2010**, 11, 1812

[Plato et al. 1991] Plato M., Möbius K., Lubitz W., in: H. Scheer (ed.). Chlorophylls, CRC Prsess, Boca Raton, Florida, **1991**

[Polìvka et al. 2010] Polìvka T., Frank H. A., *Accounts of chemical research*, **2010**, 43(8), 1125-1134

[Ros et al. 1991] Ros M., Groenen E. J. J., *J. Chem. Phys.*, **1991**, 94, 7640-7648

[Sharples et al. 1996] Sharples, F. P., Wrench, P. M., Ou, K. L., and Hiller, R. G., *Biochim. Biophys. Acta,* **1996**, *1276*, 117-123.

[Shulte et al. 2009] Shulte T., Niedzwiedzki D. M., Birge R. R., Hiller R. G., Polìvka T., Hofmann E., Frank H. A., *Proc. Natl. Acad. Sci. USA*, **2009**, 106, 20764-20769

[Shulte et al. 2009a] Schulte T., Sharples F. P., Hiller R. G., Hofmann E., *Biochemistry*, **2009**, 48(21), 4466-4475

[Shulte et al. 2010] Shulte T., Hiller R. G., Hofmann E., *FEBS Letters*, **2010**, 584, 973-978

[Standfuss et al. 2005] Standfuss, J.; Terwisscha van Scheltinga, A. C.; Lamborghini, M.; Kuehlbrandt, W. *EMBO J.* **2005**, *24*, 919-928.

[Tomasi et al. 2005] J. Tomasi, B. Mennucci and R. Cammi, *Chem. Rev.*, **2005**, 105, 2999-3094

[Vaswani et al. 2003] Vaswani H. M., Hsu C. P., Head-Gordon M., Fleming G. R., *J. Phys. Chem. B*, **2003**, 107 (31), 7940–7946

[Young et al. 1993] Young A., Britton G., Carotenoids in Photosynthesis, 1993, Chapman & Hall

[Zigmantas et al. 2002] Zigmantas D., Hiller R. G., Sundström V., Polívka T., *Proc Natl Acad Sci U S A*., **2002**; 99(26): 16760–16765

Chapter V

LHC from *Amphidinium carterae*

Biochimica et Biophysica Acta 1797 (2010) 1759–1767

Contents lists available at ScienceDirect

Biochimica et Biophysica Acta

journal homepage: www.elsevier.com/locate/bbabio

Triplet–triplet energy transfer in the major intrinsic light-harvesting complex of *Amphidinium carterae* as revealed by ODMR and EPR spectroscopies

Marilena Di Valentin [a], Enrico Salvadori [a], Giancarlo Agostini [b], Federico Biasibetti [a], Stefano Ceola [a], Roger Hiller [c], Giorgio Mario Giacometti [d], Donatella Carbonera [a,*]

[a] Department of Chemical Sciences, University of Padova, Via Marzolo 1, 35131 Padova, Italy
[b] CNR, Inst Biomol Chem, Padova Unit, I-35131, via Marzolo 1, 35131 Padova, Italy
[c] Department of Biological Sciences, Macquarie University, 2109 NSW, Australia
[d] Department of Biology, University of Padova, via U. Bassi 58/B, 35121 Padova, Italy

ARTICLE INFO

Article history:
Received 2 May 2010
Received in revised form 9 June 2010
Accepted 22 June 2010
Available online 30 June 2010

Keywords:
Triplet
LHC
Carotenoid
EPR
ODMR
Peridinin
Diadinoxanthin

ABSTRACT

We present an optically detected magnetic resonance (ODMR) and electron paramagnetic resonance (EPR) spectroscopic study on the quenching of photo-induced chlorophyll triplet states by carotenoids, in the intrinsic light-harvesting complex (LHC) from the dinoflagellate *Amphidinium carterae*.
Two carotenoid triplet states, differing in terms of optical and magnetic spectroscopic properties, have been identified and assigned to peridinins located in different protein environment. The results reveal a parallelism with the triplet–triplet energy transfer (TTET) process involving chlorophyll *a* and luteins observed in the LHC-II complex of higher plants. Starting from the hypothesis of a conserved alignment of the amino acid sequences at the cores of the LHC and LHC-II proteins, the spin-polarized time-resolved EPR spectra of the carotenoid triplet states of LHC have been calculated by a method which exploits the conservation of the spin momentum during the TTET process. The analysis of the spectra shows that the data are compatible with a structural model of the core of LHC which assigns the photo-protective function to two central carotenoids surrounded by the majority of Chl *a* molecules present in the protein, as found in LHC-II. However, the lack of structural data, and the uncertainty in the pigment composition of LHC, leaves open the possibility that this complex posses a different arrangement of the pigments with specific centers of Chl triplet quenching.

© 2010 Elsevier B.V. All rights reserved.

1. Introduction

Photosynthetic dinoflagellates are characterized by a light-harvesting system containing the carotenoid peridinin. These systems usually have two classes of light-harvesting proteins, the PCPs (peridinin–chlorophyll proteins) and the LHCs (light-harvesting complexes). PCPs are water soluble proteins and are unique to dinoflagellates. LHCs are intrinsic light-harvesting proteins which are related to the cab proteins of higher plants [1, 2] and to their algal homologous [3]. The interactions between these two classes of light-harvesting proteins are still unknown. PCPs and LHCs are present in multiple forms in dinoflagellates possibly in order to facilitate photoadaptation.

In *Amphidinium carterae*, both PCPs and LHCs are encoded by nuclear genes and synthesized with N-terminal transit peptides directing translocation to the chloroplast [4, 5].

The LHC, purified from thylakoids solubilised in digitonin or glycosidic detergents, has a 19-kDa principal component. A pigment composition of 7 Chl *a*, 4 Chl c_2, 12 peridinins and 2 diadinoxanthins has been estimated [1]. However, more recently, it has been observed that pigment content may be considerably less than that originally calculated [6] and a Car:Chl *a* ratio close to one seems to be more reasonable, on the basis of the absorption spectrum. After direct light absorption, both peridinin and Chl c_2 transfer their singlet excitation efficiently to Chl *a* [1, 6]. Although the overall identity between the sequences of LHC and LHC-II from higher plants is low (27%), the core of LHC (residues 172–330) is highly homologous (identities plus positive substitutions: 44%) to the three transmembrane helices of LHC-II. On this basis, a model characterized by three transmembrane helices, based on alignment of the sequence with the three dimensional structure of LHC-II, has been proposed [2]. The crystal structure of the spinach LHC-II complex has been obtained to a resolution of 2.72 Å [7] and that of pea LHC-II to a resolution of 2.5 Å [8]. The folding of the LHC-II protein is characterized by three

Abbreviations: LHC, light-harvesting complex; Car, carotenoid; Chl, chlorophyll; Cla, chlorophyll a; ZFS, zero field splitting; ISC, intersystem crossing; ODMR, optically detected magnetic resonance; FDMR, fluorescence detected magnetic resonance; ADMR, absorption detected magnetic resonance; T-S, triplet minus singlet; ESE, electron spin echo; FSE, field-swept echo; TR-EPR, time-resolved electron paramagnetic resonance; TTET, triplet–triplet energy transfer

* Corresponding author. Tel.: +39 498275144; fax: +39 498275161.
E-mail address: donatella.carbonera@unipd.it (D. Carbonera).

0005-2728/$ – see front matter © 2010 Elsevier B.V. All rights reserved.
doi:10.1016/j.bbabio.2010.06.011

transmembrane helices (see Fig. 1). The high-quality electron density map has permitted the location of all the 14 Chls, 8 Chl *a* and 6 Chl *b*, within one monomeric unit of the LHC-II complex. Five conserved Chl *a* ligands have been identified in LHC [2], which correspond to the ligands of Cla610-612-613-602-603 in the LHC-II structure, according to the nomenclature reported in [7]. Also the two central carotenoid (Car) binding sites (L1 and L2) are most probably preserved in LHC: within 5 Å, the identical or conserved residues are 13/18 for the L1 site and 9/13 for the L2 site. The putative conserved pigment positions are shown in Fig. 1, while the conserved protein residues of the core of LHC (residues 172–330) are shown in the Supplementary material. In LHC-II two extra carotenoid binding sites have been identified: the N1 site which is specific for a neoxanthin molecule surrounded by Chls *b* and the V1 site which binds violaxanthin, lutein, or zeaxanthin depending on light conditions [9] and is located at the periphery of the monomeric subunits. The N1 and V1 sites are not conserved in LHC. Moreover, in LHC, the total number of Chl molecules is reduced thus the additional Car molecules may be inserted in sites which are occupied by Chls in LHC-II or may form clusters as in PCP.

The main photo-protective mechanism responsible for the excess energy dissipation in LHC-II is based on the non-photochemical quenching (NPQ) mechanism, leading to the de-epoxidation of violaxanthin to antheraxanthin and zeaxanthin (VAZ) by the enzyme *violaxanthin de-epoxidase*, which is activated by low luminal pH [9, 10]. It has been suggested that the diadinoxanthin, carotenoid which is present, together with the prevailing peridinin, in the LHC complex, may play a role similar to that of violaxanthin in the NPQ process.

In isolated LHC diadinoxanthin represents only about the 1/5 of the whole Car population and contributes only marginally to the energy transfer process [6].

Carotenoids are also known to be involved in the photo-protection process as efficient, fast, and direct quenchers of the Chl triplet (^{T}Chl) states. In this way, they prevent the formation of singlet oxygen ($^{1}O_{2}^{*}$) and subsequent harmful oxidation of membrane and protein elements [11].

The study of Car triplet (^{T}Car) states formed in LHC-II complexes has been performed in the past by means of several spectroscopic techniques (EPR, Optically Detected Magnetic Resonance (ODMR), time-resolved optical spectroscopy) [12–21]. ^{T}Car states have been characterized, showing specific interactions with nearby Chl molecules [16]. Lampoura *et al.* [19] assigned the ^{T}Car populated in LHC-II specifically to the luteins sitting in the L1 and L2 sites. The majority of the ^{T}Chl states seems to be quenched by the lutein bound in the L1 site, which is in close proximity to the low-energy Chls of the complex [22]. In the past, we used ODMR to study the formation of triplet states in isolated LHC-II complexes and proved the presence of at least two distinct populations of carotenoid triplet states [14, 16]. More recently, we applied advanced EPR techniques to investigate the mechanism of carotenoid triplet state formation in LHC-II. Cla 612/603 were identified as the sites having the highest probability of the triplet formation and undergoing triplet quenching by the two central luteins [12].

The population of ^{T}Car states has also been extensively studied in the PCP proteins [23–27] In PCP, peridinins act as efficient Chl *a* triplet quenchers. According to the results obtained by EPR spectroscopy, Per614 (nomenclature as reported in ref. [28]) has been identified as the specific peridinin playing the main role in this photo-protection mechanism

In view of the similarities, but also of the differences, between the light-harvesting system of higher plants and algae, it is interesting to elucidate the mechanism of Chl triplet quenching in the LHC complex. In this work, we performed ODMR, time-resolved EPR (TR-EPR) and pulse EPR spectroscopies to study the triplet state formation in the isolated LHC complex and compared the results with those previously obtained in LHC-II and PCP complexes.

2. Materials and methods

2.1. Sample preparation

The isolated LHC complex from *A. carterae* was prepared according to the method previously described in [6]. For all the experiments, the LHC samples were dissolved in buffer (25 mM Tris at pH 7.5, 2 mM KCl) to achieve an optical density of 1.6/mm at 500 nm. Glycerol, previously degassed by several cycles of freezing and pumping, was added (60%v/v) to obtain a transparent matrix. Oxygen was removed from the samples by flushing with argon before freezing.

Samples of Chl *a* in micelles were obtained by addition of few microliters of a concentrated solution of the pigment (SIGMA) dissolved in methanol to 1 ml of 1 mM Triton X-100.

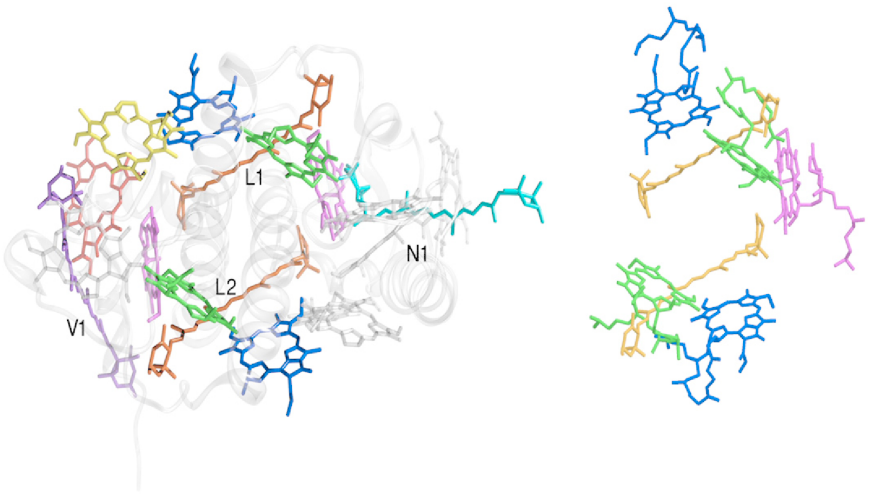


Fig. 1. *Left:* structure of the pigments associated with the basic unit of the LHC-II complex derived from the coordinates deposited in the Brookhaven Protein Data Bank (1 RWT). The protein backbone and the Chl *b* molecules are in faded grey. Orange: luteins in site L1 and L2; purple: violoxanthin in site V1; cyan: neoxanthin in site N1; blue: Cla603 (lower) and 612 (upper); pink: Cla604 (right) and 613 (left); green: Cla602 (left) and 610 (right); yellow: Cla611; red: Cla614. *Right:* conserved chlorophyll and carotenoid sites in LHC (colours as in the left panel) based on the sequence alignment with the 3D structure of LHC-II.

2.2. ODMR and fluorescence experiments

Fluorescence detected magnetic resonance (FDMR) and absorption detected magnetic resonance (ADMR) experiments were performed in the laboratory built apparatus, previously described in detail [14, 29]. ODMR is a double resonance technique based on the principle that, when a triplet steady-state population is generated by illumination, application of a resonant microwave electromagnetic field between a couple of spin sublevels of the triplet state, generally induces a change of the steady-state population of the triplet state itself, due to the anisotropy of the decay and population rates of the three spin sublevels. The induced change of the triplet population may be detected as a corresponding change of the emission and/or absorption of the system [30, 31].

Amplitude modulation of the applied microwave field is used to greatly increase the signal to noise ratio by means of a phase sensitive lock-in amplifier (EG&G 5220). In the FDMR experiments the fluorescence, excited by a halogen lamp (250 W) focused into the sample and filtered by a broadband 5 cm solution of $CuSO_4$ 1 M, was collected at 45 degrees through appropriate band-pass filters (10 nm FWHM) by a photodiode before entering the lock-in amplifier. Low temperature emission spectra were detected in the same apparatus used for ODMR experiments, using the same excitation source, but substituting the band-pass filters, before the detector, by a monochromator.

In the absorption detection mode (ADMR), the same excitation lamp was used but without filters before the sample, except for 5 cm water and heat filters. The beam was focused into the monochromator after passing the sample and finally collected by a photodiode. The modulation frequency and the microwave power were chosen depending on the experiment. By fixing the microwave frequency at a resonant value while sweeping the detection wavelength, microwave-induced Triplet –minus-Singlet (T-S) spectra can be registered.

The temperature of all the experiments performed on LHC was 1.8 K. At this temperature spin-lattice relaxation is inhibited and the ODMR signal is intense.

2.3. TR-EPR and Pulse EPR experiments

Experiments were performed on a Bruker Elexsys E580 pulsed EPR spectrometer. Laser excitation at 532 nm (10 mJ per pulse and repetition rate of 10 Hz) was provided by the second harmonic of an Nd:YAG laser (Quantel Brilliant) in a flexline dielectric resonator. The temperature was controlled by means of a helium cryostat (Oxford CF935) driven by a temperature controller (Oxford ITC503).

TR-EPR experiments were performed in direct-detection mode, taking the signal directly from the mixer, without lock-in amplification with the spectjet digitizer. Transients were accumulated both on and off-resonance field in order to eliminate the laser background signal by subtraction of the off-resonance traces. Transient signal rise time was about 50 ns. In the TR-EPR spectra, the integration period was 100–228 ns after the laser flash. The microwave power was 2 mW.

Field-swept electron spin echo (ESE) spectra (FSE spectra) were recorded using a 2-pulse ESE sequence according to the scheme: flash-DAF-$\pi/2$-τ-π-τ-echo (DAF = delay after laser flash); the value of DAF was fixed at 50 ns. ESE-detected kinetics at the triplet canonical orientations were recorded using a 2-pulse (flash-DAF-$\pi/2$- τ-π-τ-echo) ESE sequence after a variable DAF between the laser flash and the first microwave pulse. The $\pi/2$-pulse was of 16 ns and the delay τ was set at 200 ns for the FSE experiments.

2.4. EPR spectral simulations

Simulations of the powder spin-polarized triplet spectra were performed using a program written in MatLab® with the aid of the Easyspin routine (ver. 2.6.0) [32]. The program is based on the full diagonalization of the triplet state spin Hamiltonian, taking into account the Zeeman and magnetic dipole–dipole interactions, assuming a powder distribution of molecular orientations with respect to the magnetic field direction. Input parameters are the sublevel populations, the ZFS parameters, the line width at the canonical orientations, and the g-tensor components.

Calculations of the sublevel triplet state populations of the acceptor, starting from those of the donor, were performed before for the LHC-II and PCP complexes [12, 25] using a home-written program in MatLab® software, following the formalism of Akiyama et al. [33], and utilizing the x-ray coordinates of the proteins. The program for the calculation of the triplet sublevel populations works at the limit of a triplet–triplet energy transfer (TTET) which is fast, compared to the time evolution of the donor triplet spectrum, and is slow enough to allow spin alignment in the external magnetic field.

2.5. Molecular docking

Since the pigment arrangement for the LHC complex is not known, starting from the hypothesis of a structural homology of the core of LHC with that of LHC-II, as shown in Fig. 1, we used a docking procedure to introduce the peridinin molecules into the L1 and L2 sites.

All docking simulations were carried out in AutoDock (v4) using the Lamarkian genetic algorithm [34, 35].

The polypeptide backbone structure of the monomeric LHC-II, derived from the x-ray structure (PDB code 1RWT) [7], was maintained for LHC. The positions of Cla602, Cla603, Cla610, Cla612, and Cla613 in their binding sites were also conserved.

According to the sequence alignment between the spinach LHC-II and the LHC from *Amphidinium c.* (sequences aligned using BLAST; FASTA entry: tr|Q38689|Q38689_AMPCA, fragment 158–330, corresponding to the mature protein), some residues facing the carotenoid L1 and L2 binding sites within 5 Å are non-conserved in LHC. These residues were changed and their side chains were allowed to move during the docking procedure in order to minimize the energy interaction with the ligand. As starting structure for the ligand peridinin, we used the structure corresponding to PID614 in PCP [28].

The target LHC-II protein was kept rigid, therefore assuming that there are no induced conformational changes upon ligand binding, except for the residues, both conserved and not conserved, facing the L1 and L2 sites and located within 5 Å to the two carotenoids. These residues were allowed to move. Some flexibility of the peridinin molecule was also allowed, via the rotation around the single bonds of the $-OH$ and $-C(O)CH_3$ groups, while its conjugate backbone and the cyclohexyl rings were kept rigid.

For both the ligand and the target protein, all non-polar hydrogen atoms were merged to the connecting heavy atom, leaving only heavy atoms and polar hydrogen atoms. Gasteiger–Marsili atomic charges [36] were assigned using AutoDock Tools (ADT) [37].

Atomic affinity and electrostatic potentials were computed for a grid box positioned around the approximate center of the binding site, with dimensions $34.0 \times 64.0 \times 34.0$ points and spacing per point of 0.5 Å. The total number of runs was 50, and the number of energy evaluations per trial was set to 25 millions. All other docking parameters were the AutoDock default settings.

To validate the procedure, we docked the carotenoid lutein (ligand) in the LHC-II monomer (target), after removal of Lut620, using the same parameters reported above for the docking of peridinin. We obtained a stable conformation for lutein in the L1 site, which was identical to that of the crystal structure.

3. Results

3.1. ODMR

The absorption spectrum of the LHC complex from *A. carterae* taken at room temperature is shown in Fig. 2. As previously reported, the Q_y

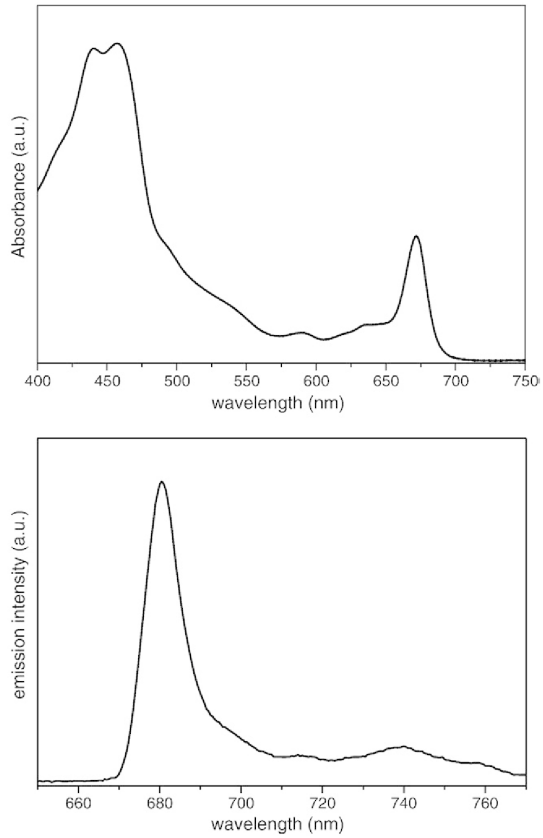


Fig. 2. *Top*: Room temperature absorbance spectrum of the LHC complex from *Amphidinium carterae*. *Bottom*: Emission spectrum of the LHC complex at 1.8 K, obtained by broad band excitation as described in Materials and methods.

band of Chl *a* is centered at 672 nm. The weak bands below 660 nm are due to the higher vibrational bands of the Q_y transition of Chl *a*, and to the Q_y band of Chl c_2 [1]. In the Soret region, there are two bands due to Chl *a* (440 nm) and Chl c_2 (458 nm). Carotenoid absorption bands overlap with the Soret bands of chlorophylls and extend further to the red. The band located at 540 nm has been assigned to the peridinin, whereas the shoulder at 495 nm belongs to both the peridinin and diadinoxanthin carotenoids [6].

The emission spectrum of LHC obtained at room temperature shows a characteristic Chl *a* fluorescence band peaking at 678 nm, in agreement with literature data (not shown) [6]. At 1.8 K, corresponding to the temperature of the ODMR experiments, the fluorescence emission spectrum, obtained by broad band excitation as described in Materials and methods, is red-shifted to about 680.5 nm, (see Fig. 2). No emission bands due to Chl c_2 molecules have been detected, demonstrating 100% energy transfer efficiency to Chl *a* in the complex even at the very low temperature.

Illumination of the sample at cryogenic temperatures induces the formation of carotenoid triplet (^{T}Car) states which can be detected by FDMR, by monitoring the emission of the sample while sweeping the microwave field, as previously reported for LHC-II and PCP [14, 16, 23]. Although carotenoids are non-fluorescing molecules, their FDMR transitions can be indirectly detected because of the energy transfer processes occurring among carotenoids and chlorophylls in the antenna complexes: a change of the steady-state population of the ^{T}Car states, induced by a resonant microwave field, is reflected by a change of the intensity of the emission of the nearby chlorophyll molecules [14].

The resulting spectra, detected at 685 nm, in the microwave field region where the 2|*E*|, the |*D*| − |*E*|, and the |*D*| + |*E*| transitions of ^{T}Car states are expected, are shown in Fig. 3. For comparison the FDMR transitions of PCP, from ref. [14] is also shown.

Two sets of three transitions with the polarization pattern usually found for ^{T}Car (intensity of transitions: 2|*E*| >> |D| + |*E*| > |*D*| − |*E*|) have been detected. This demonstrates that ^{T}Chl states in the LHC can be quenched by populating two different ^{T}Car populations. The relative contribution of the two different ^{T}Car populations (T1: |*D*| = 1237 ± 10 MHz, |*E*| = 125 ± 2 MHz; T2: |D| = 1352 ± 10 MHz, |*E*| = 138 ± 2 MHz) to the FDMR spectrum is slightly dependent on the detection wavelength in the emission spectrum (690–740 nm). The T2 contribution to the whole spectrum is about twice that of T1, as its transitions are much broader.

Together with the formation of ^{T}Car states, the low temperature illumination of the complex also results in the production of ^{T}Chl states, which are not quenched by the carotenoids. The spectral region of FDMR spectra, where the |*D*| − |*E*| and the |*D*| + |*E*| transitions of ^{T}Chl *a* states are expected [14], is shown in Fig. 4. The 2|*E*| transition was too weak to be detected, as usually found for ^{T}Chl states. The ^{T}Chl states of LHC are characterized by the following ZFS parameters: |*D*| = 868 ± 5 MHz and |E| = 137 ± 2 MHz.

To better characterize the Car and Chl molecules carrying the triplet states in terms of their absorption spectra, the microwave-induced T-S spectra were taken by setting the microwave field at different resonant frequencies. The results are shown in Fig. 4 (inset) for the ^{T}Chl and in Fig. 5 for the ^{T}Car states. In Fig. 5 (inset), the ADMR 2|E| and |D| + |E| transitions detected at some significant wavelengths are also shown. |D| − |E| transitions are not shown because they were too weak.

From the carotenoid T-S spectra, the position of the intense T-T absorption band, which is the main (positive) feature in the T-S spectrum of carotenoids and which always appears to the red side of the red-most $S_0 \rightarrow S_2$ (negative) absorption band can be determined. This band is centered at 565 nm for the triplet T2 (2|E| transition at 278 MHz) and at about 512 nm for the triplet T1 (2|E| transition at 248 MHz). In the T-S spectrum detected at 248 MHz there is also a small positive contribution at 565 nm, which is possibly due to T2

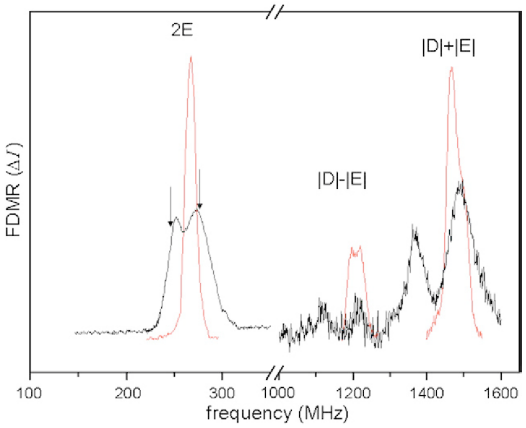


Fig. 3. FDMR spectra of the isolated LHC complex, at 1.8 K, detected at 685 nm in the microwave field region corresponding to carotenoid triplet state transitions. The 2|*E*|, the |*D*| − |*E*|, and the |*D*| + |*E*| transitions are indicated. Amplitude modulation frequency: 315 Hz, time constant 600 ms, number of scans 20. For comparison the transitions detected in PCP, in similar experimental conditions, are also shown in red (from [14]). The intensity of 2|E| transitions has been rescaled, for both samples, dividing by a factor of six.

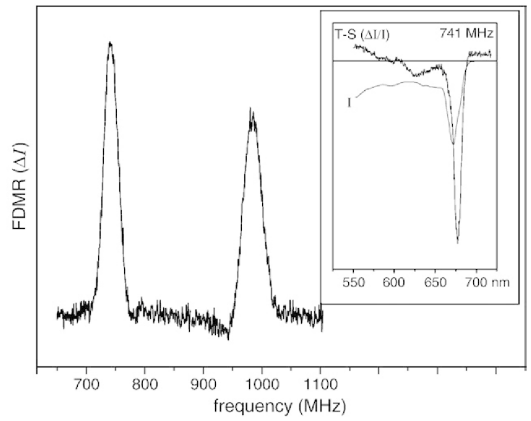


Fig. 4. FDMR spectra of the isolated LHC complex, at 1.8 K, detected at 685 nm in the microwave field region showing the $|D|-|E|$ and the $|D|+|E|$ transitions of ^{T}Chl states. Amplitude modulation frequency: 33 Hz, time constant 600 ms, number of scans 20. Inset: T-S spectrum detected at 741 MHz (other conditions as for the FDMR spectrum) and transmittance (I) of the sample.

which has broader FDMR and ADMR spectra than T1. The ADMR spectra taken at 512 and 565 nm confirm the assignment of the 2|E| and $|D|+|E|$ transitions based on the FDMR spectra. The T-T absorption bands partially overlap with the corresponding bleaching bands of the carotenoid singlet–singlet absorption ($S_0 \rightarrow S_2$), whose $0 \rightarrow 0$ transitions are positioned, respectively, at 495 and 535 nm.

In the Chl Q_y absorption region of the T-S spectra associated with the 2|E| transitions of the carotenoids, additional weak negative bands have also been detected, at 644 and 667 nm for T2 and at 649 and 670 nm for T1. These bands are due to the interaction between the Car molecule carrying the triplet state and the nearby Chls which "feel" the change of the electronic state of the Car. Similar bands have been reported in the past for several light-harvesting complexes belonging to both bacteria and plants [16, 38].

Together with the ^{T}Car states, a consistent population of ^{T}Chl unquenched states is also produced in the isolated LHC upon photo-excitation, meaning that the efficiency of the TTET to carotenoids is not 100%, at least at the low temperature of the experiments. In the chlorophyll T-S spectrum associated to the maximum of the $|D|-|E|$ transition, at 741 MHz, the absorption of the Chl *a* molecules giving the triplet states is seen as a bleaching peaking at 675 nm. This wavelength indicates that the unquenched ^{T}Chl states are located in the "red" chlorophylls of the complex. The transmittance of the sample detected at 1.8 K, in the same experimental conditions as for the detection of the T-S spectrum, shows a shoulder at 675 nm which was not resolved at higher temperature (see Fig. 4, inset).

3.2. TR-EPR and pulse EPR

Fig. 6 shows the 20 K X-band spin-polarized TR-EPR spectrum of LHC, taken at 150 ns after the laser pulse. The spectrum reveals the presence of, at least, two different species. The prevalent triplet population, having ZFS parameters: $|D| = 310 \pm 3.0$ G and $|E| = 42 \pm 3$ G, can be easily assigned to ^{T}Chl *a*, on the basis of the ZFS parameters determined by ODMR spectroscopy, reported above, and by comparison with the TR-EPR spectrum of ^{T}Chl *a* "in vitro" shown in the same figure. The latter has been obtained for Chl *a* dissolved in micelles of Triton X-100 and has been detected under the same experimental conditions as for LHC.

The presence of ^{T}Car in the composite spectrum is revealed by the transitions corresponding to the canonical orientation Z ($|D| = 452$ G $= 1268$ MHz), which do not overlap with the ^{T}Chl *a* transitions, as pointed out in Fig. 6. The observed |D| parameter is close to the average of the two |D| parameters determined by ODMR for T1 and T2.

Because of the ^{T}Car and ^{T}Chl *a* spectral overlap in the TR-EPR spectrum of LHC and of the large contribution of the ^{T}Chl *a*, it is not possible to determine the polarization pattern of the ^{T}Car by direct inspection of the TR-EPR spectrum.

Two-pulse ESE experiments have been successfully used before for the analysis of the EPR spectra of the photo-induced triplet states in LHC-II and PCP [12, 25] and were applied here to the LHC. We have previously demonstrated that for ^{T}Car states, the shape of TR-EPR and FSE spectra, taken at short DAF, are identical due to the absence of fast and anisotropic relaxation processes [26]. In contrast, porphyrin triplet states are known to show anisotropic relaxation processes which are reflected in their FSE spectra [39]. In Fig. 6, we report the FSE spectrum of ^{T}Chl dissolved in Triton X-100 1 mM, detected at the same τ and DAF as for LHC. It can be seen that the shape of the FSE spectrum of ^{T}Chl is different from the corresponding TR-EPR, shown in the same figure. The FSE spectrum of LHC is also shown. Direct comparison of the FSE and TR-EPR spectra of LHC, reveals that the spectral contribution of ^{T}Chl is strongly reduced in the FSE spectrum,

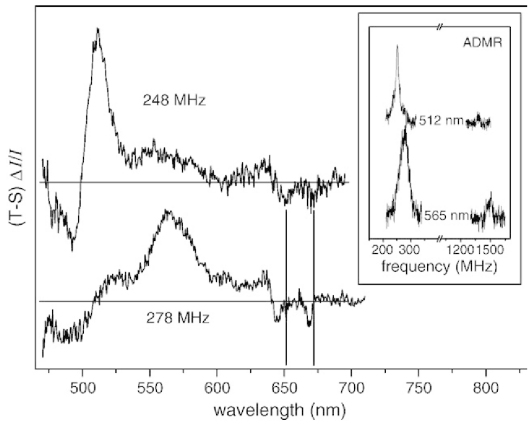


Fig. 5. T-S spectra of LHC at 1.8 K, detected at two different microwave frequencies indicated by arrows in Fig. 3. Amplitude modulation frequency 325 Hz. Slit: 1 nm. Inset: ADMR spectra detected at different wavelengths as indicated. Other conditions as for the FDMR spectrum reported in Fig. 3.

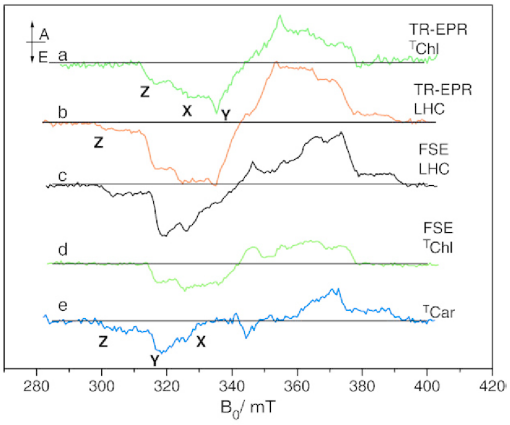


Fig. 6. X-band spin-polarized TR-EPR spectra of the photo-excited triplet state of Chl *a* dissolved in micelles of Triton X-100 (a) and of the photo-excited states populated in LHC (b). The bottom trace represents the difference (e) between the FSE spectrum of LHC (c) and the FSE spectrum of ^{T}Chl *a* (d). $T = 20$ K.

especially in correspondence to the central lines attributed to the Y canonical ZFS orientation of the ^{T}Chl. This spectral effect makes the FSE spectrum a good starting point for determining the "pure" contribution of ^{T}Car. In fact, by subtracting after smoothing, an appropriate amount of the experimental ^{T}Chl *a* FSE spectrum from that of the LHC, the "pure" contribution of ^{T}Car triplet states is obtained (relative amounts of the two components contributing to the FSE spectrum of LHC are shown in Fig. 6). The best subtraction has been obtained by minimizing the spectral features due to ^{T}Chl in the difference spectrum. Note that a contribution from a radical species is also present in the center of the spectrum. The "pure" contribution of ^{T}Car triplet state shows a polarization pattern *eeaeaa* which is similar to that obtained for LHC-II [12]; however, the central lines are much less pronounced.

The time evolution of the spin polarization has been investigated by monitoring the echo intensity as a function of DAF at the turning points corresponding to the low-field canonical orientations of the ZFS tensor of the carotenoid triplet state (*Z*, *Y*, *X* in Fig. 2) (not shown). The spin polarization of the Z component has a decay time of the order of 10 μs while the polarization of the Y component is inverted after about 10 μs. These effects are expected on the basis of the anisotropy of the decay rates of the spin sublevels, as previously reported for ^{T}Car states in other photosynthetic systems [26, 40, 41]. The time evolution of the ^{T}Car spectra is slow compared to time resolution of the setup; thus, the spectra taken at the shortest time reflect the "initial" polarization inherited from the ^{T}Chl states. The ^{T}Chl contribution of the FSE spectrum of LHC evolves independently showing no correlation with the evolution of the ^{T}Car.

3.3. Calculation of the spin polarization of the carotenoid triplet state based on spin conservation during triplet–triplet energy transfer

The ^{T}Car state formation in LHC is thought to arise from ^{T}Chl *a* quenching, since direct triplet population of carotenoids from the corresponding excited singlet state is a very low probability process. As stated above, we are able to detect a spin-polarized spectrum conserving the polarization pattern inherited from the ^{T}Chl donor. Therefore, it is possible to analyze the carotenoid triplet state polarization in terms of TTET from the ^{T}Chl *a* donor, exploiting the principle of spin conservation during TTET, as described in Materials and methods.

Due to the fast TTET, the spectral features of the ^{T}Chl *a* states which are specifically quenched by the carotenoids in LHC cannot be identified. Consequently, we have to make some assumptions in terms of the sublevel populations of the ^{T}Chl *a* to be projected from the donor to the acceptor triplet in order to calculate the ^{T}Car acceptor populations. We have already discussed in details this point in our previous work on PCP and LHC-II [12, 25]. Two sets of ^{T}Chl *a* populations, depending on the polarity of the solvent and on the ligation state of the central Mg and differing from each other in the initial polarization pattern (*eaeaea vs. eeeaaa*), have been reported from in vitro studies. A *eeeaaa* polarization pattern also characterizes the unquenched ^{T}Chl *a* contribution to the TR-EPR spectrum of LHC. In the following, we present the calculations for the acceptor triplet population rates obtained from using the ^{T}Chl *a* populations which produce the *eeeaaa* spectral pattern, although, as the calculations have demonstrated, the choice between the two polarization patterns is not influencing the main conclusions that can be drawn from the results.

An important parameter of the calculation is the relative orientation in space of the donor and acceptor moieties. Although the structure of LHC has not yet been resolved, the sequence alignment permits the hypothesis of a structural similarity with the core of the LHC-II complex. In particular, the structure of the core of pigments, composed by the two central carotenoids and the chlorophylls Cla610-612-613-602-603, seems to be conserved [2]. Thus, it is interesting to verify if the EPR data on LHC are compatible with a protein structure which conserves the strategy of photo-protection adopted by LHC-II: only two carotenoids located in the center of the protein act as ^{T}Chl quenchers, although there are extra carotenoids present somewhere in the protein scaffold. The Chls surrounding the two central carotenoids in LHC are likely reduced in number, compared to those found in LHC-II. However, five of them, having putatively conserved central ligands, are good candidate as donors in the TTET mechanism. The starting point for the calculations is to assign the two different carotenoid triplets observed in LHC by ODMR to two carotenoids sitting in the analogous of the L1/L2 binding sites of the LHC-II complex. Due to the different molecular structure of peridinin, the main carotenoid of LHC, compared to that of lutein, the molecular docking of the peridinin molecule in the two sites which accommodate the two central lutein molecules in LHC-II has been performed, taking into account the presence of different residues in the region of the carotenoid binding sites (see in Materials and methods). The starting molecular conformation chosen for the peridinin in the docking study was that corresponding to PID614 in PCP [28]. A number of conformations of minimal, comparable energy have been calculated by the docking simulation analysis (see Fig. 7).

Other parameters to be set for the calculations of the spin-polarized triplet spectrum are the values of the ZFS parameters and the directions of the ZFS axes in relation to the molecular frame, for both the donor and the acceptor molecules. The ^{T}Chl *a* ZFS axes are those used previously for ^{T}Chl a in LHC-II [12], while the ZFS axes of the docked peridinins have been obtained by the procedure used for the PCP complex [25].

Using the above assumptions, we have calculated the initial ^{T}Car spectra, expected on the basis of the TTET mechanism, for all the Cla610-612-613-602-603/Per mutual configurations derived from the docked

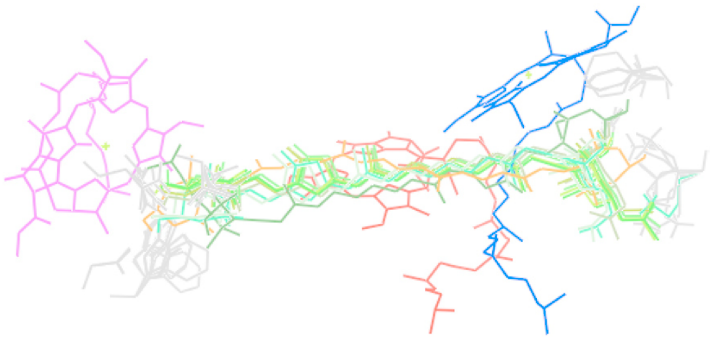


Fig. 7. Conformations of minimal, comparable energy of the peridinin molecules in the binding site of LHC, homologous to the L1 site of LHC-II, calculated by the docking procedure (green color scale). Residues allowed to move (grey) and the conserved Chls (Cla612 (red), Cla610 (blue), and Cla613 (pink)) are also shown. Corresponding Lutein 620 position in the L1 site of LHC-II [pdb file (1RWT)] is displayed in orange.

structure of peridinin in the modified L1 site of LHC-II. The overall set of parameters used for the calculations of the peridinin triplet spectra at the L1 site can be found in Supplementary material. No substantial differences were found for site L2 (not reported). All the conformations (thirteen out of fifty) showing a negative binding energy in the docking have been considered. A good agreement with the experimental data was reached only by considering TTET starting from Chl *a* 602/610 in most of the conformations (eight out of thirteen). All the remaining conformations gave a spin polarization pattern for the calculated peridinin triplet spectrum which did not reproduce the experimental data, whatever Chl molecule of the core was considered as the donor.

Since the ODMR experiments on LHC have clearly shown the presence of two distinct ^{T}Car populations, characterized by different ZFS parameters, we considered two triplet contributions in the reconstruction of TR-EPR and FSE spectra of LHC, although these two components are not clearly resolved in the spectra. A specific assignment of T1 and T2 to the carotenoid sitting in sites L1 and L2 was however not possible since, due to the symmetry of the complex, an exchange of T1/T2 in the L1/L2 sites does not produce a change of the observed triplet state polarization pattern.

An example of reconstruction of the experimental spectra is shown in Fig. 8. Firstly, on the basis of the TTET calculations of the ^{T}Car polarization in the L1/L2 sites, we have reconstructed the ^{T}Car "pure" contribution to the FSE spectrum of LHC (bottom trace in Fig. 6), by summing two triplet components, corresponding to T1 and T2, in a 1:3 ratio, as determined by ODMR; secondly, we have reconstructed the TR-EPR spectrum (reported also in Fig. 6) by adding to the calculated spectrum of the ^{T}Car state mentioned above, an appropriate amount of the smoothed TR-EPR spectrum of ^{T}Chl shown in Fig. 6.

4. Discussion

The results shown in the previous section demonstrate that in the LHC from *A. carterae* the TTET between Chl and Car is active. However, when compared to LHC-II, the efficiency of the quenching of ^{T}Chl *a* does not seem to be very high, at least at cryogenic temperatures. In fact a large population of unquenched ^{T}Chl *a* is present in the LHC complex, as shown by both the ODMR and the EPR data. This is surprising in view of the high Car/Chl ratio present in the complex, but it is in agreement with the fluorescence excitation data previously reported [6] in isolated LHC, showing that in the carotenoid region, also the efficiency of singlet–singlet energy transfer to Chl *a* is reduced. It exceeds 90% within the lowest energy peridinin band, but drops off below 525 nm. Moreover the contribution of diadinoxanthin, which is estimated to be present in a 1:5 (diadinoxanthin/peridinin) ratio in the complex, is almost missing in the fluorescence excitation spectrum, indicating that it is weakly involved in energy transfer, as confirmed by time-resolved measurements [6]. A role for diadinoxanthin similar to that of violaxanthin, which is involved in the xanthophyll cycle in LHC-II, has been suggested, and it is unlikely that the two carotenoid triplet pools observed by ODMR belong to the two different species of carotenoids present in the sample. It is more plausible that two different peridinins, having specific environments and consequently characterized by different ZFS parameters, are involved in the TTET from ^{T}Chl *a*. The effect of the environment on the spectral features of carotenoids has been discussed in the past. Recently Resonance Raman (RR) spectroscopy has been used to characterize the structures and environments of the carotenoid fucoxanthin (Fx), in the membrane-intrinsic fucoxanthin chlorophyll a/c_2 proteins (FCP) from the diatom *Cyclotella meneghiniana* [42]**.** This protein, belonging to some diatoms and brown algae, is as rich in carotenoids as LHC, and its homology with plant LHC-II implies that it has a similar organization of the transmembrane helixes [43]. In the protein, the RR spectra revealed the presence of two distinct Fx_{blue}'s , two low-energy Fx_{red}'s, and one to two intermediate-energy Fx_{green}'s, all adopting a planar all-trans conformation.

The T-S spectra associated to the two different ^{T}Car states in LHC show that one peridinin is the lowest energy peridinin present in the complex, absorbing at about 540 nm, and the other is a "bluer" peridinin absorbing at about 495 nm. It is interesting to note that also in LHC-II the ODMR experiments, performed at 1.8 K, revealed the presence of two lutein triplet states with different spectral features, having T-T absorption maxima at 507 and 525 nm and ZFS parameters |D| = 1270 and 1310 MHz, respectively. The T-S spectra of these two lutein triplets showed interactions bands in the Q_y absorption region of Chl *a*: the first with a red Chl (bleaching observed at 677 nm) and the second with a bluer Chl (bleaching at 670 nm). The two triplet states were assigned to the two luteins located in the L1 and L2 sites, respectively [19]. Similar spectral features are present in the T-S spectra of LHC, detected at the resonance frequencies maxima of the two carotenoid triplet states. In fact, as in LHC-II, the triplet T1, having smaller ZFS parameters, shows a T-T absorption maximum at shorter wavelengths (512 nm) and bleaching bands of Chls absorbing at longer wavelengths (649 and 670 nm) while T2, having larger ZFS parameters, shows a red-shifted T-T absorption maximum (565 nm) and bleaching bands of Chls at shorter wavelengths (644 and 667 nm). The bands at 644 and 649 nm correspond to the bleachings of Chl *c2*, meaning that the carotenoids involved in triplet quenching are very close not only to Chl *a* molecules but also to Chl *c2*. Similarly, bands corresponding to both Chl *a* and *b* were present in T-S spectra associated to the lutein triplet states in LHC-II [16].

The detection of only two different carotenoid triplet states among several possible, the similarity of their spectral characteristics with those found for lutein triplet states in LHC-II and, finally, the fact that in LHC-II the carotenoids involved in ^{T}Chl quenching belong to the putatively conserved protein region, has suggested as interesting to probe if the EPR data on LHC were compatible with an assignment of the triplet states to two peridinins sitting in the analogous of the L1/L2 sites.

It can be noted that the spectral shift of the T-T absorption bands of the two carotenoid triplet states is much more pronounced in LHC than in LHC-II. This could be due to the characteristics of the electronic states of peridinin molecule because of the presence of an allene and a lactone ring in conjugation with the electron system of the carbon-carbon double bonds. These group make the peridinin sensitive to the solvent

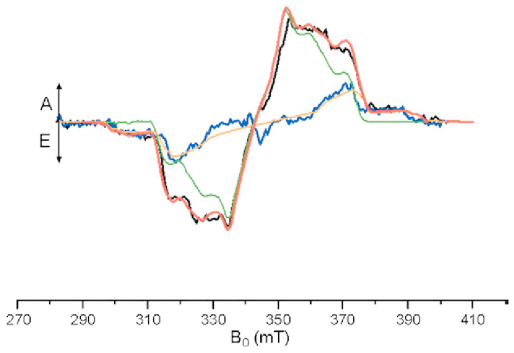


Fig. 8. TR-EPR spectrum of LHC (black line, reported also in Fig. 6) and ^{T}Car "pure" contribution to the FSE spectrum of LHC (blue line, same as in Fig. 6) and their reconstructions (red and orange lines respectively). Reconstruction of the TR-EPR spectrum was obtained by summing the ^{T}Chl contribution (green line) and the ^{T}Car contribution (orange line). The ^{T}Chl spectral contribution corresponds to the smoothed TR-EPR spectrum of ^{T}Chl reported in Fig. 6. The ^{T}Car spectrum has been calculated on the basis of the TTET mechanism starting from ^{T}Chl *a* 602/610 and a peridinin conformation as derived from the docking procedure. Calculation parameters: Px:Py:Pz = 0.35:0.20:0.45 for both T1 and T2; T1: |D| = 483 G, |E| = 49.4 G; line widths: Wx = 15 G, Wy, Wz = 20 G; T2: |D| = 442 G, |E| = 44.8 G, Wx = 15 G, Wy, Wz = 20 G; T1:T2 = 1:3.

properties [44] and might be also responsible for the enhanced response to the local protein field present in the putative L1 and L2 sites.

The spectral analysis reported in [12] has shown that the initial polarization pattern of the ^{T}Car states detected in LHC-II by TR-EPR and pulse EPR, may be well reproduced by considering a single TTET step from Chl603 to Lut621 (site L2) and/or from Chl612 to Lut620 (site L1). The initial polarization pattern of the ^{T}Car in LHC (*eeaeaa*), extracted from the FSE spectrum of LHC after subtraction of the ^{T}Chl contribution, resembles that reported for LHC-II, characterized by strong Y and weak Z emissive components in the low-field spectral region. The central absorptive X component, however, is much less pronounced that in LHC-II, indicating a similar but not identical arrangement of the Chl-Car couples involved in TTET. On the other hand, the observed polarization pattern of ^{T}Car in LHC is totally different from that detected in isolated PCP complex (*eaeaea*) [25]. Under the assumption of a conserved pigment–protein core, composed by the two central peridinins and the five Cla610-612-613-602-603 pigments as in LHC-II, and on the basis of the relative conformation of the peridinin–Chl couples obtained by the docking simulation analysis, the calculations of the expected initial polarization of ^{T}Car show that it is likely that in LHC TTET takes place starting from ^{T}Chl *a* 602/610. The experimental LHC spectrum can still be simulated starting from ^{T}Cla603/Cla612 as in LHC-II, by rotation of the carotenoid ZFS axes, about each molecular axis, of 20–30 degrees (not shown). Even tough small changes of the relative orientations of the Cla603(Cla612)-peridinin(L2/L1) couples could in principle be induced by protein-specific local effects, however, as stated above, the EPR spectra can be reproduced *without need of local rearrangement*, if the triplet states are initially formed in Cla602 and Cla610.

It is worth noting that the efficiency of the quenching of ^{T}Chl by Car is reduced in LHC compared to LHC-II. In our previous work on LHC-II we pointed out that the His and Asn residues, which coordinate the central Mg atom of Chl603 and Chl612, respectively, are able to favour the overlap of the conjugated systems, and thus the TTET process, by pulling the porphyrin ring towards the luteins. This condition is not fulfilled by the central ligands of Chl602 and Chl610. Starting from the Chl602/610 couple the global efficiency of triplet quenching by peridinins results to be reduced, compared to the corresponding quenching by luteins in LHC-II. It is possible that, since Chl 611 is missing and Chl *b* is not present in the LHC complex, the interactions among the Chls close to the carotenoid binding sites give rise to a singlet distribution of the excitation leading to a high probability of forming triplet states in the Chl602/610couple. It is also possible that the position corresponding to the Chl *a* 603/612 in LHC-II is occupied in LHC by a Chl c_2, coordinated to the conserved central ligand. This would be in agreement with the effect observed in the T-S spectra of carotenoids showing a close proximity of the Car carrying the triplet state to both Chl *a* and Chl c_2 molecules. Moreover, in the T-S spectra of LHC, the intensity of the bleaching of the Q_y band of Chl c_2 is similar to that of the Q_y band of Chl *a*, meaning that the interaction of these two pigments with the Car is comparable. The change of the Chl *b* absorption induced by the electronic state transition of the Car carrying the triplet state in LHC-II was much smaller than that observed for Chl *a* [16]. Thus, all this considerations point towards a possible closer proximity of the Chl c_2 to the central Car compared to that of Chl *b* in LHC-II.

In conclusion, the analysis shows that the EPR data are compatible with a structural model of the core of LHC which assigns the photoprotective function to two central carotenoids surrounded by the majority of the Chl *a* molecules present in the protein as found in LHC-II.

If the assignment of the quenching of ^{T}Chl states by only two peridinins located in the L1/L2 sites is correct, the role and arrangement of the extra peridinins, which are a present in each LHC monomer, remains to be clarified. It has, however, been suggested that pigment content of both the LHC [6] and FCP from diatoms [43] may be considerably less than that originally calculated. Nevertheless if a cluster of peridinins is present it does not seem to resemble the pigment arrangement observed in PCP where four peridinins surround a Chl *a* molecule and the efficiency of the quenching of the ^{T}Chl is 100%.

The Q_y absorption band of the Chl *a* molecules carrying the triplet states, which are not quenched by Car in LHC, is seen as a bleaching peaking at 675 nm in the associated T-S spectrum indicating that the "unprotected" Chls correspond to the red chlorophylls. The incomplete quenching of ^{T}Chl states in LHC could be compensated in vivo by the direct scavenging of singlet oxygen in an environment which is rich in carotenoids.

5. Conclusions

In this study on the quenching mechanism of ^{T}Chl states in isolated LHC from *A. carterae*, two carotenoid triplet states, differing in terms of optical and magnetic spectroscopic properties, have been identified and assigned to peridinins located in different protein environments. The spectral analysis shows that the results are compatible with a structural model for the core of LHC which resembles that of the LHC-II, with two central carotenoids quenching the triplet states formed in a couple of Chls, belonging to the putatively conserved pigment pool. Although this suggests a possible common strategy for ^{T}Chl quenching in the two LHCs, it must be pointed out that, due to the lack of structural data, and the uncertainty in the pigment composition, a different scenario in the pigment arrangement of LHC can not be excluded.

Acknowledgments

This work was supported by the Italian Ministry for University and Research (MURST) under the project PRIN2007. Molecular graphics image (Fig. 1) was produced using the UCSF Chimera package from the Resource for Biocomputing, Visualization, and Informatics at the University of California, San Francisco (supported by NIH P41 RR-01081). [45]

Appendix A. Supplementary data

Supplementary data associated with this article can be found, in the online version, at doi:10.1016/j.bbabio.2010.06.011.

References

[1] R.G. Hiller, P.M. Wrench, A.P. Gooley, G. Shoebridge, J. Breton, The major intrinsic light-harvesting protein of *Amphidinium*: characterization and relation to other light-harvesting proteins, Photochem. Photobiol. 57 (1993) 125–131.
[2] R.G. Hiller, P.M. Wrench, F.P. Sharples, The light harvesting chlorophyll a/c binding protein of dinoflagellates a putative polyprotein, FEBS Lett. 363 (1995) 175–178.
[3] A.R. Grossman, A. Manodori, D. Snyder, Light-harvesting proteins of diatom: their relationship to the chlorophyll *a*/*b* proteins of higher plants and their mode of transport into plastids, Mol. Gen. Genet. 224 (1990) 91–100.
[4] R.G. Hiller, M.J. Broughton, P.M. Wrench, F.P. Sharples, D.J. Mileer, J. Catmull, in: J.H. Argyroudi-Akoyunoglou, H. Senger (Eds.), Dinoflagellates Light-Harvesting Proteins: Genes, Structure and Reconstitution in the Chloroplast: From Molecular Biology to Biotechnology, Kluwer Academic Publishers, 1999, pp. 3–10.
[5] F.P. Sharples, P.M. Wrench, K.L. Ou, R.G. Hiller, Two distinct forms of the peridinin–chlorophyll alpha-protein from *Amphidinium carterae*, Biochim. Biophys. Acta 1276 (1996) 117–123.
[6] T. Polívka, I.H.M. van Stokkum, D. Zigmantas, R. van Grondelle, V. Sundström, R.G. Hiller, Energy transfer in the major intrinsic light-harvesting complex from *Amphidinium carterae*, Biochemistry 45 (2006) 8516–8526.
[7] Z. Liu, H. Yan, K. Wang, T. Kuang, J. Zhang, L. Gui, X. An, W. Chang, Crystal structure of spinach major light-harvesting complex at 2.72 resolution, Nature 428 (2004) 287–292.
[8] J. Standfuss, A.C. Terwisscha van Scheltinga, M. Lamborghini, W. Kuehlbrandt, Mechanisms of photoprotection and nonphotochemical quenching in pea light-harvesting complex at 2.5 resolution, EMBO J. 24 (2005) 919–928.
[9] A.V. Ruban, P.J. Lee, M. Wentworth, A.J. Young, P. Horton, Determination of the stoichiometry and strength of binding of xanthophylls to the photosystem II light harvesting complexes, J. Biol. Chem. 274 (1999) 10458–10465.
[10] B. Demmig-Adams, W.W. Adams, The role of xanthophyll cycle carotenoids in the protection of photosynthesis, Trends Plant Sci. 1 (1996) 21–26.
[11] H.A. Frank, R.J. Cogdell, Carotenoids in photosynthesis, Photochem. Photobiol. 63 (1996) 257–264.
[12] M. Di Valentin, F. Biasibetti, S. Ceola, D. Carbonera, Identification of the sites of chlorophyll triplet quenching in relation to the structure of LHC-II from higher

properties [44] and might be also responsible for the enhanced response to the local protein field present in the putative L1 and L2 sites.

The spectral analysis reported in [12] has shown that the initial polarization pattern of the ^{T}Car states detected in LHC-II by TR-EPR and pulse EPR, may be well reproduced by considering a single TTET step from Chl603 to Lut621 (site L2) and/or from Chl612 to Lut620 (site L1). The initial polarization pattern of the ^{T}Car in LHC (*eeaeaa*), extracted from the FSE spectrum of LHC after subtraction of the ^{T}Chl contribution, resembles that reported for LHC-II, characterized by strong Y and weak Z emissive components in the low-field spectral region. The central absorptive X component, however, is much less pronounced that in LHC-II, indicating a similar but not identical arrangement of the Chl-Car couples involved in TTET. On the other hand, the observed polarization pattern of ^{T}Car in LHC is totally different from that detected in isolated PCP complex (*eaeaea*) [25]. Under the assumption of a conserved pigment–protein core, composed by the two central peridinins and the five Cla610-612-613-602-603 pigments as in LHC-II, and on the basis of the relative conformation of the peridinin–Chl couples obtained by the docking simulation analysis, the calculations of the expected initial polarization of ^{T}Car show that it is likely that in LHC TTET takes place starting from ^{T}Chl *a* 602/610. The experimental LHC spectrum can still be simulated starting from ^{T}Cla603/Cla612 as in LHC-II, by rotation of the carotenoid ZFS axes, about each molecular axis, of 20–30 degrees (not shown). Even tough small changes of the relative orientations of the Cla603(Cla612)-peridinin(L2/L1) couples could in principle be induced by protein-specific local effects, however, as stated above, the EPR spectra can be reproduced *without need of local rearrangement*, if the triplet states are initially formed in Cla602 and Cla610.

It is worth noting that the efficiency of the quenching of ^{T}Chl by Car is reduced in LHC compared to LHC-II. In our previous work on LHC-II we pointed out that the His and Asn residues, which coordinate the central Mg atom of Chl603 and Chl612, respectively, are able to favour the overlap of the conjugated systems, and thus the TTET process, by pulling the porphyrin ring towards the luteins. This condition is not fulfilled by the central ligands of Chl602 and Chl610. Starting from the Chl602/610 couple the global efficiency of triplet quenching by peridinins results to be reduced, compared to the corresponding quenching by luteins in LHC-II. It is possible that, since Chl 611 is missing and Chl *b* is not present in the LHC complex, the interactions among the Chls close to the carotenoid binding sites give rise to a singlet distribution of the excitation leading to a high probability of forming triplet states in the Chl602/610couple. It is also possible that the position corresponding to the Chl *a* 603/612 in LHC-II is occupied in LHC by a Chl c_2, coordinated to the conserved central ligand. This would be in agreement with the effect observed in the T-S spectra of carotenoids showing a close proximity of the Car carrying the triplet state to both Chl *a* and Chl c_2 molecules. Moreover, in the T-S spectra of LHC, the intensity of the bleaching of the Q_y band of Chl c_2 is similar to that of the Q_y band of Chl *a*, meaning that the interaction of these two pigments with the Car is comparable. The change of the Chl *b* absorption induced by the electronic state transition of the Car carrying the triplet state in LHC-II was much smaller than that observed for Chl *a* [16]. Thus, all this considerations point towards a possible closer proximity of the Chl c_2 to the central Car compared to that of Chl *b* in LHC-II.

In conclusion, the analysis shows that the EPR data are compatible with a structural model of the core of LHC which assigns the photoprotective function to two central carotenoids surrounded by the majority of the Chl *a* molecules present in the protein as found in LHC-II.

If the assignment of the quenching of ^{T}Chl states by only two peridinins located in the L1/L2 sites is correct, the role and arrangement of the extra peridinins, which are a present in each LHC monomer, remains to be clarified. It has, however, been suggested that pigment content of both the LHC [6] and FCP from diatoms [43] may be considerably less than that originally calculated. Nevertheless if a cluster of peridinins is present it does not seem to resemble the pigment arrangement observed in PCP where four peridinins surround a Chl *a* molecule and the efficiency of the quenching of the ^{T}Chl is 100%.

The Q_y absorption band of the Chl *a* molecules carrying the triplet states, which are not quenched by Car in LHC, is seen as a bleaching peaking at 675 nm in the associated T-S spectrum indicating that the "unprotected" Chls correspond to the red chlorophylls. The incomplete quenching of ^{T}Chl states in LHC could be compensated in vivo by the direct scavenging of singlet oxygen in an environment which is rich in carotenoids.

5. Conclusions

In this study on the quenching mechanism of ^{T}Chl states in isolated LHC from *A. carterae*, two carotenoid triplet states, differing in terms of optical and magnetic spectroscopic properties, have been identified and assigned to peridinins located in different protein environments. The spectral analysis shows that the results are compatible with a structural model for the core of LHC which resembles that of the LHC-II, with two central carotenoids quenching the triplet states formed in a couple of Chls, belonging to the putatively conserved pigment pool. Although this suggests a possible common strategy for ^{T}Chl quenching in the two LHCs, it must be pointed out that, due to the lack of structural data, and the uncertainty in the pigment composition, a different scenario in the pigment arrangement of LHC can not be excluded.

Acknowledgments

This work was supported by the Italian Ministry for University and Research (MURST) under the project PRIN2007. Molecular graphics image (Fig. 1) was produced using the UCSF Chimera package from the Resource for Biocomputing, Visualization, and Informatics at the University of California, San Francisco (supported by NIH P41 RR-01081). [45]

Appendix A. Supplementary data

Supplementary data associated with this article can be found, in the online version, at doi:10.1016/j.bbabio.2010.06.011.

References

[1] R.G. Hiller, P.M. Wrench, A.P. Gooley, G. Shoebridge, J. Breton, The major intrinsic light-harvesting protein of *Amphidinium*: characterization and relation to other light-harvesting proteins, Photochem. Photobiol. 57 (1993) 125–131.
[2] R.G. Hiller, P.M. Wrench, F.P. Sharples, The light harvesting chlorophyll a/c binding protein of dinoflagellates a putative polyprotein, FEBS Lett. 363 (1995) 175–178.
[3] A.R. Grossman, A. Manodori, D. Snyder, Light-harvesting proteins of diatom: their relationship to the chlorophyll *a*/*b* proteins of higher plants and their mode of transport into plastids, Mol. Gen. Genet. 224 (1990) 91–100.
[4] R.G. Hiller, M.J. Broughton, P.M. Wrench, F.P. Sharples, D.J. Mileer, J. Catmull, in: J.H. Argyroudi-Akoyunoglou, H. Senger (Eds.), Dinoflagellates Light-Harvesting Proteins: Genes, Structure and Reconstitution in the Chloroplast: From Molecular Biology to Biotechnology, Kluwer Academic Publishers, 1999, pp. 3–10.
[5] F.P. Sharples, P.M. Wrench, K.L. Ou, R.G. Hiller, Two distinct forms of the peridinin–chlorophyll alpha-protein from *Amphidinium carterae*, Biochim. Biophys. Acta 1276 (1996) 117–123.
[6] T. Polívka, I.H.M. van Stokkum, D. Zigmantas, R. van Grondelle, V. Sundström, R.G. Hiller, Energy transfer in the major intrinsic light-harvesting complex from *Amphidinium carterae*, Biochemistry 45 (2006) 8516–8526.
[7] Z. Liu, H. Yan, K. Wang, T. Kuang, J. Zhang, L. Gui, X. An, W. Chang, Crystal structure of spinach major light-harvesting complex at 2.72 resolution, Nature 428 (2004) 287–292.
[8] J. Standfuss, A.C. Terwisscha van Scheltinga, M. Lamborghini, W. Kuehlbrandt, Mechanisms of photoprotection and nonphotochemical quenching in pea light-harvesting complex at 2.5 resolution, EMBO J. 24 (2005) 919–928.
[9] A.V. Ruban, P.J. Lee, M. Wentworth, A.J. Young, P. Horton, Determination of the stoichiometry and strength of binding of xanthophylls to the photosystem II light harvesting complexes, J. Biol. Chem. 274 (1999) 10458–10465.
[10] B. Demmig-Adams, W.W. Adams, The role of xanthophyll cycle carotenoids in the protection of photosynthesis, Trends Plant Sci. 1 (1996) 21–26.
[11] H.A. Frank, R.J. Cogdell, Carotenoids in photosynthesis, Photochem. Photobiol. 63 (1996) 257–264.
[12] M. Di Valentin, F. Biasibetti, S. Ceola, D. Carbonera, Identification of the sites of chlorophyll triplet quenching in relation to the structure of LHC-II from higher

plants. Evidence from EPR Spectroscopy, J. Phys. Chem. B 113 (2009) 13071–13078.
[13] D. Carbonera, G. Giacometti, G. Agostini, A. Toffoletti, ESP spectra of a carotenoid pigment in LHCII complexes, Gazz. Chim. Ital. 119 (1989) 225–228.
[14] D. Carbonera, G. Giacometti, G. Agostini, FDMR of carotenoid and chlorophyll triplets in Light-harvesting complex LHCII of spinach, Appl. Magn. Res. 3 (1992) 859–872.
[15] D. Carbonera, M. Di Valentin, G. Agostini, G. Giacometti, P.A. Liddel, D. Gust, A.L. Moore, T.A. Moore, Energy transfer and spin polarization of the carotenoid triplet state in synthetic carotenopotphyrin dyads and in natural antenna complexes, Appl. Magn. Res. 13 (1997) 487–504.
[16] R. van der Vos, D. Carbonera, A.J. Hoff, Microwave and optical spectroscopy of carotenoid triplets in light-harvesting complex LHCII of spinach by absorbance-detected magnetic resonance, Appl. Magn. Res. 2 (1991) 179–202.
[17] R. van der Vos, E.M. Franken, A.J. Hoff, ADMR study of the effect of oligomerisation on the carotenoid triplets and on triplet–triplet transfer in light harvesting complex II (LHC II) of spinach, Biochim. Biophys. Acta 1188 (1994) 243–250.
[18] V. Barzda, E.J.G. Peterman, R. van Grondelle, H. van Amerongen, The influence of aggregation on triplet formation in light-harvesting chlorophyll a/b pigment–protein complex II of green plants, Biochemistry 37 (1998) 546–551.
[19] S.S. Lampoura, V. Barzda, G.M. Owen, A.J. Hoff, H. van Amerongen, Aggregation of LHCII leads to a redistribution of the triplets over the central xanthophylls in LHCII, Biochemistry 41 (2002) 9139–9144.
[20] K.R. Naqvi, T.B. Melo, B.B.; Raju, T. Javorfi, I. Simidjiev, G. Garab, Quenching of chlorophyll a singlets and triplets by carotenoids in light-harvesting complex of photosystem II: comparison of aggregates with trimers, Spectrochim. Acta A 53 (1997) 2659–2667.
[21] E.J.G. Peterman, F.M. Dukker, R. van Grondelle, H. van Amerongen, Chlorophyll a and carotenoid triplet states in light-harvesting complex II of higher plants, Biophys. J. 69 (1995) 2670–2678.
[22] M. Mozzo, L. Dall'Osto, R. Hienerwadel, R. Bassi, R. Croce, Photoprotection in the antenna complexes of photosystem II—role of individual xanthophylls in chlorophyll triplet quenching, J. Biol. Chem. 283 (2008) 6184–6192.
[23] D. Carbonera, G. Giacometti, G. Agostini, FDMR spectroscopy of peridinin chlorophyll-a protein from *Amphidinium carterae*, Spectrochimica 51A (1995) 115–123.
[24] D. Carbonera, G. Giacometti, U. Segre, Carotenoid interactions in peridinin chlorophyll a proteins from dinoflagellates—evidence for optical excitons and triplet migration, J. Chem. Soc. Faraday Trans. 92 (1996) 989–993.
[25] M. Di Valentin, S. Ceola, E. Salvadori, G. Agostini, D. Carbonera, Identification by time-resolved EPR of the peridinins directly involved in chlorophyll triplet quenching in the peridinin–chlorophyll a–protein from *Amphidinium carterae*, Biochim. Biophys. Acta 1777 (2008) 186–195.
[26] M. Di Valentin, S. Ceola, G. Agostini, G.M. Giacometti, A. Angerhofer, O. Crescenzi, V. Barone, D. Carbonera, Pulse ENDOR and density functional theory on the peridinin triplet state involved in the photo-protective mechanism in the peridinin–chlorophyll a–protein from *Amphidinium carterae*, Biochimica et Biophysica Acta (BBA)—Bioenergetics 1777 (2008) 295–307.
[27] J.A. Bautista, R.G. Hiller, F.P. Sharples, D. Gosztola, M. Wasielewski, H.A. Frank, Singlet and triplet energy transfer in the peridinin–chlorophyll a–protein from *Amphidinium carterae*, J. Phys. Chem. A 103 (1999) 2267–2273.
[28] E. Hofmann, P.M. Wrench, F.P. Sharples, R.G. Hiller, W. Welte, K. Diederichs, Structural basis of light harvesting by carotenoids: peridininchlorophyll–protein from *Amphidinium carterae*, Science 272 (1996) 1788–1791.
[29] S. Santabarbara, E. Bordignon, R.C. Jennings, D. Carbonera, Chlorophyll triplet states associated with photosystem II of thylakoids, Biochemistry 41 (2002) 8184–8194.
[30] R.H. Clarke, Triplet State ODMR Spectroscopy, in: R.H. Clarke (Ed.), Techniques and Applications to Biophysical Systems, Wiley-Interscience, New York, 1982.
[31] A.J. Hoff, Optically detected magnetic resonance of triplet states, in: A.J. Hoff (Ed.), Advanced EPR, Elsevier, Amsterdam, 1989.
[32] S. Stoll, A. Schweiger, EasySpin, a comprehensive software package for spectral simulation and analysis in EPR, J. Magn. Reson. 178 (2006) 42–55.
[33] K. Akiyama, S. Terokubota, T. Ikoma, Y. Ikegami, Spin polarization conservation during intramolecular triplet–triplet energy-transfer studied by time-resolved EPR spectroscopy, J. Am. Chem. Soc. 116 (1994) 5324–5327.
[34] G.M. Morris, R. Huey, W. Lindstrom, M.F. Sanner, R.K. Belew, D.S. Goodsell, A.J. Olson, AutoDock4 and AutoDockTools4: automated docking with selective receptor flexibility, J. Comput. Chem. 30 (2009) 2785–2791.
[35] R. Huey, G.M. Morris, A.J. Olson, D.S. Goodsell, A semiemirical free energy force field with charge-based desolvation, J. Comput. Chem. 28 (2007) 1145–1152.
[36] J. Gasteiger, M. Marsili, Iterative partial equalization of orbital electronegativity—a rapid access to atomic charges, Tetrahedron 36 (1980) 3219–3228.
[37] M.F. Sanner, Python: a programming language for software integration and development, J. Mol. Graph. Model. 17 (1999) 57–61.
[38] A. Angerhofer, F. Bornhauser, A. Gall, R.J. Cogdell, Optical and optically detected magnetic resonance investigation on purple photosynthetic bacterial antenna complex, Chem. Phys. 194 (1995) 259–274.
[39] C.W.M. Kay, G. Elger, K. Mobius, The photoexcited triplet state of free-base porphycene: a time-resolved EPR and electron spin echo investigation, Phys. Chem. Chem. Phys. 1 (1999) 3999–4002.
[40] D. Carbonera, M. Di Valentin, C. Corvaja, G. Agostini, G. Giacometti, P.A. Liddel, D. Kuciauskas, A.L. Moore, T.A. Moore, D. Gust, Carotenoid triplet detection by time-resolved EPR spectroscopy in carotenopyropheophorbide dyads, J. Photochem. Photobiol. 105 (1997) 329–335.
[41] R. Bittl, E. Schlodder, I. Geisenheimer, W. Lubitz, R.J. Cogdell, EPR and absorption studies of carotenoid triplet formation in purple bacterial antenna complexes, J. Phys. Chem. B 105 (2001) 5525–5535.
[42] L. Premvardhan, L. Bordes, A. Beer, C. Büchel, B. Robert, Carotenoid structures and environments in trimeric and oligomeric fucoxanthin chlorophyll a/c_2 proteins from resonance Raman spectroscopy, J. Phys. Chem. B 113 (2009) 12565–12574.
[43] E. Papagiannakis, I.H.M. van Stokkum, H. Fey, C. Büchel, R. van Grondelle, Spectroscopic characterization of the excitation energy transfer in the fucoxanthin–chlorophyll protein of diatoms, Photosynth. Res. 86 (2005) 241–250.
[44] J.A. Bautista, R.E. Connors, B.B. Raju, R.G. Hiller, F.P. Sharples, D. Gosztola, M.R. Wasielewski, H.A. Frank, Excited state properties of peridinin: observation of a solvent dependence of the lowest excited singlet state lifetime and spectral behavior unique among carotenoids, J. Phys. Chem. B 103 (1999) 8751–8758.
[45] E.F. Pettersen, T.D. Goddard, C.C. Huang, G.S. Couch, D.M. Greenblatt, E.C. Meng, T.E. Ferrin, UCSF Chimera—a visualization system for exploratory research and analysis, J. Comput. Chem. 25 (2004) 1605–1612.

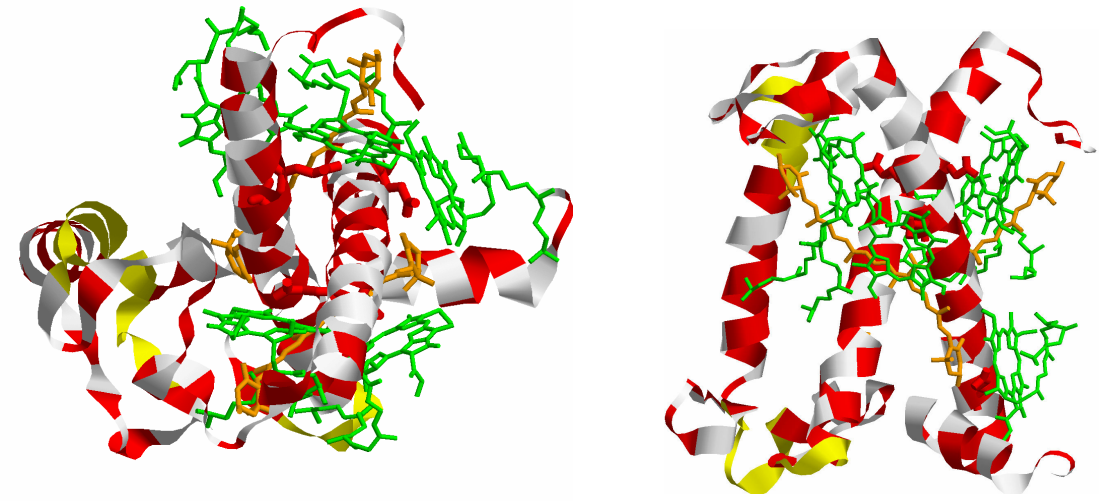
5.1 SUPPLEMENTARY MATERIALS

Triplet-triplet energy transfer in the major intrinsic light-harvesting complex of *Amphidinium carterae* as revealed by ODMR and EPR spectroscopies.

Marilena Di Valentin[1], Enrico Salvadori[1], Giancarlo Agostini[2], Federico Biasibetti[1], Stefano Ceola[1], Roger Hiller[3], Giorgio Mario Giacometti[4], Donatella Carbonera[1]*

[1] *Department of Chemical Sciences, University of Padova, Via Marzolo 1, 35131 Padova, Italy*
[2] *CNR, Inst Biomol Chem, Padova Unit, I-35131, via Marzolo 1, 35131 Padova, Italy*
[3] *Department of Biological Sciences, Macquarie University, 2109 NSW, Australia*
[3] *Department of Biology, University of Padova, via U. Bassi 58/B, 35121 Padova, Italy*

Figure S1 Residues which either are identical or correspond to positive substitutions in the BLAST alignment of LHC and LHC-II are in shown red (only the backbone is shown). Yellow parts represent gaps in the LHC structure. The structure displayed is relative to LHC-II from spinach (fragment 46-218). View from two different sides.



Calculations of the acceptor populating rates starting from those of the donor

The estimation of the acceptor populating rates of the triplet sublevels, starting from those of the donor, has been done in the limit of a TTET which is fast, compared to the time evolution of the donor triplet spectrum, and it is slow enough to allow spin alignment in the external magnetic field, in the hypothesis of spin conservation. The acceptor inherits the polarization of the donor in a way which depends on the relative geometrical arrangement of the ZFS tensor axes of the donor–acceptor couple.

Referring to the population in zero magnetic field, the relationship between the populations is the following:

$$P_i^A = \sum_j \cos_{ij}^2 \vartheta \; P_j^D$$

where $cos\,\vartheta_{ij}$ is the angle between the principal ZFS axis j of the donor (D) and the axis i of the acceptor (A). In the presence of an external magnetic field the populating rates, which determine the initial polarization of the acceptor triplet state, can be easily calculated starting from the Zero field population rates. Although the absolute values of the donor populating rates are usually not known, and only relative Px: Py: Pz values are accessible by the experiments, it can be demonstrated that the relative population rates of the acceptor, which actually determine the shape of the TR-EPR spectrum, can be calculated directly from the above reported equation, using the relative P^D_j values. The absolute intensity of the acceptor spectrum cannot be estimated.

Results of the calculations

Figure S2 The thirteen conformations (A….O) of minimal, comparable binding energy of the peridinin molecules in the protein pocket of LHC, homologous to the L1 site of LHC-II, as calculated by the docking analysis (green color scale) are shown. The residues allowed to move during the energy optimization procedure (grey), and the conserved Chls (Cla612 (red), Cla610 (blue), Cla613 (pink)) are also shown. Corresponding Lutein 620 position in the L1 site of LHC-II [pdb file (1RWT)] is displayed in orange.

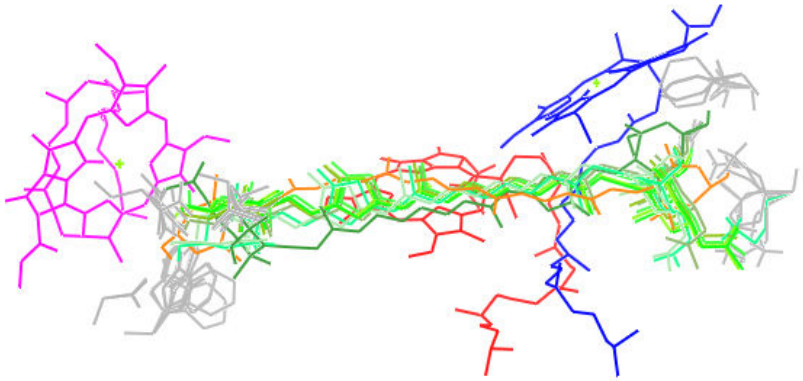
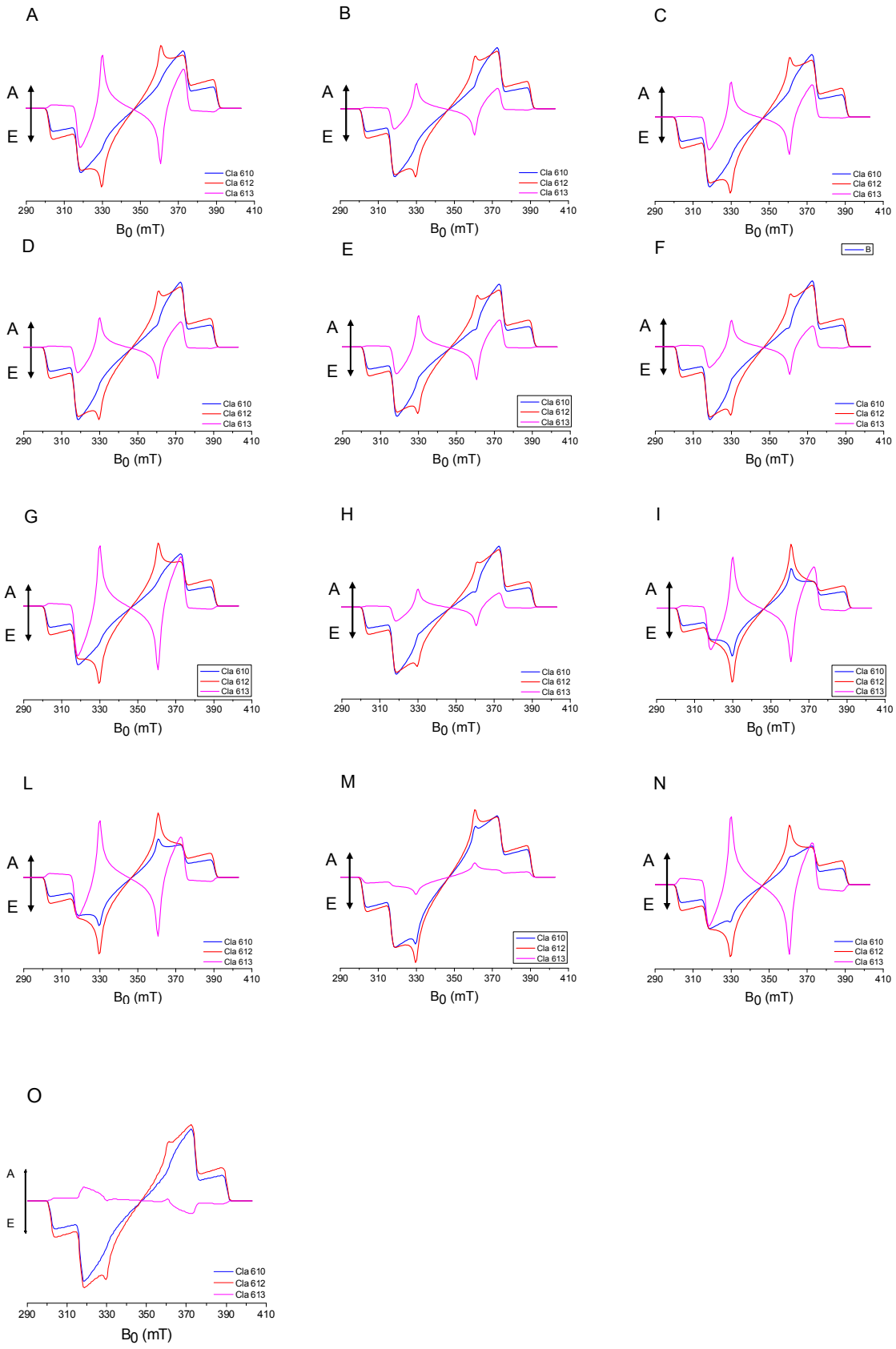


Table S1 Relative populations of the peridinin triplet state sublevels for the thirteen conformations (A---O) shown in figure S1, calculated in the hypothesis of TTET starting from each of the conserved Chls (Cla 610, 612, 613). The initial donor ^{T}Chl polarization pattern is *eeeaaa* (^{T}Cla - Px : P y : Pz = 0.36 : 0.44 : 0.20).

Conformation	**Cla 610** Px : Py : Pz	**Cla 612** Px : Py : Pz	**Cla613** Px : Py : Pz
A	0.33 : 0.23 : 0.44	0.27 : 0.25 : 0.48	0.46 : 0.23 : 0.31
B	0.34 : 0.21 : 0.45	0.28 : 0.23 : 0.49	0.40 : 0.27 : 0.33
C	0.34 : 0.21 : 0.45	0.28 : 0.24 : 0.48	0.42 : 0.25 : 0.33
D	0.34 : 0.21 : 0.45	0.28 : 0.24 : 0.48	0.41 : 0.26 : 0.33
E	0.35 : 0.21 : 0.44	0.29 : 0.24 : 0.47	0.41 : 0.26 : 0.33
F	0.35 : 0.20 : 0.45	0.29 : 0.23 : 0.48	0.40 : 0.28 : 0.32
G	0.33 : 0.25 : 0.42	0.26 : 0.28 : 0.46	0.47 : 0.21 : 0.32
H	0.36 : 0.20 : 0.44	0.30 : 0.22 : 0.48	0.38 : 0.29 : 0.33
I	0.28 : 0.29 :0.43	0.23 : 0.30 : 0.47	0.48 : 0.20 : 0.32
L	0.29 : 0.27 : 0.44	0.23 : 0.29 : 0.48	0.49 : 0.20 : 0.31
M	0.28 : 0.20 : 0.52	0.24 : 0.21 : 0.55	0.31 : 0.32 : 0.37
N	0.31 : 0.26 : 0.43	0.25 : 0.28 : 0.47	0.50 : 0.20 : 0.30
O	0.34 : 0.20 : 0.46	0.29 : 0.20 : 0.51	0.32 : 0.36 : 0.32

Figure S3 Spin polarized triplet spectra of peridinin populated by TTET calculated starting from the ^{T}Chl *a* molecules (Cla 610, 612,613 as indicated) for the thirteen conformations shown in figure S1. Only one of the two carotenoid (T2: |D| = 442 G, |E| = 44.8 G) is shown for clarity. T1 and T2 in site L1 have the same polarization and differ only for the ZFS parameters. The relative populations of the peridinin triplet state sublevels are those reported in table S1. The analogous results relative to the L2 site are not reported, since no substantial differences between the two carotenoid binding sites have been found.


A
A
E
Cla 610
Cla 612
Cla 613
290 310 330 350 370 390 410
B0 (mT)
B
C
D
E
F
G
H
I
L
M
N
O

Chapter VI

PCPs from *Amphidinium carterae* and *Heterocapsa pygmaea*

Biochimica et Biophysica Acta 1777 (2008) 1355–1363

Contents lists available at ScienceDirect

Biochimica et Biophysica Acta

journal homepage: www.elsevier.com/locate/bbabio

Spectroscopic properties of the peridinins involved in chlorophyll triplet quenching in high-salt peridinin–chlorophyll *a*-protein from *Amphidinium carterae* as revealed by optically detected magnetic resonance, pulse EPR and pulse ENDOR spectroscopies

Marilena Di Valentin [a], Stefano Ceola [a], Enrico Salvadori [a], Giancarlo Agostini [c], Giorgio Mario Giacometti [b], Donatella Carbonera [a,*]

[a] *Dipartimento di Scienze Chimiche, Università di Padova, via Marzolo 1, 35131 Padova, Italy*
[b] *Dipartimento di Biologia, Università di Padova, vi U. Bassi, 35131 Padova, Italy*
[c] *CNR, Istituto di Chimica Biomolecolare, Sezione di Padova, via Marzolo 1, 35131 Padova, Italy*

ARTICLE INFO

Article history:
Received 7 May 2008
Received in revised form 6 June 2008
Accepted 6 June 2008
Available online 18 June 2008

Keywords:
Peridinin
Carotenoid
Triplet
ODMR
EPR
ENDOR
HSPCP
MFPCP

ABSTRACT

The photoexcited triplet state of the carotenoid peridinin in the high-salt peridinin–chlorophyll *a*-protein (HSPCP) of the dinoflagellate *Amphidinium carterae* was investigated by ODMR (optically detected magnetic resonance), pulse EPR and pulse ENDOR spectroscopies. The properties of peridinins associated to the triplet state formation in HSPCP were compared to those of peridinins involved in triplet state population in the main-form peridinin–chlorophyll protein (MFPCP), previously reported. In HSPCP no signals due to the presence of chlorophyll triplet state have been detected, during either steady-state illumination or laser-pulse excitation, meaning that peridinins play the photo-protective role with 100% efficiency as in MFPCP. The general spectroscopic features of the peridinin triplet state are very similar in the two complexes and allow drawing the conclusion that the triplet formation pathway and the triplet localization in one specific peridinin in each subcluster are the same in HSPCP and MFPCP. However some significant differences also emerged from the analysis of the spectra. Zero field splitting parameters of the peridinin triplet states are slightly smaller in HSPCP and small changes are also observed for the hyperfine splittings measured by pulse ENDOR and assigned to the β-protons belonging to one of the two methyl groups present in the conjugated chain, (a_{iso} = 10.3 MHz in HSPCP vs a_{iso} = 10.6 MHz in MFPCP). The differences are explained in terms of local distortion of the tails of the conjugated chains of the peridinin molecules, in agreement with the conformational data resulting from the X-ray structures of the two complexes.

© 2008 Elsevier B.V. All rights reserved.

1. Introduction

The water soluble peridinin–chlorophyll *a*-protein (PCP) of the dinoflagellate *Amphidinium carterae*, belongs to the group of marine eukaryotic algae which employ carotenoids, such as peridinin, characterized by the presence of a carbonyl group in their molecular structure, to fulfil the light-harvesting function during photosynthesis.

The main-form PCP, MFPCP, contains peridinin and chlorophyll (Chl) *a* molecules in a stoichiometric ratio of 4:1 [1]. Along with the MFPCP, a minor component has also been isolated from *A. carterae*, which is eluted from an anion exchange column at high-salt concentration [2]. This form is denoted high-salt PCP (HSPCP) and presents 31% identity in amino acid sequence with MFPCP. It contains only six peridinins and two Chl *a* molecules and presents a larger number of positively charged amino acid residues.

The X-ray structure of MFPCP from *A. carterae* has been resolved to 2.0 Å [1]. The basic structure is a trimer. In each subunit of the trimer the pigments are arranged as two pseudo-identical domains of four peridinins and one Chl *a* molecule, as shown in Fig. 1. The pigments are located in the hydrophobic cavity formed by the protein. The peptide primary sequences of the $-NH_2$ and $-COOH$ terminal regions are largely (56%) homologous and form structurally almost identical domains, each consisting of eight alpha-helices. The MFPCP complex has a molecular weight of 32 kDa. Distances between peridinins

Abbreviations: PID, peridinin; Chl, chlorophyll; PCP, peridinin–chlorophyll protein; *A. carterae*, *Amphidinium carterae*; MFPCP, main-form PCP; HSPCP, high-salt PCP; ODMR, optically detected magnetic resonance; FDMR, fluorescence detected magnetic resonance; ADMR, absorption detected magnetic resonance; ZFS, zero field splitting; ISC, intersystem crossing; ESE, electron spin echo; ENDOR, electron nuclear double resonance; TR-EPR, Time-resolved Electron Paramagnetic Resonance; hf: hyperfine; hfcs: hyperfine constants

* Corresponding author. Tel.: +39 049 827 5144; fax: +39 049 827 5161.
E-mail address: donatella.carbonera@unipd.it (D. Carbonera).

0005-2728/$ – see front matter © 2008 Elsevier B.V. All rights reserved.
doi:10.1016/j.bbabio.2008.06.006

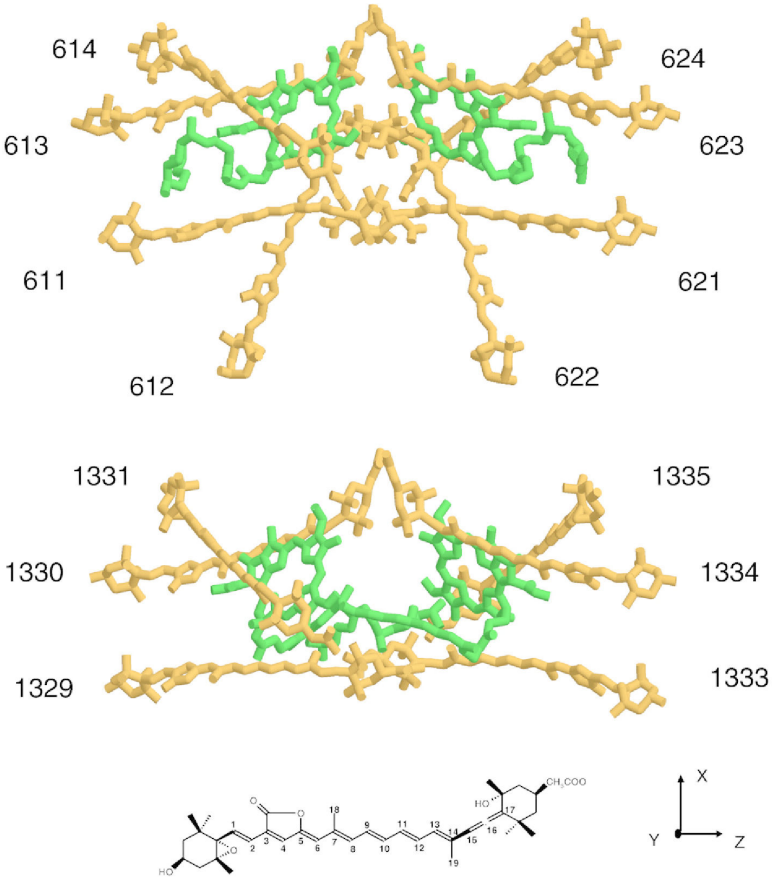


Fig. 1. (Top) Structure of the pigments associated with the monomeric basic unit of the PCP complex from *A. carterae*. Structure taken from coordinates of MFPCP complex 1PPR deposited in the Brookhaven Protein Data Bank. The numbers refer to the peridinins in the PDB files, the numbering is maintained. (Bottom) Structure of the pigments associated with the monomeric basic unit of the HSPCP complex from *A. carterae*. Structure taken from coordinates of PCP complex 2C9E deposited in the Brookhaven Protein Data Bank. The molecular structure of peridinin with the numbering of atoms and the orientation of the ZFS tensor axes is also reported.

within a single domain range from 4 to 11 Å, and the conjugated regions of the peridinins are in van der Waals contact (3.3–3.8 Å) with the tetrapyrrole rings of the Chl *a* molecules. The distance between the Mg atoms of the two Chl *a* molecules in each subunit is 17.4 Å.

Recently, the X-ray structure of HSPCP, which has a molecular weight of 34 kDa, has also been determined (T. Schulte, F.P. Sharples, R.G. Hiller, E. Hofmann, Coordinates have been deposited in the Brookhaven Protein Data Bank under ID 2C9E, unpublished) [3]. It shows a large similarity with the MFPCP structure in terms of pigment arrangement, except for the absence of two symmetry related peridinins, called PID612/PID622, according to the nomenclature of Hofmann et al. [1]. These two peridinins have been proposed to have blue-shifted absorption in the MFPCP complex [4]. An interesting difference between MFPCP and HSPCP complexes is the distance between the Mg atoms of the two Chl *a* molecules in each subunit, which is larger in the HSPCP complex (18.4 Å). Moreover, in HSPCP the phytol tails are located in the space between the two Chls, whereas in MFPCP they point to the external part of the protein. A direct comparison of the pigment arrangement in the structure of MFPCP and HSPCP is shown in Fig. 1. The different local environment of the two Chl molecules in the HSPCP complex leads to a splitting of the Chl *a* Qy absorption band at low temperature which is not observed in MFPCP [4].

After the publication of the X-ray structure of MFPCP, the number of spectroscopic studies and quantum mechanical calculations, aimed to correlate the spectroscopic properties to the arrangement of the pigments in the protein, increased quickly. Recently the study has been extended also to HSPCP which was investigated using absorption, fluorescence, fluorescence excitation, two-photon, and fast-transient optical spectroscopy [3,4]. Absorption spectra of both complexes were recorded at 10 K and analyzed in the 400–600 nm region by summing the individual 10 K spectra of Chl *a* and peridinin recorded in 2-MTHF. Fluorescence excitation spectroscopy revealed a high peridinin-to-Chl *a* energy transfer efficiency (>95%) [4]. Femtosecond time-resolved optical methods have been used to compare the energy transfer dynamics in MFPCP and HSPCP. The Chl-to-Chl energy transfer rate constant for MFPCP was found to be a factor of 4.2 larger [3].

It is well known that carotenoids bound to the light-harvesting complexes of bacteria, plants and algae, and having more than seven double bonds in the conjugated polyene chain, possess low-lying triplet states capable of trapping (B) Chl *a* triplet states, avoiding in this way the formation of potentially harmful singlet oxygen, and are able to quench active oxygen species [5]. Peridinin molecules in the isolated MFPCP complex are able to play this photo-protective role, with a 100% efficiency in terms of triplet–triplet energy transfer. The lifetime of the Chl *a* triplet state is of the order of 20 ns, within this

time a triplet state is formed on the circumferential peridinins and decays through radiationless intersystem crossing channels with a lifetime of 10 μs at room temperature [6].

In the past we used ODMR (optically detected magnetic resonance) to study the formation of triplet state in isolated MFPCP complexes [7–9]. The technique is particularly powerful in the study of photoinduced triplet states because it allows correlating the magnetic properties of the triplet state with the optical properties of the system. More recently, in a time-resolved EPR (TR-EPR) work on the peridinin triplet state generated in PCP proteins from *A. carterae*, we exploited the concept of spin conservation during triplet–triplet energy transfer, to identify the peridinin–chlorophyll pairs directly involved in the triplet energy transfer. By comparing the TR-EPR spectra of MFPCP and HSPCP and their X-ray structures, we suggested that the pathway of triplet quenching and triplet localization was quite similar in the two complexes [10]. We performed also pulse EPR and pulse ENDOR experiments on MFPCP at variable temperatures [11]. The ENDOR investigation, accompanied by DFT calculation of the hyperfine couplings, strongly supported the hypothesis of localization of the triplet state on one peridinin in each subcluster of MFPCP.

The triplet state of peridinins in HSPCP has not been characterized at the same extent. In this paper we complete the investigation on HSPCP and present an extended magnetic resonance study by using several techniques, namely ODMR, electron spin echo (ESE) and pulse ENDOR.

The results are compared to those previously obtained for MFPCP and discussed in terms of energy transfer properties, specific pathway for triplet quenching and protein structure.

2. Materials and methods

2.1. Sample preparation

The MFPCP and HSPCP complexes, extracted and purified according to Sharples et al. [2], were kindly supplied by R.G. Hiller.

2.2. Spectroscopic methods

2.2.1. ODMR and fluorescence experiments

The samples were diluted to a final Chl concentration equivalent to 100 μg/ml and 60% v/v glycerol was added in order to obtain a transparent glass upon cooling of the sample to the cryogenic temperature of the experiments. Fluorescence detected magnetic resonance (FDMR) and absorption detected magnetic resonance (ADMR) experiments were performed in the same laboratory build apparatus, previously described in detail [12,13]. The flexibility of the set up allows performing both kinds of experiments on the same sample by switching the detection mode. Briefly, ODMR is a double resonance technique based on the simple principle that, when upon illumination a triplet steady-state population is generated in a system, the application of a resonant microwave electromagnetic field between a couple of spin sublevels of the triplet state, generally induces a change of the steady-state population of the triplet state itself, due to the anisotropy of the decay and population rates of the three spin sublevels. The induced change of the triplet population may be detected as a corresponding change of the emission and/or absorption of the system [14,15]. Amplitude modulation of the applied microwave field is used to greatly increase the signal to noise ratio by means of a phase sensitive lock-in amplifier (EG&G 5220). In the FDMR experiments the fluorescence, excited by a halogen lamp (250 W) focused into the sample and filtered by a broadband 5 cm solution of $CuSO_4$ 1 M, was collected at 45 degrees through appropriate band-pass filters (10 nm FWHM) by a photodiode before entering the lock-in amplifier. Low temperature emission spectra were detected in the same apparatus used for ODMR experiments, using the same excitation source, but substituting the band-pass filters before the photodiode, coupled to a voltage-amplifier, by a monochromator.

In the absorption detection mode (ADMR) the same excitation lamp was used but without filters before the sample, except for 5 cm water and heat filters. The beam was focused into the monochromator after passing the sample and finally collected by a photodiode. The modulation frequency and the microwave power were chosen depending on the experiment. By fixing the microwave frequency at a resonant value while sweeping the detection wavelength, microwave-induced triplet-minus-singlet (T−S) spectra can be registered.

The temperature was 1.8 K. At such a temperature spin-lattice relaxation is inhibited and the ODMR signal is intense. In the experiments at higher temperatures the helium flow in the cryostat was adjusted to obtain a stable temperature.

2.2.2. Pulse EPR and pulse ENDOR experiments

The concentration of the samples was 1.0 mg protein/ml. Oxygen was removed from the samples by flushing argon in the capillary before freezing. Glycerol, previously degassed by several cycles of freezing and pumping, was added (60%v/v) to obtain a transparent matrix.

Experiments were performed on a Bruker Elexsys E580 pulsed EPR spectrometer equipped with a Bruker ENDOR accessory (E560D-P) and a radio frequency amplifier (AR751 — 150 W). Laser excitation at 532 nm (10 mJ per pulse and repetition rate of 10 Hz) was provided by the second harmonic of a Nd:YAG laser (Quantel Brilliant) in the optically transparent dielectric ring ENDOR resonator (EN4118X-MD4). The temperature was controlled with a Helium cryostat (Oxford CF935) driven by a temperature controller (Oxford ITC503).

Field-swept ESE spectra were recorded using a 2-pulse ESE sequence according to the scheme: flash-DAF-π/2-τ-π-τ-echo (DAF = delay after laser flash). ESE-detected kinetics at the triplet canonical orientations were recorded using a 2-pulse (flash-DAF-π/2-τ-π-τ-echo) ESE sequence after a variable DAF (500 ns step) between the laser flash and the first MW pulse. The π/2-pulse was of 16 ns and the delay τ was set at 200 ns for the field-swept ESE experiment and to 120 ns for the ESE-detected kinetics.

Mims ENDOR experiments were recorded using the MW pulse sequence flash-DAF-π/2-τ-π/2-*T*-π/2, with 16 ns pulse duration, in conjunction with an RF pulse of 3 μs duration, starting 0.3 μs after the second MW pulse. The DAF was 50 ns, the delay τ was variable, and the time T was 3.8 μs to accommodate the RF pulse. Mims ENDOR spectra were recorded at different τ values (from 160 ns to 240 ns) and added together to eliminate τ dependent blind spots. Pulse ENDOR spectra were accumulated for ≈15 h.

Simulations of the field-swept ESE spectra and DAF kinetics were performed according to the method previously described in Ref. [11].

3. Results

The absorption spectrum of HSPCP, taken at room temperature, was identical to the one reported by Ilagan et al. [4]. At cryogenic temperatures the splitting of the Qy band of the Chl *a* and a red shift of the carotenoid absorption in the region 450–550 nm, when compared to MFPCP, were observed, as previously reported for spectra detected at 10 K [4]. At 1.8 K the fluorescence emission maximum was at 677 nm, 2 nm red-shifted compared to the value reported for the emission at 77 K [4]. In Fig. 2, the emission spectrum at 1.8 K is shown.

3.1. Odmr

Steady-state illumination of the sample at cryogenic temperatures induces the formation of triplet states which can be detected by monitoring the change of the emission of the sample while sweeping the microwave field in the spectral region where chlorophyll and carotenoid triplet states are expected to show resonant transitions

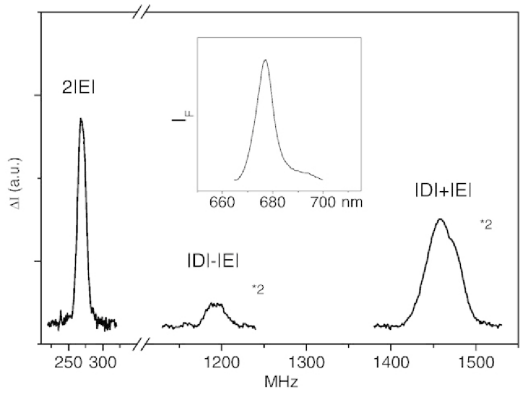


Fig. 2. FDMR spectra of peridinin triplet state in HSPCP at 1.8 K. Detection wavelength: 680 nm; modulation frequency: 323 Hz, microwave power: 1 W, 10 scans. Inset: Fluorescence emission spectra of HSPCP at 1.8 K.

between couples of spin sublevels. In principle, FDMR should not be suitable for detection of carotenoid triplet states, since carotenoids are non-fluorescing molecules. However, it has been previously demonstrated [7,16,17] that, due to the energy transfer processes going on among carotenoids and chlorophylls in the antenna complexes, a change of the steady-state population of the carotenoid triplet state, induced by a resonant microwave field, is reflected by a change of the intensity of the emission of the nearby chlorophyll molecules. In Fig. 2 the FDMR spectra, taken at wavelength corresponding to the maximum of the emission spectrum and in the microwave field region where the 2|*E*|, the |*D*|−|*E*| and the |*D*|+|*E*| transitions of carotenoids are expected, are shown. Three transitions with the polarization pattern usually found for carotenoids (intensity of 2|*E*|>> |*D*|+|*E*|>|*D*|+|*E*|) have been detected at 269, 1190 (sh1212) and 1458 (sh1470) MHz, proving the ability of the peridinins in the HSPCP complex to quench Chl triplet states by populating carotenoid triplets, even at very low temperature. The transition frequencies are slightly shifted with respect to those previously reported for MFPCP (i.e. 267, 1203(sh1229), 1465(sh1499) MHz) [7–9]. As found for most ODMR spectra of carotenoids, the |*D*|+|*E*| and |*D*|−|*E*| transitions are largely inhomogeneous. This leads to a decomposition of each triplet transition in at least two main Gaussian components (not shown) as previously found for MFPCP [8]. The resulting two triplet states are characterized by the following zero field splitting (ZFS) parameters: |*D*|=0.0440 cm^{-1}, |*E*|=0.0044 cm^{-1} and |*D*|= 0.0446 cm^{-1}, |*E*|=0.0045 cm^{-1}. The |*D*| values are both smaller than the corresponding values found for the two triplet states detected in MFPCP (|*D*|=0.0448 cm^{-1} |*E*|=0.0044 cm^{-1} and |*D*|=0.04586 cm^{-1} |*E*|= 0.0045 cm^{-1}). The results are collected in Table 1.

No signals which could be ascribed to the presence of unquenched Chl a triplet states have been detected in the steady-state conditions of the experiments, meaning that the efficiency of triplet quenching is 100%, as already found in MFPCP [7].

The microwave-induced T−S spectra taken at the maximum of the intense 2|*E*| transition (269 MHz) and at two different frequencies, chosen in the broad |*D*|+|*E*| transition, are shown in Fig. 3. The main features of the T−S spectra are very similar to those previously reported for MFPCP (thin line in Fig. 3, from [7]). Broad and complex triplet–triplet absorption bands due to peridinin triplet states are present in the whole spectral range from 450 to 650 nm. A remarkable difference is that in HSPCP the bleaching in the Q_y region of Chl *a* absorption splits clearly in two bands: a sharp feature at 675.8 nm and another broader feature at about 670 nm. A single positive band is observed at 678.7 nm. The sharp bleaching is relatively more pronounced when the spectrum is taken at 1476 MHz, in correspondence to the shoulder of the |D|+|E| transition, compared to the spectrum detected at 1457 MHz.

At 130 K and higher temperatures, the T−S spectrum becomes smoother, the sharp negative/positive features in the Q_y region of Chl absorption disappear and only a broad bleaching centred at about 670 nm remains (data not shown).

3.2. ESE and pulse ENDOR

In our previous work on triplet–triplet energy transfer in PCP from *A. carterae* we reported the TR-EPR spectrum of the HSPCP [10] and found that it was very similar to the spectrum of the MFPCP. Here we extend the characterization of the triplet state in terms of ESE and pulse ENDOR spectroscopy and compare the results to those obtained for MFPCP [11].

While kinetic measurements in time-resolved EPR are hampered by the presence of microwave-induced transition probabilities, ESE spectroscopy does not suffer of this complication since in this technique there is no microwave field present in the period between the photogeneration of the triplet state and its detection [18]. The kinetics of population and decay of the triplet spin sublevels, obtained by monitoring the echo intensity as a function of DAF at the low-field canonical orientations of the ZFS tensor (Z^-, Y^+, X^+), are shown in Fig. 4 together with the ESE-detected spectrum at a DAF of 50 ns, at 20 K. Direct comparison with the data on MFPCP taken from Ref. [11] is reported in Fig. 4. Due to the absence of fast and anisotropic relaxation processes depending on the orientation of the triplet state with respect to the magnetic field, the ESE-detected spectra taken at early times after the laser flash are substantially the same, in terms of shape, as the initial TR-EPR spectra previously reported [10].

As observed for MFPCP, the spin polarization varies in time, showing an intensity increase at the *Y* canonical resonance in the first 20 ms. Simulations of the ESE-detected spectra and ESE kinetics, according to the method described in [11], give the ZFS parameters, the relative populating rates and decay rates for the peridinin triplet sublevels in HSPCP reported in Table 1. Simulations of the ESE-detected spectra and ESE kinetics are not shown. The order of the ZFS energy levels is: $Z^2>Y^2>X^2$. As discussed before [10], the corresponding ZFS axes of the peridinin triplet state in the molecular frame are the following: the long axis is the *Z* axis, the *X* axis is along the C–H bonds in the conjugated chain and the *Y* direction is perpendicular to the conjugated *XZ* molecular plane. These axes are shown in the molecular scheme of peridinin reported in Fig. 1.

To search for possible local differences in the triplet electronic distribution of the peridinin(s) where the triplet becomes localized after triplet–triplet transfer from the Chl(s) molecule(s) we performed

Table 1
Parameters of the peridinin triplet state

	|*D*| (10^{-4} cm^{-1})	|*E*| (10^{-4} cm^{-1})	P_X: P_Y: P_Z	k_X: k_Y: k_Z (μs^{-1})	Ref.
MFPCP	449.7±0.1 (ESE)	43.9±0.1 (ESE)	0.18: 0.37: 0.45	0.15: 0.03: 0.09	[11]
	448.0±0.1 (ODMR)	44.0±0.1 (ODMR)			[8]
	458.6±0.1 (ODMR)	45.0±0.1 (ODMR)			[8]
HSPCP	443.6±0.1 (ESE)	45.1±0.1 (ESE)	0.18: 0.39: 0.43	0.135: 0.028: 0.08	
	440.0±0.1 (ODMR)	44.6±0.1 (ODMR)			
	446.0±0.1 (ODMR)	45.0±0.1 (ODMR)			

Values of the relative population rates, P_X, P_Y and P_Z, and decay constants, k_X, k_Y and k_Z, of the triplet sublevels together with the ZFS parameters |*D*| and |*E*|, derived from simulation of the time evolution of the field-swept ESE spectrum of HSPCP, according to the method described in Ref. [11]. For comparison the data relative to MFPCP from Ref. [11] are also reported. ZFS parameters resulting from the decomposition of the ODMR spectra of HSPCP with Gaussian components are also reported and compared to the equivalent data for MFPCP from Ref. [8]; line widths used in the decomposition were 8, 13, 25 MHz for both the Gaussian components contributing to each of the 2|*E*|, |*D*|−|*E*| and |*D*|+|*E*| transitions respectively.

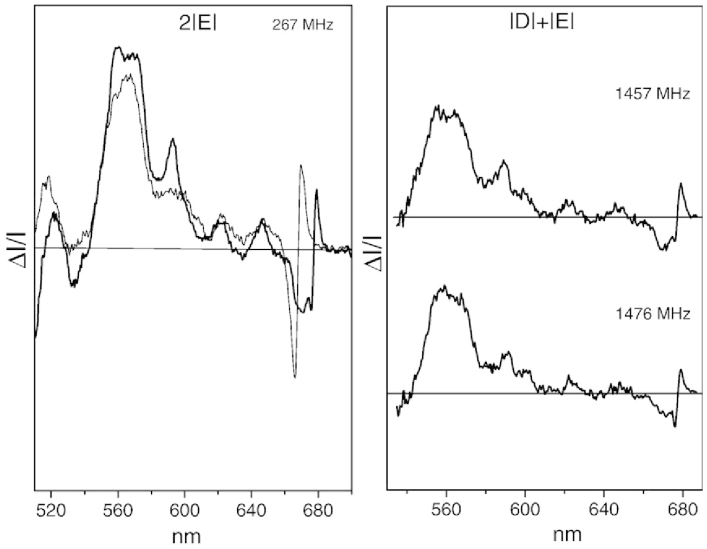


Fig. 3. T−S spectra of HSPCP detected at different resonant microwave frequencies. (Left) Comparison of the T−S spectra of HSPCP (thick line) and MFPCP (thin line) detected at the 2|*E*| transition frequency. Spectra have been rescaled to better comparison. Line corresponding to $\Delta I/I=0$ is shown. (Right) T−S spectra of HSPCP at two frequencies of the broad |*D*+|*E*| transition, as indicated. Lines corresponding to $\Delta I/I=0$ are shown. Modulation frequency: 323 Hz, microwave power: 1 W, $T=1.8$ K. Data relative to MFPCP are identical to those reported in [7]. $\Delta I/I \cong \Delta A$.

time-resolved ENDOR experiments on the triplet state and compared the results to those relative to MFPCP reported in [11]. The measurements of the ENDOR effect at the canonical magnetic field positions shown in the spectrum reported in Fig. 4, give the *Aii* hyperfine tensor components of protons in the reference frame of the ZFS tensor. These hyperfine couplings (hfc) are sensitive probe of the electronic distribution in the conjugated chain. In Fig. 5 the experimental Mims ENDOR spectra of the photoexcited triplet state of peridinin in HSPCP from *A. carterae*, at the X^+/X^- and Z^+/Z^- EPR field positions, obtained at 20 K at early times after the laser flash, are reported and compared to the corresponding spectra for MFPCP [11]. The ENDOR spectra of the Y^+/Y^- EPR field positions show an unstructured line at ν_H (the proton Larmor frequency) at short time and only spectra taken after 18 μs after the laser flash show some significant transitions. The spectrum at the Y^- field position is shown in Fig. 5 while the spectrum at the Y^+ position is omitted because it does not give any additional information showing only weak transitions due to the methyl couplings.

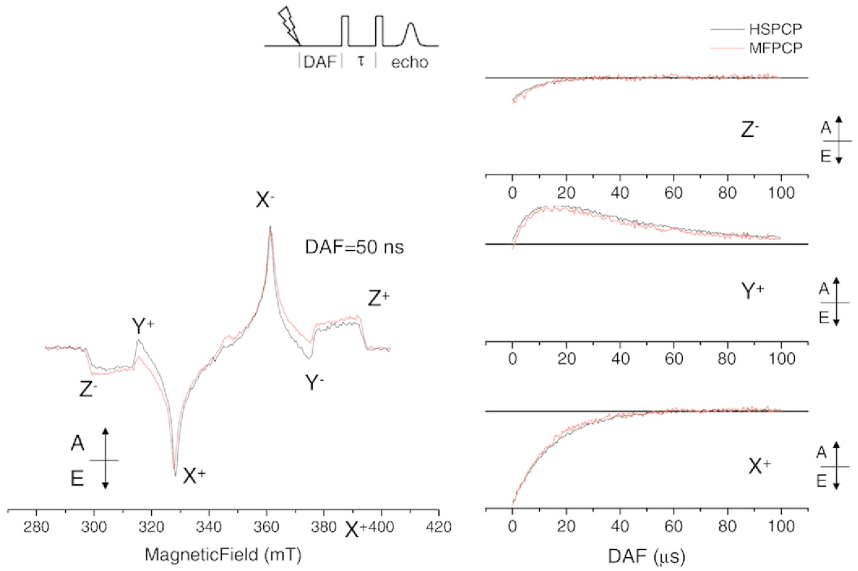


Fig. 4. (Left) Field-swept ESE spectrum of HSPCP (black) and MFPCP (red) from *A. carterae*, at $T=20$ K, at DAF=50 ns. (Right) ESE-detected kinetics, at $T=20$ K, at the low-field canonical fields Z^-, Y^+, X^+ (HSPCP: black lines; MFPCP: red lines). A = absorption, E = emission. For experimental conditions see Materials and methods. Inset: Pulse scheme of the ESE experiment for photoexcited triplet states. Order of energy for zero field triplet sublevels: |*Z*|>|*X*|>|*Y*|. Data relative to MFPCP are the same as in Ref. [11].

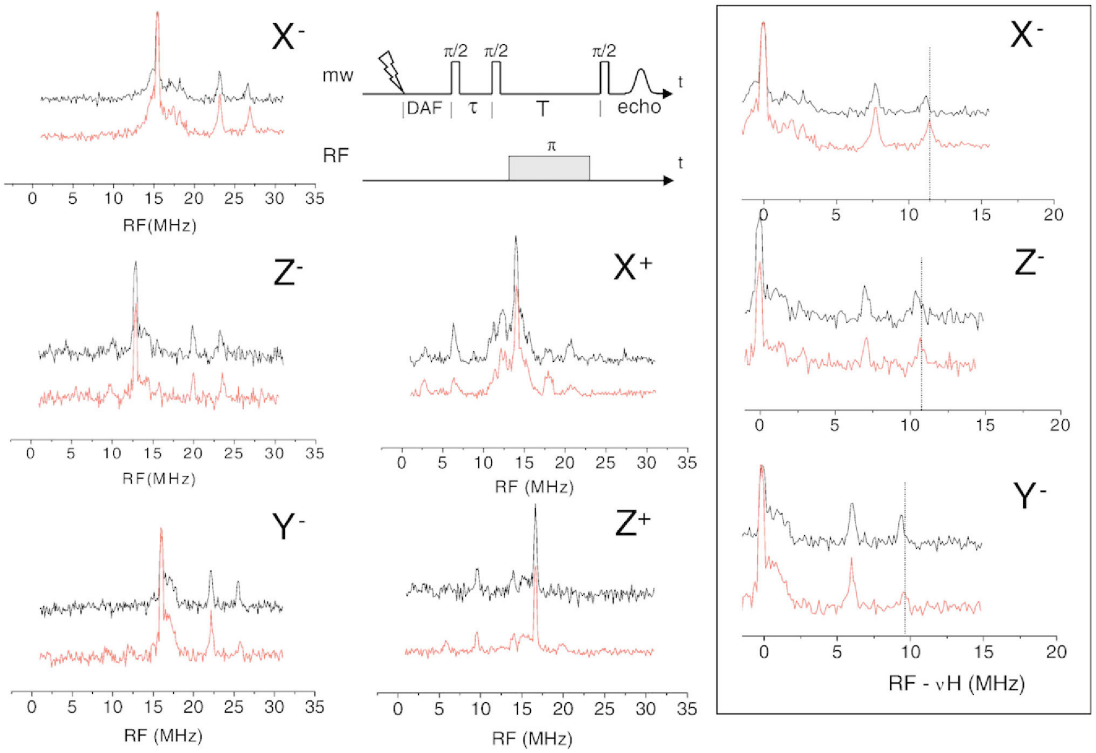


Fig. 5. Pulse Mims ENDOR spectra of HSPCP (black) and MFPCP (red) from *A. carterae* for the *X*, *Y* and *Z* EPR field positions (indicated in Fig. 4) at $T = 20$ K. The ENDOR spectra for the X^+, Y^- and Z^- EPR transitions are in emission but have been inverted for better comparison. The pulse sequence used is indicated. Right panel: region of hfcs relative to the methyl groups enlarged and with a frequency scale which gives the deviation from the ν_H. The hfcs correspond to the frequency shift between the corresponding ENDOR line and the ν_H. For experimental conditions see Materials and methods. Data relative to MFPCP are the same as in Ref. [11].

The two narrow ENDOR transitions, appearing on the low RF (radio frequency) side from ν_H in the X^+ and Z^+ spectra and on the high RF side from ν_H in the X^- and Z^- spectra, correspond to positive hfcs which have been assigned to rotating methyl group at positions 18 and 19 in the molecular structure shown in Fig. 1 [11]. In HSPCP one of the two methyl groups shows hyperfine couplings which are smaller compared to the values found in MFPCP ($A_{XX} = 11.1$ MHz/$A_{YY} = 9.5$ MHz/$A_{ZZ} = 10.3$ MHz versus $A_{XX} = 11.4$ MHz/$A_{YY} = 9.8$ MHz/$A_{ZZ} = 10.7$ MHz), while the other methyl shows the same hfc values: $A_{XX} = 7.6$ MHz, $A_{YY} = 6.2$ MHz $A_{ZZ} = 7.1$ MHz. The values of the hfcs along the three ZFS directions lead to estimate an $a_{iso} = 10.3$ MHz for HSPCP, to be compared to the value 10.6 MHz previously found for MFPCP. In Fig. 5 the ENDOR transitions assigned to the methyl protons, for the three canonical orientations, are shown in a scale (RF-ν_H) which allows the direct estimation of the couplings.

The use of Mims ENDOR was aimed to detect the small hyperfine couplings with more sensitivity to search for possible differences between the two complexes also in the region close to ν_H. However no significant differences were observed in this region. The Davies ENDOR spectra performed on the samples did not give additional information (not shown).

4. Discussion

In HSPCP, peridinins play the photo-protective role with 100% efficiency as in MFPCP. In both complexes no signals due to the presence of chlorophyll triplet state have been detected, during either steady-state illumination or laser-pulse excitation.

Triplet–triplet energy transfer has a very stringent distance requirement and is very sensitive to the mutual orientation of the molecular π orbitals of the molecules involved. In our previous work on MFPCP we have shown that localization of the triplet state mainly in one peridinin in each subcluster is likely to occur [10]. The peridinin–chlorophyll pair, directly involved in the triplet–triplet energy transfer, coincides with the one having the shortest centre to centre distance and the water molecule, which is coordinated to the central Mg atom of the Chl *a* molecule, placed at the interface between the two pigments (PID614/624 in Fig. 1). In our analysis of the TR-EPR data, in terms of triplet–triplet transfer, also PID612 and PID622 resulted to be possible sites of Chl triplet quenching in MFPCP. However, their involvement was supposed to be inessential on the basis of the comparison of the TR-EPR spectra of MFPCP with those obtained for HSPCP because in the latter the analogous of the PID612/622 couple is missing but the TR-EPR spectrum is very similar to that of MFPCP [10]. While the polarization pattern of TR-EPR spectrum of peridinin triplet state is strongly dependent on the relative geometry of the donor-acceptor couple, ODMR and ENDOR spectroscopies are more sensitive to the local environment of the triplet state itself. For this reason we have performed a complete study searching for possible significant differences in triplet localization and molecular environment in HSPCP compared to MFPCP.

4.1. Odmr

The three FDMR transitions are inhomogenously broadened and show two distinct components as previously observed for MFPCP (see

Table 1). The ZFS parameters |*D*| and |*E*| are slightly different in the two complexes; this can be due to the local environment and/or to a distortion of the peridinin molecular skeleton. The two components give a slightly different contribution to the T−S spectrum but overlap at each wavelength. In the TR-EPR and ESE spectra these two components are not distinguishable due to the powder distribution of the anisotropic ZFS tensor and to the hyperfine broadening. The presence of more components with very similar ZFS parameters is a common feature of the ODMR spectra of carotenoid triplet states, in natural systems, taken at very low temperature. We have recently assigned the components to slightly different conformations of the same pigment rather than to different pigments [19,10].

The comparison of the T−S spectra of HSPCP and MFPCP reported in Fig. 3 shows that the general features due to the peridinin triplet states are the same in the two complexes. The main T–T absorption band is centred at about the same wavelength (565 nm) and the red-most bleaching in the peridinin absorption region is observed at about 535 nm in both complexes. In this respect the characteristics of the absorption of the peridinin(s) where the triplet state is localized and the possible interactions with the nearby peridinins, which would be reflected in the T−S spectrum, seem to be similar. Moreover the possibility of a direct involvement of the red-most peridinin of MFPCP, which has been proposed to absorb at 544 nm by Ilagan et al. [3], in the localization of the triplet state may be ruled out because a large difference in the T−S spectra should be expected, being this red absorption absent in HSPCP [3]. On the contrary they are very similar.

Some significant differences are present in the T−S spectrum of the two complexes in the region of the Qy absorption bands of the Chls. The bleaching observed in this region has been assigned to a change in the interaction between peridinin and Chl which takes place when the carotenoid changes the electronic state (from singlet to triplet). This is a common feature observed in all the T−S spectra of carotenoids in natural photosystems reported up to date [19–22]. It is interesting to note that, at least at 1.8 K, both the Chls of the HSPCP complex contribute to the bleaching in the Qy absorption region. The bleaching of the red-shifted Chl, centred at 676 nm, is very sharp, while the second component is broader and centred at about 670 nm. The observation of the bleaching of both the Chls of the complex seems to indicate that, in the experimental conditions of the ODMR experiments (continuous illumination in the range 400–700 nm), carotenoid triplet states are populated in both the subclusters and are localized in close proximity to the two Chl molecules. A possible different explanation of the observed feature in the T−S spectrum could be the presence of a strongly coupled Chl dimer interacting with the peridinin carrying the triplet state. However, this last possibility must be excluded on the basis of the results reported by Ilagan et al. [3], who showed the presence of distinct spectral forms of Chl in HSPCP, and on the basis of the large distance between the Chls planes resulting from the X-ray structure (18.4 Å centre to centre).

4.2. ESE and pulse ENDOR

The absence of significant differences in the ESE (or in the TR-EPR) spectra taken at initial times after the laser flash and in the kinetics of HSPCP with respect to those of MFPCP, indicates that the peridinins responsible for the Chl quenching in the two clusters of HSPCP are substantially similar to those of MFPCP in terms of relative orientation with the triplet donor, the ^{T}Chl, and in terms of ZFS axes directions in the peridinin molecular structure. As already proposed [10,11], the similarity in the polarization pattern of the spectra and in the pigment arrangement of the two protein complexes, strongly suggests a localization of the triplet state on PID1331/1335, the analogous of PID614/624 in MFPCP (see Fig. 1). For sake of precision and completeness, we performed the calculations of the initial ESE triplet spectra for the triplet–triplet energy transfer from each of the two Chls to the three surrounding peridinins in the symmetry related subclusters of the HSPCP complex. The method, described in detail for MFPCP [10], exploits the concept of spin conservation during the triplet–triplet energy transfer. The acceptor (peridinin) inherits the polarization of the donor in a way which depends on the relative geometrical arrangement of the donor-acceptor couple. Although homologous Chl-peridinin couples in the MFPCP and HSPCP structures are slightly different in terms of relative orientation and carotenoid backbone distortions (see Fig. 6), the calculations show that these differences do not produce any significant effect on the calculated spectra and therefore in the assignment of triplet localization. In fact, the best agreement with the experimental spectrum is obtained for triplet transfer to PID1331 and/or 1335. Details of the calculations are reported in the Supplementary material.

At the temperature of the experiments, 20 K, the Chl–Chl transfer rate of the excitation is fast 20 ps [3] and the probability to form the triplet state is likely higher for the Chl absorbing at about 677 nm (Chl 1327 in the X-ray structure of HSPCP). The prevailing triplet is therefore localized mainly on the PID1331 which is close to Chl1327. However the ODMR results indicate that the possibility to form triplet states in both subclusters is not negligible, at least under continuous illumination. With a pulse duration of laser flash of 9 ns, as that used in the time-resolved and ESE experiments, a contribution to the triplet population coming from Chl 1328 is still plausible. The calculation ESE spectra of PID1335 and PID1331, at short DAF, show that they are almost identical (see the Supplementary material). This means that we are not able to evaluate the relative contribution of these peridinins to the triplet quenching. To similar conclusions lead the analysis of the TR-EPR spectra of MFPCP [10].

Interestingly, the water molecule coordinated to the central Mg of the Chl molecules, which has been suggested to play a key role in the triplet–triplet transfer in MFPCP, is present also in HSPCP, forming a bridge between Chl1327(1328) and PID-1331(1335).

Although similarities between HSPCP and MFPCP in terms of pigment arrangement are clearly found, however, looking carefully to the homologous carotenoids in the respective X-ray structures, it is possible to point out some local different conformations of the peridinins. In particular the differences between the homologous PID614/PID1131 are shown in Fig. 6, where the comparison has been made superimposing the planes of the Chls which are close to these peridinins in the two proteins. In principle, these differences should produce a variation of the ZFS parameters and of the spin density distribution of the associated triplet states. Indeed a decrease of the |D| parameter is observed in the ODMR spectra of HSPCP, showing a possible larger delocalization of the electron density in the molecular skeleton. A measurable decrease of the hyperfine couplings, previously assigned to the protons of the methyl group located in position 19 in the molecular structure (see Fig. 1), has also been detected in the time- resolved ENDOR spectra of the triplet state of HSPCP. The methyl groups have been used in our previous work [11] as markers of the electronic structure of the triplet state and the satisfactory agreement between the experimental and computed hyperfine couplings, assigned to the rotating methyl groups on the conjugated chain, provided a critical test of the triplet state wavefunction. DFT calculations showed that the unpaired spins are quite delocalized over the whole conjugated system, with an alternate spin pattern with positive spin densities alternating with gradually smaller negative spin densities. This alternate pattern is lost in the central region of the conjugated chain where all positive densities are found. Similar description of the spin density distribution in the peridinin triplet state was given by Niklas et al. [23] on the basis of the ENDOR data relative to the reconstituted N-domain of PCP. The decrease of the hfcs observed for methyl 19 in HSPCP compared to the values reported for MFPCP indicates that the tail of the conjugated chain where the allenic group is present is a site of molecular distortion. The calculations have shown that this region of the molecular structure is indeed the more

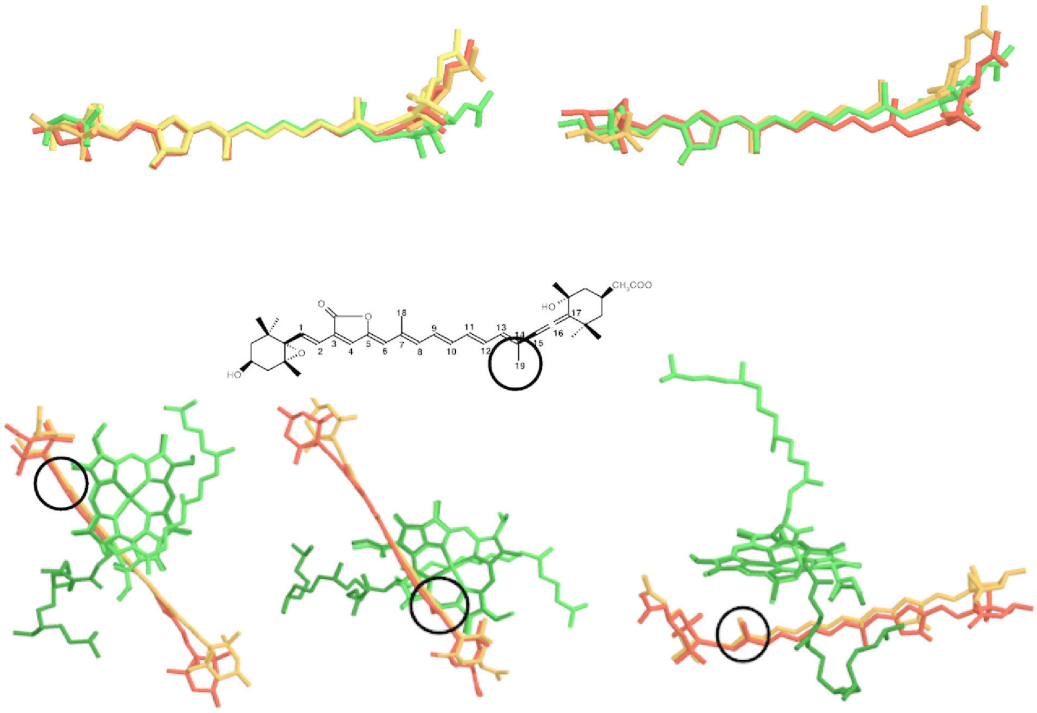


Fig. 6. (Top) Superimposition of the structure of the peridinins associated with one subcluster of MFPCP (left) and HSPCP (right). Green: PID611/1329; yellow: PID612; orange: PID613/1330; red: PID614/1331. (Bottom) Superimposition of the structures of the Chl-PID614 and Chl-PID1331 couples associated with MFPCP and HSPCP respectively. Three different views are shown. Structure taken from coordinates of 1PPR and 2C9E PDB files deposited in the Brookhaven Protein Data Bank. The methyl in position 19 is highlighted both in the molecular structure of peridinin and in the X-ray structures.

affected by conformational disorder [11] as evident also by inspection of Fig. 6 where the superimposition of the peridinins belonging to the same subcluster, of both MFPCP and HSPCP, is shown. The different degrees of bending of the peridinin tails in the conformations assumed by the pigments in the complexes are shown in Fig. 6. The direct comparison between PID614 in MFPCP and PID1331 in HSPCP, which are assumed to be the site of triplet quenching together with PID614 and PID1335, is also shown in Fig. 6. In this figure the methyl group 19 is highlighted by a circle. When the Chl planes relative to the homologous subclusters are superimposed in the two complexes the differences between the peridinins are clearly seen. The methyl in position 18 is located in the central part of the molecules which is more conserved, while methyl 19 is in the region where the two molecules differ the most. On the opposite tail of the molecule there is also a local distortion which should produce a change of the spin density especially at the proton in position 1, where the spin density has been shown to be large from the DFT calculations [11]. Unfortunately the hfcs relative to this proton have not been assigned in our spectra because they have broad transitions which do not easily emerge from the noise. Actually, in the Mims time-resolved ENDOR spectra on the triplet states of the two proteins many expected hfcs are missing, because of the large anisotropy, thus the whole redistribution of the spin density in the skeleton due to the different conformations of the tails cannot be fully described. Nevertheless the methyl marker can be used as evidence of the local distortion of the molecule.

In conclusion, HSPCP and MFPCP share most of the properties relatively to the triplet formation pathway and to the triplet localization in specific peridinins. However some significant differences also emerged from the analysis of the spectra which can be explained in terms of local distortion of the conjugated chains of the peridinins molecules, in agreement with the conformational data resulting from the X-ray structures of the two complexes.

Acknowledgements

This work was supported by the Italian Ministry for University and Research (MURST) under the project PRIN2005. We are grateful to Prof. Giovanni Giacometti for his continuous interest in this work and to Roger Hiller for his interest in the work and for kindly supplying the samples.

Appendix A. Supplementary data

Supplementary data associated with this article can be found, in the online version, at doi:10.1016/j.bbabio.2008.06.006.

References

[1] E. Hofmann, P.M. Wrench, F.P. Sharples, R.G. Hiller, W. Welte, K. Diederichs, Structural basis of light harvesting by carotenoids: peridinin–chlorophyll–protein from *Amphidinium carterae*, Science 272 (1996) 1788–1791.
[2] F.P. Sharples, P.M. Wrench, K.L. Ou, R.G. Hiller, Two distinct forms of the peridinin–chlorophyll alpha-protein from *Amphidinium carterae*, Biochim. Biophys. Acta 1276 (1996) 117–123.
[3] R.P. Ilagan, J.F. Koscielecki, R.G. Hiller, F.P. Sharples, G.N. Gibson, R.R. Birge, H.A. Frank, Femtosecond time-resolved absorption spectroscopy of main-form and high-salt peridinin–chlorophyll proteins at low temperatures, Biochemistry 45 (2006) 14052–14063.
[4] R.P. Ilagan, S. Shima, A. Melkozernov, S. Lin, R.E. Blankenship, F.P. Sharples, R.G. Hiller, R.R. Birge, H.A. Frank, Spectroscopic properties of the main-form and high-

salt peridinin–chlorophyll a proteins from *Amphidinium carterae*, Biochemistry 43 (2004) 1478–1487.
[5] H.A. Frank, R.J. Cogdell, Carotenoids in photosynthesis, Photochem. Photobiol. 63 (1996) 257–264.
[6] J.A. Bautista, R.G. Hiller, F.P. Sharples, D. Gosztola, M. Wasielewski, H.A. Frank, Singlet and triplet energy transfer in the peridinin–chlorophyll a-protein from *Amphidinium carterae*, J. Phys. Chem. A 103 (1999) 2267–2273.
[7] D. Carbonera, G. Giacometti, U. Segre, Carotenoid interactions in peridinin chlorophyll a proteins from dinoflagellates — evidence for optical excitons and triplet migration, J. Chem. Soc. Faraday Trans. 92 (1996) 989–993.
[8] D. Carbonera, G. Giacometti, G. Agostini, FDMR spectroscopy of peridinin chlorophyll-a protein from *Amphidinium-carterae*, Spectrochimica 51A (1995) 115–123.
[9] D. Carbonera, G. Giacometti, U. Segre, A. Angerhofer, U. Gross, Model for triplet–triplet energy transfer in natural clusters of peridinin molecules contained in dinoflagellate's outer antenna proteins, J. Phys. Chem. B 103 (1999) 6357–6362.
[10] M. Di Valentin, S. Ceola, E. Salvadori, G. Agostini, D. Carbonera, Identification by time-resolved EPR of the peridinins directly involved in chlorophyll triplet quenching in the peridinin–chlorophyll a-protein from *Amphidinium carterae*, Biochim. Biophys. Acta 1777 (2008) 186–195.
[11] M. Di Valentin, S. Ceola, G. Agostini, G.M. Giacometti, A. Angerhofer, O. Crescenzi, V. Barone, D. Carbonera, Pulse ENDOR and density functional theory on the peridinin triplet state involved in the photo-protective mechanism in the peridinin–chlorophyll a-protein from *Amphidinium carterae*, Biochim. et Biophys. Acta 1777 (2008) 295–307.
[12] D. Carbonera, G. Giacometti, G. Agostini, FDMR of carotenoid and chlorophyll triplets in light-harvesting complex LHCII of spinach, Appl. Magn. Reson. 3 (1992) 361.
[13] S. Santabarbara, E. Bordignon, R.C. Jennings, D. Carbonera, Chlorophyll triplet states associated with photosystem II of thylakoids, Biochemistry 41 (2002) 8184.
[14] R.H. Clarke, Triplet State ODMR Spectroscopy. Techniques and Applications to Biophysical Systems, in: R.H. Clarke (Ed.), Wiley-Interscience, New York, 1982.
[15] A.J. Hoff, Optically Detected Magnetic Resonance of Triplet States. Advanced EPR, in: A.J. Hoff (Ed.), ELSEVIER, Amsterdam, 1989.
[16] D. Carbonera, G. Giacometti, G. Agostini, A. Angerhofer, V. Aust, ODMR of carotenoid and chlorophyll triplets in CP43 and CP47 complexes of spinach, Chem. Phys. Lett. 194 (1992) 275–281.
[17] D. Carbonera, E. Bordignon, G. Giacometti, G. Agostini, A. Vianelli, Fluorescence and absorption detected magnetic resonance of chlorosomes from green bacteria *Chlorobium tepidum* and *Chloroflexus aurantiacus*. A comparative study, J. Phys. Chem B 105 (2001) 246–255.
[18] T.S. Lin, Electron spin echo spectroscopy of organic triplets, Chem. Rev. 84 (1984) 1–15.
[19] D. Carbonera, G. Agostini, T. Morosinotto, R. Bassi, Quenching of chlorophyll triplet states by carotenoids in reconstituted Lhca4 subunit of peripheral light-harvesting complex of photosystem I, Biochemistry 44 (2005) 8337–8346.
[20] R. Van der Vos, D. Carbonera, A.J. Hoff, Microwave and optical spectroscopy of carotenoid triplets in light-harvesting complex LHCII of spinach by absorbance-detected magnetic resonance, Appl. Magn. Res. 2 (1991) 179–202.
[21] T. Javorfi, G. Garab, K. Razi Naqvi, Reinvestigation of the triplet-minus-singlet spectrum of chloroplasts, Spectrochim. Acta Part A 56 (2000) 211–214.
[22] A. Angerhofer, F. Bornhauser, A. Gall, R.J. Cogdell, Optical and optically detected magnetic resonance investigation on purple photosynthetic bacterial antenna complexes, Chem. Phys. 194 (1995) 259–274.
[23] J. Niklas, T. Schulte, S. Prakash, M. van Gastel, E. Hofmann, W. Lubitz, Spin-density distribution of the carotenoid triplet state in the peridinin–chlorophyll–protein antenna. A Q-band pulse electron-nuclear double resonance and density functional theory study, J. Am. Chem. Soc. 129 (2007) 15442–15443.

Biochimica et Biophysica Acta 1787 (2009) 168–175

Contents lists available at ScienceDirect

Biochimica et Biophysica Acta

journal homepage: www.elsevier.com/locate/bbabio

Triplet–triplet energy transfer in Peridinin-Chlorophyll *a*-protein reconstituted with Chl *a* and Chl *d* as revealed by optically detected magnetic resonance and pulse EPR: Comparison with the native PCP complex from *Amphidinium carterae*

Marilena Di Valentin [a], Giancarlo Agostini [c], Enrico Salvadori [a], Stefano Ceola [a], Giorgio Mario Giacometti [b], Roger G. Hiller [d], Donatella Carbonera [a,*]

[a] *Dipartimento di Scienze Chimiche, Università di Padova, via Marzolo 1, 35131 Padova, Italy*
[b] *Dipartimento di Biologia, Università di Padova, vi U. Bassi, 35131 Padova, Italy*
[c] *CNR, Istituto di Chimica Biomolecolare, Sezione di Padova, via Marzolo 1, 35131 Padova, Italy*
[d] *Department of Biological Sciences, Macquarie University, 2109 NSW, Australia*

ARTICLE INFO

Article history:
Received 16 October 2008
Received in revised form 11 December 2008
Accepted 12 December 2008
Available online 24 December 2008

Keywords:
PCP
Peridinin
Carotenoid
Triplet
ODMR
EPR

ABSTRACT

The triplet state of the carotenoid peridinin, populated by triplet–triplet energy transfer from photoexcited chlorophyll triplet state, in the reconstituted Peridinin-Chlorophyll a-protein, has been investigated by ODMR (Optically detected magnetic resonance), and pulse EPR spectroscopies. The properties of peridinins associated with the triplet state formation in complexes reconstituted with Chl *a* and Chl *d* have been compared to those of the main-form peridinin-chlorophyll protein (MFPCP) isolated from *Amphidinium carterae*. In the reconstituted samples no signals due to the presence of chlorophyll triplet states have been detected, during either steady state illumination or laser-pulse excitation. This demonstrates that reconstituted complexes conserve total quenching of chlorophyll triplet states, despite the biochemical treatment and reconstitution with the non-native Chl *d* pigment. Zero field splitting parameters of the peridinin triplet states are the same in the two reconstituted samples and slightly smaller than in native MFPCP. Analysis of the initial polarization of the photoinduced Electron-Spin-Echo detected spectra and their time evolution, shows that, in the reconstituted complexes, the triplet state is probably localized on the same peridinin as in native MFPCP although, when Chl *d* replaces Chl *a*, a local rearrangement of the pigments is likely to occur. Substitution of Chl *d* for Chl *a* identifies previously unassigned bands at ~ 620 and ~ 640 nm in the Triplet-minus-Singlet (T−S) spectrum of PCP detected at cryogenic temperature, as belonging to peridinin.

© 2008 Elsevier B.V. All rights reserved.

1. Introduction

Dinoflagellates belong to the group of marine eukaryotic algae which possess two different light harvesting complexes, an intrinsic membrane bound LHC, and the water soluble peridinin–chlorophyll-a protein (PCP) which contains only peridinin and Chl *a*.

Depending on the species, the PCP complex consists of either an apoprotein of 32 kDa binding 8 peridinin and 2 Chl *a* molecules, or is a dimer of 15 kDa monomers each binding 4 peridinins and 1 Chl *a* [1]. The amino acid sequence of the 32 kDa protein form indicates that it arose by a gene duplication and fusion as it consists of two parts with 56% identity and joined by a spacer region. Moreover, the 15 kDa PCP of *Heterocapsa pygmaea* also has high homology with both domains of the 32 kDa species [1].

The X-ray structure of the main form of PCP (MFPCP) from *A. carterae* has been resolved to 2.0 Å [2]. The basic structure is a trimer. In each subunit of the trimer the pigments are arranged as two pseudo-identical domains of 4 peridinins, and a Chl *a* molecule, as shown in Fig. 1. The pigments are located in the hydrophobic cavity formed by the protein. The peptide primary sequences of the -N and -C terminal regions form structurally almost identical domains, each consisting of eight alpha-helices. Recently, the X-ray structure of high-salt PCP (HSPCP), which has a molecular weight of 34 kDa, has also been determined (T. Schulte, F.P. Sharples, R.G. Hiller, E. Hofmann, coordinates have been deposited in the Brookhaven Protein Data Bank under ID 2C9E, unpublished) [3]. It shows considerable similarity with the MFPCP structure in terms of pigment arrangement, except for the absence of two symmetry related peridinins, called PID612/PID622 in MFPCP [2].

PCP has been extensively investigated with many different spectroscopic techniques as well as by theoretical studies, in order

Abbreviations: PID, peridinin; Chl, chlorophyll; PCP, peridinin-chlorophyll protein; *A. carterae*, *Amphidinium carterae*; MFPCP, main form PCP; ODMR, optically detected magnetic resonance; FDMR, fluorescence detected magnetic resonance; ADMR, absorption detected magnetic resonance; ZFS, zero field splitting; ISC, intersystem crossing; ESE, electron spin echo

* Corresponding author. Tel.:+39 049 827 5144; fax: +39 049 827 5161.
E-mail address: donatella.carbonera@unipd.it (D. Carbonera).

0005-2728/$ – see front matter © 2008 Elsevier B.V. All rights reserved.
doi:10.1016/j.bbabio.2008.12.004

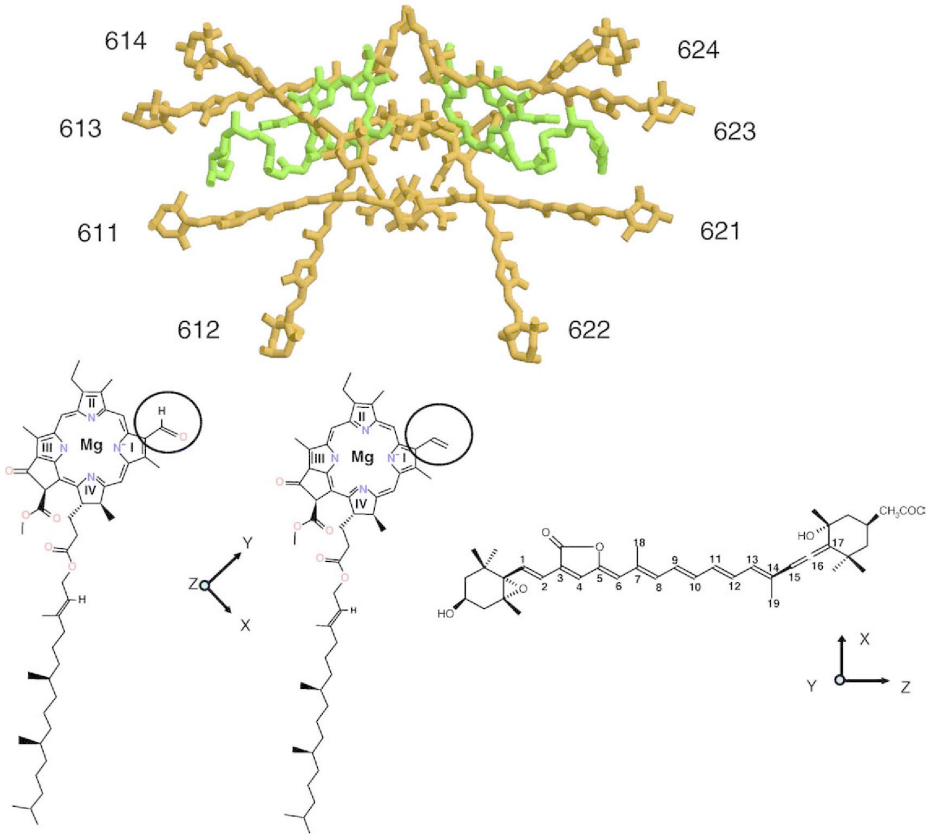


Fig. 1. (Top) Structure of the pigments associated with the monomeric basic unit of the PCP complex from *A. carterae*. Structure taken from coordinates of MFPCP complex 1PPR deposited in the Brookhaven Protein Data Bank. The numbers refer to the peridinins in the PDB files (Bottom) Molecular structure of Chl *d* (left) and Chl *a* (right) and peridinin with the orientation of the ZFS tensor axes.

to correlate the spectroscopic properties with the arrangement of the pigments in the protein, as resolved by the X-ray structure [4–9]. More recently, reconstitution of functional PCP from heterologously-expressed apoprotein mixed with pigments extracted from native PCP, has been obtained [10]. Constructs of full-length, and also N-terminal domain alone PCP (N-PCP), have been produced and reconstituted in vitro with both native and altered pigment composition. The N-PCP is a 16 kDa protein which corresponds to the "half-mer" of the monomeric PCP from *A. carterae*. When the unfolded N-PCP is reconstituted with the same pigments as those present in native PCP, the protein forms a 32 kDa homo-dimer [10–12]. The Circular Dichroism, absorption, fluorescence and florescence excitation spectra, have shown that the reconstituted samples are characterized by spectroscopic properties very similar to those of the native samples [5,10].

The genetic and biochemical manipulations of PCP have opened the way to a better understanding of the energy transfer between peridinins and Chls. [13,16]. It has been shown that the substitution of Chl *a* by Chl *b*, Chl *d*, acetyl-Chl *a* and BChl *a* does not alter significantly the singlet energy transfer pathway and its efficiency. The minor differences observed have been rationalized in terms of specific effects due to diverse spectral overlaps between the pigments [13,15]. Experimental results on hetero-chlorophyllous N-PCP complexes, obtained by adding mixture of different Chls during the reconstitution process, indicate specific binding affinities in the protein [12,13,14].

In addition to their main light harvesting function, peridinin molecules in PCP also play a photo-protective role [17–19]. The low-lying triplet state of peridinin is capable of trapping Chl *a* triplet states, avoiding the formation of potentially harmful singlet oxygen. In MFPCP the lifetime of the Chl *a* triplet state is of the order of 20 ns; within this time a triplet state is formed on the peridinins and decays through radiationless intersystem crossing channels with a lifetime of 10 μsec at room temperature [19].

In MFPCP, HSPCP and also in N-PCP reconstituted with the native pigments, the triplet-triplet energy transfer takes place with 100% efficiency [5,20–23]. To study the formation of triplet state in native PCP complexes, we have used in the past different spectroscopic techniques: ODMR (optically detected magnetic resonance), to correlate the magnetic properties of the triplet state with the optical properties of the system [18,21,24–25]; time-resolved EPR (TR-EPR) [20–21] to identify the peridinin-chlorophyll pairs directly involved in the triplet energy transfer, and pulse-ENDOR for insights into the electronic structure of the peridinin triplet state [21,23]. By comparing the TR-EPR spectra of MFPCP and HSPCP and their X-ray structures, we suggested that the pathway of triplet quenching and triplet localization was very similar in the two complexes [21]. We also performed pulse-EPR and pulse-ENDOR experiments on MFPCP and HSPCP. The ENDOR investigation, accompanied by DFT calculation of the hyperfine couplings strongly supported the hypothesis of localization of the triplet state on one peridinin in each subcluster of both MFPCP and HSPCP complexes [21,23]. The triplet state of

peridinins in N-PCP has not been characterized to the same extent although a pulse-ENDOR experiment on the triplet state of the Chl *a* N-PCP has been reported [22].

In this work we compare the properties of peridinin triplet states, populated by triplet –triplet energy transfer from photoexcited chlorophyll triplet state, in complexes reconstituted with Chl *a* with those previously reported for peridinins involved in triplet state population in the native MFPCP from *A. carterae*. We also extend the study to Chl *d* N-PCP to explore the effect of the structure of the Chl on the properties of the triplet-triplet energy transfer process. Chl *d* has a Q_y band at 700 nm, red-shifted compared to the Chl *a* Q_y band (670 nm). A splitting of the Soret and Qy bands observed in Chl *a* N-PCP, but not in Chl *d* N-PCP complexes, has been suggested to be due to the different configurations that the vinyl group in Ring I can adopt (see Fig. 1). In contrast the carbonyl group in Ring I of Chl *d* may adopt only a single configuration [4]. Moreover, while the Chl-protein interaction induces a blue-shift of the Q_y band in the low temperature spectra of Chl *a*, Chl *b*, and 3-Acetyl-Chl *a*, compared to the spectra taken in 2-MTHF at low temperature, no shift is observed for Chl *d* [4].

The efficiency of the triplet-triplet transfer depends strictly on the relative geometry of the donor and the acceptor and requires optimization in terms of wavefunction overlap and pigment interactions. In this work we try to rationalize the effect induced by the insertion of Chl *d* on the triplet quenching mechanism occurring in PCP. The results are compared to those previously obtained for native MFPCP and discussed in terms of energy transfer properties, specific pathway for triplet quenching and protein structure.

2. Materials and methods

2.1. Sample preparation

Reconstitution of N-PCP complexes from heterologously expressed N-Domain PCP apoprotein was as described previously [10]. Samples of purified reconstructed PCP were stored in aliquots at −70 °C and diluted with buffer immediately prior to use. Absorbance at the Chl Qy band was 0.8 for the ODMR experiments and about 2.0 times for EPR experiments. Pigments for reconstituting Chl *a* N-PCP were extracted from MFPCP and Chl *d* was extracted from cells of *Acaryochloris marina* by the procedure of Martinson and Plumley and purified by reverse phase HPLC [26].

2.2. Spectroscopic methods

2.2.1. ODMR experiments

60% v/v glycerol was added to the samples in order to obtain a transparent glass upon cooling of the sample to 1.8 K. At cryogenic temperatures spin-lattice relaxation is inhibited and the ODMR signal is intense. Fluorescence and Absorption detected magnetic resonance (FDMR, ADMR) experiments were performed in a home built apparatus, previously described in detail [27–28]. ODMR is a double resonance technique based on the simple principle that, when a triplet steady state population is generated upon illumination, the application of a resonant microwave electromagnetic field between two spin sublevels of the triplet state, generally induces a change of the steady state population of the triplet state itself, due to the anisotropy of the decay and population rates of the three spin sublevels. The induced change of the triplet population may be detected as a corresponding change of the emission and/or absorption of the system [24–25]. Amplitude modulation of the applied microwave field (on–off) is used to increase the S/N ratio by means of a phase sensitive lock-in amplifier (EG&G 5220) detection.

In the FDMR experiments the fluorescence, excited by a halogen lamp (250 W) focused into the sample and filtered by a broadband 5 cm solution of $CuSO_4$ 1 M, was collected at 45 °C through appropriate band-pass filters (10 nm FWHM) by a silicon photodiode (Centronic OSI 5) before entering the lock-in amplifier. Low temperature emission spectra were detected in the same apparatus used for ODMR experiments, using the same excitation source, but substituting the band-pass filters before the photodiode by a monochromator (Jobin Yvon HR250, 3 nm/mm dispersion).

In the absorption detection mode (ADMR) the sample is excited by a halogen lamp (250 W) focused into the sample and filtered by 5 cm water and heat filters. The transmitted light, modulated by the on–off of the microwave field, after passing a monochromator, is detected by a photodiode and the signal is finally amplified and demodulated in the lock-in amplifier.

By fixing the microwave frequency at a resonant value while sweeping the detection wavelength, microwave-induced Triplet-minus-Singlet (T−S) spectra can be registered.

2.2.2. Pulse EPR experiments

Oxygen was removed from the samples by flushing argon in the EPR capillary before freezing. Glycerol, previously degassed by several cycles of freezing and pumping, was added (60%v/v) to obtain a transparent matrix.

Experiments were performed on a Bruker Elexsys E580 pulsed EPR spectrometer. Laser excitation at 532 nm (10 mJ per pulse and repetition rate of 10 Hz) was provided by the second harmonic of a Nd:YAG laser (Quantel Brilliant) in a dielectric cavity. The temperature was controlled with a Helium cryostat (Oxford CF935) driven by a temperature controller (Oxford ITC503).

Field-swept ESE spectra were recorded using a 2-pulse ESE sequence according to the scheme: flash-DAF-π/2-τ-π-τ-echo (DAF = delay after laser flash); the value of DAF was fixed at 50 ns. ESE-detected kinetics at the triplet canonical orientations were recorded using a 2-pulse (flash-DAF-π/2-τ-π-τ-echo) ESE sequence after a variable DAF between the laser flash and the first MW pulse. The π/2-pulse was of 16 ns and the delay τ was set at 200 ns for the field-swept ESE experiment and to 120 ns for the ESE-detected kinetics.

2.3. EPR spectral analysis

Calculation of the sublevel triplet state populations of the acceptor starting from those of the donor has been performed using a home-written program in Mathematica® software following the formalism of ref. [20–21] in the limit of a triplet-triplet energy transfer which is fast, compared to the time evolution of the donor triplet spectrum and is slow enough to allow spin alignment in the external magnetic field. Simulations of the powder spin polarised triplet spectra were performed using a program written in MatLab® with the aid of the Easyspin routine (ver. 2.6.0) [29]. The program is based on the full diagonalization of the triplet state spin Hamiltonian, taking into account the Zeeman and magnetic dipole-dipole interactions, assuming a powder distribution of molecular orientations with respect to the magnetic field direction.

Simulations of the DAF kinetics were performed according to the method previously described in ref. [20].

3. Results

The absorption spectra of the reconstituted samples, taken at room temperature, are identical to those reported by Ilagan et al. 2006 [4]. At 1.8 K the fluorescence emission maximum is at 672 nm, for Chl *a* N-PCP, and 700 nm for Chl *d* N-PCP, values in agreement with those reported for the emission at 77 K [4].

3.1. ODMR

Steady state illumination of PCP at cryogenic temperatures leads to the formation of peridinin triplet states, which can be detected by monitoring the change of the Chl emission induced by a microwave field swept in the spectral region where carotenoid triplet states are

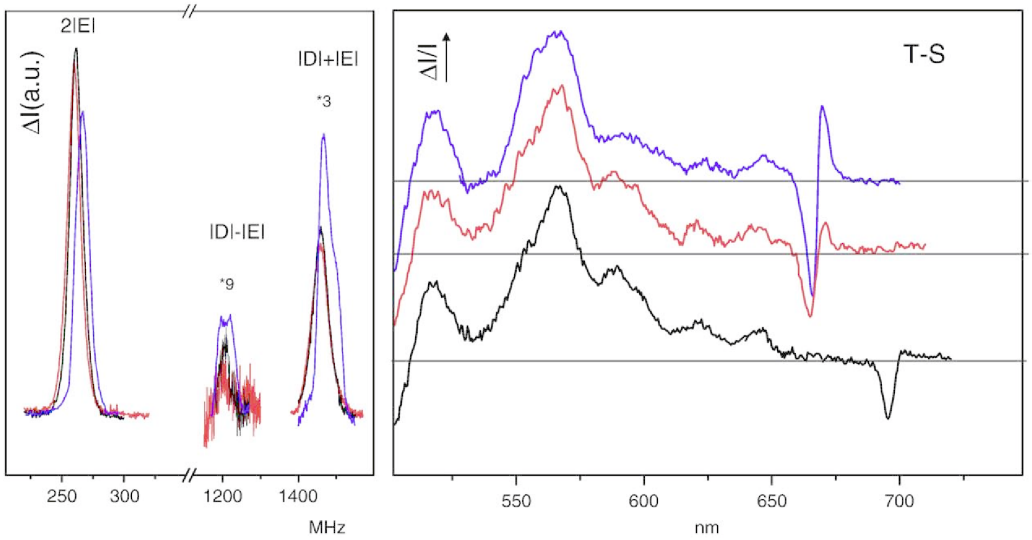


Fig. 2. (Left) FDMR spectra of peridinin triplet state in Chl *a* N-PCP (red), Chl *d* N-PCP (black) and MFPCP (blue) at 1.8 K. MFPCP curves from [18]. Detection wavelength: 670 nm for Chl *a* N-PCP, 700 nm for Chl *d* N-PCP; mod. freq. 323 Hz, Mw power 1 W, 10 scans. (Right) T−S spectra of Chl *a* N-PCP (red), Chl *d* N-PCP (black) detected at the maximum of 2|E| transition. T−S spectrum of MFPCP (blue) from [34]. Spectra have been rescaled for better comparison. The lines corresponding to ΔI/I = 0 are shown. Modulation frequency: 323 Hz, Microwave power: 1 W, *T* = 1.8 K. ΔI/I ≡ ΔA.

expected to show resonant transitions between pairs of spin sublevels [18,27,30–32].

FDMR spectra of Chl *a* N-PCP and Chl *d* N-PCP, in the microwave field region where the 2|E|, the |D|−|E| and the |D|+|E| transitions of peridinins are expected, are shown in Fig. 2 (left).

Three transitions, characterized by the polarization pattern usually found for carotenoids (intensity of $2|E| \gg |D|+|E| > |D|-|E|$), have been detected at 261, 1206, 1460 MHz for Chl *d* N-PCP and 260, 1202, 1460 MHz for Chl *a* N-PCP giving essentially the same ZFS parameters ($|D| = 0.0443 \pm 0.0001$ cm^{-1} $|E| = 0.0043 \pm 0.0005$ cm^{-1}). The transition frequencies are slightly shifted with respect to those previously reported for native MFPCP (i.e. 267, 1203(sh1229), 1465 (sh1499) MHz) [18,33–34]. The |D|+|E| and |D|−|E| transitions are largely inhomogeneous for both the N-PCP complexes but lack the two well-resolved components present in native MFPCP ($|D| = 0.0448$ cm^{-1}, $|E| = 0.0044$ cm^{-1} and $|D| = 0.04586$ cm^{-1}, $|E| = 0.0045$ cm^{-1}).

In both reconstituted samples, as in native MFPCP [18,20,34], no signals which could be ascribed to the presence of unquenched Chl *a* triplet states have been detected under steady state illumination.

The microwave-induced T−S spectra, taken by fixing the microwave frequency at the maximum of the intense 2|E| transition (260–261 MHz), are shown in Fig. 2 (right). The T−S spectra of Chl *a* N-PCP is very similar to that, previously reported, for native MFPCP (shown also in Fig. 2, from [34]) and is almost identical to the spectrum of Chl *d* N-PCP in the range from 450 to 650 nm. The main difference between the two reconstituted samples is in the spectral position, and relative intensity, of the bleaching corresponding to the Q_y band of Chl (665 nm for Chl *a* N-PCP vs 695 nm for Chl *d* N-PCP). The bleaching is accompanied at longer wavelength by a small positive band which is more pronounced in Chl *a* N-PCP than in Chl *d* N-PCP.

3.2. Pulse EPR

We have previously shown that, in the case of carotenoid triplet state, kinetic measurements in time-resolved EPR are hampered by the presence of microwave-induced transition probability effects. Pulse EPR is more appropriate, because it does not suffer from the above complication as there is no microwave field present in the period between the photo-generation of the triplet state and its detection [23]. The kinetics of population and decay of the triplet spin sublevels, obtained by monitoring the echo intensity as a function of DAF, at the low-field canonical orientations of the ZFS tensor (Z^-, Y^+, X^+), are shown in Fig. 3 together with the ESE-detected spectrum at a DAF of 50 ns, at 20 K.

Due to the absence of fast and anisotropic relaxation processes depending on the orientation of the triplet state with respect to the magnetic field, the ESE detected spectra taken at early times after the laser flash are substantially the same, in terms of shape, as the initial TR-EPR spectra (data not shown), as already observed for native MFPCP. No signals which could be ascribed to the presence of unquenched Chl triplet states have been detected in either TR-EPR or ESE detected spectra at early and late times after the laser flash in the two reconstituted samples, in agreement with the ODMR results. Direct comparison of the ESE-detected spectra and decay curves, with the corresponding data on native MFPCP taken from ref [23] are reported in Fig. 3.

Simulations of the ESE-detected spectra and ESE kinetics, according to the method described in [23], give the ZFS parameters, the relative populating rates and decay rates for the peridinin triplet sublevels in Chl *a* N-PCP and Chl *d* N-PCP reported in Table 1. Simulated DAF curves are shown in Fig. 3. As previously discussed [20–21], the ZFS axes correspond to those shown in the molecular structure of peridinin in Fig. 1. The order of the ZFS energy levels is: $Z^2 > Y^2 > X^2$. It can be seen that the ZFS parameters, the decay rates and the population probabilities, obtained from the simulation of the triplet spectra of Chl *a* N-PCP, are slightly different from those of native MFPCP. The introduction of Chl *d* in place of Chl *a* leads to a measurable effect on the relative population probabilities, but does not change the polarization pattern of the initial triplet spectrum (*eaeaea*), the ZFS parameters and the decay rates of the spin sublevels compared to Chl *a* N-PCP.

3.3. Triplet–triplet energy transfer

Calculations of the initial ESE triplet spectra based on the concept of spin conservation during the triplet-triplet energy transfer can be

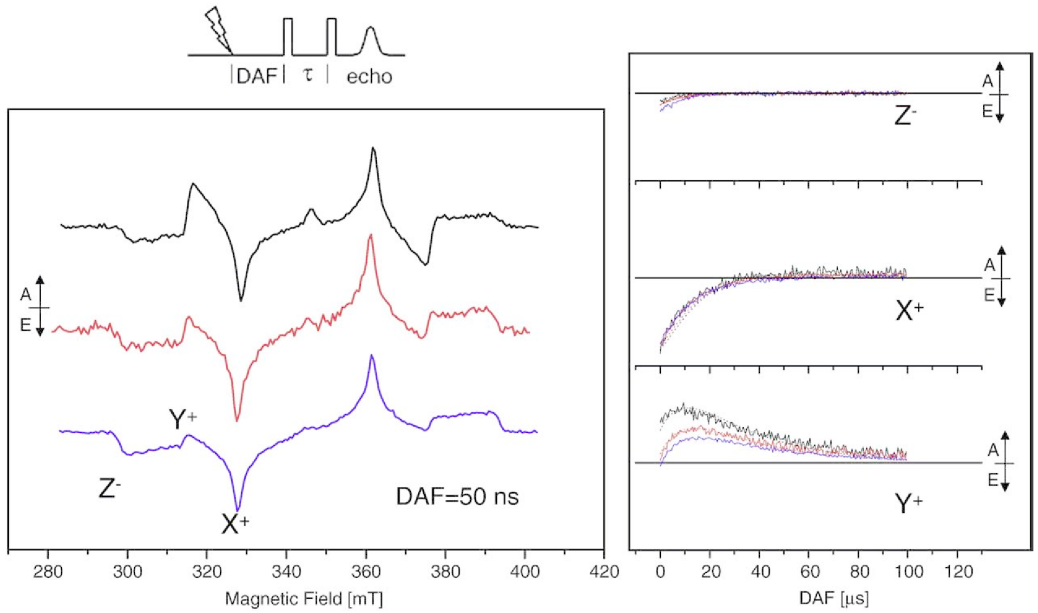


Fig. 3. (Left) Field-swept ESE spectrum of Chl *a* N-PCP (red), Chl *d* N-PCP (black) from *A. carterae*, at $T=20$ K, at DAF=50 ns. (Right) ESE-detected kinetics, at $T=20$ K, at the low-field canonical fields Z−, Y+, X+ (Chl *a* N-PCP (red), Chl *d* N-PCP (black)). A=absorption, E=emission. Simulated traces of Chl *a* N-PCP (red) and Chl *d* N-PCP (black) are superimposed on the experimental ones (dots). For experimental conditions see Section 2. Inset: Pulse scheme of the ESE experiment for photoexcited triplet states. Order of energy for zero field triplet sublevels: |Z|>|X|>|Y|. Data for MFPCP are from ref. [23].

performed by the method, previously described for native MFPCP [20,21]. Briefly, the acceptor (peridinin) inherits the spin polarization of the triplet donor in a way which depends on the relative geometrical arrangement of the donor-acceptor couple. Calculations for Chl *a* N-PCP have been performed assuming the same pigment arrangement of the N-domain of native MFPCP as derived from the X-ray structure, and initial Chl *a* spin level populations as those used for the calculations previously done on the native PCP [20]. The results (data not shown) inicate that in the reconstituted N-domain, the protein maintains the same characteristics of the triplet-triplet transfer as the full-length native protein, and the peridinins for which the calculations give a spectrum in agreement with the experimental one, are the same as in native PCP, namely PID614 and PID612 [20].

Calculations for Chl *d* N-PCP have been performed starting from a Chl *d* triplet state having the initial polarization pattern reported for isolated Chl *d* in 2-Me-THF glass: (Px:Py:Pz 0.34:0.50:0.16) [35]. The calculations assume the same relative geometry of the pigments as in the N-domain of MFPCP and in particular the same orientation of Chl *d* as Chl *a* in the binding pocket. The results are shown in Fig. 4 (left), where the spectra calculated for each Chl *d*→PID pair in the complex, are compared to the experimental spectrum. It can be seen that the best agreement with the experimental spectrum is achieved by assuming a localization of the triplet state on PID612. A good agreement with the experimental spectrum may be obtained also for PID 614 by rotating the ZFS axes of Chl *d* 15–20° around the axis perpendicular to the porphyrin plane (see Fig. 4, right). On the contrary the other two peridinins, PID611 and PID613, do not show the correct polarization pattern by small rotation of the ZFS axes (not shown).

4. Discussion

It is well established that triplet-triplet energy transfer, via the Dexter mechanism, is a process which depends strictly on the relative

Table 1
Parameters of the peridinin triplet state

	$\|D\|$ (10^{-4} cm^{-1})	$\|E\|$ (10^{-4} cm^{-1})	P_X: P_Y: P_Z	k_X: k_Y: k_Z (μs^{-1})	Ref
MFPCP	449.7±0.1 (ESE)	43.9±0.1 (ESE)	0.18:0.37:0.45	0.15: 0.03:0.09	[23]
	448.0±0.1 (ODMR)	44.0±0.1 (ODMR)			[18]
	458.6±0.1 (ODMR)	45.0±0.1 (ODMR)			[18]
Chl *a*	443.1±0.1 (ESE)	43.0±0.1 (ESE)	0.175:0.405:0.42	0.13: 0.034:0.09	
N-PCP					
	443.0±0.1 (ODMR)	43.0±0.5 (ODMR)			
Chl *d*	443.1±0.1 (ESE)	43.0±0.1 (ESE)	0.19: 0.435:0.375	0.13: 0.034:0.09	
N-PCP					
	443.0±0.1 (ODMR)	43.0±0.5 (ODMR)			

Values of the relative population rates, P_X, P_Y and P_Z, and decay constants, k_X, k_Y and k_Z, of the triplet sublevels in zero field together with the ZFS parameters |D| and |E|, derived from simulation of the time evolution of the field-swept ESE spectrum of Chl *a* N-PCP and Chl *d* N-PCP, according to the method described in ref [23]. For comparison the data relative to MFPCP from ref. [23] are also reported.
ZFS parameters resulting from the decomposition of the ODMR spectra of Chl *a* N-PCP and Chl *d* N-PCP with Gaussian components are also reported and compared to the equivalent data for MFPCP from ref. [18].

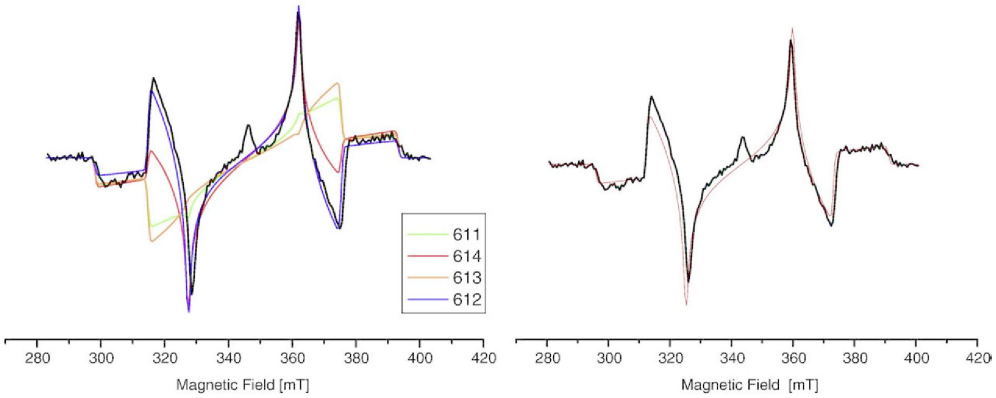


Fig. 4. (Left) Calculated initial triplet powder spectra of peridinins based on the triplet-triplet energy transfer mechanism, with the initial relative populations for the donor Chl *d* triplet: *Px:Py:Pz* = 0.34:0.50:0.16. Other parameters are reported in Table 1. The spectra are calculated for each Chl-Per pair of the N-domain as indicated. The spectra are compared to the experimental one, already reported in Fig. 3. (Right) Spectrum calculated for the Chl-PID614 pair after rotation (20°) of the ZFS axes of Chl *d* as discussed in the text.

geometry of donor and acceptor molecular frames. The efficiency of the photo-protection mechanism played by carotenoid molecules in the light harvesting complexes depends on the stringent overlap requirement between the chlorophyll and carotenoid wave functions. Any change in relative pigment geometry and/or in the electronic properties of the two partners in the triplet energy transfer may affect the efficiency of the process. In principle, by inserting Chl *d* in place of Chl *a* in N-PCP, some influence in the triplet-triplet transfer is expected, due to the different molecular structure (see Fig. 1) of the pigments.

4.1. ODMR

It is well kwon that the high sensitivity of the ODMR technique allows detection of very small amount of Chl triplet state. However no signals which could be ascribed to the presence of either Chl *a*, or Chl *d* triplet states have been detected in the N-PCP complexes. This means that the efficiency of triplet quenching is 100%, as in native PCP [21] and is not affected, either by the reconstitution process, or by the substitution of Chl *d* for Chl *a*.

The comparison of the T−S spectra of Chl *a* N-PCP and native MFPCP reported in Fig. 2 shows that the general features are maintained in the two complexes. The main T–T absorption band is centred at the same wavelength (567 nm) and the red-most bleaching in the peridinin absorption region is at ~535 nm in both complexes. However in Chl *a* N-PCP the main absorption band is less broad and more asymmetric. On the other hand, the T−S spectra of Chl *a* N-PCP and Chl *d* N-PCP are identical in the range from 450 to 650 nm. The ZFS parameters measured for the peridinin triplet state of Chl *a*-N-PCP and Chl *d* N-PCP differ less from each other than from those of native MFPCP. The small differences observed in the ZFS parameters and in the features of the carotenoid spectral region of the T−S spectra of the two N-PCP complexes compared to those of native MFPCP, could be due to the reconstitution process. Although the PCP complex reconstituted using the N-domain forms a dimer in solution, and aligning the duplicated N-domains on the published PCP structure, requires almost no spatial adjustment [36], the presence of only half protein may well introduce small changes in the molecular environment of the peridinins carrying the triplet states. In fact, looking closer at the interface between the two monomers, a deviation from a perfect matching is found, due to a relatively low identity between the N- and C-domains of MFPCP. The main deviations are in the loops surrounding the terminal ring close to the allene group of PID614/624 and where the tails of PID612/622 point toward the external solvent. Due to the length of the peridinins spanning the protein scaffold and to the close proximity of all the pigments in the two clusters, some effect could be transmitted to the whole interface producing a small structural rearrangement. This could influence the optical and magnetic properties of the peridinin carrying the triplet state as observed. The best overlay of the MFPCP structure with the dimer of two N-domains is shown in Supplementary material.

Significant differences in the T−S spectra of Chl *a* N-PCP and Chl *d* N-PCP, are present only in the region of the Qy absorption bands of the Chls. As expected the bleaching of Chl *d* is red-shifted compared to Chl *a* and is centered at 695 nm. If the T−S spectra of Chl *a* N-PCP and Chl *d* N-PCP are normalized at 570 nm, the intensity of the Q_y bleaching is 1.5 times greater for Chl *a* compared to Chl *d*. Since the extinction coefficient is about the same, or even higher, for Chl *d* in PCP [4] the difference can be ascribed to a different interaction strength between the Chl (*a* or *d*) and the peridinin carrying the triplet state, as proposed by Angerhofer et al. [37] to explain the results on triplet-triplet transfer efficiency in bacterial light harvesting complexes.

It is interesting to note that the up to now unassigned triplet–triplet absorption bands, appearing between 580–660 nm in the T−S spectra, must belong to the peridinin triplet manifold since they are not influenced by the change in electronic properties following substitution of Chl *a* by Chl *d*.

4.2. Pulse EPR and triplet–triplet transfer

The presence of only minor differences in the ESE (or in the TR-EPR) spectra taken at initial times after the laser flash and in the kinetics of Chl *a* N-PCP compared to those of native MFPCP, indicates that the peridinins responsible for the Chl triplet quenching are substantially unaltered, in terms of their relative orientation with respect to the ^{T}Chl donor, and in terms of their ZFS axes in the peridinin manifold. The minor differences observed may be due to the interface effects mentioned above in discussing the ODMR results.

Calculations of the initial polarization of the ESE spectra in Chl *a* N-PCP, based on the assumption of spin conservation during triplet-triplet energy transfer, show that the best agreement with the experimental data is achieved, as in native MFPCP, by localising the triplet on PID614 and, possibly, in PID612. In the case of native MFPCP significant contribution of PID612 was considered to be unlikely, based on comparison with HSPCP which shows similar initial polarization of the ESE spectra but lacks PID612 although maintaining a similar pigment arrangement [21]. The same consideration can be extended to Chl *a* N-PCP.

The comparison between the relative populations of the peridinin triplet spin sublevels of Chl *d* N-PCP and Chl *a* N-PCP, show that the introduction of Chl *d*, leads to a significant change of the initial population probabilities, while the ZFS parameters and the decay rates are conserved. The calculations of the initial ESE spectra reported in Fig. 4, for Chl *d* N-PCP seem to indicate a preferential quenching by PID612 compared to PID614, while the other two peridinins (PID611-613) are characterized by a wrong polarization pattern and their contribution must be negligible. This result is however surprising because PID612 is postulated to be a blue-shifted peridinin, absorbing at ~485 nm in native MFPCP. If high energy absorption is maintained in the N-PCP reconstituted domain, a preferential localization of the triplet state on the blue-absorbing peridinin would produce a large effect on the associated T−S spectrum. The main bleaching should be blue-shifted and the T–T absorption band would be expected at shorter wavelengths. On the contrary the T−S spectrum of the Chl *d* N-PCP is almost identical to that of Chl *a* N-PCP and similar to that of native PCP in the peridinin absorption region. According to Ilagan et al. [4] the 10 K absorption spectrum of Chl *d* N-PCP results from contribution of four spectrally distinct forms of peridinin with spectral origins at 490, 513, 530, 546 nm, substantially the same as in Chl *a* N-PCP (486, 510, 529, 548 nm) and very similar to those of the native PCP (485, 522, 526, 544 nm). If the localization of the triplet state changed upon reconstitution with Chl *d*, large effects on the T−S spectrum would be expected, but this is not observed. The ODMR data clearly indicate no changes in terms of magnetic and optical properties of the peridinin(s) triplet state(s) involved in the Chl triplet quenching. Furthermore the decay rates of spin sublevels, determined by the simulations of ESE spectra, are the same as those found for Chl *a* N-PCP (Table 1).

As mentioned above, the calculation of triplet–triplet energy transfer in Chl *d* N-PCP, is based on the assumptions of an initial Chl *d* triplet state having the polarization pattern reported for isolated Chl *d* in 2-MTHF glass (Px:Py:Pz 0.34:0.50:0.16) [33], the same ZFS axes directions as for Chl *a*, the same relative geometry of the pigments as in the N-domain of the native MFPCP and in particular the same orientation of Chl *d* in the binding pocket of Chl *a*. The effect of the polarization of Chl *d* triplet donor has been checked by determining the population probabilities of Chl *d* in partially denatured samples of Chl *d* N-PCP where the Chl *d* triplet state becomes detectable due to reduced triplet-triplet energy transfer efficiency. This experiment gives the following parameters: Px:Py:Pz 0.33:0.43:0.24 for Chl *d*. Using this different set of initial Chl triplet state populations does not change the results significantly, meaning that the best agreement between the experimental and calculated triplet spectra is still reached by localising the triplet preferentially on PID612 (data not shown). This makes the choice of the Chl *d* initial population probabilities, within the range of population above mentioned, not crucial for the assignment of the peridinin involved in the triplet energy transfer. Out of the range the agreement becomes poor for small changes of the Pz population, while the Px and Py values are less restrictive. Instead, a change of the ZFS axes directions in the Chl molecular structure, or a rotation of the Chl ring in the protein, could both account for the observed effects. In fact, when we calculate the acceptor spectrum by rotating the ZFS axes of Chl *d* 15–20° around the axis perpendicular to the porphyrin plane, we obtain a good agreement, with the experimental spectrum, for PID 614 (see Fig. 4). In principle, a change of the axes directions with respect to Chl *a*, due to the substitution in ring 1 (R1) of the porphyrin, is possible. Unfortunately, the directions of the ZFS axes in Chl *d* have not yet been determined either in vitro or in vivo. This leaves open the other possibility for the interpretation of the data: the results are still compatible with a localization of the triplet state on PID614, as in native PCP, if, instead of rotating the ZFS axes in the molecular plane, a rotation of the Chl *d* ring takes place, when the pigment is placed in the binding pocket of Chl *a*. It is interesting to note that such a rotation could be accompanied by the formation of a H-bond of the carbonyl group with the -OH group of the terminal ring of PID612 (see Supplementary material for details). This pigment rearrangement would also be in agreement with the ODMR measurements showing a small change of Chl-peridinin interaction, as revealed by the different intensity of the Q_y bleaching in T−S spectra of Chl *a* N-PCP and Chl *d* N-PCP. A local effect in the binding of Chl *d* in PCP has been invoked also by Ilagan et al. [4] who suggested that the carbonyl group of Chl *d* in R1 unlike the vinyl group of Chl *a* (see Fig. 1) is unable to assume different conformations, explaining in this way the lack of splitting of the Chl Soret band on binding Chl *d* into PCP.

In our previous work on MFPCP and HSPCP we have suggested that the water molecule coordinated to the central Mg of the Chl molecules, plays a key role in the triplet-triplet transfer in MFPCP, and in HSPCP, by forming a bridge between the Chl and PID614/624 (PID1331/1335 in HSPCP) [21]. Since the rotation of Chl *d* does not preclude the possibility of forming a water bridge between Chl *d* and PID614 in N-PCP, the localization of the triplet state on PID614 could still predominate.

5. Conclusions

The N-PCP complexes maintain a 100% efficiency for the quenching of chlorophyll despite the biochemical treatment and reconstitution process, suggesting a substantially conserved pigment structure and arrangement, compared to the native MFPCP. Analysis of the T−S spectra, initial polarization of the photoinduced field-swept ESE spectra and their time evolution, show that, in the reconstituted complexes, the triplet state is probably localized on the same peridinin as in the native complex, although, when Chl *d* replaces Chl *a* in the binding pocket, a local rearrangement of the pigments could occur.

Acknowledgements

This work was supported by the Italian Ministry for University and Research (MURST) under the project PRIN2005. We are grateful to Prof. Giovanni Giacometti for his continuous interest in this work.

Appendix A. Supplementary data

Supplementary data associated with this article can be found, in the online version, at doi:10.1016/j.bbabio.2008.12.004.

References

[1] A. Macpherson, R.G. Hiller, Light-harvesting system in Chl *c*-containing algae in: light-harvesting antennas, in: B Green, W Parson (Eds.), Photosynthesis, Kluwer, Dordrecht, 2003, pp. 323–352.
[2] E. Hofmann, P.M. Wrench, F.P. Sharples, R.G. Hiller, W. Welte, K. Diederichs, Structural basis of light harvesting by carotenoids: Peridinin-chlorophyll-protein from *Amphidinium carterae*, Science 272 (1996) 1788–1791.
[3] F.P. Sharples, P.M. Wrench, K.L. Ou, R.G. Hiller, Two distinct forms of the peridinin-chlorophyll a-protein from Amphidinium carterae, Biochim. Biophys. Acta 1276 (1996) 117–123.
[4] R.P. Ilagan, T.W. Chapp, R.G. Hiller, F.P. Sharples, T. Polívka, H.A. Frank, Optical spectroscopic studies of light-harvesting by pigment-reconstituted peridinin-chlorophyll-proteins at cryogenic temperatures, Photosynth. Res. 90 (2006) 5–15.
[5] R.P. Ilagan, S. Shima, A. Melkozernov, S. Lin, R.E. Blankenship, F.P. Sharples, R.G. Hiller, R.R. Birge, H.A. Frank, Spectroscopic properties of the main-form and high-salt peridinin-chlorophyll a proteins from *Amphidinium carterae*, Biochemistry 43 (2004) 1478–1487.
[6] F.J. Kleima, M. Wendling, E. Hofmann, E.J.G. Peterman, R. van Grondelle, H. van Amerongen, Peridinin chlorophyll a protein: relating structure and steady-state spectroscopy, Biochemistry 39 (2000) 5184–5195.
[7] D. Carbonera, G. Giacometti, U. Segre, E. Hofmann, R.G. Hiller, Structure-based calculations of the optical spectra of the light-harvesting peridinin-chlorophyll-protein complexes from *Amphidinium carterae* and *Heterocapsa pygmaea*, J. Phys. Chem., B 103 (1999) 6349–6356.
[8] E. Papagiannakis, M. Vengris, D.S. Larsen, I.H.M. van Stokkum, R.G. Hiller, R. van Grondelle, Use of ultrafast dispersed pump-dump-probe and pump-repump-probe spectroscopies to explore the light-induced dynamics of peridinin in solution, J. Phys. Chem., B 110 (2006) 512–521.

[9] A. Damjanovic, T. Ritz, K. Schulten, Excitation transfer in the peridinin-chlorophyll-protein of *Amphidinium carterae*, Biophys. J. 79 (2000) 1695–1705.
[10] D.J. Miller, J. Catmull, R. Puskeiler, H. Tweedale, F.P. Sharples, R.G. Hiller, Reconstitution of the peridinin-chlorophyll *a*-protein (PCP): evidence for functional flexibility in chlorophyll binding, Photosynth. Res. 86 (2005) 229–240.
[11] T.H.P. Brotosudarmo, H. Hofmann, R.G. Hiller, S. Wörmke, S. Mackowski, A. Zumbusch, C. Bräuchle, H. Scheer, Peridinin-chlorophyll-protein reconstituted with chlorophyll mixtures: preparation, bulk and single molecule spectroscopy, FEBS Lett. 580 (2006) 5257–5262.
[12] T.H.P. Brotosudarmo, S. Mackowski, E. Hofmann, R.G. Hiller, C. Bräuchle, H. Scheer, Relative binding affinities of chlorophylls in peridinin-chlorophyll-protein reconstituted with heterochlorophyllous mixtures, Photosynth. Res. 94 (2008) 247–252.
[13] T. Polivka, T. Pascher, V. Sundstrom, R.G. Hiller, Tuning energy transfer in the peridinin-chlorophyll complex by reconstitution with different chlorophylls, Photosynth. Res. 86 (2005) 217–227.
[14] T. Polivka, T. Pascher, R.G. Hiller, Energy transfer in the peridinin-chlorophyll protein complex reconstituted with mixed chlorophyll sites, Biophys. J. 94 (2008) 3198–3207.
[15] S. Mackowski, S. Wörmke, T.H.P. Brotosudarmo, C. Jung, R.G. Hiller, H. Scheer, C. Bräuchle, Energy transfer in reconstituted peridinin-chlorophyll-protein complexes: ensemble and single molecule spectroscopy studies, Biophys. J. 93 (2007) 3249–3258.
[16] S. Mackowski, S. Wörmke, T.H.P. Brotosudarmo, H. Scheer, C. Bräuchle, Fluorescence spectroscopy of reconstituted peridinin-chlorophyll-protein complexes, Photosynth. Res. 95 (2008) 253–260.
[17] H.A. Frank, R.J. Cogdell, Carotenoids in photosynthesis, Photochem. Photobiol. 63 (1996) 257–264.
[18] D. Carbonera, G. Giacometti, G. Agostini, FDMR spectroscopy of peridinin chlorophyll-a protein from amphidinium-carterae, Spectrochimica 51A (1995) 115–123.
[19] J.A. Bautista, R.G. Hiller, F.P. Sharples, D. Gosztola, M. Wasielewski, H.A. Frank, Singlet and triplet energy transfer in the peridinin-chlorophyll a-protein from *Amphidinium carterae*, J. Phys. Chem., A 103 (1999) 2267–2273.
[20] M. Di Valentin, S. Ceola, E. Salvadori, G. Agostini, D. Carbonera, Identification by time-resolved EPR of the peridinins directly involved in chlorophyll triplet quenching in the peridinin-chlorophyll a-protein from *Amphidinium carterae*, Biochim. Biophys. Acta 1777 (2008) 186–195.
[21] M. Di Valentin, S. Ceola, E.o. Salvadori, G. Agostini, G.M. Giacometti, D. Carbonera, Spectroscopic properties of the peridinins involved in chlorophyll triplet quenching in high-salt peridinin-chlorophyll a-protein from Amphidinium carterae as revealed by optically detected magnetic resonance, pulse EPR and pulse ENDOR spectroscopies, Biochim. Biophys. Acta 1777 (2008) 1355–1363.
[22] J. Niklas, T. Schulte, S. Prakash, M. van Gastel, E. Hofmann, W. Lubitz, W. Spin, Density distribution of the carotenoid triplet state in the peridinin-chlorophyll-protein antenna. A Q-band pulse electron-nuclear double resonance and density functional theory study, J. Am. Chem. Soc. 129 (2007) 15442–15443.
[23] M. Di Valentin, S. Ceola, G. Agostini, G.M. Giacometti, A. Angerhofer, O. Crescenzi, V. Barone, D. Carbonera, Pulse ENDOR and density functional theory on the peridinin triplet state involved in the photo-protective mechanism in the peridinin-chlorophyll a-protein from Amphidinium carterae, Biochim. Biophys. Acta 1777 (2008) 295–307.
[24] R.H. Clarke, Triplet state ODMR spectroscopy, in: R.H. Clarke (Ed.), Techniques and Applications to Biophysical Systems, Wiley-Interscience, New York, 1982.
[25] A.J. Hoff, Optically detected magnetic resonance of triplet states, in: A.J. Hoff (Ed.), Advanced EPR, Elsevier, Amsterdam, 1989.
[26] T.A. Martinson, G.F. Plumley, One-step extraction and concentration of pigments and acyl lipids by *sec*-butanol from *in vitro* and *in vivo* samples, Anal. Biochem. 228 (1995) 123–130.
[27] D. Carbonera, G. Giacometti, G. Agostini, FDMR of carotenoid and chlorophyll triplets in Light-harvesting complex LHCII of spinach, Appl. Magn. Reson. 3 (1992) 361.
[28] S. Santabarbara, E. Bordignon, R.C. Jennings, D. Carbonera, Chlorophyll triplet states associated with photosystem II of thylakoids, Biochemistry 41 (2002) 8184.
[29] S. Stoll, A. Schweiger, EasySpin, a comprehensive software package for spectral simulation and analysis in EPR, J. Magn. Reson. 178 (2006) 42–55.
[30] D. Carbonera, G. Giacometti, G. Agostini, A. Angerhofer, V. Aust, ODMR of carotenoid and chlorophyll triplets in CP43 and CP47 complexes of spinach, Chem. Phys. Lett. 194 (1992) 275–281.
[31] D. Carbonera, E. Bordignon, G. Giacometti, G. Agostini, A. Vianelli, Fluorescence and absorption detected magnetic resonance of chlorosomes from green bacteria Chlorobium tepidum and *Chloroflexus aurantiacus*. A comparative study, J. Phys. Chem., B 105 (2001) 246–255.
[32] D. Carbonera, G. Agostini, T. Morosinotto, R. Bassi, Quenching of chlorophyll triplet states by carotenoids in reconstituted Lhca4 subunit of peripheral light-harvesting complex of photosystem I, Biochemistry 44 (2005) 8337–8346.
[33] D. Carbonera, G. Giacometti, U. Segre, A. Angerhofer, U. Gross, Model for triplet-triplet energy transfer in natural clusters of peridinin molecules contained in Dinoflagellate's outer antenna proteins, J. Phys. Chem., B 103 (1999) 6357–6362.
[34] D. Carbonera, G. Giacometti, U. Segre, Carotenoid interactions in peridinin chlorophyll a proteins from dinoflagellates — evidence for optical excitons and triplet migration, J. Chem. Soc., Faraday Trans. 92 (1996) 989–993.
[35] M. Di Valentin, S. Ceola, G. Agostini, A. Telfer, J. Barber, F. Böhles, S. Santabarbara, D. Carbonera, The photo-excited triplet state of chlorophyll *d* in methyl-tetrahydrofuran studied by optically detected magnetic resonance and time-resolved EPR, Mol. Phys. 105 (2007) 2109–2117.
[36] R.G. Hiller, L.G. Crossley, P.M. Wrench, N. Santucci, E. Hofmann, The 15-kDa forms of apo-peridinin-chlorophyll *a* protein (PCP) in dinoflagellates show high identity with the apo-32-kDa PCP forms, and have similar N-terminal leaders and gene arrangements, Gent. Genomics 266 (2001) 254–259.
[37] A. Angerhofer, F. Bornhauser, A. Gall, R.J. Cogdell, Optical and optically detected magnetic resonance investigation on purple photosynthetic bacterial antenna complexes, Chem. Phys. 194 (1995) 259–274.

Appl Magn Reson (2010) 37:191–205
DOI 10.1007/s00723-009-0046-y

Applied
Magnetic Resonance

Pulsed EPR and ENDOR on the Peridinin Triplet State Involved in the Photoprotective Mechanism in Peridinin–Chlorophyll *a*–Proteins

Marilena Di Valentin · E. Salvadori · S. Ceola · D. Carbonera

Received: 30 April 2009 / Revised: 2 June 2009 / Published online: 15 November 2009
© Springer 2009

Abstract The photoexcited triplet state of the carotenoid peridinin in the peridinin–chlorophyll *a*–protein (PCP) of the dinoflagellate *Heterocapsa pygmaea* has been investigated by pulsed electron paramagnetic resonance (EPR) and pulsed electron-nuclear double resonance (ENDOR) spectroscopies. The α- and β-protons hyperfine couplings of the peridinin-conjugated chain have been derived from Davies and Mims ENDOR experiments. The spectroscopic results have been compared to those obtained for the main form of the PCP complex and for the high-salt PCP form from *Amphidinium carterae*. The EPR features of the peridinin triplet state are very similar in the antenna complexes belonging to the two different dinoflagellate species, proving that the triplet formation pathway and the triplet localization on one specific peridinin per subcluster are common features of different PCP antennas. No significant variation of the hyperfine couplings of the peridinin triplet state has been detected between the main form of the PCP complex from *A. carterae* and *H. pygmaea*. The spectroscopic results confirm the close relationship between the *Amphidinium* PCP and the corresponding *Heterocapsa* complex at least in terms of mutual arrangement of the chlorophyll *a*–peridinin pair involved in photoprotection and in terms of conformation of the peridinin-conjugated chain.

1 Introduction

Marine photosynthetic organisms utilize an efficient light-harvesting strategy based primarily on carotenoids (Cars) rather than chlorophyll (Chl) pigments. Among the variety of light-harvesting proteins of marine algae, the water-soluble protein peridinin–chlorophyll *a*–protein (PCP) is an ideal model for investigating singlet–

M. Di Valentin (✉) · E. Salvadori · S. Ceola · D. Carbonera
Dipartimento di Scienze Chimiche, Università di Padova, via Marzolo 1, 35131 Padua, Italy
e-mail: marilena.divalentin@unipd.it

singlet energy transfer from Cars to Chls and triplet–triplet energy transfer from Chls to Car pigments. PCP is the peripheral light-harvesting complex of photosynthetic dinoflagellates, it contains only peridinin (Per) and Chl *a* in a stoichiometric ratio of 4:1. A high carotenoid content and the presence of Per, an unusual light-harvesting carotenoid (the molecular structure is reported in Fig. 1), are distinctive characteristics of the PCP antenna protein. Peridinin is an asymmetric and highly substituted carotenoid with a C_{37} carbon skeleton (rather than C_{40} as in most carotenoids) together with a lactone ring, an allene moiety in conjugation with the π-electron system and two terminal β-rings with epoxy and acetate substituents.

The structure of the main form of PCP (MF-APCP) from *Amphidinium carterae* (*A. carterae*), resolved at 2.0 Å resolution [1], reveals a trimer of protein subunits with densely packed pigments. As shown in Fig. 1, in each subunit the pigments are organized in two pseudo-identical domains of four Pers in van der Waals contact (3.3–3.8 Å) with the tetrapyrrole ring of one Chl *a* molecule. Pers are in an almost extended all-*trans* configuration and show small distortions from their average geometry, which derive from the interaction with the surrounding protein. Distances among Pers within a single domain range from 4 to 11 Å. The peptide primary sequence of the N- and C-terminal regions form structurally almost identical domains, each consisting of eight alpha-helices.

Besides the main form of the PCP complex from *A. carterae*, a minor component is eluted from the anion exchange columns at high-salt concentration [2]. This form, denoted high-salt PCP (HS-APCP), has a molecular weight of 34 kDa, a 31% identity in amino acid sequence and contains only six Pers and two Chl *a* molecules.

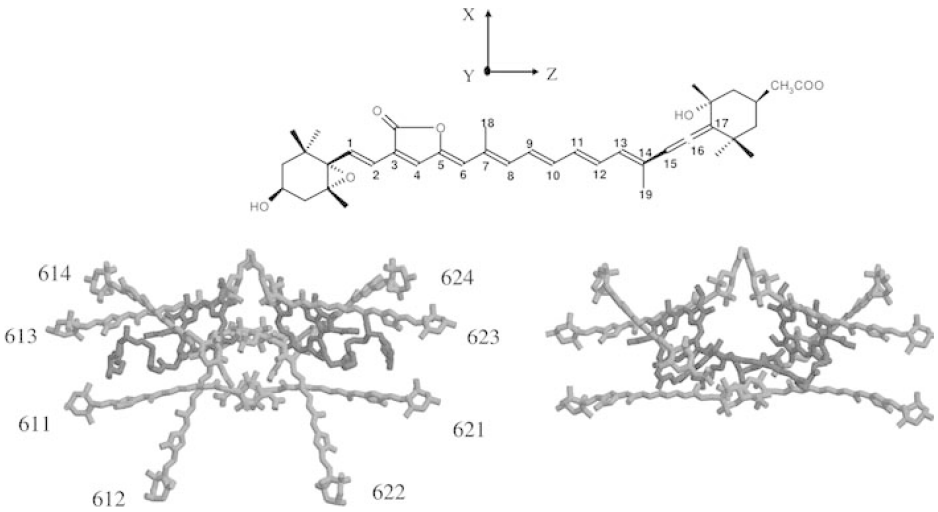


Fig. 1 *Top* molecular structure of peridinin with the numbering of atoms and the orientation of the zero-field splitting (ZFS)-tensor axes. *Bottom left* arrangement of the pigments associated with the monomeric basic unit of the MF-APCP complex from *A. Carterae*. The coordinates are taken from PDB-file 1PPR deposited in the Brookhaven Protein Data Bank [1]. The PDB-file numbering for the peridinins is maintained. *Bottom right* arrangement of the pigments associated with the monomeric basic unit of the HS-APCP complex from *A. Carterae*. The coordinates are taken from PDB-file 2C9E deposited in the Brookhaven Protein Data Bank [3]

Recently, the X-ray structure of HS-APCP has also been determined [3]. It shows a large similarity with the MF-APCP in terms of pigment arrangement, except for the absence of the two symmetry-related peridinins, Per612/Per622, according to the nomenclature of Hofmann et al. [1]. Differences between MF-APCP and HS-APCP have been found in the inter-distance between the two Chl *a* molecules belonging to each subunit, which is larger in the case of HS-APCP, and in the location of the phytol tails which point to the external part of the protein in MF-APCP while they are directed in the region between the two Chls in the HS-APCP complex. A direct comparison between the two different pigment arrangements is shown in Fig. 1. Differences in the low-temperature absorption spectra of the MF-APCP and HS-APCP have been reported [4–6].

The PCP complexes isolated from another dinoflagellate species *Heterocapsa pygmaea* (HPCP) shows only some minor differences in the spectroscopic properties compared to the MF-APCP complex from *A. carterae* [7, 8]. The HPCP complex has the same pigment stoichiometry as MF-APCP but the apoprotein has a 15.5 kDa molecular mass (half size compared to MF-APCP) and contains half the number of pigments. HPCP is present in solution as a homodimer. The degree of identity of HPCP with the C-terminal domain of *A. carterae* is about 70%. Although the structure of HPCP is unknown, modeling of the HPCP amino acid sequence on to the high-resolution structure of *A. carterae* PCP shows that the protein regions in contact with the pigments are highly conserved in sequence [9].

Pers have a dual function in the PCP complexes: they act as light-harvesting pigments and as photoprotective agents. Their role as antenna pigments is fulfilled by absorbing light in the blue-green spectral region where Chls absorb weakly and delivering excitation energy to these pigments by rapid singlet–singlet energy transfer. They play the photoprotective role by virtue of their low-lying triplet states. They quench Chl triplet states, which can be populated under high light conditions, by triplet–triplet energy transfer [10, 11]. In this way they prevent the formation of the highly reactive singlet oxygen species, which would lead to the damage of the light-harvesting apparatus. This photoprotective function is therefore essential for photosynthesis in an oxygen-containing environment.

In the isolated form of PCP, the Chl *a* pigments, once excited, cannot transfer their energy to other antenna complexes and de-excitation mainly proceeds through fluorescence or intersystem crossing and triplet formation. The lifetime of the Chl *a* triplet state in PCPs is of the order of 20 ns; within this time a triplet state is formed on one of the circumferential Pers and decays through radiationless intersystem crossing channels with a lifetime of 10 μs at room temperature [11, 12].

Electron paramagnetic resonance (EPR) spectroscopy is a fundamental tool for understanding the electronic structure of the photoexcited triplet state. Porphyrin, chlorophyll and bacteriochlorophyll model systems [13–16] and photosynthetic primary donors [17–20] have been extensively investigated by time-resolved and pulse electron-nuclear double resonance (ENDOR) in order to derive the triplet hyperfine couplings (hfcs) and the spin density distribution of the triplet state. Only recently, the advanced EPR techniques have proved to be powerful also in studying the triplet state of the carotenoid species populated by triplet energy transfer in antenna systems.

In a time-resolved EPR study, we exploited the concept of spin angular momentum conservation during triplet–triplet energy transfer in order to investigate the mechanism of photoprotection in the MF-APCP and HS-APCP from *A. carterae* [21]. We suggested a specific path for triplet–triplet energy transfer, common to both PCP forms, involving the Chl–Per pair characterized by the shortest center-to-center distance (Chl601/602 and Per614/624 according to the nomenclature used in Ref. [21] and reported in Fig. 1. This particular pair is characterized by the presence of a water molecule in a bridging position which is coordinated to the central Mg atom of the Chl.

Later, we extended the spectroscopic study of the peridinin triplet state in MF-APCP and HS-APCP to the pulsed ENDOR spectroscopy, in order to gain insight into the triplet state electronic structure [22, 23]. Comparison of the proton hfcs obtained from ENDOR experiments on the MF-APCP with those predicted from density functional theory (DFT) allowed to determine the triplet spin density on the conjugated chain of the peridinin molecule correlate it with the structural requirements for efficient triplet–triplet energy transfer. Small differences in the hfcs assigned to the β-protons belonging to one of the two methyl groups present in the Per-conjugated chain have been found in MF-APCP compared to HS-APCP. The discrepancy has been explained in terms of local distortion of the tails of the conjugated chain in the two PCP forms, in agreement with X-ray structural data.

A Q-band ENDOR and DFT study was also performed on the Per triplet state in a refolded N-domain PCP complex (RF-PCP) [24]. Dimerization of the N-domain, expressed in *Escherichia coli*, occurs upon refolding. Spectroscopic features of MF-APCP are maintained in the RF-PCP complex as reported in Refs. [6, 25, 26].

Only preliminary ENDOR experiments on the peridinin triplet state in the PCP complex from *H. pygmaea* have been reported [27], not allowing a comparison between light-harvesting complexes of different marine organisms, because of the absence of a complete set of hfcs and corresponding assignment.

The present work is a comparative investigation by pulse EPR and ENDOR spectroscopies on HPCP from *H. pygmaea* and MF-APCP, HS-APCP from *A. carterae*, devoted to recognize common features and differences in the triplet state electronic structure of Pers in diverse PCP forms.

2 Materials and Methods

2.1 Sample Preparation

PCP proteins, extracted and purified according to Refs. [2, 28, 29], were kindly supplied by R. G. Hiller. Sample concentrations were $\approx$1 mg/ml. Oxygen was removed from the samples by flushing argon in the EPR tube before freezing, residual oxygen was removed using glucose/glucose oxidase. Glycerol, previously degassed by several cycles of freezing and pumping, was added (60% v/v) to obtain a transparent matrix.

2.2 Pulsed EPR and ENDOR Measurements

Pulsed EPR and ENDOR were performed on a Bruker Elexsys E580 pulsed EPR spectrometer equipped with a Bruker ENDOR accessory (E560D-P) and a radio frequency (RF) amplifier (AR751–150W). Laser excitation at 532 nm (10 mJ per pulse and repetition rate of 10 Hz) was provided by the second harmonic of a Nd:YAG laser (Quantel Brilliant) in the optically transparent dielectric ring ENDOR resonator (EN4118X-MD4). The resonator was placed in a helium cryostat (Oxford CF935) for the cryogenic temperature experiments. After pulsed laser excitation, the EPR and ENDOR signals were directly detected and had a non-derivative shape (A = enhanced absorption, E = emission).

Field-swept electron spin echo (ESE) spectra were recorded using a 2-pulse (flash-DAF-π/2-τ-π-τ-echo) ESE sequence for a delay between the laser flash and the first microwave pulse (DAF) of 50 ns. ESE-detected kinetics at the triplet canonical orientations were recorded using a 2-pulse (flash-DAF-π/2-τ-π-τ-echo) ESE sequence after a variable DAF (500 ns step) between the laser flash and the first microwave pulse. The π/2-pulse was of 16 ns and the delay τ was set at 200 ns for the field-swept ESE experiment and to 120 ns for the ESE-detected kinetics.

Davies-ENDOR experiments were performed using the microwave pulse sequence (flash-DAF-π-T-π/2-τ-π-τ-echo) with an inversion π pulse of 128 ns, T of 3.8 μs and a RF pulse of 3 μs. The detection sequence was similar to the field-swept ESE experiment but with τ of 300 ns. The DAF was normally 50 ns or 18 μs for Y transition.

Mims ENDOR experiments were recorded using the microwave pulse sequence (flash-DAF-π/2-τ-π/2-T-π/2-echo), with 16 ns pulse duration, in conjunction with an RF pulse of 3 μs duration, starting 0.3 μs after the second microwave pulse. The DAF was 50 ns normally or 18 μs for Y transition, the delay τ was variable, and the time T was 3.8 μs to accommodate the RF pulse. Mims ENDOR spectra were recorded at different τ values (from 160 to 240 ns) and added together to eliminate τ-dependent blind spots. Pulse ENDOR spectra were accumulated for $\approx$15 h.

2.3 EPR Spectral Analysis

A program written in MatLab® was employed to analyze the pulse EPR spectra. The program calculates both the line shape and the time profile of the spin-polarized triplet EPR spectrum. The program is based on a spin Hamiltonian in which only the Zeeman and magnetic dipole–dipole interaction, zero-field splitting (ZFS) parameters D and E, are explicitly taken into account to calculate the line shape of the spectrum for an ensemble of randomly oriented molecules.

The time-evolution of the EPR spectrum has been calculated in terms of the photoexcited triplet state dynamics, as previously described [30].

Since the kinetics at the X and Y canonical fields are strongly mixed because of the superposition of several transitions, the transient traces detected at the canonical transitions are not simulated in the simplified view of single canonical transitions. The calculated time-traces are extracted, in correspondence of the X, Y and Z spectral turning-points, from a bidimensional simulation of the EPR spectrum of the

peridinin triplet state as a function of both the static magnetic field and delay from the laser pulse.

3 Results

3.1 EPR

Figure 2 depicts the field-swept ESE EPR spectra of the photoexcited triplet state of peridinin in MF-APCP, HS-APCP from *A. carterae* and *HPCP* from *H. pygmaea*, recorded immediately after the laser flash (DAF of 50 ns) at 20 K. The spectra for MF-APCP and HS-APCP were already reported in Refs. [21, 23] and assigned to the peridinin triplet state. The spectra show the same *eaeaea* spin-polarization pattern and ZFS parameters which are only slightly different among the different PCP forms (see Table 1). The polarization pattern is inherited from the Chl *a* triplet donor during the triplet–triplet energy transfer as demonstrated in Ref. [21]. No difference in spectral profiles is observed when comparing the corresponding time-resolved EPR spectra and the field-swept ESE spectra (data not shown), proving that the spin–spin relaxation time is not orientation dependent or sufficiently longer than the τ value of 200 ns used in the pulsed EPR experiments.

In Fig. 3 the experimental field-swept ESE spectrum at DAF = 50 ns for HPCP is superimposed with the spectral simulation. Canonical orientations of the ZFS tensor are also indicated. The order of the ZFS energy levels is: $Z^2 > Y^2 > X^2$. The corresponding ZFS axes of the peridinin triplet state have been chosen analogously to those determined for β-carotene in crystals [31, 32]: the long axis is the Z axis, the X axis is along the C–H bonds in the conjugated chain and the Y direction is perpendicular to the conjugated XZ molecular plane (see Fig. 1).

We have also investigated the kinetics of population and decay of the triplet spin sublevels by monitoring the echo intensity as a function of DAF, the delay of the

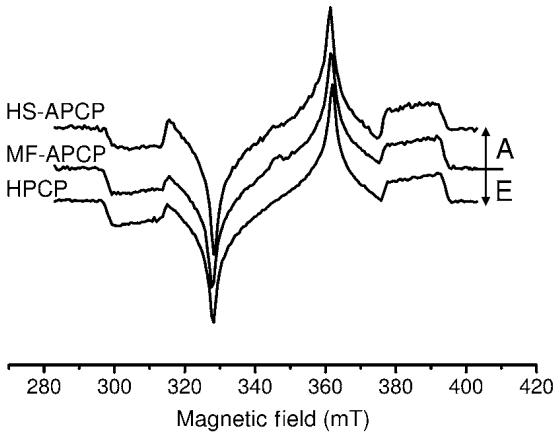


Fig. 2 Comparison between field-swept ESE spectra of HS-APCP, MF-APCP from *A. carterae* and HPCP from *H. pygmaea* recorded at $T = 20$ K. Data relative to MF-APCP and HS-APCP are the same as in Refs. [22] and [23], respectively. For experimental conditions see Sect. 2. *A* absorption, *E* emission

Table 1 Values of the ZFS parameters $|D|$ and $|E|$, relative population rates P_X, P_Y, P_Z and decay constants k_X, k_Y, k_Z obtained from the simulation of the time-evolution of the field-swept ESE spectrum of HPCP from *H. pygmaea*

	D (10^{-4} cm^{-1})	E (10^{-4} cm^{-1})	P_X:P_Y:P_Z	k_X:k_Y:k_Z	Ref.
HPCP	448.7	44.8	0.18:0.37:0.45	0.135:0.035:0.085	
MF-APCP	449.7	43.9	0.18:0.37:0.45	0.15:0.03:0.09	[14]
HS-APCP	443.6	45.1	0.18:0.39:0.43	0.135:0.028:0.08	[15]

The simulation procedure is described in Sect. 2. For comparison, the data relative to MF-APCP [22] and HS-APCP [23] from *A. carterae* are also reported

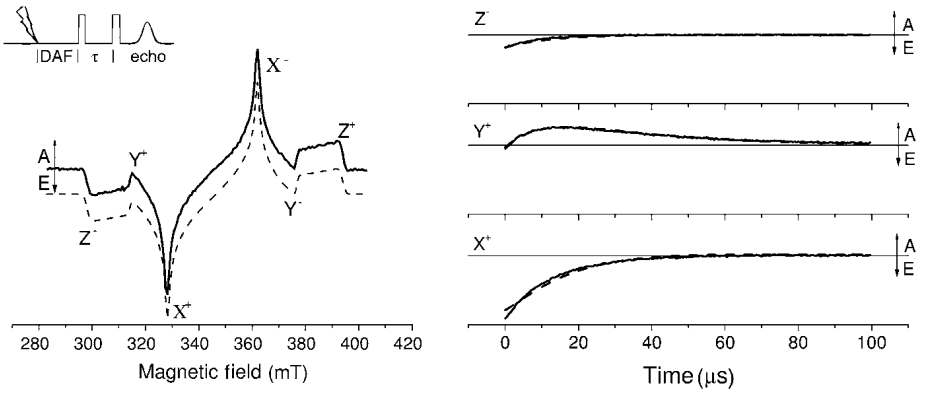


Fig. 3 *Left* field-swept ESE spectrum of HPCP (*solid line*) from *H. pygmaea* recorded at $T = 20$ K and DAF = 50 ns and corresponding simulation (*dashed line*); *inset* pulse scheme of the ESE experiment for photoexcited triplet states. *Right* ESE-detected kinetics at the low-field canonical orientations Z^-, Y^+, X^+ (*solid line*) recorded at $T = 20$ K, superimposed to the corresponding simulation (*dashed line*). Order of energy for zero-field triplet sublevels: $|Z| > |Y| > |X|$. Simulation parameters are reported in Table 1. *A* absorption, *E* emission

microwave pulse sequence with respect to the laser flash. While kinetic measurements in time-resolved EPR are hampered by the presence of microwave-induced transition probabilities, ESE spectroscopy does not suffer of this complication since in this technique there is no microwave field present in the period between the photogeneration of the triplet state and its detection. The overall ESE-detected kinetics in function of DAF at the low-field canonical orientations of the ZFS tensor (Z^-, Y^+, X^+), superimposed to the simulated traces, are reported in Fig. 3. The time-evolution of the EPR spectrum was calculated in terms of the photoexcited triplet state dynamics [30], assuming that the echo decay reflects the decay kinetics of the triplet populations connected by the microwave pulses. The delay τ between the two microwave pulses was adjusted to a minimum value in order to avoid also spin–spin relaxation effects.

In Table 1 we summarize the simulation parameters, ZFS parameters, relative populating rates and decay rates for the peridinin triplet levels, for HPCP and compare them to the corresponding values reported previously for MF-APCP and HS-APCP [21, 23]. The time-dependent changes of the spin polarization are satisfactorily reproduced by simulations based on a strongly anisotropic decay of the

three spin sublevels of the peridinin triplet state to the ground singlet state. The time-evolution of the spin-polarization, leading to a final polarization pattern of the type *eaeaea*, is not only a common feature of the peridinin triplet from different PCP forms but has also been found for all the carotenoid triplet states in all the different photosynthetic systems, as demonstrated in Refs. [33, 34].

3.2 ENDOR

Pulse ENDOR experiments were performed on HPCP and compared to previously reported experiments on MF-APCP and HS-APCP from *A. carterae* [22, 23], and RF-PCP [24].

ENDOR experiments on the triplet state, carried out at the canonical magnetic field positions in the EPR spectrum, permit measurement of the hfc tensor components A_{ii} of protons in the reference frame of the ZFS tensor, yielding single-crystal-like spectra. The hyperfine couplings are sensitive probes of the electronic distribution on the conjugated chain.

The triplet spin energy levels for one of the three canonical orientations, including first-order hyperfine interaction with one proton A_{ii}, for $D < 0$ as expected for the Per molecule characterized by a long axis, are shown in Fig. 4. For each EPR transition, there are two ENDOR resonance frequencies at:

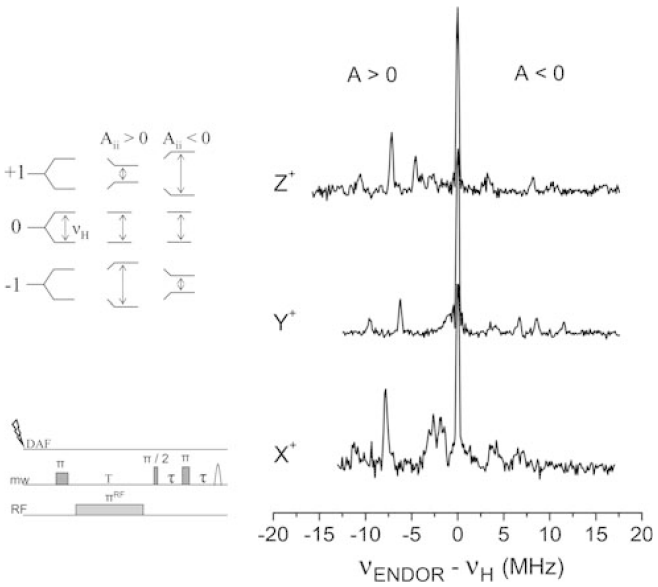


Fig. 4 *Top left* spin energy levels of a triplet state, showing positive and negative hyperfine interaction with one nucleus with spin $I = 1/2$ for the field parallel to one of the canonical axes of the ZFS tensor. *Bottom left* pulse scheme for Davies-ENDOR experiment for photoexcited triplet states. *Right* Davies-ENDOR spectra of HPCP from *H. pygmaea* for the X^+, Y^+ and Z^+ field position (indicated in Fig. 3) at $T = 20$ K. The frequency scale gives the deviation of the resonance line from ν_H. For experimental conditions see Sect. 2

$\nu_{ENDOR}(0) = \nu_H$
$\nu_{ENDOR}(1) = \nu_H - A_{ii}$ if $A_{ii} > 0$ or $\nu_{ENDOR}(1) = \nu_H + A_{ii}$ if $A_{ii} < 0$

corresponding to the X^+, Y^+ or Z^+ EPR transition or

$\nu_{ENDOR}(0) = \nu_H$
$\nu_{ENDOR}(-1) = \nu_H + A_{ii}$ if $A_{ii} > 0$ or $\nu_{ENDOR}(-1) = \nu_H - A_{ii}$ if $A_{ii} < 0$

corresponding to the X^-, Y^- or Z^- EPR transition.

The ENDOR transitions corresponding to the $\Delta m_S = \pm 1$ EPR transitions in the low-field and high-field spectra are reflected on opposite sides of the transition at ν_H. For the $\Delta m_S = +1$ transition, depending on the sign of A_{ii}, the ENDOR lines occur on the low (if $A_{ii} > 0$) or high (if $A_{ii} < 0$) frequency side. An opposite situation is encountered for the $\Delta m_S = -1$ transition. Therefore, if the sign of the ZFS parameter D is known, the sign of the hfcs can be directly derived from the spectral position corresponding to the low- or high-field lines.

The Davies-ENDOR spectra of the photoexcited triplet state of peridinin in HPCP for the X^+, Y^+ and Z^+ EPR field positions, obtained at 20 K, are reported in Fig. 4. While the ENDOR spectra corresponding to the X^+, Z^+ transitions have been recorded at DAF = 50 ns, the spectra corresponding to the Y^+ transitions have been taken at DAF = 18 μs in order to exploit the maximum intensity of the spin polarization. The initial spin-polarized spectrum at the Y^- transition is very weak and is characterized only by an unstructured free proton Larmor line (ν_H). The frequency scale in this figure is plotted as deviation from ν_H and the hfcs correspond to the frequency shift between the corresponding ENDOR line and the ν_H. On the basis of the scheme reported in Fig. 4, ENDOR lines have been labeled in terms of positive or negative hfcs.

Table 2 Experimental values of the proton hyperfine tensor components in the ZFS axes system of the peridinin triplet state in HPCP from *H. pigmaea*

A_{XX} (MHz)	A_{YY} (MHz)	A_{ZZ} (MHz)
+11.4	+9.8	+10.7
+7.6	+6.2	+7.1
+3.2[a]	+1.8[b]	+4.6[a]
+2.7	+1.1	+3.9[a]
+1.9[b]	−0.9[b]	+2.8
+1.4[b]	−4.0	+1.5[b]
+0.8[b]	−6.8	+0.9[b]
−1.0[b]	−8.6[a]	−1.3[b]
−3.6	−11.6[a]	−3.2
−4.0[a]		−8.1[a]
−6.8		−10.5[a]
		−16.0[a]

The ZFS reference frame is reported in Fig. 1

[a] *hfcs* present only in Davies-ENDOR spectra

[b] *hfcs* present only in Mims ENDOR spectra

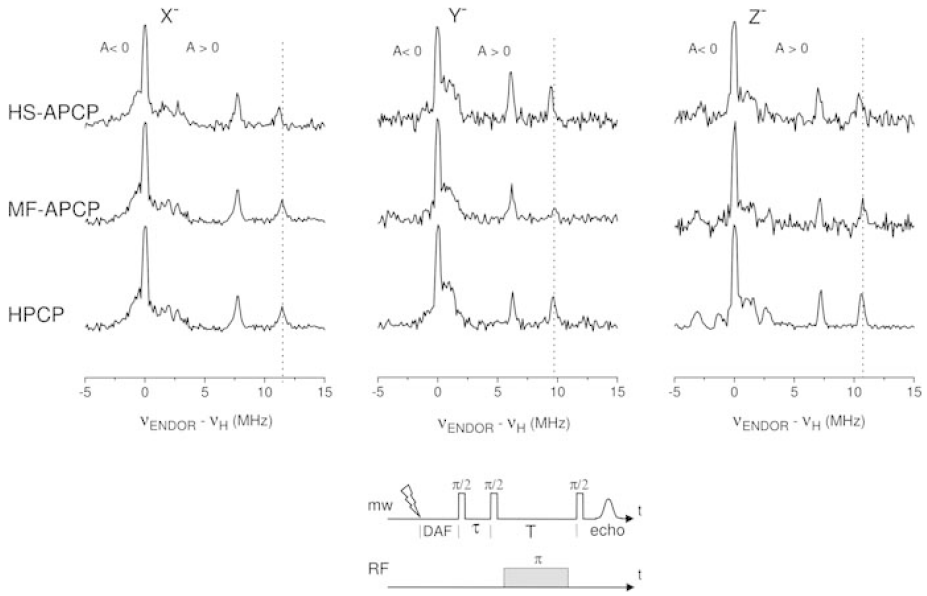


Fig. 5 Mims ENDOR spectra of HS-APCP, MF-APCP from *A. carterae* and HPCP form *H. pygmaea* for the X^-, Y^- and Z^- EPR field positions (indicated in Fig. 3) recorded at $T = 20$ K. The frequency scale gives the deviation of the resonance line from ν_H. For experimental conditions see Sect. 2. Data relative to MF-APCP and HS-APCP are taken from Refs. [22] and [23], respectively. *Inset* pulse scheme of the Mims ENDOR experiment for photoexcited triplet states

All hf tensor components, measured along the three canonical directions of the ZFS reference frame, are summarized in Table 2. Assignment of the ENDOR transitions, based on DFT calculation of the hyperfine tensors, was reported for MF-APCP from *A. carterae* in Ref. [22] and for RF-PCP in Ref. [24].

The Mims ENDOR spectra of the photoexcited triplet state of peridinin in HPCP for the X^-, Y^- and Z^- EPR field positions, obtained at 20 K, are reported in Fig. 5 and compared to the corresponding spectra from MF-APCP and HS-APCP [22, 23]. The ENDOR spectra for the Z^- transition are spin-polarized in emission as the corresponding EPR transition, but it has been inverted for better comparison with the other transitions.

The use of the Mims ENDOR technique was aimed at detecting small hfcs with higher sensitivity compared to Davies ENDOR in order to search for possible differences among the PCP complexes under investigation. For this reason, a narrow RF frequency region, reaching the methyl groups lines, is shown in Fig. 5. Indeed, all the ENDOR spectra at the canonical EPR field positions show partially resolved lines in the vicinity of the Larmor frequency, corresponding to positive and negative hfcs. These small hfcs components have been assigned to α-protons. No variations in this spectral range have been found among the different PCP forms. The large positive hfcs have been assigned to rotating methyl groups at position 18 and 19 in the molecular structure shown in Fig. 1. While, as already pointed out in our previous report [23], in HS-APCP one of the two methyl groups shows hfcs which

Table 3 Experimental ENDOR values of the *hfcs* relative to methyl groups 18 and 19 (see Fig. 1) of HPCP from *H. pygmaea*

	A_{XX} (MHz)		A_{YY} (MHz)		A_{ZZ} (MHz)		a_{iso} (MHz)		Ref.
	Me18	Me19	Me18	Me19	Me18	Me19	Me18	Me19	
HPCP	7.6	11.4	6.2	9.8	7.1	10.7	7.0	10.6	
MF-APCP	7.6	11.4	6.2	9.8	7.1	10.7	7.0	10.6	[14]
HS-APCP	7.6	11.1	6.2	9.5	7.1	10.3	7.0	10.3	[15]

For comparison, the data relative to MF-APCP [22] and HS-APCP [23] from *A. carterae* are also reported

are smaller compared to the values found for MF-APCP, no variation in any of the A_{ii} components has been found in HPCP compared to MF-APCP.

All the three hyperfine tensor components in the ZFS-tensor frame, for both methyl groups, have been determined from the ENDOR spectra shown in Figs. 4 and 5. Values are reported in Table 3 and compared to those corresponding to MF-APCP and HS-APCP [22, 23]. Based on the approximate collinearity between the ZFS and hfc tensor principal axes, the hfc components measured in the ZFS frame can be considered the principal components of the proton hyperfine tensors. For this reason, the isotropic hfc constants for the two rotating methyl groups for HPCP can be directly derived from the set of measured hfc components: $a_{iso} = 7.0$ MHz and $a_{iso} = 10.6$ MHz.

4 Discussion

The key light-harvesting pigment in the PCP antenna complex is the peridinin carotenoid. The crystal structure of the MF-APCP complex revealed that the eight Pers, surrounding two Chl *a* molecules, are not structurally equivalent [1]. The numerous spectroscopic studies and quantum mechanical calculations indicate that the peridinins are inhomogeneous in terms of local environment and occupy binding sites with different energies [12, 35–37]. In addition, the minor component of *A. carterae*, denoted HS-APCP, lacks the peridinin equivalents of Per612 and Per622 in the MF-APCP and the Chl phytol tails reside between the two Chls in the space occupied by Per612 and Per622 in the MF-APCP [5]. Although strong similarities between MF-APCP and HS-APCP can be found in terms of pigment arrangement, local distortions of the polyene chain can be recognized by comparison between the homologous peridinins in the respective X-ray structures [3, 5, 23]. Differences in pigment structure and stoichiometry are accompanied by variations in the amino acid environment surrounding the pigment cluster, attributed to the larger number of positively charged amino acid residues. Altogether these differences among Pers inside and between subcluster and their occurrence in different PCP forms might lead to different electronic density distribution on the Per molecule.

Triplet–triplet energy transfer, based on the Dexter mechanism, depends on stringent overlap requirement between the donor and acceptor wave functions and is very sensitive to distance and mutual orientation between the π orbitals of the

molecules involved [38]. Small differences in the relative geometry of the donor–acceptor pair are expected to lead to preferential pathways in the triplet quenching. In the PCP complex the X-ray structure has shown the complexity of the system in terms of pigment arrangement: all four peridinins surrounding the Chl *a* molecule are at van der Waals distance from the tetrapyrrole ring but the contact involves different parts of the donor and acceptor conjugated systems. Therefore, the distance requirement is fulfilled for all four carotenoid molecules and other factors based on fine-tuning of the relative geometry of the pair and on the electron density distribution on the extended conjugated systems play the major role. In principle different pathways could be activated by these tuning effects. Detailed knowledge of the electronic structure of the triplet state of the Per carotenoid is fundamental in order to investigate the issue. This information has been provided by the extensive ENDOR studies performed on MF-APCP, HS-APCP from *A. carterae* and RF-PCP [22–24].

We have demonstrated by advanced EPR techniques that the triplet state is localized on a specific peridinin both in MF-APCP and HS-APCP complexes, named Per 614(624) in MF-APCP. This peridinin is placed at the shortest center-to-center distance to the Chl *a* molecule and is bridged to this pigment by a water molecule which is coordinated to the central Mg atom of the pyrrole ring. This is a unique feature of Per614(624) which is conserved also in HS-APCP. A recent ultrafast transient absorption investigation has pointed out the stronger interaction of Per(614)624 with Chl *a* compared to the other Pers of each cluster [39].

As an extension of previous investigations on MF-APCP and HS-APCP, we have performed pulsed EPR and ENDOR experiments on the photoexcited peridinin triplet state in the HPCP antenna complex from *H. pygmaea*. Because the structure of HPCP is not known, despite of the close relationship between MF-APCP and HPCP [9], the possibility exists that subtle differences in cluster arrangement and pigment conformation might lead to important variations in terms of triplet–triplet energy transfer properties.

As already proposed by a comparative study of MF-APCP and HS-APCP [21], the close similarities in terms of the spin-polarization pattern of the triplet state field-swept ESE spectra among all the PCP complexes strongly suggest that homologous peridinins, occupying equivalent positions in the cluster arrangement in terms of relative orientation to the Chl *a* triplet donor, are populated by triplet–triplet energy transfer not only in the PCP complexes of *A. carterae* but also in the PCP complex of *H. pygmaea*. The absence of any significant difference between the PCP complexes of the two different organisms in the spectroscopic and kinetic parameters, derived from simulations of the time-evolution of the field-swept ESE spectra (reported in Table 1), rules out the possibility that different triplet–triplet energy transfer pathways are active in HPCP or that there is a rearrangement of the donor/acceptor pair. Variations of the spin-polarization pattern, when detected, strongly suggest a pigment rearrangement in the binding pocket as in the case of Chl *d* reconstituted PCP complexes [40].

Davies and Mims ENDOR spectra of the photoexcited peridinin triplet state on HPCP from *H. pygmaea*, measured at all canonical orientations where the static magnetic field is parallel to the ZFS-tensor axes, have allowed to obtain a full set of

hyperfine tensor values for all three canonical orientations. All the positive hyperfine coupling tensor components in the ZFS reference frame, corresponding to the two different rotating methyl groups at positions 18 and 19 (see Fig. 1) of the peridinin-conjugated chain, have been derived. Negative hyperfine components, showing large anisotropy in the three canonical orientations, are assigned to α-protons. In Mims experiments small positive and negative hyperfine components belonging to α-protons have also been detected. The full set of hfcs for the peridinin triplet state has been measured (reported in Table 2). Assignment of the experimental hfcs to the molecular positions along the peridinin chain is based on DFT calculation of the hyperfine tensors reported for MF-APCP [22] and RF-PCP [24].

When comparing the full set of experimental hfcs to the corresponding hfcs for MF-APCP and RF-PCP, no significant variation can be found in any of the characteristic spectral region, in proximity to the Larmor frequency, in the positive methyl proton hfc region and in the range corresponding to large hfcs of α-protons.

In the previous report on HS-APCP [23], the two methyl groups at positions 18 and 19 of the peridinin-conjugated chain (see Fig. 1) have been used as markers of variation of the electronic structure of the triplet state. A measurable decrease of the hyperfine tensor components assigned to the protons of the rotating methyl group at position 19 has been detected in the triplet ENDOR spectra for HS-APCP compared to MF-APCP. This result has been interpreted in terms of redistribution of the electron spin density at the tail of the conjugated chain where the allenic group is located. This is the site where molecular distortion is located, as revealed by the X-ray structures of the two complexes [3]. While the methyl group at position 18 is positioned at the center of the conjugated chain which is more conserved, the methyl group at position 19 is a probe in the region where the Pers belonging to the two different complexes differ the most. In contrast, the ENDOR frequencies corresponding to both methyl 18 and 19 do not show any variation when comparing the spectra of MF-APCP and HPCP.

In principle, some differences might be expected because HPCP is a homodimer analogue, showing high sequence homology with the C-domain of MF-APCP. The spectroscopic result confirms the close relationship between the MF-APCP and the corresponding complex from *H. pygmaea* at least in terms of mutual arrangement of the Chl–Per pair involved in photoprotection and in terms of the conformation of the peridinin-conjugated chain. A trimeric model for HPCP, based on the X-ray structure of the MF-APCP trimer, indeed shows that the protein regions in contact with the pigment cluster are highly conserved and can accommodate an unaltered pigment arrangement [9]. The differences between the two complexes are in the two regions located at the putative trimer contacts and on the solvent-exposed surface of the protein. In any case, these differences do not affect the overall structural features of the trimer interface. The hydrophobic pocket and the hydrophilic region including cofactor headgroups are conserved in agreement with our spectroscopic evidence.

No significant differences in hfcs and consequently in triplet spin density on the Per molecule have been detected in native and reconstituted PCP complexes [24], with the exception for the variant HS-APCP, whose X-ray structure is showing local distortions of the pigments compared to the main form complex. On the other hand, when comparing HPCP, which is a homodimer with a high degree of identity with

the C-terminal domain of MF-APCP, with the heterodimer MF-APCP and with the reconstituted homodimer RF-PCP, the triplet probe should allow subcluster differences to be revealed. The invariance of the Per triplet hfcs demonstrates that the differences in pigment arrangement between the N-terminal and C-terminal domains, at least in the photoprotection site, do not affect the triplet state electronic distribution.

Recently, a delocalized triplet model, in which the carotenoid triplet state is shared with the adjacent Chl *a* molecule, has been proposed by Alexandre et al. [41] to interpret step-scan Fourier transform infrared spectroscopy data obtained for MF-APCP. The study has been extended to HPCP and the same conclusions have been drawn for the antenna complex from the *Hetercocapsa* dinoflagellate species [42]. However, all the hfcs derived from the ENDOR experiments on MF-APCP and HPCP have been assigned to protons belonging to the peridinin molecule, proving that in the ENDOR time scale the triplet state is completely localized on the peridinin. No indication of any Per-Chl *a* delocalization in the triplet state is coming from DFT calculations. Computations carried out on Chl601–Per614 pair led to the identification of two distinct low-lying triplet states, localized, respectively, on the Chl *a* and on the Per moiety [22].

This comparative study reinforces the hypothesis of localization of the triplet state on one specific peridinin in the PCP antenna complexes. The ENDOR data, supported by DFT calculations, prove that the peridinin involved in the photoprotective mechanism shows high spin density particularly at the carbon atom position in close contact with the water ligand to the Chl *a* pigment, as demonstrated by inspection of the high-resolution X-ray data on MF-APCP [1]. This result has been interpreted in terms of involvement of the water ligand, functioning as an efficient superexchange mediator, in the triplet–triplet energy transfer between the Chl *a* donor and the Per614(624) acceptor in the PCP antenna [21, 22]. We expect that the water molecule at the interface of the photoprotective Chl–Per pair is conserved also in HPCP.

Acknowledgments This work was supported by the Italian Ministry for University and Research (MURST) under the project PRIN2007. We thank Prof. Giovanni Giacometti for fruitful discussions and advice and Roger Hiller for kindly providing samples of PCP proteins.

References

1. E. Hofmann, P.M. Wrench, F.P. Sharples, R.G. Hiller, W. Welte, K. Diederichs, Science **272**, 1788–1791 (1996)
2. F.P. Sharples, P.M. Wrench, K.L. Ou, R.G. Hiller, BBA-Bioenerg. **1276**, 117–123 (1996)
3. T. Schulte, F.P. Sharples, R. Hiller, E. Hofmann, Biochemistry **48**, 4466–4475 (2009)
4. R.P. Ilagan, S. Shima, A. Melkozernov, S. Lin, R.E. Blankenship, F.P. Sharples, R.G. Hiller, R.R. Birge, H.A. Frank, Biochemistry **43**, 1478–1487 (2004)
5. R.P. Ilagan, J.F. Koscielecki, R.G. Hiller, F.P. Sharples, G.N. Gibson, R.R. Birge, H.A. Frank, Biochemistry **45**, 14052–14063 (2006)
6. T. Polivka, R.G. Hiller, H.A. Frank, Arch. Biochem. Biophys. **458**, 111–120 (2007)
7. D. Carbonera, G. Giacometti, U. Segre, J. Chem. Soc., Faraday Trans. **92**, 989–993 (1996)
8. D. Carbonera, G. Giacometti, U. Segre, E. Hofmann, R.G. Hiller, J. Phys. Chem. B **103**, 6349–6356 (1999)

9. R.G. Hiller, L.G. Crossley, P.M. Wrench, N. Santucci, E. Hofmann, Mol. Genet. Genomics **266**, 254–259 (2001)
10. H.A. Frank, R.J. Cogdell, Photochem. Photobiol. **63**, 257–264 (1996)
11. J.A. Bautista, R.G. Hiller, F.P. Sharples, D. Gosztola, M. Wasielewski, H.A. Frank, J. Phys. Chem. A **103**, 2267–2273 (1999)
12. F.J. Kleima, M. Wendling, E. Hofmann, E.J.G. Peterman, R. van Grondelle, H. van Amerongen, Biochemistry **39**, 5184–5195 (2000)
13. C.W.M. Kay, M. Di Valentin, K. Möbius, Sol. Energ. Mat. Sol. C. **38**, 111–118 (1995)
14. C.W.M. Kay, M. Di Valentin, K. Möbius, J. Chem. Soc., Perkin Trans **2**, 2563–2568 (1997)
15. C.W.M. Kay, U. Gromadecki, J.T. Torring, S. Weber, Mol. Phys. **99**, 1413–1420 (2001)
16. A. Marchanka, W. Lubitz, M. van Gastel, J. Phys. Chem. B **113**, 6917–6927 (2009)
17. M. Di Valentin, C.W.M. Kay, G. Giacometti, K. Möbius, Chem. Phys. Lett. **248**, 434–441 (1996)
18. F. Lendzian, R. Bittl, W. Lubitz, Photosynth. Res. **55**, 189–197 (1998)
19. W. Lubitz, Phys. Chem. Chem. Phys. **4**, 5539–5545 (2002)
20. F. Lendzian, R. Bittl, A. Telfer, W. Lubitz, BBA-Bioenerg. **1605**, 35–46 (2003)
21. M. Di Valentin, S. Ceola, E. Salvadori, G. Agostini, D. Carbonera, BBA-Bioenerg. **1777**, 186–195 (2008)
22. M. Di Valentin, S. Ceola, G. Agostini, G.M. Giacometti, A. Angerhofer, O. Crescenzi, V. Barone, D. Carbonera, BBA-Bioenerg. **1777**, 295–307 (2008)
23. M. Di Valentin, S. Ceola, E. Salvadori, G. Agostini, G.M. Giacometti, D. Carbonera, BBA-Bioenerg. **1777**, 1355–1363 (2008)
24. J. Niklas, T. Schulte, S. Prakash, M. van Gastel, E. Hofmann, W. Lubitz, J. Am. Chem. Soc. **129**, 15442–15443 (2007)
25. T. Polivka, T. Pascher, V. Sundstrom, R.G. Hiller, Photosynth. Res. **86**, 217–227 (2005)
26. D.J. Miller, J. Catmull, R. Puskeiler, H. Tweedale, F.P. Sharples, R.G. Hiller, Photosynth. Res. **86**, 229–240 (2005)
27. S. Parrish, A. Angerhofer, (Annual report NHFML, Talahasse, FL, 1999) pp. 22–23
28. B.B. Prezelin, F.T. Haxo, Planta **128**, 133 (1976)
29. K. Steck, T. Wacker, W. Welte, F.P. Sharples, R.G. Hiller, FEBS Lett. **268**, 48–50 (1990)
30. T.S. Lin, Chem. Rev. **84**, 1–15 (1984)
31. J. Frick, J.U. Vonschutz, H.C. Wolf, G. Kothe, Mol. Cryst. Liq. Cryst. **183**, 269–272 (1990)
32. Frick J., Phd thesis 1992, Universitaet Stuttgart, Stuttgart
33. D. Carbonera, M. Di Valentin, G. Agostini, G. Giacometti, P.A. Liddell, D. Gust, A.L. Moore, T.A. Moore, Appl. Magn. Res. **13**, 487–504 (1997)
34. R. Bittl, E. Schlodder, I. Geisenheimer, W. Lubitz, R.J. Cogdell, J. Phys. Chem. B **105**, 5525–5535 (2001)
35. R. Spezia, M. Aschi, A. Di Nola, M. Di Valentin, D. Carbonera, A. Amadei, Biophys. J. **84**, 2805–2813 (2003)
36. S. Shima, R.P. Ilagan, N. Gillespie, B.J. Sommer, R.G. Hiller, F.P. Sharples, H.A. Frank, R.R. Birge, J. Phys. Chem. A **107**, 8052–8066 (2003)
37. M. Krikunova, H. Lokstein, D. Leupold, R.G. Hiller, B. Voigt, Biophys. J. **90**, 261–271 (2006)
38. D.L. Dexter, J. Chem. Phys. **21**, 836–850 (1953)
39. I.H.M. van Stokkum, E. Papagiannakis, M. Vengris, J.M. Salverda, T. Polivka, D. Zigmantas, D.S. Larsen, S.S. Lampoura, R.G. Hiller, R. van Grondelle, Chem. Phys. **357**, 70–78 (2009)
40. M. Di Valentin, G. Agostini, E. Salvadori, S. Ceola, G.M. Giacometti, R.G. Hiller, D. Carbonera, BBA-Bioenerg. **1787**, 168–175 (2009)
41. M.T.A. Alexandre, D.C. Luhrs, I.H.M. van Stokkum, R. Hiller, M.L. Groot, J.T.M. Kennis, R. Van Grondelle, Biophys. J. **93**, 2118–2128 (2007)
42. C. Bonetti, M.T.A. Alexandre, R.G. Hiller, J.T.M. Kennis, R. van Grondelle, Chem. Phys. **357**, 63–69 (2009)

Conservation of Spin-polarization during Triplet-Triplet Energy transfer in Reconstituted Peridinin-Chlorophyll *a*-Proteins from *Amphidinium carterae*

Marilena Di Valentin[§], Claudia Tait[§], Enrico Salvadori[§], Stefano Ceola[§], Hugo Scheer [⊥], Roger Hiller[‖], Donatella Carbonera[§]

[§]*Dipartimento di Scienze Chimiche, Università di Padova, via Marzolo 1, 35131 Padova, Italy*
[‖]*Department of Biological Sciences, Macquarie University, North Ryde, NSW 2109, Australia*
[⊥] *Department of Biologie I – Bereich Botanik, Ludwig-Maximilians-Universität München, Menziger Str. 67, D-80638 München, Germany*

KEYWORDS: Light-harvesting, PCP, carotenoids, chlorophylls, protein reconstitution, energy transfer, triplet state, EPR.

Abstract

Reconstituted peridinin-chlorophyll *a*-protein (PCP) complexes, where the N-terminal domain of native PCP from *Amphidinium carterae* has been reconstituted with different chlorophyll (Chl) species, are investigated by time-resolved EPR (TR-EPR) in order to elucidate the fine details of the triplet-triplet energy transfer mechanism. This spectroscopic approach exploits the concept of spin conservation during triplet-triplet energy transfer, which leads to recognizable spin polarization effects in the observed TR-EPR spectra. The spin polarization produced at the acceptor site (peridinin) depends on the initial polarization of the donor (chlorophyll) and on the relative geometrical arrangement of the donor-acceptor spin axes. A variation of donor triplet-state properties in terms of population probabilities or triplet spin axes directions, as produced by replacement of chlorophyll *a* with non-native chlorophyll species in the reconstituted complexes (ZnChl *a* and BacterioChl *a*), is reflected in the polarization pattern of the carotenoid triplet state.

The spectroscopic results have been compared to those obtained for the main form of the PCP complex and the high-salt PCP form from *Amphidinium carterae*. Both in the native and in the complexes reconstituted with ZnChl *a* and BacterioChl *a*, the

triplet state is localized on a single peridinin, peridinin 614, according to X-ray nomenclature [Hofmann et al., 1996]. The identification of same chlorophyll-peridinin pair involved in the triplet energy transfer for the three different systems, characterized by different donor properties confirms the validity of the assumption of spin conservation in the EPR spectral analysis adopted. Above all, the results reinforce the hypothesis that peridinin 614 is the carotenoid of election in PCP proteins in the photo-protection mechanism based on triplet-triplet energy transfer.

ABBREVIATIONS: Per, peridinin; Chl, chlorophyll; PCP peridinin-chlorophyll *a* protein; ZFS, Zero Field Splitting; ISC, Intersystem Crossing. TR-EPR. Time-resolved Electron Paramagnetic Resonance *A. carterae, Amphidinium cartarae*; MFPCP, Main form PCP; RFPCP, Refolded PCP.

1. Introduction

Photosynthetic light harvesting is achieved by a variety of chlorophyll and carotenoid pigments bound to distinct types of light-harvesting proteins depending on the organisms [Polivka et al., 2010].

Marine algae contribute to photosynthetic CO_2 fixation. They possess an efficient light-harvesting system optimized for light-harvesting capacity especially in the blue-green spectral region because water functions as a filter of light in the red.

Dinoflagellates contain a unique soluble antenna, the peridinin-chlorophyll *a*-protein (PCP), which differs from other antennas in using the carotenoid peridinin (Per) as the main light-harvesting pigment instead of chlorophyll (Chl). The high resolution X-ray structure of the main form of PCP (MFPCP) from the dinoflagellate *Amphidinium carterae* (*A. carterae*) has been available for a decade [Hofmann et al., 1996] and has been of valuable support in the understanding of the energy transfer pathways investigated by spectroscopic methods [Carbonera et al., 1995, 1996, Di Valentin et al., 2008 A, 2008 B, 2008 C, 2009 A, 2010, Bautista et al., 1999, Krueger et al., 2001, Zigmantas et al., 2002, Ilagan et al., 2006].

The PCP antenna contains only peridinin and Chl *a* in a stoichiometric ratio of 4:1. The basic structure is a trimer. In each subunit of the trimer the pigments are arranged as two pseudo-identical domains of four peridinins and one Chl *a* molecule, as shown

in Figure 1. The pigment clusters are located in the hydrophobic cavity formed by the protein. Distances between peridinins within a single domain range from 4 to 11 Å, and the conjugated regions of the peridinins are in Van der Waals contact (3.3–3.8 Å) with the tetrapyrrole rings of the Chl *a* molecules. The distance between the Mg atoms of the two Chl *a* molecules in each subunit is 17.4 Å.

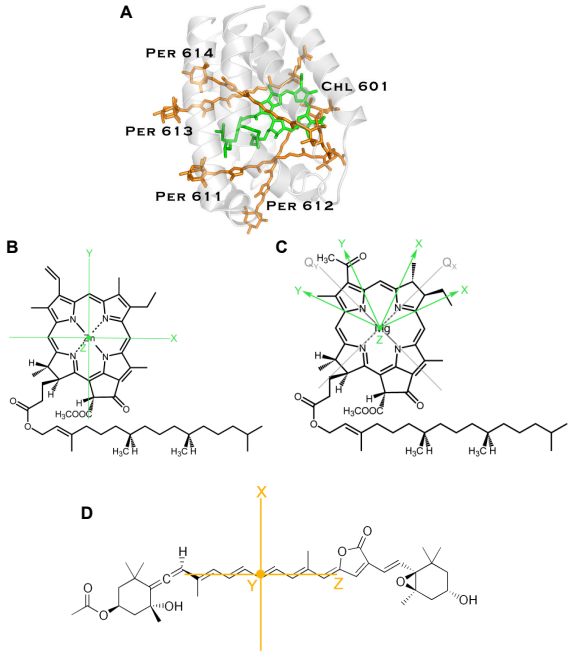


Figure 1: Structure of RFPCP (A) derived from the coordinates deposited in the Brookhaven Protein Data Bank (3IIS) and molecular structures of ZnChl *a* (B), BChl *a* (C) and peridinin (D) with the orientation of the ZFS tensor axes as defined in the text.

Along with the MFPCP, a minor component has also been reported which is eluted from an anion exchange column at high-salt concentration. This form, denoted high-salt PCP (HSPCP), presents 31% identity in amino acid sequence with MFPCP and contains only six peridinins and two Chl *a* molecules [Sharples et al., 1996]. The X-ray structure of HSPCP has been determined [Schulte et al., 2009 B]. It shows a large similarity with the MFPCP structure in terms of pigment arrangement, except for the absence of two symmetry related peridinins called PID612/PID622 in the two subclusters respectively, according to the nomenclature of Hofmann et al. of MFPCP (Per612-Per622 in Figure 1).

The high-resolution structure determination has been coupled with pigment substitution and reconstitution or site-directed mutation of the PCP antenna in order to elucidate the fine details of energy transfer among carotenoid and Chl pigments. For

this purpose Hiller and coworkers [Miller et al., 2005] have developed an heterologous expression system of the PCP apoprotein, which is finally reconstituted with peridinin and a variety of Chls species or BChl *a* in order to obtain reconstituted PCP (called RFPCP). Hetero-chlorophyllous complexes, containing two different Chls have also been successfully produced [Brotosudarmo et al., 2006, 2008]. Investigations on RFPCP by various optical spectroscopic techniques have demonstrated the excellent stability of RFPCP proteins which maintain high efficiency of peridinin-to-chlorophyll energy transfer function in the presence of non-native Chl species.

Recently, the X-ray structures of RFPCPs reconstituted with Chl *a*, Chl *b*, Chl *d* and BChl *a* have been published [Schulte et al., 2009 A, 2010]. The Chl *a* RFPCP complex does not deviate from the native PCP complex. The pigment arrangement is almost identical in all Chl RFPCPs, and the different Chl species replace Chl *a* almost perfectly, even though a slight translational shift of BChl *a* in the Chl binding site of ≈ 0.4 Å has been observed.

The authors have principally focused their attention on the triplet-triplet energy transfer (TTET) pathways in the main light-harvesting complexes of different organisms.

Carotenoids (Car) bound to the light-harvesting complexes of bacteria, plants and algae and having more than seven double bonds in the conjugated polyene chain, possess low-lying triplet states capable of trapping (B)Chl *a* triplet states, by TTET, avoiding the formation of the potentially harmful singlet oxygen and quenching active oxygen species [Frank et al., 1996]. In the case of dinoflagellates, the peridinin molecules in the isolated PCP complex satisfactorily play the photo-protective role, with a 100% efficiency in terms of TTET.

The study on carotenoid triplet states formed in different antenna systems has been performed by means of several advanced magnetic resonance techniques: time-resolved electron spin resonance (TR-EPR), pulsed EPR and double resonance techniques, i.e. pulsed electron-nuclear double resonance (ENDOR) and optically detected magnetic resonance (ODMR), starting from the dinoflagellate PCP antenna and extending the investigation to Chl *d* RFPCP [Di Valentin et al., 2009 A], LHCII of higher plants [Di Valentin et al., 2009 B] and the dinoflagellate intrinsic LHC [Di Valentin et al., 2009 C].

A common motif has been identified in the photo-protection strategy of the diverse antenna complexes adopting selected Chl *a*-Car pairs for TTET. In the specific case of the PCP antenna, the authors suggested an exclusive path for triplet quenching in MFPCP, involving Per 614/624 (PID614/PID624 according to [Hofmann et al., 1996]) as the quencher of the Chl *a* triplet states. Only one among the four peridinins in Van der Waals contact with each Chl *a* of the pigment cluster is devoted to photo-protection. The distinctive structural property for the selected peridinin is the presence of a water molecule coordinated to the central Mg atom of the Chl *a* donor at the interface between the donor-acceptor pair.

In this work we have extended and verified the spectroscopic approach adopted in the previous investigations on the photo-protection mechanism in diverse antenna systems to PCP complexes successfully reconstituted with ZnChl *a* or BChl *a*. The approach is based on the assumption of spin angular momentum conservation during TTET [El-Sayed et al., 1969, Brenner et al., 1978]. TTET takes place by an electron exchange mechanism and since in the theoretical description no spin dependent terms are explicitly considered, the spatial orientation of the triplet spin angular momentum must be conserved when resonance transfer occurs. If the molecular axes of the acceptor are rotated with respect to those of the donor molecule, the population probabilities of the donor triplet sublevels are transferred into the acceptor sublevels with relative probabilities given by the squared cosines of the angles relating the principal magnetic axes of the donor and the acceptor [El-Sayed et al., 1969, Brenner et al., 1978].

The specific choice of ZnChl *a* and BChl *a* as possible donor molecules for TTET in the reconstituted proteins has been driven by the triplet-state magnetic properties of these pigments which allowed to verify the main assumption of spin conservation in all the previous EPR investigations on the antenna photo-protection. ZnChl *a* is characterized by a distinct initial spin polarization of the photo-excited triplet state compared to Chl *a* due to a different selectivity in the intersystem-crossing (ISC) population of the triple-state spin sublevels attributed to the introduction of zinc into the Chl ring system. On the other hand, while the ISC populations of the BChl *a* triplet state are not altered significantly, the Zero Field Splitting (ZFS) axes direction in the macrocycle are rotated with respect to those of the Chl *a* triplet state, due to the substantial change in spin density of the triplet state of the tetrahydroporphyrin

compared to the dihydroporphyrin. Linear-dichroic (LD-) absorbance-detected magnetic resonance (ADMR) studies have allowed to define the position of the ZFS axes *X* and *Y* of BChl *a* at angles of ~ 73° and ~ 20° with respect to the optical axis Q_Y, while an angle of ~ 45° has been found for the *X* and *Y* ZFS axes of Chl *a* [Vrieze et al., 1995].

In the present investigation we have demonstrated that indeed the variation of the donor triplet state properties is reflected in the spin polarization pattern of the carotenoid triplet state as expected in the framework of spin angular momentum conservation and at the same time the spectral analysis has allowed to unambiguously confirm the path proposed in previous works for triplet quenching in wild-type PCP proteins and the unique role of a special Chl *a*-Per pair strongly coupled via an interfacial water molecule.

2. Materials and Methods

Sample preparation. RFPCP proteins were prepared according to [Miller et al., 2005]. Absorbance at the Chl Q_Y band for RFPCP was ~ 0.5 for EPR samples.

Oxygen was removed from the RFPCP samples by flushing argon in the EPR capillary before freezing. Glycerol, previously degassed by several cycles of freezing and pumping, was added (60% v/v) to obtain a transparent matrix.

The EPR samples of BChl *a* and ZnChl *a* in methyl-tetrahydrofuran (Me-THF), were prepared dissolving them in Me-THF to a final Chl concentration of ~10^{-5} M sealed in a capillary tube after several pumping/freezing cycles in order to remove the oxygen from the sample. The solvent was distilled from sodium before usage. BChl *a* was purchased from Sigma-Aldrich while ZnChl *a* was prepared according to [Kass et al., 1998].

TR-EPR measurements. Experiments were performed on a Bruker Elexsys E580 pulsed EPR Spectrometer at 9.7 GHz. Laser excitation at 532 nm (10 mJ per pulse and repetition rate of 10 Hz) was provided by the second harmonic of an Nd:YAG laser (Quantel Brilliant) in a flexline dielectric resonator. The temperature was controlled by means of a helium cryostat (Oxford CF935) driven by a temperature controller (Oxford ITC503). TR-EPR experiments in direct-detection mode, taking the signal directly from the mixer, without lock-in amplification with the SpecJet digitizer. Transients were accumulated both on and off-resonance in order to

eliminate the laser background signal by subtraction of the off-resonance traces. Transient signal rise time was about 50 ns. In the TR-EPR spectra, the integration period was 100–228 ns after the laser flash. The microwave power was 2mW.

Spectral analysis. Simulations of the powder spin-polarized triplet spectra were performed using the Easyspin [Stoll et al., 2006] routine in Matlab®. The program is based on the full diagonalization of the triplet state spin Hamiltonian, comprehending the Zeeman and magnetic dipole-dipole interactions, the lineshape of the EPR spectrum is calculated assuming a powder-like distribution of molecular orientations with respect to the magnetic field direction. The ordering of the triplet sublevels has been chosen in agreement with previous studies: $|Z|>|X|>|Y|$ for ZnChl *a*, $|Z|>|Y|>|X|$ for BChl *a* and $|Z|>|X|>|Y|$ for Per.

The sublevel population probabilities of the acceptor (peridinin) triplet state were calculated with a home-written program in Matlab®, according to the formalism of spin angular momentum conservation [El-Sayed et al., 1969, Brenner et al., 1978], assuming that the TTET process is fast compared to the time evolution of the donor triplet spectrum, but slow enough to allow spin alignment in the external magnetic field. The triplet state populations of the acceptor are determined by the triplet state populations of the donor and by the relative orientation of the ZFS axes of the pigments according to the following expression:

$$P_i^A = \sum_j \cos \vartheta_{ij}^{\,2} P_j^D$$

where ϑ_{ij} is the angle between the principal axis j of the donor and the axis i of the acceptor. The resulting relative populations of the three sublevels are used as input parameters for the computation of the spectra in the simulation program for powder triplet-state EPR spectra.

The ZFS axes of peridinin triplet state were obtained through principal components analysis using the Matlab® function “princomp”. The method is based on the solution of the covariance matrix of the data, in which the eigenvalues represent the amount of variance attributed to each eigenvector. The data set used in the calculations contained the spatial coordinates of the atoms of the conjugated chain of each peridinin molecule, as reported in the PDB files 3IIS and 2X21, respectively for ZnChl *a* and BChl *a* RFPCP. The resulting eigenvectors are a good approximation of the ZFS axes due to their particular orientation in carotenoids: the solution vector

with the greatest eigenvalue lies along the main axis (*Z*) of the peridinin molecule, the vector with the intermediate eigenvalue lies along the C-H bonds (*X*) and the vector with the smallest eigenvalue is perpendicular to the molecular plane.

The directions of the ZFS axes of ZnChl *a* and BChl *a* used in the calculations were taken as defined in literature for the Chl *a* and BChl *a* triplet states [Vrieze et al., 1995, Lendzian et al., 2003].

The relative orientation of the ZFS axes of donor and acceptor triplet states was determined based on the pigment arrangement in the X-ray structures of PCP reconstituted with Chl *a* (3IIS) for ZnChl *a* RFPCP and PCP reconstituted with BChl *a* (2X21) for BChl *a* RFPCP.

3. Results

3.1 Photo-excited triplet-states in ZnChl a RFPCP

Figure 2 shows the X-band spin-polarized TR-EPR spectra of the donor triplet states, ^{T}ZnChl *a* and ^{T}Chl *a* in Me-THF glass, and those corresponding to the acceptor triplet states in Chl *a* RPCP and ZnChl *a* RFPCP shortly after the laser pulse.

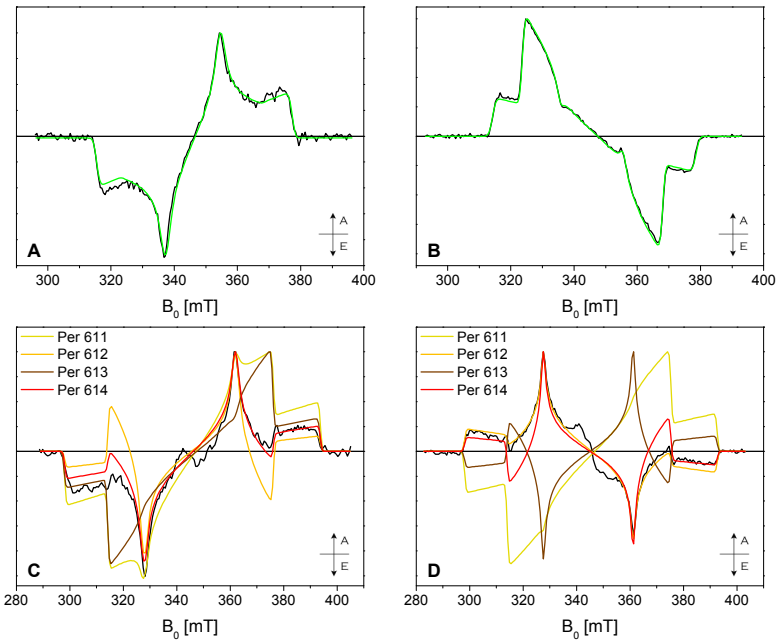


Figure 2: Top - Experimental and simulated TR-EPR spectra of ^{T}Chl *a* (A) (adapted from [Di Valentin et al., 2008 D]) and ^{T}ZnChl *a* (B) in Me-THF glass at 90 K. Order of energy for zero field triplet sublevels: $|Z|>|X|>|Y|$. Bottom - Experimental TR-EPR spectrum for Chl *a* RFPCP (C) and ZnChl *a* RFPCP (D) at 150 K with the corresponding calculated EPR spectra of ^{T}Per for each Per surrounding the chlorophyll donor. The simulation parameters are reported in Table 1. $|Z|>|Y|>|X|$. A=Absorption, E=Emission.

Table 1

Parameters for the triplet state simulations[a]

Chl *a* in Me-THF glass					**ZnChl *a* in Me-THF glass**				
$\mathbf{P_X}$	0.33				$\mathbf{P_X}$	0.00			
$\mathbf{P_Y}$	0.56				$\mathbf{P_Y}$	0.41			
$\mathbf{P_Z}$	0.11				$\mathbf{P_Z}$	0.59			
D = 30.2±0.5 mT					D = 32.2±0.5 mT				
E = -4.4±0.1 mT					E = -4.1±0.1 mT				
$W_X : W_Y : W_Z$ = 2.0 : 2.0 : 2.0 mT					$W_X : W_Y : W_Z$ = 1.5 : 1.5 : 2.0 mT				
Peridinins in Chl *a* RFPCP					**Peridinins in ZnChl *a* RFPCP**				
	Per611	Per612	Per613	Per614		Per611	Per612	Per613	Per614
$\mathbf{P_X}$	0.28	0.15	0.35	0.14	$\mathbf{P_X}$	0.33	0.57	0.14	0.54
$\mathbf{P_Y}$	0.25	0.45	0.19	0.39	$\mathbf{P_Y}$	0.25	0.28	0.44	0.21
$\mathbf{P_Z}$	0.47	0.40	0.46	0.47	$\mathbf{P_Z}$	0.42	0.15	0.42	0.25
D = -47.90±0.75 mT					D = -47.30±0.75 mT				
E = -4.60±0.25 mT					E = -4.60±0.25 mT				
$W_X : W_Y : W_Z$ = 2.0 : 1.0 : 1.0 mT					$W_X : W_Y : W_Z$ = 1.0 : 1.0 : 1.0 mT				

[a] P_X, P_Y, P_Z: zero-field populations of the triplet states; D, E: ZFS parameters; W: line-widths at the canonical positions in the EPR powder spectrum. Isotropic g value g_{iso}=2.0023.

The TTET from Chl to Per in MFPCP occurs in about 17 ns [Bautista et al., 1999]. Since the time resolution of the set-up is about 50 ns, only the acceptor triplet state can be detected, as observed experimentally. The absence of any ^{T}Chl signal in the spectra proves that peridinins play their photo-protective role, consisting in the quenching of the potentially harmful ^{T}Chl, with 100% efficiency also in the reconstituted proteins.

The initial carotenoid polarization, detected by TR-EPR, has been analyzed in the framework of spin angular momentum conservation during TTET, as described in detail in Materials and Methods. The three sublevel populations of the donor triplet state are transferred into the acceptor sublevels with relative probabilities given by the squared cosines of the projections of the donor ZFS axes onto the acceptor axes. Population probabilities for the Chl *a* and ZnChl *a* triplet states were derived from simulation of the corresponding experimental TR-EPR spectra. The absence of any donor triplet signal in the TR-EPR spectra of the RFPCPs, which is consistent with a TTET time of the order of tens of ns, allows to state that the initial polarization pattern of donor triplet state does not evolve significantly under the effect of spin relaxations before the transfer to the peridinin(s). We calculated the peridinin spectra

for all four mutual Chl *a*-peridinin configurations derived from the X-ray structure of Chl *a* RFPCP [Schulte et al., 2009 A, 2010], as previously done for MFPCP. The corresponding calculations are reported in Figure 2 and the parameters are reported in Table 1 for both antenna complexes.

As shown in Figure 2, the calculated spectra have the same polarization pattern of the corresponding experimental spectra only for two of the mutual arrangements of the Chl-Per pigments triplet axes present in the pigment subcluster. In both cases the selected arrangements correspond to the pairs (Zn)Chl *a*601-Per614 and (Zn)Chl *a*601-Per612. Not only the spin polarization of the acceptor triplet state populated in Chl *a* RFPCP, as expected on the basis of the equivalence between the X-ray structure of MFPCP and RFPCP with the same pigments [Schulte et al., 2009 A], but also the spin polarization for ZnChl *a* RFPCP is reproduced by the same arrangements of pigments selected in the investigation on MFPCP [Di Valentin et al., 2008 A], despite the important variation of spin polarization induced by the substitution of the central metal ion. This is a strong evidence that the condition of spin-polarization conservation is satisfied for the systems under investigation.

An active role of Per612(622) in the TTET was ruled out in previous investigations on MFPCP and HSPCP by the fact that in the absence of this pigments, as in the HSPCP complex, the triplet-state polarization is exactly the same [Di Valentin et al., 2008 C]. The same argument can be used to exclude the pair (Zn)Chl *a*601-Per612 in the present analysis, based on the equivalence of the X-ray structures of MFPCP and RFPCPs and consequently of the energy-transfer pathways [Schulte et al., 2009 A]. The outcome of the spectral analysis is that Per614 remains the best candidate for efficient triplet quenching not only in native PCP complexes (Per614/Per624) but also in RFPCP.

The agreement between the experimental and calculated triplet-state TR-EPR spectra has been optimized considering only the (Zn)Chl *a*601-Per614 pair by small rotations (± 20°) around each of the ^{T}Per ZFS axes, as initially determined by principal component analysis. The best agreement is obtained through simultaneous optimization of the correspondence between the calculated and experimental spectra for both reconstituted complexes. The result is reported in Figure 3 and corresponds to a 12° rotation of the ^{T}Per *X* and *Y* ZFS axes around the *Z* axis.

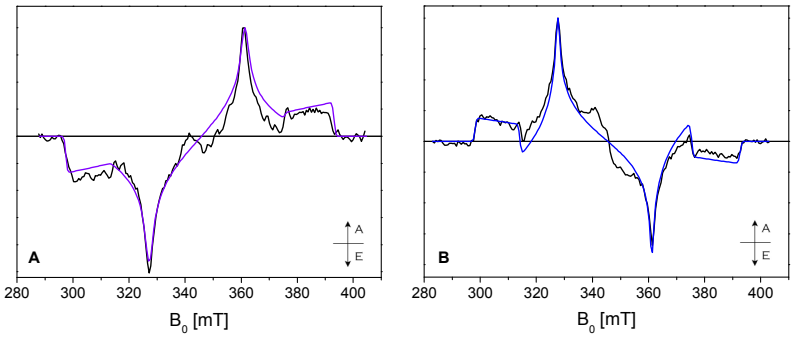


Figure 3: Experimental TR-EPR spectrum for Chl *a* RFPCP (A) and ZnChl *a* RFPCP (B) at 150 K with the corresponding calculated TR-EPR spectra of ^{T}Per614 after a 12° rotation of the peridinin's *X*, *Y* ZFS axes around the *Z* axis as defined in the text. $|Z|>|Y|>|X|$. A=Absorption, E=Emission.

The optimization through exclusive rotation around the acceptor triplet state axes is justified by the higher uncertainty in the orientations of the ^{T}Per ZFS axes compared those of ^{T}Chl *a*. While the latter have been identified by LD-ADMR and confirmed by ENDOR spectroscopy [Vrieze et al., 1995, Lendzian et al., 2003], the ^{T}Per ZFS axes have been determined by principal component analysis as explained in detail in Materials and Methods. Unfortunately, computational methods available for the calculation of the ZFS tensor of triplet states are still not reliable as regards the determination of the principal axes. For this reason, starting from the only information available from experimental data on the triplet state of β-carotene single crystal [Frick et al., 1990], we have used the approach based on principal component analysis in order to take into account the effects produced by the distortion of the carbon-skeleton induced by the protein surroundings.

The results for rotations of ± 20° around all the ZFS axes of both donor and acceptor triplet state are shown in the Supporting information for the ZnChl *a*-Per614 pair in ZnChl *a* RFPCP. No significant variation of the spin polarization pattern is produced, demonstrating that the uncertainty in the directions of the ZFS axes does not affect the outcome of the spectral analysis.

3.2 Photo-excited triplet-states in BChl a RFPCP

Figure 4 shows the X-band spin-polarized TR-EPR spectra of the donor triplet state, ^{T}BChl *a* in Me-THF glass, and of the acceptor triplet state for BChl *a* RFPCP shortly after the laser pulse.

The spin-polarized TR-EPR spectrum of ^{T}BChl *a* in Me-THF glass has been simulated as shown in the superimposed simulations reported in Figure 4 using the ZFS parameters and ISC population probabilities indicated in Table 2, which are in perfect agreement with parameters previously reported [Plato et al., 1991]. The spin polarization is slightly different from that of ^{T}Chla because of small variation in the population probabilities and because of the sign inversion of the ZFS parameter *E* [Vrieze et al., 1995, Marchanka et al., 2009].

As for Chl *a* RPCP and ZnChl *a* RFPCP, the TR-EPR spectrum corresponding to BChl *a* RFPCP has been simulated considering only one triplet-state species which can be directly assigned to the peridinin molecule [Carbonera et al., 1995]. The absence of any ^{T}BChl *a* contribution in the spectrum proves that the TTET process is characterized by 100% efficiency in this reconstituted protein as well.

The same approach used for the other reconstituted proteins has been adopted to analyze the initial carotenoid polarization in the framework of spin angular momentum conservation. We calculated the peridinin spectra for all four mutual Chl *a*-peridinin configurations derived from the X-ray structure of BChl *a* RFPCP [Schulte et al., 2010]. The corresponding calculations are reported in Figure 4 and the parameters in Table 2.

In this case, the spectral analysis should reproduce the effects of a rotation of the triplet principal axes of the donor molecule compared to those of Chl *a* on the spin polarization of the acceptor triplet state. In fact, while the ISC populations of the ^{T}BChl *a* triplet state are not altered significantly, the ZFS axes direction in the macrocycle are rotated with respect to those of the ^{T}Chl *a* triplet state as proved experimentally [Vrieze et al., 1995]. LD-ADMR studies have allowed to define the position of the ZFS axes *X* and *Y* of BChl *a* at angles of ~ 73° and ~ 20° with respect to the optical axis Q_Y, while an angle of ~ 45° has been found for the ZFS axes of Chl *a*. The LD-ADMR experiments allow only an estimation of the angles between Q_Y and the *X* and *Y* axes, leaving two possible orientations of the ZFS axes with respect to the molecular axes (see Figure 2). This ambiguity has been removed only for the ZFS axes of ^{T}Chl *a* in a pulse ENDOR investigation on the photo-excited ^{T}Chl *a* [Lendzian et al., 2003]. An analogous ENDOR study on the photo-excited ^{T}BChl *a*, although assuming a precise orientation for the data analysis, does not remove the

ambiguity [Marchanka et al., 2009]. For this reason the spectral analysis has been carried out for both positive and negative angles with respect to the optical axes.

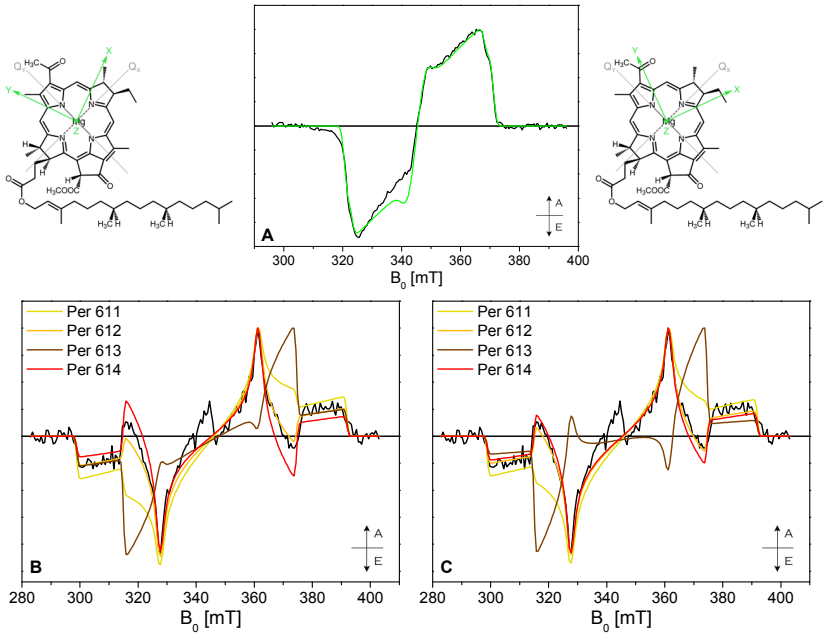


Figure 4: Top - Experimental and simulated TR-EPR spectra of ^{T}BChl *a* in Me-THF glass at 90 K (A).$|Z|>|Y|>|X|$. Bottom - Experimental TR-EPR spectrum for BChl *a* RFPCP at 150 K and calculated EPR spectra of ^{T}Per for each Per surrounding the chlorophyll donor and for two possible orientations of the donor's in-plane ZFS axes [Vrieze et al., 1995]: at an angle of -20° (B) and +20° (C) with respect to the corresponding optical axes (Q_x and Q_y). The simulation parameters are reported in Table 2. The molecular structures with the two possible orientations of the ZFS axes are shown above the corresponding spectra. $|Z|>|Y|>|X|$. A=Absorption, E=Emission.

The outcome of the analysis is perfectly in line with the results obtained for MFPCP and for (Zn)Chl *a* RFPCP, as discussed in the previous section: the spin-polarization pattern is reproduced only for two mutual arrangements of the BChl *a*-Per triplet axes. Exclusion of the BChl *a*601-Per612 pair, on the basis of the results on HSPCP allows to select the BChl *a*601-Per614 pair as the best arrangement in terms of triplet axes orientations to reproduce the carotenoid experimental spin polarization, in perfect agreement with all the other results [Di Valentin et al., 2008 A]. The ambiguity regarding the sign of the angle between the optical and magnetic axes does not significantly alter the results, Figure 4 shows a very similar trend for the four pairs of donor-acceptor pigments for both a positive and a negative angle between the in-plane triplet and optical axes of ^{T}BChl *a*. To reinforce the conclusions, since these angles are also defined with a great uncertainty (± 15°) the spectra have been calculated for different angles to find the best correspondence between the calculated

and experimental spectra for the three BChl *a*-Per pairs. These results, available in the Supporting information, prove that the uncertainty in the directions of the donor's in-plane ZFS axes is not affecting the outcome of the spectral analysis since there is no significant variation of the spin polarization pattern of either BChl *a*-Per pair. The best agreement is still obtained for the BChl *a*601-Per614 pair, as for native PCP and the other RFPCP complexes [Di Valentin et al., 2008 A].

Table 2

Parameters for the triplet state simulations[a]

BChl *a* in Me-THF glass

$\mathbf{P_X}$ 0.44

$\mathbf{P_Y}$ 0.40

$\mathbf{P_Z}$ 0.16

D = 25.25±0.5 mT

E = 6.55±0.1 mT

$W_X : W_Y : W_Z$ = 4.0 : 2.0 : 2.0 mT

Peridinins in BChl *a* RFPCP

-20° [b]

	Per611	Per612	Per613	Per614
$\mathbf{P_X}$	0.29	0.20	0.36	0.19
$\mathbf{P_Y}$	0.32	0.37	0.26	0.41
$\mathbf{P_Z}$	0.39	0.43	0.38	0.40

+20° [b]

	Per611	Per612	Per613	Per614
$\mathbf{P_X}$	0.31	0.19	0.38	0.19
$\mathbf{P_Y}$	0.33	0.39	0.26	0.40
$\mathbf{P_Z}$	0.36	0.42	0.36	0.41

D = -46.60±0.75 mT

E = -4.30±0.25 mT

$W_X : W_Y : W_Z$ = 2.0 : 1.0 : 1.0 mT

[a] P_X, P_Y, P_Z: zero-field populations of the triplet states; D, E: ZFS parameters; W: line-widths at the canonical positions in the EPR powder spectrum. Isotropic g value g_{iso}=2.0023.

[b] Orientation of the *X* and *Y* ZFS axes of BChl *a* with respect to the corresponding optical axes Q_X and Q_Y used for the calculation of the TTET.

On the basis of the TR-EPR results we propose a definite orientation of the ZFS axes with respect to the optical axes. The best agreement between the experimental and calculated spectra is obtained for an angle of +30° between the *Y* triplet axes and Q_Y. This would also explain why the carotenoid spin polarization detected in BChl *a* RFPCP does not differ significantly from the corresponding polarization found for MFPCP and Chl *a* RFPCP despite the expected rotation of the triplet axes. This final assignment would reduce the reorientation between the two macrocycles to only 15° (see Figure 2).

4. Discussion

Structure-function relationships in enzymatic proteins are an important goal for biophysical studies. Structure is heavily based on X-ray analysis at atomic resolution, while function is often revealed by the complementary use of optical or magnetic spectroscopy.

While advanced EPR techniques have been largely applied to photosynthetic reaction center proteins and have revealed important details of the electron transfer process in photosynthesis, they have not been used in the same extent in the structure-function investigation on antenna proteins. In this context, identification of the pigments involved in the triplet-triplet energy transfer from chlorophyll molecules to carotenoids is an important issue related to the photo-protective function of carotenoids in the light-harvesting complexes of the photosynthetic apparatus.

TTET, based on Dexter's exchange mechanism, requires stringent distance and geometrical conditions in the arrangement of the partners. The electronic coupling V_{TT}, which governs the rate of energy transfer, depends on the two-electron exchange integral involving the LUMO and the HOMO of donor and acceptor molecules and for this reason is extremely sensitive to the mutual orientation of the molecular π orbitals of the molecules involved. Even small differences in the relative geometry of the donor-acceptor pair may lead to preferential pathways in triplet quenching. For example, inspection of the X-ray structure of the PCP proteins in terms of pigment arrangements does not allow to draw any conclusions on the TTET: the presence of several peridinins surrounding the Chl *a* molecules, at comparable Van der Waals distances from the conjugated Chl *a* macrocycle, makes the question on TTET pathways not trivial and requires the support from spectroscopic tools.

In previous manuscripts, we addressed this question and we identified the pairs of pigments involved in TTET not only for the PCP proteins but also for other antenna complexes, LHCII from higher plants and LHC from the dinoflagellate *A. cartarae* [Di Valentin et al., 2009 B, 2009 C]. We have proved that by exploiting the spin angular momentum conservation condition, which is an intrinsic property of the electron exchange mechanism, it is possible to gain insight into the structural requirements of TTET. Spin conservation is fulfilled only if the TTET transfer results from a pure electrostatic exchange mechanism and not from magnetic type

interactions, if no spin-orbit interactions are present both in the donor and acceptor molecules and if the transfer occurs in a time scale which is too short to allow spin alignment with respect to the external magnetic field [Brenner et al., 1978]. In X-band EPR this limit is about 20 ps. In systems where either of these assumptions becomes invalid the spin directions are not necessarily conserved in the energy transfer. In the past, spin angular momentum conservation has been experimentally confirmed for many systems at zero-field and in the presence of the external magnetic field, both in single-crystal studies and in randomly oriented systems [El-Sayed et al., 1969, 1971, Imamura et al., 1984, Akiyama et al., 1994]. In a few cases the spin polarization conservation was not found because of dynamic complications like fast TTET or intervention of excited triplet states [Kim, 1978]. Since the peridinin triplet rise-time is 17 ns [Bautista et al., 1999], the condition of spin alignment is definitely satisfied, but the other conditions have not been verified for large molecular systems and in the presence of heavy nuclei like the ones under investigation. The complexity of the problem compared to previous investigations is intrinsic in its biological relevance.

In the present investigation we have further addressed the question of TTET in antenna complexes, considering PCP proteins reconstituted with Chl pigments opportunely selected in order to verify the consistency of the spectroscopic approach we have proposed [Di Valentin et al., 2008 A]. Among the possible Chls suitable to take the role of donors in TTET, ZnChl *a* and BChl *a* are both characterized by triplet state properties which differ from those of Chl *a* in a manner that allows verification of spin angular momentum conservation during the transfer mechanism. ZnChl *a* is characterized by a different selectivity in the ISC population of the triplet-state spin sublevels compared to Chl *a* [Clarke et al., 1976]. On the other hand, while the ISC populations of the BChl *a* triplet state are not altered significantly, the ZFS axes direction in the macrocycle are rotated with respect to those of the Chl *a* triplet state [Vrieze et al., 1995]. Indeed, even a simple and qualitative inspection of the TR-EPR spectra of the Chl *a* and ZnChl *a* triplet states and of the corresponding Chl *a* RFPCPs shows how the inversion of the spin polarization pattern in the donor spectra is reflected in the spin polarization of the acceptor triplet state in the RFPCPs. The spectral effects produced by the triplet-axes rotation when comparing Chl *a* to BChl *a* RFPCP are not as straightforward but the spectral analysis, which has been

made in parallel to that of Chl *a* and ZnChl *a* RFPCP, is perfectly consistent in the framework of spin conservation, selecting the same donor-acceptor pair (Chl 601-Per614) in all the three RFPCP antenna complexes under investigation and in perfect agreement with previous results on PCP proteins [Di Valentin et al., 2008 A, 2009 A].

The coherence of the results is reinforced by additional information coming from X-ray crystallography and optical spectroscopic studies on RFPCPs [Miller et al. 2005, Ilagan et al. 2006, Schulte et al., 2009 A, 2010]. The pigment arrangement is almost identical in all Chl RFPCPs and indistinguishable from that in MFPCP. Where slight deviations are present, as for BChl *a* RFPCP, they are taken into account in the spectral analysis, since the mutual arrangement of the triplet axes is based on the X-ray data of the corresponding reconstituted complex [Schulte et al., 2009 A, 2010]. The invariance in the pigment arrangement is reflected in a high efficiency of both the singlet-singlet [Ilagan et al., 2006] and TTET processes. No structural or spectroscopic information is available at the moment for ZnChl *a* RFPCP, but the same outcome is expected as for the other RFPCPs since in this case substitution of the central metal, while significantly affecting the ISC properties of the system, should have no effect on the structural and electronic properties of the Chl macrocycle [Kass et al., 1998].

Consequently, the TR-EPR spectral analysis reported in the Results section shows unequivocally that the initial polarization of the donor triplet state is projected into the acceptor triplet state according to the relative spin axes directions of the two molecules involved in TTET. It is worth noting that this result does not depend critically on the assumptions that have to be made to perform the spectral analysis. While the donor populations have been derived directly from simulations of the experimental TR-EPR spectra of the donor triplet state populated via ISC in organic solvent, the ZFS principal axes directions have been derived from literature data [Vrieze et al., 1995]. For ZnChl *a* RFPCP the assumption has been made that the triplet axes directions of the ZnChl *a* triplet state are not varied compared to those of Chl *a* on the basis of ENDOR studies on the corresponding radical cations which found no significant alteration of the spin density in the zinc-substituted compound [Kass et al., 1998]. A possible source of inaccuracy in the calculation for the BChl *a* RFPCP derives from the large uncertainty on direction of the BChl *a* triplet state ZFS

axes as derived from LD-ADMR [Vrieze et al., 1995]. As far as the acceptor is concerned, an inaccuracy might derive from the choice of the directions of the ZFS axes of the peridinins molecules in both systems due to the fact that the peridinins are slightly distorted in the X-ray structure, and that the triplet state geometry could be different with respect to that of the ground state. Taking into account all the mentioned sources of uncertainty, the sensitivity of the calculations to the triplet axes direction has been tested showing that within ±20° the spin-polarization pattern of the calculated spectrum for the Per614 triplet state does not change significantly and thus does not alter the outcome of the spectral analysis. Furthermore, while a possible reorientation of the Chl ring, although not expected, could be responsible for a variation of the triplet axes orientations with respect to those reported in the literature in the case of Zn Chl *a* RFPCP, for which the crystallographic structure of the reconstituted protein is not available, a reorientation cannot be invoked for BChl *a* RFPCP, since the corresponding X-ray data have been used for the spectral calculations [Schulte et al., 2010].

As a conclusive remark, the present investigation on RFPCP not only validates the correctness of the spectroscopic approach adopted in the characterization of the TTET pathways in antenna complexes but above all strengthens the conclusions drawn in the previous EPR investigations on this topic [Di Valentin et al., 2008 A, 2009 B, 2010]. The present results confirm the concept of localization of the triplet state on one specific peridinin (Per614/624) in each of the two pigment subclusters related by a pseudo-C_2 symmetry and containing four carotenoids pigments surrounding the Chl a macrocycle with Van der Waals contact in the MFPCP. As previously pointed out, the specific peridinin-chlorophyll pair involved in the photo-protective mechanism is characterized by the shortest center-to-center distance and by the presence of a water molecule which is coordinated to the central Mg atom of Chl *a*. This water molecule is present in all RFPCPs, whose X-ray structural data are available [Schulte et al., 2009 A, 2010] and there is no reason to expect a different structural motif for ZnChl *a* RFPCP, since among the divalent metals Zn is considered the most suited to replace Mg without affecting the structural and coordination properties of the porphyrin macrocycle [Kass et al., 1998]. For this interfacial water molecule, which is an unique feature of the identified photo-protective pair of pigments, the role of super-exchange mediator in TTET has been

suggested [Di Valentin et al., 2008 A, 2008 B]. Further experiments on MFPC are underway to finally prove this hypothesis.

Finally, the application of the proposed spectroscopic approach to artificial antenna systems [Carbonera et al., 1997 A, 1997 B] in order to identify the structural requirements for efficient TTET should be considered when designing new biomimetic devices for which photo-protection might play an important role in order to extend the life-time under prolonged and wide-spread illumination conditions.

Acknowledgements

This work was supported by the Italian Ministry for University and Research (MURST) under the project PRIN2008.

Supporting information available

Additional Figures are presented showing the effects of the rotation in the range ±20° around each of the ^{T}Per, ^{T}ZnChl *a* and ^{T}BChl *a* ZFS axes, as determined by multicomponent analysis or as directed on the basis of literature data, on the outcome of the calculation for the ZnChl *a*-Per614 pair in ZnChl *a* RFPCP and for the BChl *a*-Per614 pair in BChl *a* RFPCP. For the rotation around the *Z* ZFS axis of ^{T}BChl *a* the BChl *a*-Per611 and BChl *a*-Per613 pairs are also shown.

References

[Akiyama et al., 1994] Akiyama K., Terokubota S., Ikoma T., Ikegami Y., *J. Am. Chem. Soc.*, **1994**, 116, 5324-5327.

[Bautista et al., 1999] Bautista J. A., Hiller R. G., Sharples F. P., Gosztola D., Wasielewski M., Frank H. A., *J. Phys. Chem. A*, **1999**, 103, 2267-2273.

[Brenner et al., 1978] Brenner H. C. B., J. C.; Harris C. B., *Chem. Phys.*, **1978**, 31, 137-164.

[Brotosudarmo et al., 2006] Brotosudarmo T. H. P., Hofmann E., Hiller R. G., Wormke S., Mackowski S., Zumbusch A., Brauchle C., Scheer H., *FEBS Lett.*, **2006**, 580, 5257-5262.

[Brotosudarmo et al., 2008] Brotosudarmo T. H. P., Mackowski S., Hofmann E., Hiller R. G., Brauchle C., Scheer H., *Photosynth. Res.*, **2008**, 95, 247-252.

[Carbonera et al., 1995] Carbonera D., Giacometti G., Agostini G., *Spectrochim. Acta, Part A*, **1995**, 51, 115-123.

[Carbonera et al., 1996] Carbonera D., Giacometti G., Segre U., *J. Chem. Soc.,Faraday Trans.*, **1996**, 92, 989-993.

[Carbonera et al., 1997 A] Carbonera D., Di Valentin M., Agostini G., Giacometti G., Liddell P. A., Gust D., Moore A. L., Moore T. A., *Appl. Magn. Reson.*, **1997**, 13, 487-504.

[Carbonera et al., 1997 B] Carbonera D., Di Valentin M., Corvaja C., Giacometti G., Agostini G., Liddell P. A., Moore A. L., Moore T. A., Gust D., *J. Photochem. Photobiol., A*, **1997**, 105, 329-335.

[Clarke et al., 1976] Clarke R. H. C., R. E.; Schaafsma, T. J.; Kleibeuker, J. F.; Platenkamp, R. J., *J. Am. Chem. Soc.*, **1976**, 98, 3674-3677.

[Di Valentin et al., 2008 A] Di Valentin M., Ceola S., Salvadori E., Agostini G., Carbonera D., *Biochim. Biophys. Acta, Bioenerg.*, **2008**, 1777, 186-195.

[Di Valentin et al., 2008 B] Di Valentin M., Ceola S., Agostini G., Giacometti G. M., Angerhofer A., Crescenzi O., Barone V., Carbonera D., *Biochim. Biophys. Acta, Bioenerg.*, **2008**, 1777, 295-307.

[Di Valentin et al., 2008 C] Di Valentin M. C., S.; Salvadori, E.; Agostini, G.; Giacometti, G. M.; Carbonera, D., *Biochim. Biophys. Acta*, **2008**, 1777, 1355-1363.

[Di Valentin et al., 2008 D] Di Valentin M., Ceola S., Salvadori E., Agostini G., Carbonera D., *Biochim. Biophys. Acta, Bioenerg.*, **2008**, 1777, 186-195.

[Di Valentin et al., 2009 A] Di Valentin M., Agostini G., Salvadori E., Ceola S., Giacometti G. M., Hiller R. G., Carbonera D., *Biochim. Biophys. Acta, Bioenerg.*, **2009**, 1787, 168-175.

[Di Valentin et al., 2009 B] Di Valentin M., Biasibetti F., Ceola S., Carbonera D., *J. Phys. Chem. B*, **2009**, 113, 13071-13078.

[Di Valentin et al., 2009 C] Di Valentin M., Salvadori E., Agostini G., Biasibetti F., Ceola S., Hiller R., Giacometti G. M., Carbonera D., *Biochim. Biophys. Acta, Bioenerg.*, **2009**, 1797, 1759-1767.

[Di Valentin et al., 2010] Di Valentin M., Salvadori E., Ceola S., Carbonera D., *Appl. Magn. Reson.*, **2010**, 37, 191-205.

[El-Sayed et al., 1969] El-Sayed M. A., Tinti D. E., Yee E. M., *J. Chem. Phys.*, **1969**, 51, 5721-5723.

[El-Sayed, 1971] El-Sayed M. A., *J. Chem. Phys.*, **1971**, 54, 680-692.

[Frank et al., 1996] Frank H. A.,Cogdell R. J., *Photochem. Photobiol.*, **1996**, 63, 257-264.

[Frick et al., 1990] Frick J., Vonschutz J. U., Wolf H. C., Kothe G., *Mol. Cryst.Liq. Cryst.*, **1990**, 183, 269-272.

[Hofmann et al., 1996] Hofmann E., Wrench P. M., Sharples F. P., Hiller R. G., Welte W., Diederichs K., *Science*, **1996**, 272, 1788-1791.

[Ilagan et al., 2006] Ilagan R. P., Chapp T. W., Hiller R. G., Sharples F. P., Polivka T., Frank H. A., *Photosynth. Res.*, **2006**, 90, 5-15.

[Imamura et al., 1984] Imamura T. O., O., Murai, H.; Obi, K., *J. Phys. Chem.*, **1984**, 88, 4028-4031.

[Kass et al., 1998] Kass H., Lubitz W., Hartwig G., Scheer H., Noy D., Scherz A., *Spectrochim. Acta, Part A*, **1998**, 54, 1141-1156.

[Kim, 1978] Kim S. S., *J. Chem. Phys.*, **1978**, 68, 333-334.

[Krueger et al., 2001] Krueger B. P., Lampoura S. S., van Stokkum I. H. M., Papagiannakis E., Salverda J. M., Gradinaru C. C., Rutkauskas D., Hiller R. G., van Grondelle R., *Biophys. J.*, **2001**, 80, 2843-2855.

[Lendzian et al., 2003] Lendzian F., Bittl R., Telfer A., Lubitz W., *Biochim. Biophys. Acta, Bioenerg.*, **2003**, 1605, 35-46.

[Marchanka et al., 2009] Marchanka A., Lubitz W., van Gastel M., *J. Phys. Chem. B*, **2009**, 113, 6917-6927.

[Miller et al., 2005] Miller D. J., Catmull J., Puskeiler R., Tweedale H., Sharples F. P., Hiller R. G., *Photosynth. Res.*, **2005**, 86, 229-240.

[Plato et al., 1991] Plato M. M., K.; Lubitz, W., *Chlorophylls*, ed. H. Scheer. 1991, Florida: CRC Press.

[Polivka et al., 2010] Polivka T.,Frank H. A., *Acc. Chem. Res.*, **2010**, 43, 1125-1134.

[Schulte et al., 2009 A] Schulte T., Niedzwiedzki D. M., Birge R. R., Hiller R. G., Polivka T., Hofmann E., Frank H. A., *Proc. Natl. Acad. Sci. U. S. A.*, **2009**, 106, 20764-20769.

[Schulte et al., 2009 B] Schulte T., Sharples F. P., Hiller R. G., Hofmann E., *Biochemistry*, **2009**, 48, 4466-4475.

[Schulte et al., 2010] Schulte T., Hiller R. G., Hofmann E., *FEBS Lett.*, **2010**, 584, 973-978.

[Sharples et al., 1996] Sharples F. P., Wrench P. M., Ou K. L., Hiller R. G., *Biochim. Biophys. Acta, Bioenerg.*, **1996**, 1276, 117-123.

[Stoll et al., 2006] Stoll S.,Schweiger A., *J. Magn. Reson.*, **2006**, 178, 42-55.

[Vrieze et al., 1995] Vrieze J.,Hoff A. J., *Chem. Phys. Lett.*, **1995**, 237, 493-501.

[Zigmantas et al., 2002] Zigmantas D., Hiller R. G., Sundstrom V., Polivka T., *Proc. Natl. Acad. Sci. U. S. A.*, **2002**, 99, 16760-16765.

6.4.1 Supporting Information

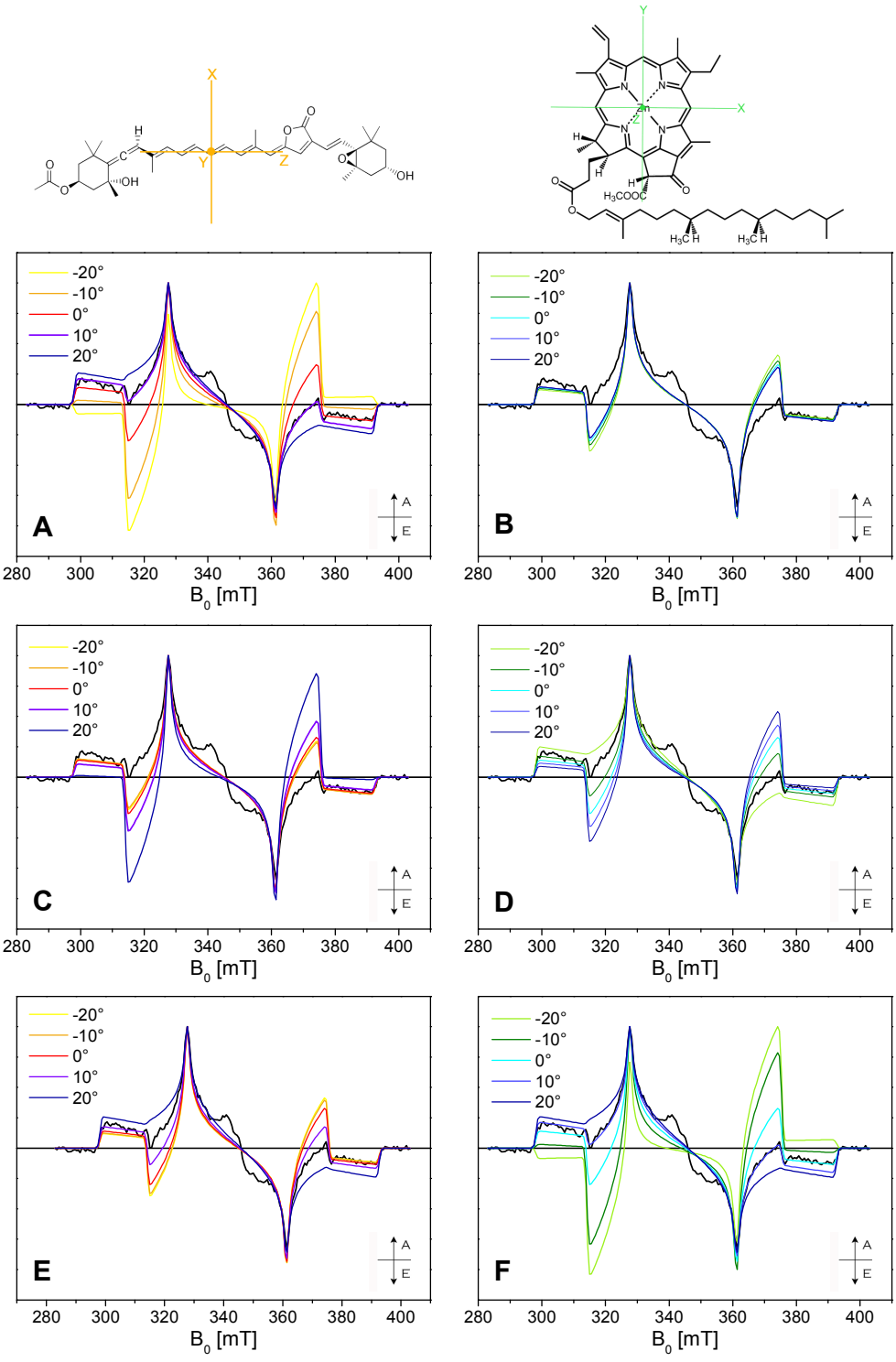


Figure 1': Experimental TR-EPR spectrum for ZnChl *a* RFPCP at 150 K with the corresponding calculated TR-EPR spectra of ^{T}Per614 after rotation around the ZFS axes of the pigments: around the *X* axis of Per614 (A), around the *X* axis of ZnChl *a*601 (B), around the *Y* axis of Per614 (C), around the *Y* axis of ZnChl *a*601 (D), around the *Z* axis of Per614 (E), around the *Z* axis of ZnChl *a*601 (F). $|Z|>|Y|>|X|$. A=Absorption, E=Emission.

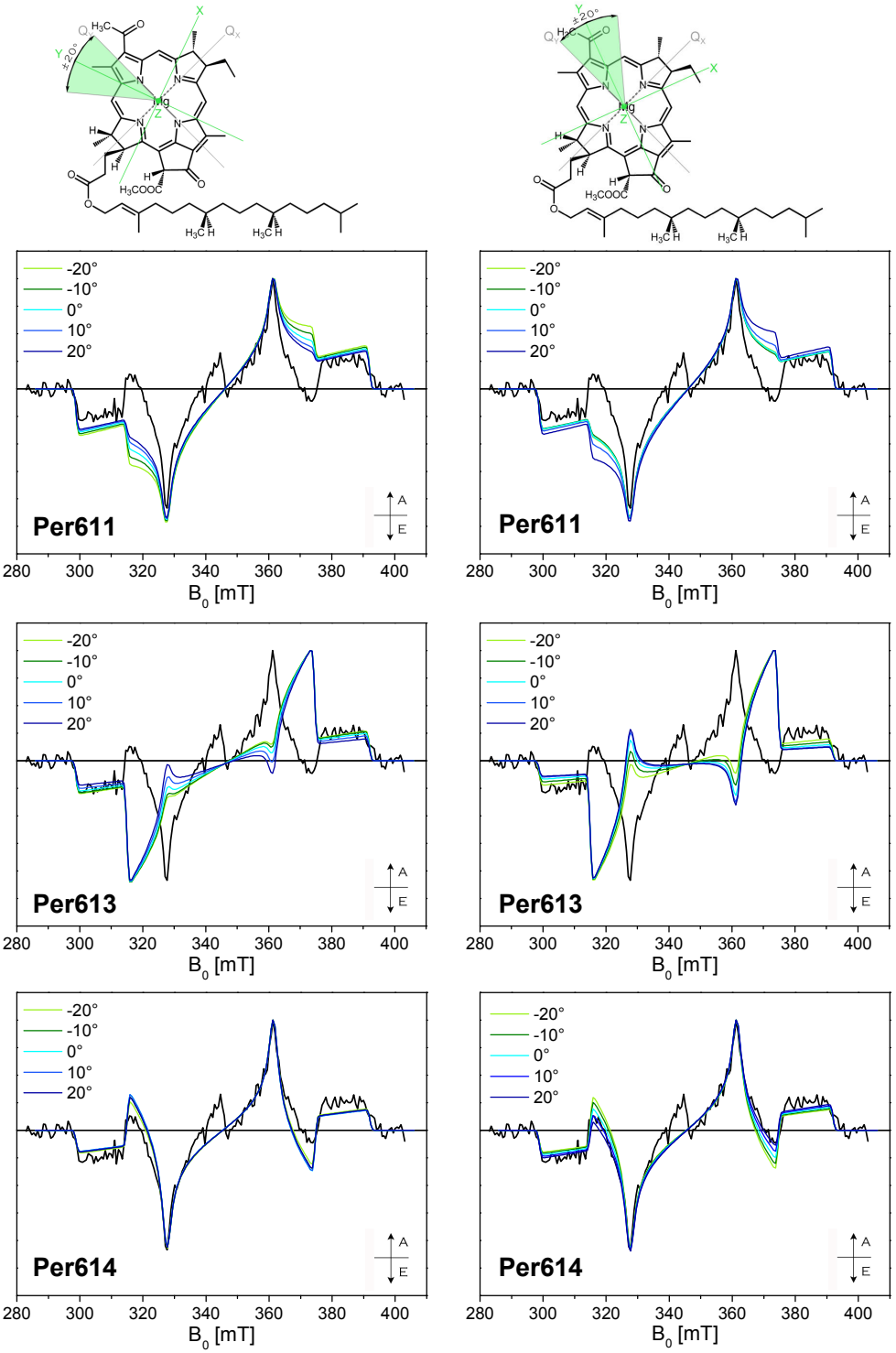


Figure 2': Experimental TR-EPR spectrum for BChl *a* RFPCP at 150 K with the corresponding calculated TR-EPR spectra of ^{T}Per for different orientations of the in-plane ZFS axes of BChl *a* in a 40° interval around the two possible orientations of the ZFS *X* and *Y* axes reported in [Vrieze et al, 1995]: at -20° and at +20° with respect to the corresponding optical axes. $|Z|>|Y|>|X|$. A=Absorption, E=Emission. The interval of considered angles is depicted above with respect to the molecular structure.

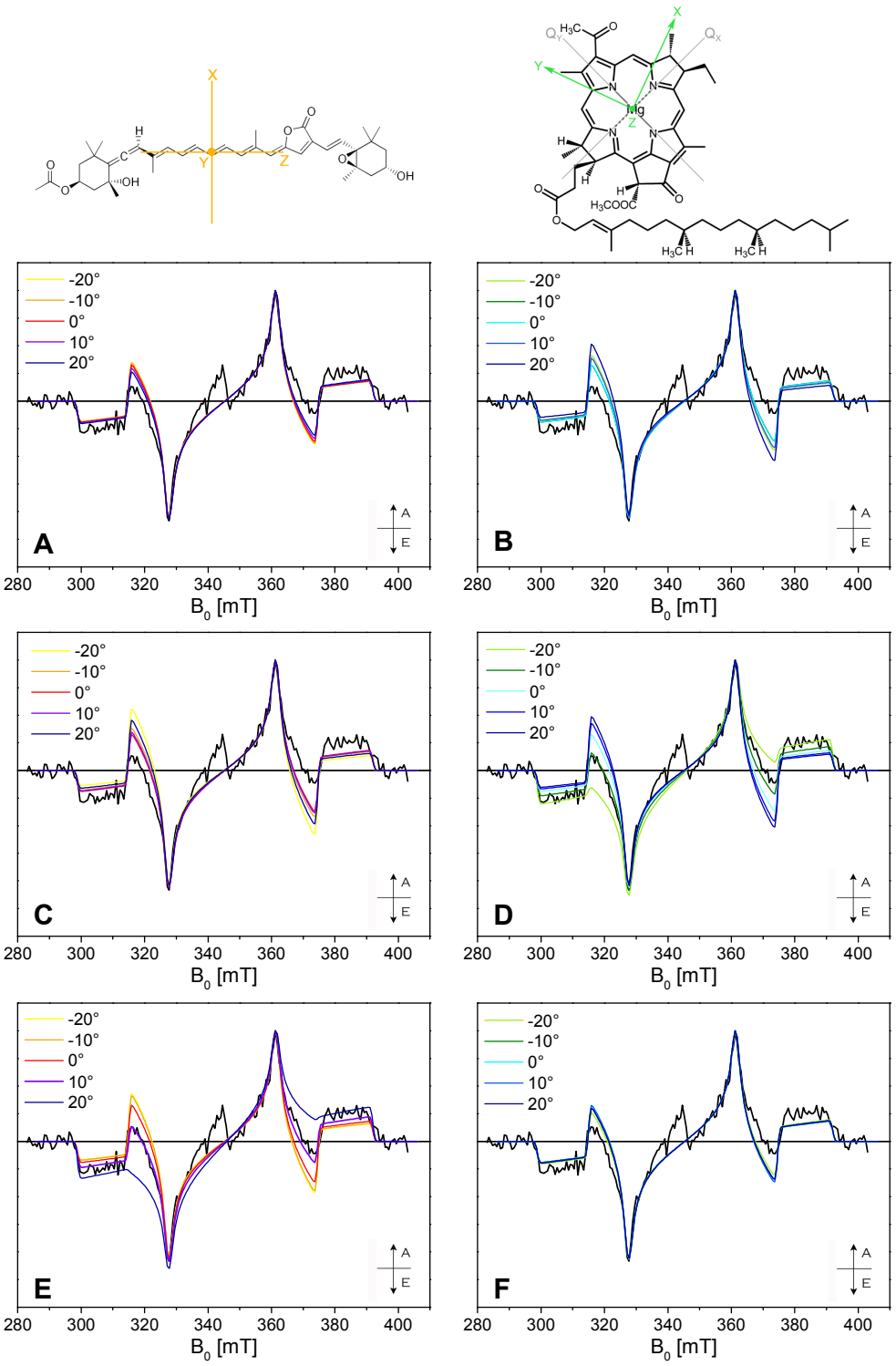


Figure 3': Experimental TR-EPR spectrum for BChl *a* RFPCP at 150 K with the corresponding calculated TR-EPR spectra of ^{T}Per614, assuming the in-plane ZFS axes at an angle of -20° from the corresponding optical axes, after rotation around the ZFS axes of the pigments: around the *X* axis of Per614 (A), around the *X* axis of ZnChl *a* 601 (B), around the *Y* axis of Per614 (C), around the *Y* axis of ZnChl *a* 601 (D), around the *Z* axis of Per614 (E), around the *Z* axis of ZnChl *a* 601 (F). $|Z|>|Y|>|X|$. A=Absorption, E=Emission.

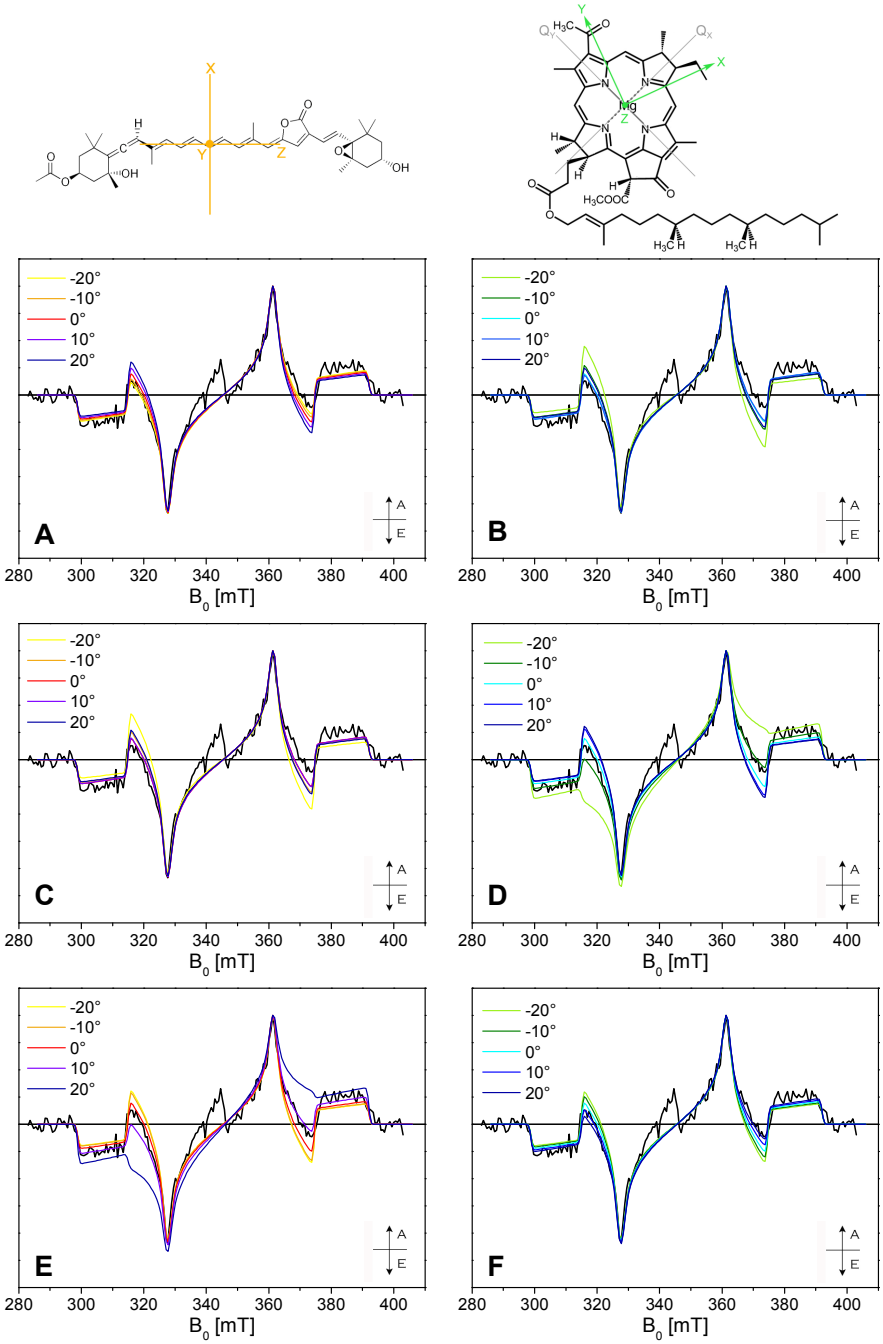


Figure 4': Experimental TR-EPR spectrum for Chl *a* RFPCP (A) and ZnChl *a* RFPCP (B) at 150 K with the corresponding calculated TR-EPR spectra of ^{T}Per614, assuming the in-plane ZFS axes at an angle of +20° from the corresponding optical axes, after rotation around the ZFS axes of the pigments: around the *X* axis of Per614 (A), around the *X* axis of ZnChl *a* 601 (B), around the *Y* axis of Per614 (C), around the *Y* axis of ZnChl *a* 601 (D), around the *Z* axis of Per614 (E), around the *Z* axis of ZnChl *a* 601 (F). $|Z|>|Y|>|X|$. A=Absorption, E=Emission.

Chapter VII

Chlorosomes from *Chlorobaculum tepidum*

A time-resolved EPR investigation of the triplet-triplet energy transfer in the chlorosomes of *Chlorobaculum tepidum* reveals the molecular organization of the pigments in the baseplate

Enrico Salvadori[1], Marilena Di Valentin[1], Marco Albertini[1], Christopher W. M Kay[2], Vianelli Alberto[3], Donatella Carbonera[1]

[1]Department of Chemical Sciences, University of Padua, via Marzolo 1, 35131 Padova, Italy

[2]Department of Structural and Molecular Biology, University College London, Gower Street, London WC1E 6BT, U.K.,

[3]Department of Structural & Functional Biology, University of Insubria, I-21100 Varese, Italy

TITLE RUNNING HEAD: triplet-triplet energy transfer in chlorosomes

Abstract

Chlorosomes are light-harvesting systems of particular interest since they allow green bacteria to perform photosynthesis in extremely low light conditions. This extraordinary ability is due to the supramolecular aggregates of BChl *c* molecules that are present in the chlorosome interior. Despite many attempts, the chlorosome crystal structure has not been resolved yet.

The great attention around these structures is focused on their efficiency in terms of collected photons and energy transfer rate to the reaction centres. A fundamental role in this energy transfer process is played by the baseplate (CsmA-BChl *a* complex), a pigment-protein para-crystalline structure connecting the BChls *c* of the chlorosome to the BChls *a* of the reaction centres. In a recent paper [Pedersen et al., *Photosynth. Res.*, **2010**, 104, 233-243] a model for the baseplate assembly has been proposed which takes into account many experimental constrains for the CsmA protein structure and for the orientations of the BChl *a* molecules. However, no experimental data have been presented to support the orientations of the carotenoids in the baseplate obtained by molecular dynamics.

In this contribution, we exploit the photo-protection mechanism, based on triplet-triplet energy transfer, to derive some structural constrains concerning the carotenoid molecules directly involved in the BChl *a* triplet quenching in the baseplate and critically discuss the validity of the structural model.

1. Introduction

Light-harvesting is a fundamental process preceding the charge separation events that drive the photosynthesis in natural organisms. To accomplish this task, the photosynthetic organisms have developed many different antenna complexes (light harvesting complexes) adapted to various habitat conditions. The largest and most efficient antenna system known is the chlorosome, common to green sulphur bacteria (Chlorobi) and green filamentous bacteria (Chloroflexi) [Blankenship et al. 2003]. The chlorosome is an unusual antenna system since it is characterized by a protein to pigments ratio which is the lowest found among the different species and its structure is dominated by pigment-pigment rather than protein-pigment interactions. In fact,

chlorosomes hold several thousands of bacteriochlorophyll (BChl) molecules (*c*, *d*, or *e* types, depending on the species) that aggregate and form supramolecular structures [Pedersen et al. 2010, Oostergetel et al. 2010]. This self-aggregating organization of the pigments is responsible for the high light-harvesting efficiency. In contrast to other antenna complexes, chlorosomes do not have a constant stoichiometry and a fixed size, although usually they exhibit an ellipsoidal shape (100-200 nm l, 50-100 nm w, 10-30 nm h). Quinones and carotenoids (Car) are also present and the whole pigments' cluster is embedded in a lipid monolayer which also lodges several proteins (at least ten) and waxes esters.

In the green sulphur bacterium *Chlorobaculum tepidum*, the supra-molecular assembly is made of BChl *c* molecules and is connected to the Fenna-Mettew-Olson (FMO) proteins via the so called "baseplate" structure. The FMO proteins collect the energy from the chlorosomes and finally transfer the excitation to the reaction centers (RCs). Figure 1 shows a scheme of the photosynthetic apparatus of *Chlorobaculum tepidum*.

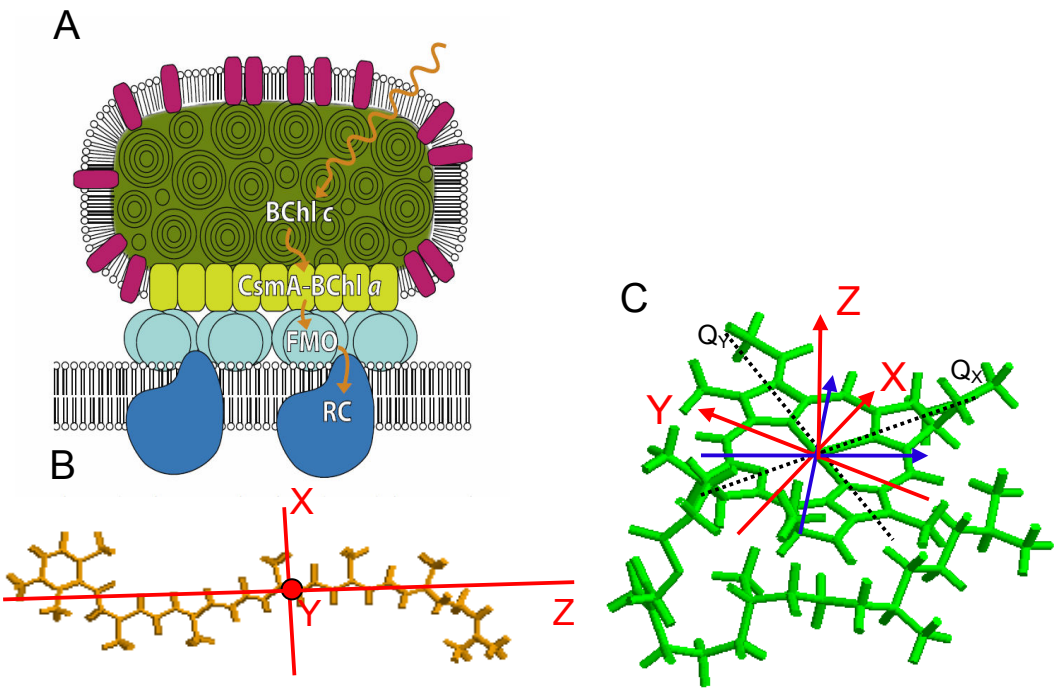


Figure 1: (A) cartoon model of the photosynthetic apparatus of *Chlorobaculum tepidum*, the singlet energy transfer pathways are represented by orange arrows (the figure has been extracted from [Pederesen et al. 2008]); (B) molecular structure of carotenoid chlorobactene with the orientation of ZFS axes (left);. (C) molecular structure of BChl *a* with the orientation of the optical transition dipole moments Q_X and Q_Y (black lines), and the two possible sets of ZFS axes as derived by linear-dichroism ODMR experiments (blue and red lines).

The baseplate is a two-dimensional para-crystalline array of CsmA proteins: each CsmA binds one BChl *a* molecule and one or two carotenoids molecules. CsmA binds exclusively BChl *a* and this selectivity is fundamental to assure a quick and efficient energy transfer from the BChl *c* molecules of the chlorosomes to the RCs BChl *a* special pairs. Moreover, CsmA is the most abundant among the chlorosomal proteins. It accounts for about 50% of the protein content, and is the only protein which is fundamental for the chlorosome formation [Sakuragi et al. 1999, Bryant et al. 2002, Montaño et al. 2003, Pedersen et al. 2008a]. A lot of work to elucidate the arrangement of pigment aggregates of the chlorosomes has been done and several models have been proposed in which the BChl pigments were organized into either rods or lamellae [Holzwarth et al. 1994, Arellano et a. 2005 Jochum et al. 2008, Linnato et al. 2008, Pšenčík et al. 2010, Akutsu et al. 2010]. On the other hand, much less is known about the baseplate structure which has the fundamental role in the funnelling of the excitation toward the RCs. In a recent paper Pedersen at al. [Pedersen et al. 2010] proposed a model for the baseplate of the chlorosomes of photosynthetic green bacteria, by combining the NMR data on the structure of the isolated CsmA protein [Pedersen et al. 2008] with a molecular dynamics analysis of the supramolecular assembly forming the baseplate. The model consists in a repetition of a close interacting dimer of CsmA-BChl *a* proteins in which a BChl *a* dimer is located between the two CsmA proteins. These dimers are in turn aligned to produce a flat structure of CsmA-BChl *a* complexes. In the basic unit, eight CsmA protein, eight BChl *a* molecules and ten chlorobactene molecules are present. The eight BChls *a* are divided into four groups related by symmetry, and five different classes of carotenoids are distinguishable, as can be clearly seen in figure 2. To build up the model several experimental constrains have been taken into account: (i) the NMR structure of CsmA protein as derived by the NMR experiments performed in methanol:chloroform solution [Pedersen et al. 2008]; (ii) the orientation of the transition dipole moment Q_Y of BChl *a* with respect the long axis of the chlorosome, as inferred by the fluorescence anisotropy measurements on single chlorosomes [Shibata et al. 2009]; (iii) the presence of exciton coupling between BChl *a* molecules as revealed by circular dichroism (CD) experiments performed either on baseplate preparations from *Chl. Limicola* or on reconstituted CsmA-BChl *a* complexes [Gerola and Olson 1986, Pedersen et al. 2008a, Pedersen et al. 2010]. To

prove the reliability of the computed baseplate structure, the BChl *a* spectroscopic properties have been simulated, in particular the near infra-red CD spectrum of BChl *a* [Pedersen et al. 2010].

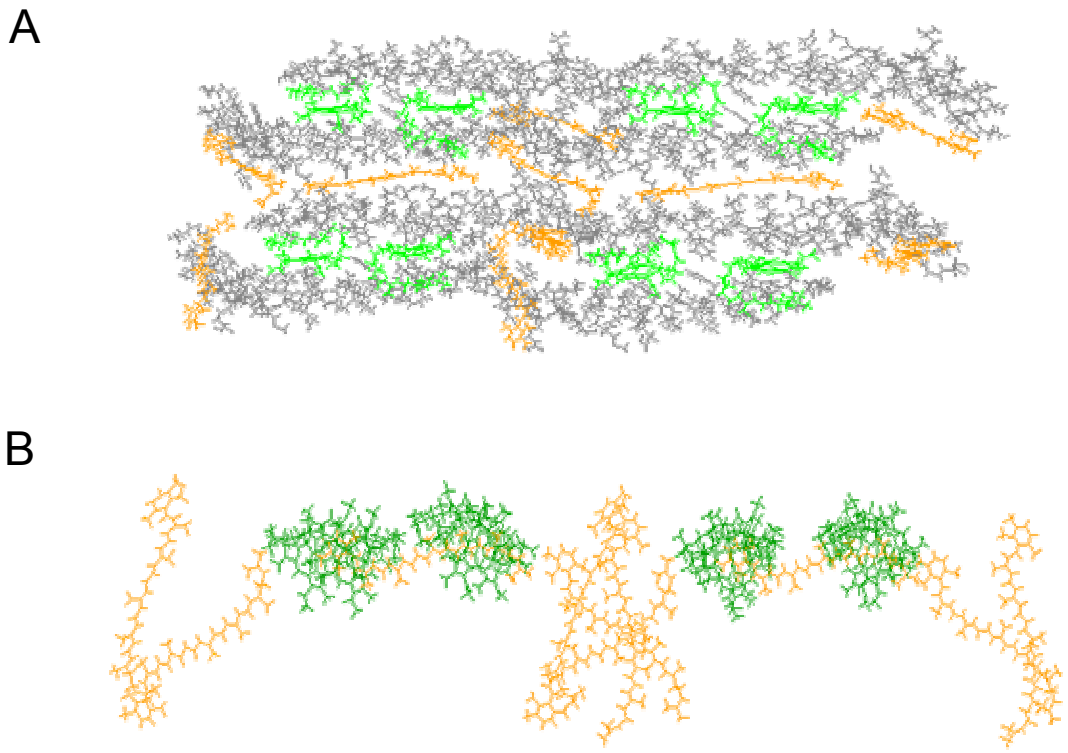


Figure 2: (A) Top view of baseplate model presented in [Pedersen et al. 2010]: grey, CsmA protein; green, BChl a molecules; orange, chlorobactene molecules. (B) A side view of the pigments present in the baseplate.

Chlorobactene molecules have been also introduced in the structure since they are always associated with the CsmA-BChl *a* complexes. Based on the molecular dynamics calculations, the energetically favourable positions for the chlorobactene molecules resulted to be between two adjacent CsmA proteins of separated dimers. Moreover if more than one carotenoid molecule for each dimer is included, as experimentally found, the remaining molecules result to be located around the C-terminal regions of CsmA [Pedersen et al. 2010]. It is worth noting that no experimental constrains have been used for the calculation of the carotenoid orientations in the baseplate structure.

It is well known that, besides having a structural role, carotenoids are present in the antenna complexes also to protect the apparatus from the possible damage induced

by the photo-formation of singlet oxygen. It has been demonstrated [Carbonera et al. 2001] that, in the chlorosomes, the carotenoids located in the baseplate are able to play the photo-protective role by quenching the BChl *a* triplet states which are formed during illumination. The mechanism is based on triplet-triplet energy transfer (TTET).

Carotenoids have been proposed to be arranged also between the farnesyl tails of the BChls *c*, filling up the hydrophobic environment between the lamellar aggregates [Pšenčík et al. 2006]. Kim et al. [Kim et al. 2007] showed that aggregates of BChl c molecules are naturally protected from harmful singlet oxygen production by the formation of triplet excitonic states with state energies that lie below the energy of singlet oxygen. The quenching of BChl c triplet states by carotenoids has been reported at room temperature [Kim et al. 2007, Melø et al 2000] but not at low temperature [Carbonera et al. 2001], indicating a temperature dependence of the energy transfer processes in the chlorosomes [Melø et al 2000].

In this work, we analyze the TR-EPR spectra of the carotenoid triplet states which become populated via TTET upon illumination of isolated chlorosomes and evaluate the compatibility of the baseplate model, proposed by Pedersen et al., with the experimental observations. Indeed, in our previous investigations on TTET occurring in antenna complexes of algae and higher plants, we have shown that the spin quantum number conservation which characterizes the TTET process, can be exploited to derive structural information on the system since the spectral shape of the TR-EPR spectrum strictly depends on the relative geometry of the Car/BChl couples involved in the TTET [Di Valentin 2008, Di Valentin 2009].

2. Materials and Methods

2.1 Sample preparation

Isolated Chlorosomes of *Chlorobaculum tepidum* were prepared in according to the procedure of Gerola et al. and decribed in [Carbonera et al. 2001] to a final concentration of 1 mg mL^{-1} BChl *c*. The samples were poised at pH 7.4 in 10 mM potassium phosphate buffer and added with 20 mM dithionite under nitrogen. Oxygen was removed from the sample by bubbling argon in the EPR tubes before freezing.

2.2 TR-EPR experiments

Experiments were performed on a Bruker Elexsys E580 pulsed EPR spectrometer. Laser excitation at 532 nm (10 mJ per pulse and repetition rate of 10 Hz) was provided by the second harmonic of a Nd:YAG laser (Quantel Brilliant) in a flexline dielectric resonator. The temperature was controlled by means of a helium cryostat (Oxford CF935) driven by a temperature controller (Oxford ITC503).

TR-EPR experiments were performed in direct-detection mode, taking the signal directly from the mixer, without lock-in amplification with the specjet digitizer. Transients were accumulated both on and off-resonance fields in order to eliminate the laser background signal by subtraction of the off-resonance traces. Transient signal rise time was about 50 ns. The microwave power was 2 mW. The microwave frequency was 9.70 GHz. Time-resolved spectra?

2.3 EPR spectral simulations

Simulations of the powder spin-polarised triplet spectra were performed using a program written in MatLab® with the aid of the Easyspin routine (ver. 2.6.0) [Stoll et al. 2006]. As previously described [Di Valentin et al. 2008, 2009, 2010], the program is based on the full diagonalization of the triplet state spin Hamiltonian, taking into account the Zeeman and magnetic dipole-dipole interactions, assuming a powder distribution of molecular orientations with respect to the applied magnetic field. Input parameters are: the sublevel populations, the ZFS parameters, the line-width at the canonical orientations and the g-tensor components assumed to be isotropic and equal to g_e.

Calculations of the sublevel triplet state populations of the acceptor, starting from those of the donor, were performed following the procedure described before [Di Valentin 2008, 2009, 2010], using a home-written program in MatLab® software, based on the formalism of [Akiyama et al. 1994], and utilizing the atomic coordinates of the pigments in the baseplate according to the model proposed by Pedersen et al [Pedersen et al. 2010]. The program for the calculation of the triplet sublevel populations, works in the limit of a triplet-triplet energy transfer (TTET) which is fast, compared to the time evolution of the donor triplet spectrum, and is slow enough to allow spin alignment in the external magnetic field. Referring to the three

triplet sublevels with no applied magnetic field, the relationship between the populations of the acceptor and those of the donor is:

$$P_i^A = \sum_j \cos^2 \theta_{ij} \; P_j^D$$

where θ_{ij} is the angle between the principal axis *j* of the donor and the axis *i* of the acceptor. With an applied magnetic field, the populating rates of the three sublevels, at any field position, which determine the initial polarization of the acceptor triplet state, can be calculated starting from those at zero field. Although only the relative populating rates *Px:Py:Pz* of the donor are accessible experimentally and usually the absolute values are not known, the relative populating rates of the acceptor can be calculated directly from the equation reported above using the relative rates P_j^D.

3. Results

3.1 TR-EPR

The 95 K X-band spin-polarized TR-EPR spectrum of chlorosomes from *Chlorobaculum tepidum*, taken at 150 ns after the laser pulse is shown in Figure 3. The spectrum clearly reveals the presence of two different species. The triplet population with the wider spectrum, having ZFS parameter |D| = 350 G, can be easily assigned to ^{T}Car, on the basis of the ZFS parameters previously determined by ODMR spectroscopy on the same type of preparations [Carbonera et al. 2001]. The other contribution is attributed to unquenched ^{T}BChl *c* characterized by |D| = 250 G and |E| = 31 G, in good agreement with the ODMR analysis presented in [Carbonera et al. 2001]. No detectable ^{T}BChl *a* states are present, while a photo-induced radical is visible in the central part of the TR-EPR spectrum. The poor signal to noise ratio of the spectrum is due to the low triplet yield which characterizes the chlororsomes [Carbonera et al. 2001].

As a result of the spectral analysis (not shown), and as already found for other antenna systems [Di Valentin et al. 2008, 2009, 2010], the time evolution of the ^{T}Car spectrum is slow compared to the time resolution of the instrumental set-up, thus the spectrum taken at the shortest time is representative of the “initial” polarization inherited from the ^{T}BChl states during the TTET process. The ^{T}BChl *c* contribution

of the TR-EPR spectrum evolves independently showing no correlation with the spectral evolution of the ^{T}Car (not shown).

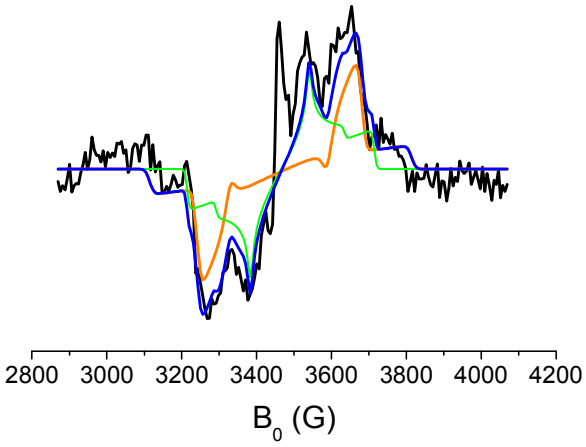


Figure 3: 95 K photo-excited TR-EPR spectrum of chlorosomes from *Chlorobaculum tepidum* (black line). Reconstruction (blue) of the experimental spectrum obtained by summing up two distinct contributions: the BChl *c* triplet state spectrum (green: |D| = 250 ± 3 G, |E| = 31 ± 3 G; *Px:Py:Pz* = 0.36:0.44:0.20) and the carotenoid contribution (orange: |D| = 350 ± 3 G, |E| = 30 ± 3 G; *Px:Py:Pz* = 0.38 : 0.22 : 0.39).

The experimental spectrum has been reconstructed as shown in figure 3, by simulating the two contributions of ^{T}BChl *c* and ^{T}Car and fitting the experimental spectrum by summing them in proper relative amount. A similar procedure was used before for the reconstruction of the TR-EPR spectrum of the LHC from *Amphidinium Carterae* [Di Valentin et al. 2010]. Since the populating sublevel rates of isolated ^{T}BChl *c* are not known, we have considered the strong similarity between the electronic and magnetic properties of BChl *c* and Chl *a*: in fact, the BChl *c* structural characteristics closely resemble those of Chl *a* and the electronic spectra are also very similar [Blankenship et al. 2003]. For these reasons, we have assumed, for the simulation of the ^{T}BChl *c* spectrum, values for the sublevels populations of ^{T}BChl *c* similar to those, which are well known, of ^{T}Chl *a* in MTHF, only slightly modified to better fit the experimental spectrum [Di Valentin et al. 2008]. Although the BChl *c* molecules giving the triplet states are present in oligomeric forms in the chlorosomes [Carbonera et al. 2001, Kim et al. 2007, Pšenčík et al. 1997], their ZFS populations are expected to be very similar to those of the corresponding monomers because of

the parallel arrangements of the pyrrole rings suggested by the models of the aggregates present in the literature [Arellano et al. 2005]. Finally, the ZFS parameters of the ^{T}BChl c and ^{T}Car were those reported in the ODMR work [Carbonera et al. 2001], while the sublevel populations of the ^{T}Car have been determined by a fitting procedure which minimizes the difference between the experimental spectrum and the one obtained by summing the ^{T}Car and ^{T}BChl *c* contributions in a proper relative amount. The best reconstruction is shown in figure 3, where the contribution of the carotenoid to the TR-EPR spectrum is seen to be characterized by the polarization pattern *eeaeaa* (Px:Py:Pz = 0.38:0.22:0.39).

3.2Calculations of the TR-EPR spectra based on TTET

The ^{T}Car spectral contribution to the TR-EPR spectrum (see the orange trace in figure3) represents the experimental result which allows us to critically discuss the baseplate structural model.

According to the results obtained before the carotenoid triplet states observed at low temperature are populated by TTET mainly from the ^{T}BChl *a* states formed in the baseplate [Carbonera et al. 2001]. Even though some carotenoids molecules are thought to be located close to the BChl *c* molecules, they seem to have a minor capacity of triplet quenching at low temperature. For this reason we have neglected in our analysis the possible contribution of ^{T}BChl *c* states to the TTET.

The ^{T}Car inherits the polarization of the ^{T}BChl *a* in a way which depends on the relative orientation of the ZFS axes, as already discussed in our previous work on other light-harvesting complexes [Di Valentin 2008, 2009, 2010]. To check the compatibility of the baseplate model with the EPR results we have calculated the expected initial TR-EPR spectrum for each BChl *a*/Car couple in the structure proposed by Pedersen et al. [Pedersen et al. 2010], according to the procedure described below.

To perform the calculations it is needed to know: (i) the relative geometrical position of the BChl *a* and carotenoid moieties; (ii) the orientation of the ZFS axes on the molecular frames; and (iii) the triplet sublevel populations of the ^{T}BChl *a* formed by ISC process.

The relative position of each BChl *a* /Car couple has been derived from the coordinates of the atoms constituting the pigments structural model presented by

Pedersen et al. [Linnato personal communication]. The orientation of the ZFS axes of the carotenoid molecules in the molecular frame have been determined by using the procedure already described in [Di Valentin et al. 2009], giving the Z axis approximately parallel to the long molecular axis, a deviation being induced by the presence of the aromatic ring present in the molecular structure, the X axis almost parallel to the C-H bond direction of the conjugated chain, and the Y axis perpendicular to the ZX plane (see figure 1) [Frick et al. 1990]. The orientation of ZFS axes of BChl *a* with respect to the orientation of Qy transition dipole moment was determined before by linear-dichroism ODMR [Vrieze et al. 1995]: from those experiments it was possible to derive the angle between the X and Y ZFS axes in the porphyrin plane and the Qy vector but not the sign of the rotation which remains undetermined. The two possible orientations of the ZFS frame in the BChl *a* molecular structure are shown in figure 1. Marchanka et al. tried to remove this ambiguity, by means of pulsed ENDOR measurements of the photoexcited ^{T}BChl *a* state, and selected the red configuration in figure 1 [Marchanka et al. 2009]. However, since the assignment maintains a degree of uncertainty, we preferred to consider, in our calculations, both possibilities.

The last input parameters are the triplet sublevel populations generated by ISC in the BChl *a* molecules: since the energy transfer rate from ^{T}BChl *a* to ^{T}Car is faster compared to the experimental time resolution we were not able to detect the ^{T}BChl *a* spectrum directly. For this reason we assumed the triplet sublevel populations to be equal to those derived for a photoexcited sample of isolated BChl *a* in methyl-THF (not shown). In fact, iIn this solvent there is a penta-coordination to the central Mg atom as in the natural system. The ^{T}BChl *a* spectrum was characterized by $|D| = 252 \pm 3.0$ G and $|E| = 65 \pm 3$ G and by relative populations Px : Py : Pz = 0.44 : 0.40 : 0.16 (not shown).

For each of the eight BChl *a* molecules of the basic structural unit of the baseplate we considered the closest carotenoid molecule and calculated the expected ^{T}Car spectrum. The results are shown in figure 4, relatively to the two possible orientations of the ZFS axes in the BChl *a* molecular frame.

By comparison of the spectra of figure 4 with the experimental ^{T}Car contribution to the experimental TR-EPR spectrum, it can be seen that most BChl *a*-Car couples give rise to a polarization pattern which is compatible with the observed one

(*eeaeaa*). For most of these couples the results are only slightly influenced by the choice of ZFS axes on the BChl *a* molecular structure.

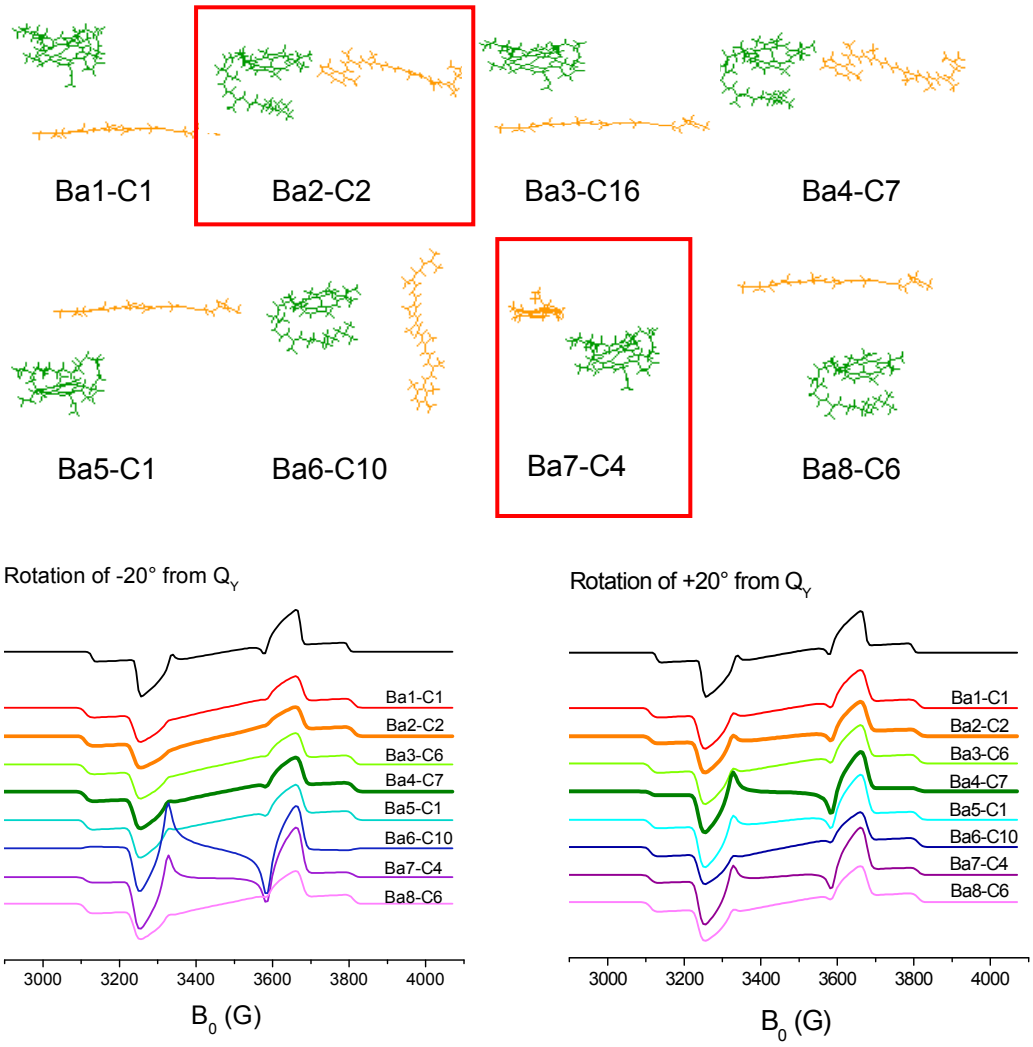


Figure 4: Top - Molecular structure of BChl *a*/Car pairs as derived by the structural model presented in [Pedersen et al. 2010]. Bottom - Spectra of the ^{T}Cars (C1..C10) calculated on the basis of TTET from the 8 BChl *a* molecules (Ba1…Ba8) of the baseplate together with the spectrum deriving from the reconstruction of the experimental TR-EPR spectrum (black). The two BChl a/Car couples with the closest proximity are highlighted. Both the possible orientations of ZFS axes of ^{T}BChl *a* with respect to the orientation of Qy transition dipole moment have been considered.

4. Discussion

The whole chlorosome machinery is of great interest since it represents a model to develop efficient artificial light-harvesting devices. The crystal structure is not

available yet and in literature many works have been devoted to elucidate the nature of the supramolecular BChl *c* aggregates. The baseplate of the chlorosomes is the functional link between the BChl *c* aggregates and the FMO proteins. For its position in the apparatus, the baseplate is a sort of energy converter and for this reason it is very important to know its structure and to understand the energy transfer pathways in which it is involved. Only one structural model of the baseplate has been proposed up to now. This model accounts for the position and the orientation of CsmA proteins [Frigaard et al. 2005, Li et al. 2006] and for many optical properties of the BChl *a* [Gerola and Olson 1987, Pedersen et al. 2008a, Pedersen et al. 2010] but it lacks of any experimental results about the carotenoids properties. Although they are a small fraction of the total pigments content (10% in *Chlorobaculum tepidum*), carotenoids in chlorosomes play a fundamental role not only in the light harvesting but also as molecular glue [Carbonera et al. 2001, Ikonen et al. 2007]. It has been demonstrated that the inhibition of carotenoids results in the inability of properly assembling the baseplate [Arellano et al. 2001], leading to round-shape chlorosomes [Frigaard et al. 2005]. The interaction between the CsmA-BChl *a* complex and the associated carotenoids is very strong: even a gel filtration column is not able to separate them [Pedersen at al. 2008]. Thus, the presence and the location of carotenoids molecules are not of secondary importance in determining the functional and structural properties of the baseplate structure.

The TTET mechanism is a collateral energy transfer path activated in high light (stress) conditions which may allow gaining structural information about the location of specific carotenoid molecules in the baseplate. TTET is a demanding mechanism since it implies a close contact between the partners involved in the energy transfer to assure a good overlap between their electronic wavefunctions. The TR-EPR experiments at 95 K described in the previous section show that, as expected, carotenoid triplet states are populated under illumination of the isolated chlorosomes. On the basis of the ODMR results obtained before in the chlorosomes of *Chlorobaculum tepidum*, it has been proven that, at low temperature, most of these carotenoid triplet states become populated by TTET occurring between BChls *a* and carotenoids (most likely chlorobactene, the most abundant species) located in the baseplate. Thus the TR-EPR experiments can be useful for determining the relative

position of these, specific, carotenoid- BChl *a* couples in the baseplate and verify the accuracy of the proposed model.

According to the calculations reported above, most of the BChl *a*- Car couples considered, present a polarization pattern of the TR-EPR spectrum of the acceptor ^{T}Car compatible with the observed one. However, among these, only the two symmetry-related couples (BChl2-Car2 and BChl4-Car7) have a minimum distance between the carotenoid conjugate chain and the porphyrin ring of about 6.5 Å (see figure 4 and table 1) and are not separated by the interposed protein residues. For all the others the distance is larger than 10 Å. Thus it seems reasonable that only these two couples would be able to perform TTET in the proposed structure of the baseplate, since the two partners are close enough to allow the triplet transfer to occur.

BChl a – Carotenoid couple	**π – π shortest distance (Å)**
Ba1-C1	14 Å
Ba2-C2	7 Å
Ba3-C6	15 Å
Ba4-C7	6 Å
Ba5-C1	15 Å
Ba6-C10	15 Å
Ba7-C4	13 Å
Ba8-C6	16 Å

Table 1: Shortest distances obtained from the atomic coordinates between the π-systems of the eight bacteriochlorophyll molecules present in the model and the corresponding closest carotenoid [Linnato personal comunication]. The nomenclature refers to figure 4.

In all the other possible couples the partners are too far apart to have any physical meaning in terms of TTET. This would leaves several unprotected BChl *a* molecules in the baseplate, unless BChl2 and BChl4 represent the red most BChls of the baseplate where the excitation is funnelled. However it must be noted that, from a theoretical point of view, also the 6.5 Å measured minimum distance between the BChl2-Car2 represents a limit for an efficient TTET. Therefore we think that a refining of the model of the baseplate should be considered, based on a closer packing of at least some of the carotenoids, relatively to the BChl *a* molecules (< 5 Å considering the distance between the two π-systems, as already found for other

natural antenna complexes [Di Valentin 2008, 2009]). According to the EPR constrains the pairs should be in a relative geometry that could allow to reproduce the experimental carotenoid triplet state polarization pattern.

As a final remark, the presence of unquenched BChl *c* triplet states is in agreement with previous works on triplet states interaction and energy transfer in chlorosomes [Arellano et al. 2000, Carbonera et al. 2001]. As already suggested the biological meaning of these large triplet population could imply that BChl *c* supra-aggregates triplet state energy fall below that of singlet oxygen and triplet carotenoids, representing in this way a non dangerous energy dissipation pathway [Kim et al. 2007]. The polarization pattern observed for the BChl *c* triplet states is in agreement with a parallel arrangement of the porphyrin planes in the aggregates.

5. References

[Akiyama et al. 1994] Akiyama K., Terokubota S., Ikoma T., Ikegami Y., *J. Am. Chem. Soc.*, **1994**, 116, 5324-5327

[Akutsu et al. 2010] Akutsu H., Ayako Egawa A., Fujiwara T., *Photosynth. Res.*, **2010**, 104(2-3), 221-231

[Arellano et al. 2000] Arellano J. B., Melo T. B., Borrego C. M., Garcia-Gil J., Naqvi K.R., *Photochem. Photobiol.*, **2000**, 72, 669-675

[Arellano et al. 2001] Arellano J. B., Borrego C. M., Martinez-Planelles A., Garcia-Gil L. J., *rch. Microbiol.*, **2001**, 175, 226-233

[Arellano et al. 2005] Arellano J. B., Borrego C. M., Butcher S. J., Ikonen T., Laurinmaki P., Psencik J., Serimaa R. E., Tuma R., *Biophys. J.*, **2005**, 88(1), 175A

[Blankenship et al. 2003] Blankenship R. E., Matsuura K., Antenna complex from green photosynthetic bacteria. In: Green B.R., Parson W. W. (eds), Light harvesting antennas in photosynthesis. Kluwer, Dordrecht, The Netherlands

[Bryant et al. 2002] Bryant D. A., Vassilieva E. V., Frigaard N. U., et al., *Biochemistry*, **2002**, 41, 14403-14411

[Carbonera et al. 2001] Carbonera D., Bordignon E., Giacometti G., Agostini G., Vianelli A.,Vannini C., *J. Phys. Chem. B*, **2001**, 105, 246-255

[Di Valentin et al. 2008] Di Valentin M., Ceola S., Salvadori E., Agostini G., Carbonera D., *Biochimica et Biophysica Acta*, **2008**, 1777, 186-195.

[Di Valentin et al. 2009] Di Valentin M., Biasibetti F., Ceola S., Carbonera D., *J. Phys. Chem. B*, **2009**, 113, 13071-13078

[Di Valentin et al. 2010] Di Valentin M., Salvadori E., Agostini G., Biasibetti F., Ceola S., Hiller R., Giacometti G. M., Carbonera D., *BBA-Bioenergetics*, **2010**, 1797, 1759-1767

[Frick et al. 1990] Frick J., Von Schutz J. U., Wolf H. C., Kothe G., *Mol. Cryst. Liq. Cryst.*, **1990**, 183, 269-272

[Frigaard et al. 2005] Frigaard N.-U., Li H., Martinsson P., Das S. K., Franck H. A., Aartsma T. J., Bryant D. A., *Photosynth. Res.*, **2005**, 86, 101-111

[Gerola and Olson 1986] Gerola P. D., Olson J. M., *Biochim. Biophys. Acta*, **1986**, 848, 69-76

[Holzwarth et al. 1994] Holzwarth A. R., Schaffner K., *Photosynth. Res.*, **1994**, 41, 225-233

[Ikonen et al. 2007] Ikonen T. P., Li H., Psencik J., Laurinmaki P. A., Butcher S. J., Frigaard N.-U., Serimaa R. E., Bryant D. A., Tuma R., *Biophys. J.*, **2007**, 93(2), 620-628

[Jochum et al. 2008] Jochum T., Reddy C. M., Eichhofer A., Buth G., Szmytkowski J., Kalt H., Moss D., Balaban T. S., *Proceedings of the national academy of sciences of the united states of America*, **2008**, 105(35), 12736-12741

[Kim et al. 2007] Kim H., Maresca J. A., Bryant D. A., Savikhin S., *Biophys. J.*, **2007**, 93, 192-201

[Li et al. 2006] Li H., Frigaard N.-U., Bryant D. A., *Biochemistry*, **2006**, 45, 9095-910

[Linnato et al. 2008] Linnanto J. M., Korppi-Tommola J. E. I., *Photosynth. Res.*, **2008**, 96(3), 227-245

[Marchanka et al. 2009] Marchanka A., Lubitz W., van Gastel M., *J. Phys. Chem. B.*, **2009**, 113(19), 6917-6927

[Melø et al. 2000] Melø T. B., Frigaard N. U., Matsuura K., Naqvi K. R., *Spectrochimica Acta part - Molecular and Biomolecular Spectroscopy*, **2000**, 56(10), 2001-2010

[Montaño et al. 2003] Montaño G. A., Wu H. M., Lin S., et al., *Biochemistry*, **2003**, 42, 10246-10251

[Oostergetel et al. 2010] Oostergetel G. T., van Amerongen H., Boekema E. J., *Photosynth. Res.*, **2010**, 104, 245-255

[Pedersen et al. 2008] Pedersen M. Ø., Underhaug J., Dittmer J., Miller M., Nielsen N. C., *FEBS Letters*, **2008**, 582, 2869-2874

[Pedersen et al. 2008a] Pedersen M. Ø., Pham L., Steensgaard D. B., Miller M., *Biochemistry* **2008**, 47, 1435-1441

[Pedersen et al. 2010] Pedersen M. Ø., Linnato J., Frigaard N.-U., Nielsen N. C., Miller M., *Photosynth. Res*., **2010**, 104, 233-234

[Pšenčík et al. 1997] Pšenčík J., Schaafsma T. J., Searle G. F. W., Hala J., *Photosynth. Res.*, **1997**, 52, 83-92

[Pšenčík et al. 2006] Pšenčík J., Arellano J. B., Ikonen T. P., Borrego C. M., Laurinmäki P. A., Butcher S. J., Serimaa R. E., Tuma R., *Biophys. J.*, **2006**, 91, 1433-1440[Pšenčík et al. 2010] Pšenčík J., Torkkeli M., Zupčanová A., Vácha F., Serimaa R. E., Tuma R., *Photosynth. Res*., **2010**, 104(2-3), 211-219u

[Sakuragi et al. 1999] Sakuragi Y., Frigaard N. U., Shimada K., Matsuura K., *Biochemistry*, **2007**, 46, 7062-7068

[Shibata et al. 2009] Shibata Y, Saga Y., Tamiaki H., Itoh S., *Photosynth. Res.*, **2009**, 100, 67-78

[Stoll et al. 2006] Stoll S., Schweiger A., *J. Magn. Reson.*, **2006**, 178, 42-55

[Vrieze et al. 1995] Vrieze J., Hoff A. J., *Chem. Phys. Lett.*, **1995**, 237, 493-501

Acknowledgements

I would like to thank all the Biophysics research group of the Chemical Science Department at the University of Padova:

Prof. Donatella Carbonera
Dr. Marilena Di Valentin
Dr. Stefano Ceola
Dr. Giancarlo Agostini
Prof. Giovanni Giacometti
Fedrico Biasibetti
Marco Albertini
Claudia Tait

I would also gratefully thank all the collaborators from other research groups:

Prof. Vincenzo Barone
Dr. Alfonso Pedone
Dr. Christopher M. W. Kay
Prof. Alberto Vianelli
Prof. Roger H. Hiller
Prof. Hugo Scheer
Prof. Juha Linnato